

Freie Universität



Berlin

Synthesis of Novel Ligands Based on 2-(2'-Pyridyl)-4,6-diphenylphosphinine: Coordination Chemistry and Reactivity

Inaugural-Dissertation

to obtain the academic degree

Doctor rerum naturalium (Dr. rer. nat.)

submitted to the Department of Biology, Chemistry, and Pharmacy
of Freie Universität Berlin

by

M. Sc. Marlene Bruce Vázquez del Mercado

from León, Guanajuato, Mexico

November 17th 2016

1. reviewer: Prof. Dr. C. Müller
2. reviewer: Prof. Dr. Nora Kulak

Date of disputation: November 17th 2016

The described work was carried out within the time period of September 2012 until June 2016 under the supervision of Prof. Dr. Christian Müller at the Freie Universität Berlin.

Declaration

I herewith confirm that I have prepared this dissertation without the help of any impermissible resources. All citations are marked as such. The present thesis has neither been accepted in any previous doctorate degree procedure nor has it been evaluated as insufficient.

Marlene Bruce Vázquez del Mercado

Berlin, September 2016

List of publications

- Lithium salts of 2,4,6-triaryl- λ^4 -phosphinine Anions – A Comparison Study.
Authors: Marlene Bruce, Gisa Meissner, Manuela Weber, Jelena Wiecko, Christian Müller.
Reference: *European Journal of Inorganic Chemistry* **2014** 1719-1726
- Recent Developments in the Chemistry of Pyridyl-functionalized, Low-coordinate Phosphorus Heterocycles.
Authors: Christian Müller, Julian A. W. Sklorz, Iris de Krom, Antonia Loibl, Marija Habicht, Marlene Bruce, Gregor Pfeifer, Jelena Wiecko.
Reference: *Chemistry Letters*, **2014**, (43) 1390-1404

Manuscripts in Preparation:

- Pyridyl-functionalized Phosphabarrelenes: Synthesis, Coordination Chemistry and Reactivity of Novel Phosphorus Cage Compounds.
Authors: Marlene Bruce, Julian A. W. Sklorz, Manuela Weber, Marija Habicht, Dieter Lentz, Nicolas Mézailles, Christian Müller
Manuscript in preparation
- Rhodium complexes of 1-ferrocenyl- λ^4 -phosphinine anions: Structural Characterization and Reactivity
Authors: Marlene Bruce, Sebastian Ponath, Christoph Hein, Manuela Weber, Christian Müller

Poster presentations:

- 2013 European Workshop on Phosphorus Chemistry. Regensburg, Germany.
- 2014 International Conference on Phosphorus Chemistry. Dublin, Ireland.
- 2015 European Workshop on Phosphorus Chemistry. Kassel, Germany.
- 2016 European Workshop on Phosphorus Chemistry. Berlin, Germany.

Acknowledgement

First of all, I would like to thank Prof. Dr. Christian Müller for giving me the trust and opportunity to work in his group. I appreciate the experience of being part of a new group, which started growing very rapidly in a very friendly and collaborative atmosphere. I am thankful for his advice, support, and guidance through all these years.

I would also like to thank Prof. Dr. Nora Kulak for being the second reviewer of this thesis and taking the time to read it.

I am very thankful to all the people that contributed to this work in one or another way:

* Dr. Jelena Wiecko, Manuela Weber and Dr. Dieter Lentz for the X-ray crystal structure analyses presented in this work.

* Dr. Dieter Lentz for his support on the synthesis of the phosphabarrelene with the hexafluoro-2-butyne.

* Dr. Simon Steinhauer and Antonia Loibl for all the help with the NMR experiments and the explanations.

* Antonia, Marija, Julian, Massimo, Fanni, Gregor, Steven, Martin, Wiebke, Jelena and Annika, for all the help, discussions, support, the food, the cakes, the drama and mostly all those fun days. Special thanks to those who read and corrected the chapters of this work!

* My students Sebastian Ponath, Christoph Hein, Vico Adjedje, Fabian Eberle, Michael Katan, Gisa Meißner, and Waldemar Hoffmann.

* Markus Peschke, and the workers in the mechanical and glass workshops.

I would like to thank my family who has always supported me, the last five years from the distance, yet being always present: My parents, for encouraging me to go after what I like and being very loving. My sisters Mariana, Marcelle, and Michelle for the unconditional support, fun, long talks, and visits. My very numerous and caring mexican family (grandparents, aunts, uncles, cousins, nephews and nieces). To Nat, who has been very understanding and accurate to push me into having some fun during days of stress

but also motivating me to work harder when it appeared that the energy was disappearing.

Many thanks to my new Berlin family, who throughout the years has made the time in this foreign city feel like home. Valentina, Lothar, Amalia, Killian, Miriam, Massimo, Antonia, Fanni, Emma, Iliusi, Sofia, the MvB crew, and all the nice friends I've made here.

Abstract

This work focuses on a detailed investigation of 2-(2'-pyridyl)-4,6-diphenylphosphinine (PN) and the outcome of this work is the development of three different classes of ligands based on this aromatic phosphorus heterocycle: an anionic pyridyl-functionalized λ^4 -phosphinine, a pyridyl-functionalized phosphabarrelene and a pyridyl-functionalized phosphasemibullvalene. The coordination chemistry and reactivity of all three ligands with transition metals was further investigated in detail.

Coordination compounds with some transition metals and the **PN** ligand have been explored and reported in literature. In this work, the first pyridyl-substituted phosphinine-based complexes of copper, iron and gold were synthesized and structurally characterized. The preparation of other complexes starting with from different rhodium and tungsten precursors were explored and compared to the ones reported in literature. Interesting coordination modes of the **PN** ligand were noticed for different complexes. The reactivity of the obtained iron complexes towards alkene coordination and protonation was explored as well.

By means of an alkylation reaction with lithium reagents, the **PN** compound was successfully converted into anionic λ^4 -phosphinines with different substituents on the phosphorus atom (methyl, phenyl, and ferrocenyl). These anionic species are more similar to phosphines than phosphinines due to the aromatic disruption on the phosphorus ring that leads to a strong pyramidalization of the phosphorus atom. They are reactive towards protic reagents such as water and alcohols, yielding a lithium salt and a neutral compound, where a proton has been added selectively to one of the P-C double bonds within the heterocycle. The selectivity of this reaction is dependent on the pK_a of the base formed. Nevertheless, the electronic and steric situation of this class of ligands differs substantially from phosphines, thus making them very interesting ligands for metal complexes with different properties than “classical” phosphine-based metal complexes. One of the outstanding differences is that pyridyl-substituted λ^4 -phosphinine ligands show an interesting coordination mode besides the expected η^1 -P- η^1 -N chelating

mode. They are able to coordinate a second metal center *via* the delocalized π -system along the carbocyclic part of the phosphorus heterocycle resulting in ligands that can donate up to 8 electrons.

The first pyridyl-substituted phosphabarrelene was synthesized *via* a [4+2] cycloaddition reaction of the **PN** ligand and hexafluoromethyl-2-butyne. Despite the poor donating properties of phosphabarrelenes in general, several transition metal complexes could be synthesized and characterized with this new ligand. In the case of gold complexes, it was observed that the coordination occurs only *via* the phosphorus atom. The obtained complexes undergo a photochemical rearrangement when irradiated in solution with UV light yielding different products. The selectivities of such reactions appear higher for the transition metal complexes than for the free ligand. From the reaction mixtures of rhodium and tungsten complexes the main product was purified and characterized. The product corresponds to a pyridyl-substituted phosphasemibullvalene derivative. From these findings a rearrangement mechanism is proposed. IR analyses and crystallographic data of the complexes obtained suggest, that in general, phosphasemibullvalenes are better net-donors than phosphabarrelenes.

Kurzbeschreibung

Die vorliegende Arbeit beschäftigt sich mit einer detaillierten Untersuchung des 2-(2'-pyridyl)-4,6-diphenylphosphinins (**PN**-Ligand) sowie der Entwicklung von drei neuen, aus letzterem abgeleiteten, Ligandensystemen: ein anionisches, pyridyl-funktionalisiertes λ^4 -Phosphinin, ein pyridyl-funktionalisiertes Phosphabarrelen und ein pyridyl-funktionalisiertes Phosphasemibullvalen. Die Koordinationschemie von allen drei Systemen mit Übergangsmetallen wurde detailliert untersucht.

Einige Komplexe des **PN**-Liganden mit bestimmten Übergangsmetallen wurden in der Vergangenheit bereits synthetisiert und in der Literatur beschrieben. Hier wurden nun die ersten Pyridylphosphininkomplexe mit Kupfer, Eisen und Gold dargestellt und charakterisiert. Die Synthese von weiteren Koordinationsverbindungen, ausgehend von anderen Rhodium- und Wolfram-Prekursoren wurden untersucht und mit den literaturbekannten Komplexen verglichen. Für verschiedene Metallkomplexe konnten interessante Koordinationsmodi erhalten werden. Weiterhin wurde die Reaktivität der erhaltenen Eisenkomplexe näher untersucht.

Durch Alkylierung mit Lithiumreagenzien wurde die **PN**-Verbindung erfolgreich in anionische λ^4 -Phosphinine mit unterschiedlichen Substituenten am Phosphoratom (Methyl, Phenyl und Ferrocenyl) überführt. Diese anionischen Spezies sind durch die Störung des aromatischen Systems sowie die daraus folgende Pyramidalisierung des Phosphoratoms den Phosphinen ähnlicher als den Phosphininen. Sie reagieren mit protischen Reagenzien, wie z.B. Wasser oder Alkoholen, zu Lithiumsalzen und einer Phosphorverbindung, die durch selektive Protonierung an eine der P-C-Doppelbindungen elektrisch neutral ist. Die Selektivität der Reaktion ist vom pK_a -Wert der entstehenden konjugierten Base abhängig. Auf Grund der dennoch entscheidenden sterischen und elektronischen Unterschiede zwischen dieser Ligandenklasse und den Phosphinen sind λ^4 -Phosphinine sehr interessante Liganden für Metallkomplexe mit anderen Eigenschaften als herkömmliche Phosphinmetallkomplexe sie aufweisen. Ein auffallender Unterschied ist beispielsweise der interessante Koordinationsmodus von

pyridylsubstituierten λ^4 -Phosphininen neben dem erwarteten η^1 -P- η^1 -N-Chelatkomplex. Über das delokalisierte π -System entlang des Kohlenstoffgerüsts des Phosphorheterozyklus kann ein zweites Metall gebunden werden, wodurch diese Liganden bis zu 8 Elektronen zur Verfügung stellen können.

Das erste pyridylsubstituierte Phosphabarrelen wurde durch [4+2]-Zykloaddition von Hexafluoromethyl-2-butin an den PN-Liganden synthetisiert. Trotz der generell schwachen Donoreigenschaften von Phosphabarrelenen konnten mehrere Übergangsmetallkomplexe dieses neuen Liganden dargestellt und charakterisiert werden. Im Falle von Goldkomplexen konnte ausschließlich Koordination über das Phosphoratom beobachtet werden. Generell durchlaufen die erhaltenen Koordinationsverbindungen unter Bestrahlung mit UV-Licht eine Umlagerung zu verschiedenen Produkten. Die Selektivität dieser Reaktionen scheint für Metallkomplexe höher zu sein als für den freien Liganden. Aus den Reaktionsgemischen der Rhodium- und Wolframkomplexe konnte das Hauptprodukt, ein pyridylsubstituierter Phosphasemibullvalen-Derivat, isoliert und charakterisiert werden. Auf Grund dieser Ergebnisse wird ein Mechanismus für die Umlagerung vorgeschlagen. Phosphasemibullvalene sind laut IR Analysen und Molekülstrukturdaten der erhaltenen Komplexe bessere Netdonoren als Phosphabarrelene.

Table of contents

1	Introduction to phosphinine.....	3
1.1	Introduction	3
1.2	Synthetic routes	3
1.3	Electronic properties	6
1.4	Steric properties	7
1.5	Coordination modes and transition metal complexes.....	8
1.6	P,N – hybrid ligands	11
1.7	Aim of this thesis.....	14
1.8	References.....	15
2	Coordination Chemistry of 2-(2'-Pyridyl)-4,6-diphenylphosphinine	21
2.1	Introduction	21
2.2	Results and discussion.....	28
	Group XI metal complexes	29
	Group X metal complexes	40
	Group IX metal complexes	42
	Group VIII metal complexes	45
	Group VI metal complexes	60
2.3	Conclusions.....	62
2.4	Experimental.....	63
	General remarks	63
	[(PN)Cu(MeCN)] ₂ [PF ₆] ₂ (5)	63
	[(PN) ₂ Cu][PF ₆] (6)	64
	[Ag(PN)][OTs] (7).....	64
	[Ag(PN) ₂][OTs] (8).....	65
	[Ag(PN) ₃][OTs] (9).....	65
	[Ag(PN) ₃][OTf] (10).....	66
	[Au(PN)Cl] (11).....	66
	[Au(I)-Au(III)(μ-PN)Cl ₄] (12).....	67
	[Ni(PN)CO] ₂ (15)	67
	[Rh(PN)Cl(CO)] ₂ (16)	67
	[Fe(PN)(CO) ₃] (17).....	68
	[Fe(PN)(η ² -methylacrylate)(CO) ₂] (18)	68
	[Fe(PN)(η ² -(1,3-butadiene))(CO) ₂] (19).....	68

$[\mu\text{-(pdt)Fe}_2(\text{PN})(\text{CO})_4]$ (20)	69
$[\mu\text{-(pdt)Fe}_2(\text{PN})_2(\text{CO})_2]$ (21)	69
$[\text{W}(\text{PN})_2(\text{CO})_2]$ (22)	70
X-ray crystal structure determinations	70
2.5 References	73
3 λ^4-Phosphinines	81
3.1 Introduction	81
3.2 Coordination chemistry of λ^4-phosphinines	83
3.3 Results and discussion	85
3.4 Conclusions	103
3.5 Experimental	104
General remarks	104
1-Ferrocenyl-(2,6-diphenyl-4-(p-tolyl))-cyclophosphahexadienyllithium (17)	104
1-Methyl-4,6-triphenyl-2-(2'pyridyl)-phosphacyclohexadienyllithium (18)	105
1,4,6-triphenyl-2-(2'pyridyl)-phosphacyclohexadienyllithium (19)	105
1-Ferrocenyl- (2-Pyridyl)-4,6-diphenylphosphinine (20)	106
$[(\text{cod})\text{Rh}(\eta^1\text{-19})]$ (25)	106
$[(\text{cod})\text{Rh}(\eta^1\text{-20})]$ (26)	107
$[(\text{cod})\text{Rh}(\eta^1\text{-(H)20})]$ (27)	107
$[(\text{cod})_2\text{Rh}_2(\eta^1\text{-}\eta^5\text{-20})]$ (28)	108
$[(\text{cod})_2\text{Rh}_2(\eta^1\text{-}\eta^6\text{-17})]$ (29)	109
X-ray crystal structure determinations	109
3.6 References	111
4 Phosphabarrelenes	115
4.1 Introduction	115
4.2 Results and discussion	121
4.3 Conclusions	140
4.4 Experimental	140
General remarks	140
Phosphabarrelene (1)	141
$[\text{Au}(\text{1})\text{Cl}]$ (2)	142
$[(1,5\text{-cyclooctadiene})(\text{1})\text{rhodium}]$ tetrafluoroborate (3)	142
$[(\text{CO})\text{ClRh}(\text{1})]$ (4)	143
$[(\text{CO})_4\text{W}(\text{1})]$ (5)	144
$[(\text{CO})_3\text{Fe}(\text{1})]$ (6)	145

[(CO)ClRh(phosphasemibullvalene)] (7)	145
[(CO) ₄ W(phosphasemibullvalene)] (8).....	145
X-ray crystal structure determinations.....	145
4.5 References	148
5 Summary and conclusions	153

Table of abbreviations

IUPAC	International Union of Pure and Applied Chemistry
BArF	[Bis(trifluoromethyl)phenyl]borate
bpy	Bipyridine
cod	Cyclooctadiene
CV	Cyclic voltammetry
cym	Cymene
DCM	Dichloromethane
DFT	Density functional theory
DMS	Dimethyl sulfide
dmsO	Dimethyl sulfoxide
DPEphos	(Oxydi-2,1-phenylene)bis(diphenylphosphine)
dppe	1,2-Bis(diphenylphosphino)ethane
dppm	1,2-Bis(diphenylphosphino)methane
dppp	1,2-Bis(diphenylphosphino)propane
dppv	1,2-Bis(diphenylphosphino)ethylene
ee	Enantiomeric excess
E°	Electrode potential
Et	Ethyl
Fc	Ferrocene
Fc^+	Ferrocenium
h	Planck constant
HMBC	Heteronuclear Multiple Bond Correlation
HOMO	Highest Occupied Molecular Orbital
HPLC	High Performance Liquid Chromatography
HSAB	Hard-Soft Acid-Base
IR	Infrared
J	Coupling constant
k	Rate of exchange

K_{Tc}	Equilibrium constant at coalescence temperature
LUMO	Lowest Unoccupied Molecular Orbital
<i>m</i> -	Meta
M:L	Metal to ligand ratio
Me	Methyl
MeCN	Acetonitrile
MO	Molecular Orbital
N_A	Avogadro Number
nbd	Norbornadiene
<i>n</i> Bu	<i>n</i> -Butyl
NICS	Nucleus Independent Chemical Shift
NIPHOS	2-(2'-Pyridyl)-4,5-dimethylphosphinine
NMR	Nuclear Magnetic Resonance
Ortep	Oak Ridge Thermal Ellipsoid Plot
pa	Anodic potential
pc	Catodic potential
pdt	Propane dithiolate
Ph	Phenyl
Py	Pyridine
R	Gas constant
<i>t</i> Bu	<i>tert</i> -Butyl
Tc	Critical temperature
THF	Tetrahydrofuran
TMBP	Tetramethylbiphosphinine
TMS	Trimethylsilyl
TON	Turn Over Number
UV	Ultra Violet
$\tilde{\nu}$	wave number

Chapter 1

Introduction to Phosphinines: Synthesis,
Electronic and Steric Properties and
Coordination Modes

1	Introduction to phosphinines	3
1.1	Introduction.....	3
1.2	Synthetic routes.....	3
1.3	Electronic properties	6
1.4	Steric properties.....	7
1.5	Coordination modes and transition metal complexes	8
1.6	P,N- hybrid ligands	11
1.7	Aim of this thesis	14
1.8	References	15

1 Introduction to phosphinines

1.1 Introduction

Phosphinines, also known as phosphabenzenes or phosphorins, are six-membered fully unsaturated planar aromatic heterocycles bearing a phosphorus atom. They are the phosphorus analogues of pyridines. The phosphorus atom in phosphinines is trivalent and it is bound to two carbon atoms. This is represented by the descriptors λ and σ , respectively leading to the formal IUPAC name: $\lambda^3\sigma^2$ -phosphinines (figure 1.1).

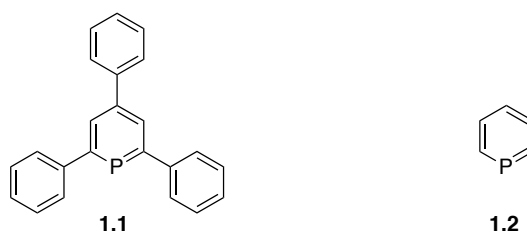
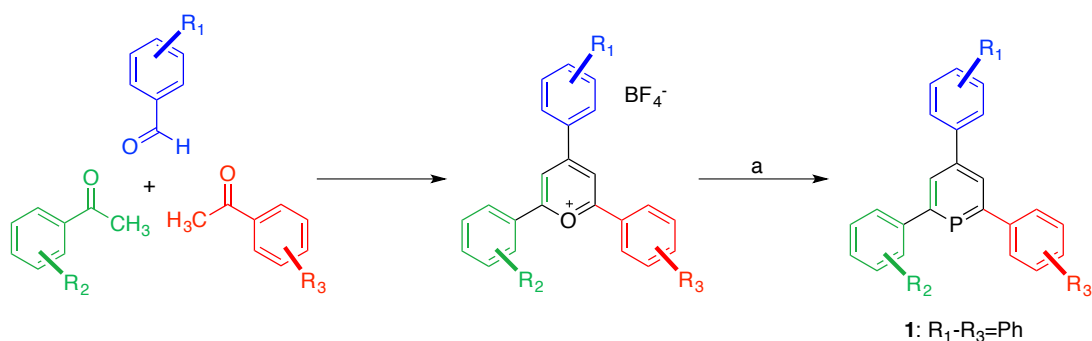


Figure 1.1 $\lambda^3\sigma^2$ -phosphinines

Phosphinines were long considered as scientific curiosities because they represent an exception of the double bond rule. Until the late sixties, Märkl and Ashe III developed state-of-the-art synthetic methodologies that allowed the systematic functionalization of these compounds and permitted their exploration in more detail.

1.2 Synthetic routes

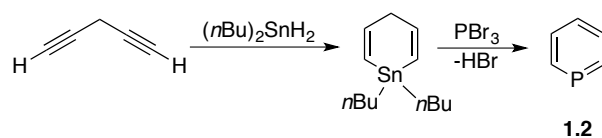
Märkl used benzaldehyde and acetophenone to synthesize the corresponding pyrylium salt used to prepare the 2,4,6-triphenylphosphinine (**1.1**), the first phosphinine to be published (figure 1.1).¹ Later, Müller²⁻⁶ and Breit⁷ used a modular approach using functionalized benzaldehydes and acetophenones to obtain a considerably large library of substituted pyrylium salts, which can be converted to phosphinines (scheme 1.1).



Scheme 1.1 Modular synthesis of phosphinines from the corresponding pyrylium salt.

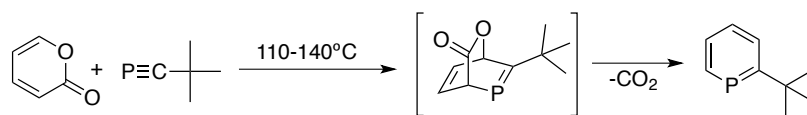
1.1: Märkl's triphenylphosphinine; a=P(CH₂OH)₃/py; R₁-R₃=Ph

The tin-route (scheme 1.2) developed by Ashe III, allowed the synthesis of the unsubstituted phosphinine **1.2**, although it is not air stable.⁸



Scheme 1.2 The tin route: Synthesis of the unsubstituted phosphinine

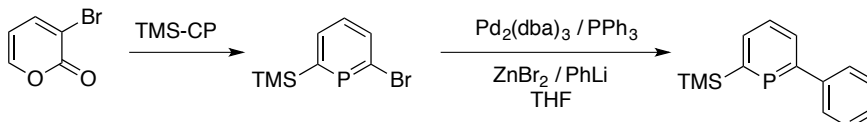
Several methodologies have been developed for the synthesis of phosphinines with different substitution pattern. Regitz *et al.* described the reactivity of phosphalkynes as dienophiles in [4+2] cycloaddition reactions with cyclopentadienones or pyrones to obtain alkyl-substituted phosphinines after exclusion of CO or CO₂, respectively (scheme 1.3).^{9,10}



Scheme 1.3 [4+2] cycloaddition reaction between pyrone and a phosphalkyne

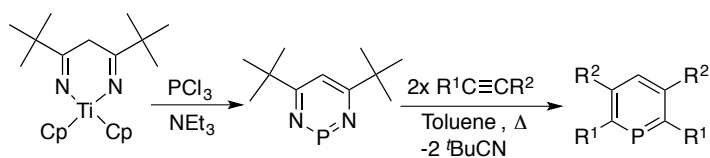
Very recently, Müller reported on the synthesis of 2,6-disubstituted phosphinines using TMS-phosphalkyne and 3-bromopyrone. This interesting observation allows further functionalization of phosphinines, which was achieved in this case *via* a Negishi cross-coupling reaction of PhLi

and bromo-phosphinine leading to 6-phenyl-2-trimethylsilyl-phosphinine (scheme 1.4). The molecular structure of the substituted phosphinine was verified by means of X-ray crystallography of the corresponding W(0) complex.¹¹



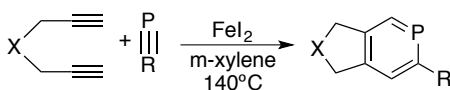
Scheme 1.4 Synthesis of 6-phenyl-2-trimethylsilylphosphinine *via* Negishi coupling

Le Floch and Mathey used (di)azaphosphinines as precursors to obtain phosphinines, mainly with substituents in the 2- and 6- positions of the heterocyclic framework (scheme 1.5).¹²



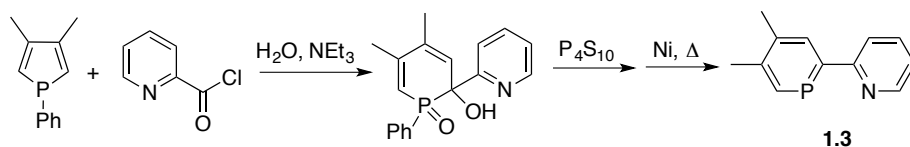
Scheme 1.5 Synthesis of phosphinines from diazaphosphinines

Recently the groups of Nishibayashi and Sakata published an FeI₂-catalyzed [2+2+2] cycloaddition of diynes with phosphalkynes in *m*-xylene to give a variety of 2,4,5-trisubstituted phosphinines (scheme 1.6).¹³



Scheme 1.6 Synthesis of phosphinines *via* the FeI₂-catalyzed [2+2+2] cycloaddition of diynes with phosphalkynes

For the synthesis of 2-substituted phosphinines, Mathey and co-workers investigated ring-expansion reactions of phospholes by formal insertion of methylene fragments. With this method, the first phosphinine derivative of 2,2'-bipyridine (NIPHOS, **1.3**) was synthesized (Scheme 1.7).¹⁴



Scheme 1.7 Synthesis of NIPHOS *via* phosphole ring-expansion

1.3 Electronic properties

As shown by photoelectron and electron transmission spectroscopy, phosphinines behave significantly different compared to their lighter analogues, the pyridines.^{15–18} While pyridines are fully aromatic, the aromaticity in phosphinines has been calculated to be as high as 88-90% of that of benzene.^{19,20} The molecular orbital diagram of the unsubstituted phosphinine and pyridine is depicted in figure 1.2. The nitrogen atom has its largest coefficient in the HOMO of the pyridine, which represents the electron lone pair. On the other hand, the phosphorus lone pair is best represented by the HOMO-2 of the phosphinine, which is a more diffuse and less directional orbital than that of pyridine. Upon coordination to a metal center *via* the phosphorus lone pair, the HOMO and HOMO-1 can contribute to the formation of a M-P bond *via* π -donation according to the shape of these orbitals.

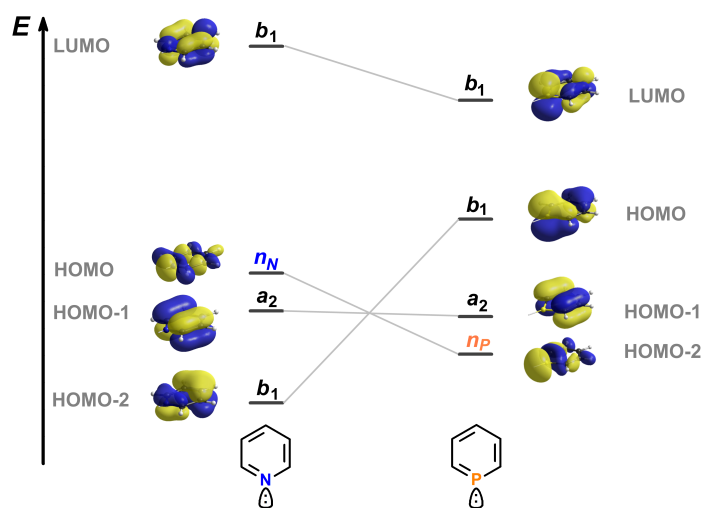


Figure 1.2 Qualitative MO-diagram of the frontier orbitals of phosphinine and pyridine.

The large coefficient at the phosphorus atom is the LUMO (lowest unoccupied molecular orbital) and its geometry enables π -accepting features of the heterocycle, which are less pronounced in the case of pyridine, where the LUMO is higher in energy. Consequently, phosphinines are much better π -accepting ligands, but worse σ -donors compared to pyridines.

The lone pair of the phosphorus atom in phosphinines has a strong $3s$ -orbital character, which is about 64% vs. 29% found in the lone pair of the nitrogen atom in pyridines.²¹ The low basicity of the phosphorus center ($pK_a(\text{C}_6\text{H}_5\text{P}^+) = -16.1 \pm 1.0$ in aqueous solutions)²² is therefore explained by its poor hybridization ability.

In the $^{31}\text{P}\{^1\text{H}\}$ NMR spectrum, phosphinines show a typical down-field shift of about $\delta = +200$ ppm. The signals for the peripheral protons appear more down-field in the ^1H NMR spectrum compared to those of benzene. Nucleus independent chemical shift values (NICS) of phosphinines conclude that these phenomena can be attributed to the presence of a diamagnetic ring current typical for aromatic systems.²¹

As for most phosphorus ligands, Tolman's electronic parameter χ (chi) quantifies the electronic properties of phosphinines.²³ The values can be obtained by IR-spectroscopy from the CO-stretching frequencies of the corresponding $[\text{LNi}(\text{CO})_3]$ complexes, where L is the ligand of interest. The reference has been set for the strong σ -donor $(t\text{Bu})_3\text{P}$ with a χ value of zero, so a strong σ -donating ligand will have a small value while a strong π -acceptor will have a large χ value. Due to the high toxicity of nickel complexes, correlations to the *trans*- $[\text{L}_2\text{Rh}(\text{CO})\text{Cl}]$ complex have been made in order to compare the electronic properties between different phosphorus ligands in a safer manner.²⁴ The χ values for phosphinines place these compounds close to the electronic properties of phosphites, suggesting that they are also electron withdrawing (π -acceptors) as had been already anticipated from the corresponding MO diagram.

1.4 Steric properties

For phosphorus(III) compounds, such as phosphines and phosphites, Tolman's cone angle (θ) has been the preferred parameter to describe the steric situation of the molecule. Nevertheless, it does not seem to be appropriate for the description of phosphinines. In 2006, Müller *et al.* reported the first molecular structure in the crystal of a λ^3 -triarylphosphinine derivative.³ As has

been demonstrated later for several aryl-phosphinines, the heterocycle is an essentially planar distorted hexagon, due to the larger size of the phosphorus atom compared to a carbon atom. Consequently, a special descriptor for the steric situation of phosphinines has been introduced.

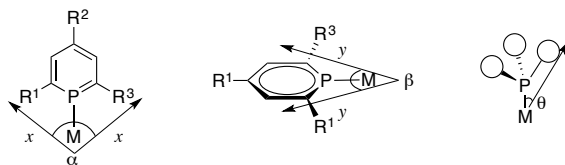


Figure 1.3 Steric properties of 2,4,5-triarylphosphinines in comparison to classical phosphorus ligands

The occupancy angles α and β depicted in figure 1.3 show that the main steric demand occurs in the x plane. In this sense, phosphinines are similar to their pyridine analogues. On the other hand, the internal C-P-C angle (between $98.38(12)^\circ$ and $101.37(11)^\circ$) is somewhat smaller than the C-N-C angle in pyridine (117°).^{5,25,26} The P-C bond length (between 1.76 and 1.74 Å) lies in between a P-C single bond (triphenylphosphine: 1.83 Å) and a P=C double bond (diphenylmethylenephosphaalkyne: 1.66 Å).^{27,28} Between the C-C bonds on the rest of the ring and the P-C bonds there is no bond length alternation, which indicates delocalization of the π -system and the presence of an aromatic system.

Another parameter to measure the bulkiness of a ligand has been introduced by Nolan and Cavallo and it is called “the percent buried volume” ($\% V_{\text{bur}}$).^{29,30} The percentage of occupied volume by a ligand in a sphere of a defined radius with the metal center at the core is calculated using crystallographic data. The group of Müller has calculated this value for 2,4,6-triphenylphosphinine **1.1**, which is $\% V_{\text{bur}} = 33.1\%$ at a P-M distance of 2.28 Å.

1.5 Coordination modes and transition metal complexes

Because of their particular electronic and steric properties, phosphinines are intriguing ligand candidates for transition metal complexes. Figure 1.4 shows the most common coordination modes of phosphinines.

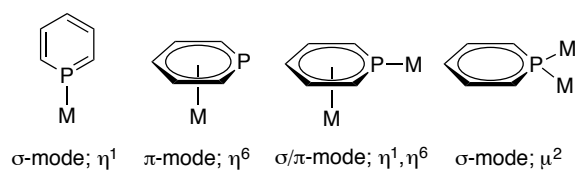


Figure 1.4 Selected coordination modes of phosphinines

The phosphorus lone pair (HOMO-2) and the aromatic π -system (HOMO and HOMO-1) can potentially lead to η^1 - and η^6 -coordination, respectively as well as to bridging ligands (μ^2 -coordination) or a combination of any of these.^{31–35} The most common η^1 -coordination mode is mainly achieved with metal centers in low oxidation states, due to the pronounced π -accepting properties of the ligand.^{7,36–41} An η^6 -coordination mode is generally imposed by steric effects, or when the metal has no particular affinity to phosphorus or is in a higher oxidation state.^{42–48} A mixed η^1 - η^6 binding mode, where the phosphinine acts as an 8-electron donor, has been found in few cases for metals such as manganese and chromium.^{49,50} Complexes where the phosphorus atom in the heterocycle bridges two metal centers have also been reported, most of them being hetero-donor functionalized phosphinine ligands.^{51–57}

Some of the complexes mentioned above have found interesting and promising applications in fields such as homogeneous catalysis,^{2,42,58–61} including water oxidation,⁶² photocatalysis⁶³ and material chemistry⁶⁴ among others. In the next chapters, some examples will be described in more detail.

Müller *et al.* reported on the C-H activation of 2,4,6-triphenylphosphinine **1.1** by late transition metal complexes. *Ortho*-metalation of **1.1** in complexes of the type $[\text{MCl}(\text{Cp}^*)(\text{P}^{\wedge}\text{C})]$ (**1.4** and **1.5**, figure 1.5) were isolated and structurally characterized.

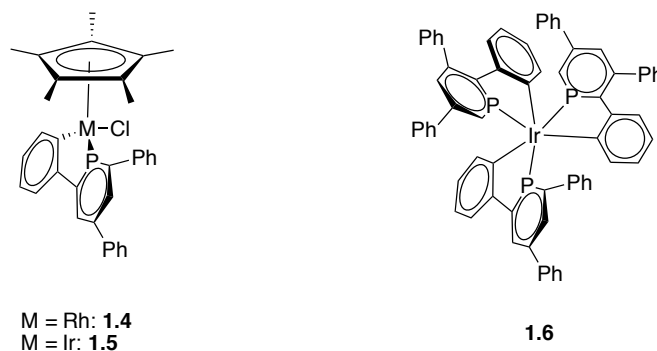


Figure 1.5 Cyclometalated complexes with **1.1**

Furthermore, the *fac*-isomer of the homoleptic complex *fac*-[Ir(P[∧]C)₃] (**1.6**, figure 1.5) was obtained quantitatively from the mixture of **1.1** and [Ir(acac)₃]. The access to these type of complexes opens a route to the development of new homogeneous (photo)catalysts and molecular materials.^{25,65,66}

The preparation of phosphinine complexes with metals in intermediate oxidation states is rather challenging. One strategy to enhance the σ-coordination mode *via* the phosphorus atom is the introduction of a hetero-donor functionality that yields a potential chelating ligand. The chelating stabilization can also prevent the fast ligand dissociation from the metal fragment.

Le Floch and Mathey prepared and characterized the first diphosphinine **1.7** and studied its coordination chemistry with several transition metals, leading, for example, to complex **1.8** (figure 1.6).^{53,61,67–72}

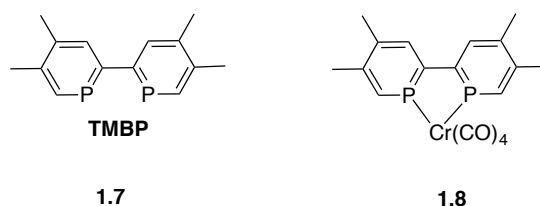


Figure 1.6 Bidentate phosphinine TMBP and its chromium complex

Le Floch reported on nickel(II)-promoted homocoupling reactions of (2-phosphininy)halogenozirconocene complexes for the synthesis of diphosphinines with different substitution patterns.⁷³ Müller reported on the synthesis of diphosphinine **1.9** that coordinates to rhodium in a *trans*-fashion yielding complex **1.10** (figure 1.7).⁷⁴

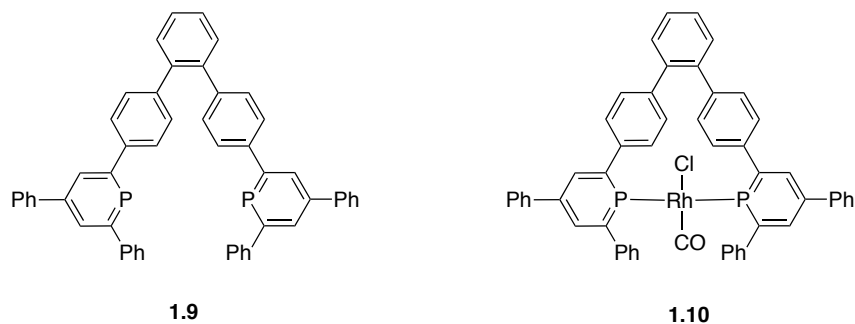


Figure 1.7 Diphosphinine **1.5** and its corresponding rhodium complex **1.6**

Many other examples of hetero-donor functionalized phosphinines have been reported, and some examples are presented in the following chapters. On the next pages the focus will be set on phosphorus ligands with a nitrogen-based functionality.

1.6 P,N- hybrid ligands

Hybrid ligands are molecules that contain at least two functionalities that can bind to metal centers. Through the years, bi- or polydentate ligands have been designed and developed for a plethora of applications. A very popular combination of heteroatoms for the synthesis of such ligands is phosphorus and nitrogen. Phosphorus is considered as a soft atom and nitrogen as a hard atom according to Pearson's HSAB concept. The formation and stabilization of new complexes can be achieved due to mainly three factors: 1) The good σ -donating properties of the nitrogen-containing functionality, 2) the good π -accepting properties of the phosphorus-containing functionality, and 3) the possibility of the formation of a chelate complex.

For example, 2-(diphenylphosphino)pyridine (**1.11**, figure 1.8) has been known for several decades. It has the ability to connect to identical metal centers or to different ones either acting as a monodentate ligand or as a chelating ligand (figure 1.8). Its small bite angle and its rigidity are thought to enhance the formation of M-M bonds and to bridge two metal centers. These features made possible the formation of very different types of metal complexes that have interesting applications.⁷⁵⁻⁸²

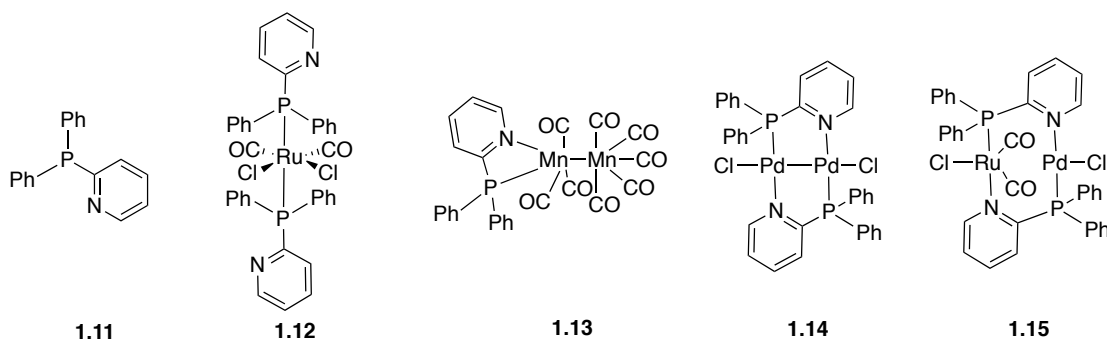


Figure 1.8 2-(Diphenylphosphino)pyridine and its different coordination modes in metal complexes

The electronic and steric properties of the pyridyl-substituted phosphine **1.11** and pyridyl-substituted-phosphinine **1.3** differ substantially. This opens the possibility to prepare and design novel transition metal complexes taking advantage of the different properties of this PN ligand.

Even though the parent phosphorus derivative of 2,2'-bipyridine (**1.16**, figure 1.9) has not yet been synthesized, DFT calculations of its frontier orbitals predict the electronic situation of such hybrid ligands.⁸³

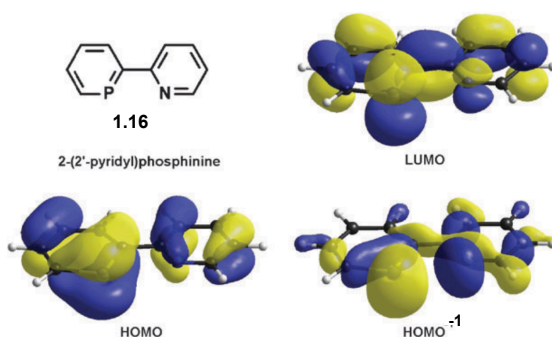
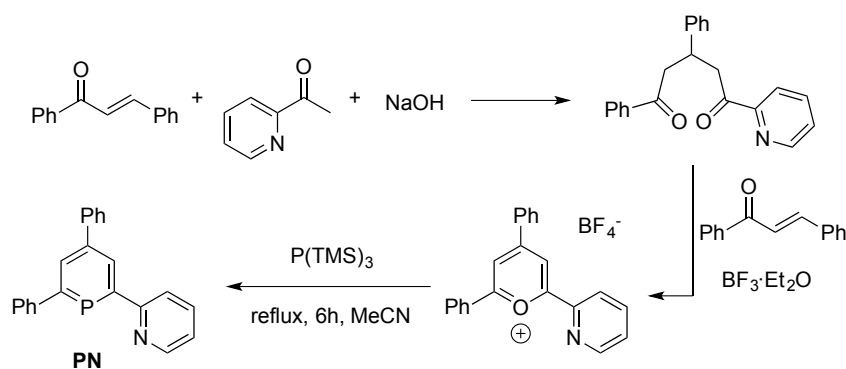


Figure 1.9 Selected frontier orbitals of 2-(2'-pyridyl)phosphinine assuming a planar geometry of the ligand.

The LUMO of **1.16** indicates that the phosphinine moiety acts as a strong π -acceptor according to the size and distribution of the coefficients of this orbital. The HOMO indicates π -donation from the phosphorus to a metal center while the lone pairs of both heteroatoms are represented at the HOMO-1, representing the σ -donor properties of this ligand.

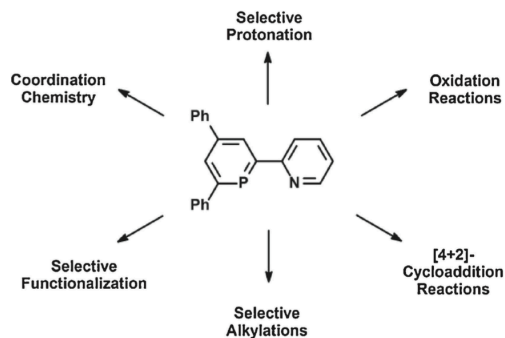
NIPHOS (**1.3**, figure 1.3) was the first example of a pyridyl-substituted phosphinine. Nevertheless, only a few studies on the coordination chemistry of NIPHOS have been reported. This is probably due to the high nucleophilicity of the phosphorus atom, the facile protonation at the nitrogen atom, and its multistep synthesis. Carbonyl complexes of group VI transition metals were obtained with NIPHOS ($[(\mathbf{1.3})M(\text{CO})_4]$, $M = \text{W, Mo, Cr}$) as well as with Rh(I), Ir(I) ($[(\text{cod})M(\mu\text{-}\mathbf{1.3})_2]$, $M = \text{Rh, Ir}$). Highly reactive complexes of Pt(II) and Pd(II) ($[\text{MCIL}(\mathbf{1.3H}\cdot\text{OH})][\text{MCl}_3(\text{L})]$, $M = \text{Pt, Pd}$) were identified by means of NMR spectroscopy but their isolation was not successful. These examples will be described in more detail in the following chapters.

Müller *et al.* reported on the synthesis of 2-(2'-pyridyl)-4,6-diphenylphosphinine (**PN**) via the pyrylium salt route using $P(TMS)_3$ as the phosphorus source. The modular synthesis starts by preparing the corresponding diketone from *trans*-chalcone, acetylpyridine and NaOH. After recrystallization, the product of this reaction is refluxed with *trans*-chalcone and an excess of trifluoroborane etherate. The pyrylium salt obtained is recrystallized and reacts further with $P(TMS)_3$ in acetonitrile to obtain an air- and water-stable pyridyl-substituted phosphinine, which is purified by means of column chromatography (scheme 1.8).



Scheme 1.8 Synthesis of pyridyl-substituted phosphinine **PN**

It turned out that the phenyl rings in 2- and 4-position of the heterocycle create a higher kinetic stability to the phosphinine, making it less prone to nucleophilic attack on the phosphorus atom in comparison to NIPHOS. This is probably one of the reasons why there are now more reports on the chemistry of this **PN** ligand.



Scheme 1.9 Selected reactions with **PN**

1.7 Aim of this thesis

The motivation of this work comes from the very interesting results that have been obtained from several studies on this particular phosphinine, some of which are depicted in scheme 1.9. The aim of this thesis is to continue exploring the fascinating chemistry that 2-(2'-pyridyl)-4,6-diphenylphosphinine has to offer. It is also important to examine the different coordination modes that this pyridyl-substituted compound can adopt besides the usual P,N-chelating mode.

On the other hand, the reactivity of the **PN** phosphinine is of interest due to the possibility of obtaining phosphorus compounds derived from the latter, which have different electronic and steric properties. The first example is the alkylation reaction with lithium reagents to form pyridyl-functionalized λ^4 -phosphinines. The second example is the [4+2] cycloaddition reaction of hexafluorobutyne and the **PN** phosphinine. This reaction leads to a phosphabarrelene compound. λ^4 -phosphinines and the obtained phosphabarrelene are also explored as ligands for transition metal complexes.

The previous literature reports on this phosphinine and in some cases on NIPHOS are discussed in the introduction of the corresponding chapters of this thesis, which have been divided as follows. Chapter two presents the results obtained in this work on the coordination chemistry of the **PN** phosphinine with several transition metal complexes, such as Cu, Ag, Au, Fe and W. In chapter three, selective alkylations and arylations are discussed. These results were obtained by reacting the **PN** phosphinine with lithium reagents such as MeLi, PhLi and FcLi. The coordination chemistry of the corresponding phosphorus compounds obtained is also presented in this chapter. Chapter four focuses on [4+2] cycloaddition reactions. The results of the first pyridyl-substituted phosphabarrelene are described, as well as its photochemical reactivity and its coordination chemistry. Oxidation reactions and selective protonation of the **PN** phosphinine are also reviewed in the introduction of this chapter.

Throughout this work, some of the synthesized complexes are investigated for future applications, such as homogeneous catalysis, models for enzymes that contain metal centers, and for the synthesis of novel phosphorus compounds.

1.8 References

- (1) Märkl, G. *Angew. Chem.* **1966**, 78 (18-19), 907.
- (2) Müller, C.; López, L. G.; Kooijman, H.; Spek, A. L.; Vogt, D. *Tetrahedron Lett.* **2006**, 47 (12), 2017.
- (3) Müller, C.; Lutz, M.; Spek, A. L.; Vogt, D. *J. Chem. Crystallogr.* **2006**, 36 (12), 869.
- (4) Müller, C.; Pidko, E. A.; Totev, D.; Lutz, M.; Spek, A. L.; van Santen, R. A.; Vogt, D. *Dalton Trans.* **2007**, 46, 5372.
- (5) Müller, C.; Wasserberg, D.; Weemers, J. J. M.; Pidko, E. A.; Hoffmann, S.; Lutz, M.; Spek, A. L.; Meskers, S. C. J.; Janssen, R. A. J.; van Santen, R. A.; Vogt, D. *Chem. Eur. J.* **2007**, 13 (16), 4548.
- (6) Müller, C.; Pidko, E. A.; Staring, A. J. P. M.; Lutz, M.; Spek, A. L.; van Santen, R. A.; Vogt, D. *Chem. Eur. J.* **2008**, 14 (16), 4899.
- (7) Breit, B.; Winde, R.; Mackewitz, T.; Paciello, R.; Harms, K. *Chem. Eur. J.* **2001**, 7 (14), 3106.
- (8) Ashe III, A. J. *J. Am. Chem. Soc.* **1971**, 93 (13), 3293.
- (9) Rösch, W.; Regitz, M. *Z. Naturforsch. B* **1986**, 41b, 931.
- (10) Regitz, M.; Binger, P. *Angew. Chem.* **1988**, 100 (11), 1541.
- (11) Habicht, M. H.; Wossidlo, F.; Weber, M.; Müller, C. *Chem. Eur. J.* **2016**.
doi:10.1002/chem.201602012
- (12) Avarvari, N.; Le Floch, P.; Mathey, F. *J. Am. Chem. Soc.* **1996**, 118 (47), 11978.
- (13) Nakajima, K.; Takata, S.; Sakata, K.; Nishibayashi, Y. *Angew. Chem. Int. Ed.* **2015**, 54 (26), 7597.
- (14) Alcaraz, J.-M.; Breque, A.; Mathey, F. *Tetrahedron Lett.* **1982**, 23 (15), 1565.
- (15) Modelli, A.; Hajgató, B.; Nixon, J. F.; Nyulászi, L. *J. Phys. Chem. A* **2004**, 108 (36), 7440.
- (16) Nyulászi, L.; Veszprémi, T. *J. Phys. Chem.* **1996**, 100 (16), 6456.
- (17) Nyulászi, L. *Chem. Rev.* **2001**, 101 (5), 1229.
- (18) Burrow, P. D.; Ashe, A. J.; Bellville, D. J.; Jordan, K. D. *J. Am. Chem. Soc.* **1982**, 104 (2), 425.
- (19) Nyulaszi, L.; Veszpremi, T.; Reffy, J.; Burkhardt, B.; Regitz, M. *J. Am. Chem. Soc.* **1992**, 114 (23), 9080.
- (20) Baldrige, K. K.; Gordon, M. S. *J. Am. Chem. Soc.* **1988**, 110 (13), 4204.
- (21) Frison, G.; Sevin, A.; Avarvari, N.; Mathey, F.; Le Floch, P. *J. Org. Chem.* **1999**, 64 (15), 5524.
- (22) Pham-Tran, N.-N.; Bouchoux, G.; Delaere, D.; Nguyen, M. T. *J. Phys. Chem. A* **2005**, 109 (12), 2957.

- (23) Tolman, C. A. *Chem. Rev.* **1977**, 77 (3), 313.
- (24) Kühn, O. *Coord. Chem. Rev.* **2005**, 249 (5-6), 693.
- (25) Broeckx, L. E. E.; Güven, S.; Heutz, F. J. L.; Lutz, M.; Vogt, D.; Müller, C. *Chem. Eur. J.* **2013**, 19 (39), 13087.
- (26) Ashe III, A. J.; Six-membered Rings with One Arsenic, Antimony, or Bismuth Atom. In *Comprehensive Hetrocyclic Chemistry II*; Katritzky, A. R., Rees, C. W., Scriven, E. F. V., Eds.; New York, 1996; p 669.
- (27) Daly, J. J. *J. Chem. Soc.* **1964**, 3799.
- (28) Bart, J. C. J. *Angew. Chem., Int. Ed.* **1968**, 7 (9), 730.
- (29) Clavier, H.; Nolan, S. P. *Chem. Commun.* **2010**, 46 (6), 841.
- (30) Poater, A.; Cosenza, B.; Correa, A.; Giudice, S.; Ragone, F.; Scarano, V.; Cavallo, L. *Eur. J. Inorg. Chem.* **2009**, 2009 (13), 1759.
- (31) Le Floch, P.; Mathey, F. *Coord. Chem. Rev.* **1998**, 178-180, 771.
- (32) Mézailles, N.; Mathey, F.; Le Floch, P. *Prog. Inorg. Chem.* **2001**, 49, 455.
- (33) Le Floch, P. *Coord. Chem. Rev.* **2006**, 250 (5-6), 627.
- (34) Müller, C.; Vogt, D. *Dalton Trans.* **2007**, 9226 (47), 5546.
- (35) Kollár, L.; Keglevich, G. *Chem. Rev.* **2010**, 110 (7), 4257.
- (36) Elschenbroich, C.; Nowotny, M.; Behrendt, A.; Harms, K.; Wocadlo, S.; Pebler, J. *J. Am. Chem. Soc.* **1994**, 116 (14), 6217.
- (37) Mao, Y.; Mathey, F. *Org. Lett.* **2012**, 14 (4), 1162.
- (38) Wallis, C.; McGuinness, D.; Newman, P. D.; Tooze, R. P.; Edwards, P. G. *Dalton Trans.* **2009**, 12, 2178.
- (39) Dash, K. C.; Eberlein, J.; Schmidbaur, H. *Synth. React. Inorg. M.* **1973**, 3 (4), 375.
- (40) Elschenbroich, C.; Nowotny, M.; Behrendt, A.; Massa, W.; Wocadlo, S. *Angew. Chem.* **1992**, 104 (10), 1388.
- (41) Elschenbroich, C.; Six, J.; Harms, K. *Chem. Commun.* **2006**, 32, 3429.
- (42) Knoch, F.; Kremer, F.; Schmidt, U.; Zenneck, U.; Le Floch, P.; Mathey, F. *Organometallics* **1996**, 15, 2713.
- (43) Le Floch, P.; Knoch, F.; Kremer, F.; Mathey, F.; Scholz, J.; Scholz, W.; Thiele, K.-H.; Zenneck, U. *Eur. J. Inorg. Chem.* **1998**, 1998 (1), 119.
- (44) Deberitz, J.; Nöth, H. *Chem. Ber.* **1970**, 103 (8), 2541.
- (45) Deberitz, J.; Nöth, H. *Chem. Ber.* **1973**, 106 (7), 2222.
- (46) Vahrenkamp, H.; Nöth, H. *Chem. Ber.* **1972**, 105 (4), 1148.
- (47) Doux, M.; Ricard, L.; Mathey, F.; Floch, P. Le; Mézailles, N. *Eur. J. Inorg. Chem.* **2003**, 2003 (4), 687.
- (48) Mézailles, N.; Ricard, L.; Mathey, F.; Le Floch, P. *Organometallics* **2001**, 20 (15), 3304.

- (49) Nainan, K. C.; Sears, C. T. *J. Organomet. Chem.* **1978**, *148* (3), C31.
- (50) Nief, F.; Charrier, C.; Mathey, F.; Simalty, M. *J. Organomet. Chem.* **1980**, *187* (2), 277.
- (51) Chen, X.; Li, Z.; Yanan, F.; Grützmacher, H. *Eur. J. Inorg. Chem.* **2016**, *5*, 633.
- (52) Mao, Y.; Lim, K. M. H.; Li, Y.; Ganguly, R.; Mathey, F. *Organometallics* **2013**, *32* (12), 3562.
- (53) Bakker, M. J.; Vergeer, F. W.; Hartl, F.; Goubitz, K.; Fraanje, J.; Rosa, P.; Le Floch, P. *Eur. J. Inorg. Chem.* **2000**, *2000* (5), 843.
- (54) Bakker, M. J.; Vergeer, F. W.; Hartl, F.; Rosa, P.; Ricard, L.; Le Floch, P.; Calhorda, M. *J. Chem. Eur. J.* **2002**, *8* (7), 1741.
- (55) Reetz, M. T.; Bohres, E.; Goddard, R.; Holthausen, M. C.; Thiel, W. *Chem. Eur. J.* **1999**, *5* (7), 2101.
- (56) Schmid, B.; Venanzi, L. M.; Gerfin, T.; Gramlich, V.; Mathey, F. *Inorg. Chem.* **1992**, *31* (1), 5117.
- (57) Arce, A. J.; Deeming, A. J.; Sanctis, Y. De; Manzur, J. *J. Chem. Soc., Chem. Commun.* **1993**, *3*, 325.
- (58) Müller, C.; Vogt, D. Phosphinine-Based Ligands in Homogeneous Catalysis: State of the Art and Future Perspectives. In *Phosphorus Compounds*; Peruzzini, M., Gonsalvi, L., Eds.; Springer, Netherlands, 2011; p 151.
- (59) Breit, B. *Chem. Commun.* **1996**, 2071.
- (60) Reetz, M. T.; Guo, H. *Synlett* **2006**, *13*, 2127.
- (61) Miyake, Y.; Isomura, E.; Iyoda, M. *Chem. Lett.* **2006**, *35* (8), 836.
- (62) Broeckx, L. E. E.; Bucci, A.; Zuccaccia, C.; Lutz, M.; Macchioni, A.; Müller, C. *Organometallics* **2015**, *34* (12), 2943.
- (63) Loibl, A.; Müller, C. *Unpublished results*.
- (64) Roesch, P.; Nitsch, J.; Lutz, M.; Wiecko, J.; Steffen, A.; Müller, C. *Inorg. Chem.* **2014**, *53* (18), 9855.
- (65) Broeckx, L. E. E.; Delaunay, W.; Latouche, C.; Lutz, M.; Boucekkine, A.; Hissler, M.; Müller, C. *Inorg. Chem.* **2013**, *52* (19), 10738.
- (66) Broeckx, L. E. E.; Lutz, M.; Vogt, D.; Müller, C. *Chem. Commun.* **2011**, *47* (7), 2003.
- (67) Rosa, P.; Ricard, L.; Le Floch, P.; Mathey, F.; Sini, G.; Eisenstein, O. *Inorg. Chem.* **1998**, *37* (13), 3154.
- (68) Le Floch, P.; Carmichael, D.; Ricard, L.; Mathey, F. *J. Am. Chem. Soc.* **1991**, *113* (2), 667.
- (69) Le Floch, P.; Carmichael, D.; Ricard, L.; Mathey, F.; Jutand, A.; Amatore, C. *Organometallics* **1992**, *11* (7), 2475..
- (70) Le Floch, P.; Ricard, L.; Mathey, F.; Jutand, A.; Amatore, C. *Inorg. Chem.* **1995**, *34*, 11.
- (71) Mathey, F.; Le Floch, P. *Chem. Ber.* **1996**, *129* (3), 263.
- (72) Le Floch, P.; Ricard, L.; Mathey, F. *Bull. Soc. Chim. Fr.* **1996**, *133*, 691.

- (73) Rosa, P.; Mézailles, N.; Mathey, F.; Le Floch, P. *J. Org. Chem.* **1998**, *63* (14), 4826.
- (74) Müller, C.; Freixa, Z.; Lutz, M.; Spek, A. L.; Vogt, D.; van Leeuwen, P. W. N. M. *Organometallics* **2008**, *27* (5), 834.
- (75) Kartashova, K.; Mallet-Ladeira, S.; Axet, M. R. *J. Organomet. Chem.* **2015**, *799*, 226.
- (76) Chen, K.; Shearer, J.; Catalano, V. J. *Inorg. Chem.* **2015**, *54* (13), 6245.
- (77) Lin, Y.-M.; Guan, Z.-J.; Liu, K.-G.; Jiang, Z.-G.; Wang, Q.-M. *Dalton Trans.* **2015**, *44* (5), 2439.
- (78) Tang, C.-M.; Li, X.-L.; Wang, G.-Y. *Korean J. Chem. Eng.* **2012**, *29* (12), 1700.
- (79) Jamali, S.; Mazloomi, Z.; Nabavizadeh, S. M.; Milić, D.; Kia, R.; Rashidi, M. *Inorg. Chem.* **2010**, *49* (6), 2721.
- (80) Coetzee, M.; Purcell, W.; Visser, H. G.; Venter, J. A. *Acta Cryst.* **2007**, *E63*, m3165.
- (81) Párkányi, L.; Szalontai, G.; Besenyei, G. *Inorg. Chim. Acta* **2006**, *359* (9), 2933.
- (82) Kuang, S.-M.; Zhang, Z.-Z.; Xue, F.; Mak, T. C. *Polyhedron* **1999**, *18* (26), 3465.
- (83) Campos-Carrascos, A.; Pidko, E. A.; Masdeu-Bultó, A. M.; Lutz, M.; Spek, A. L.; Vogt, D.; Müller, C. *New J. Chem.* **2010**, *34*, 1547

Chapter 2

Coordination Chemistry of 2-(2'-Pyridyl)- 4,6-diphenylphosphinine

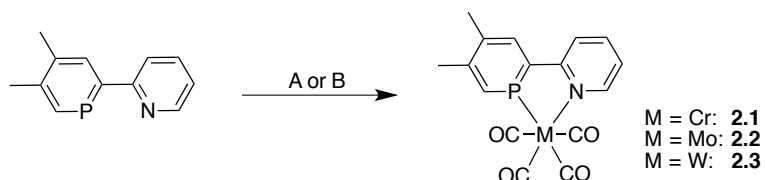
2	Coordination Chemistry of 2-(2'-Pyridyl)-4,6-diphenylphosphinine.....	21
2.1	Introduction	21
2.2	Results and discussion	28
	Group XI metal complexes	29
	Group X metal complexes	40
	Group IX metal complexes	42
	Group VIII metal complexes	45
	Group VI metal complexes	60
2.3	Conclusions	62
2.4	Experimental	63
	General remarks	63
	[(PN)Cu(MeCN)] ₂ [PF ₆] ₂ (5)	63
	[(PN) ₂ Cu][PF ₆] (6)	64
	[Ag(PN)][OTs] (7)	64
	[Ag(PN) ₂][OTs] (8)	65
	[Ag(PN) ₃][OTs] (9)	65
	[Ag(PN) ₃][OTf] (10)	66
	[Au(PN)Cl] (11)	66
	[Au(I)-Au(III)(μ-PN)Cl ₄] (12)	67
	[Ni(PN)CO] ₂ (15)	67
	[Rh(PN)Cl(CO)] ₂ (16)	67
	[Fe(PN)(CO) ₃] (17)	68
	[Fe(PN)(η ² -methylacrylate)(CO) ₂] (18)	68
	[Fe(PN)(η ² -(1,3-butadiene))(CO) ₂] (19)	68
	[μ-(pdt)Fe ₂ (PN)(CO) ₄] (20)	69
	[μ-(pdt)Fe ₂ (PN) ₂ (CO) ₂] (21)	69
	[W(PN) ₂ (CO) ₂] (22)	70
	X-ray crystal structure determinations	70
2.5	References	73

2 Coordination Chemistry of 2-(2'-Pyridyl)-4,6-diphenylphosphinine

2.1 Introduction

As described in the previous section, phosphinines are versatile ligands not only because of their special electronic properties but also due to several different coordination modes they can adopt in metal complexes. When a pyridyl-functionality is introduced to the phosphinine framework, one more possibility adds to the list of coordination modes. Depending on the position of this second donor functionality, the formation of a chelating complex or the coordination to a second metal center can be enabled. In this section, a review of the reported complexes in literature with 2-(2'-pyridyl)-substituted phosphinines will be presented.

The first reported pyridyl-substituted phosphinine was NIPHOS (**1.3**, scheme 1.6). Mathey *et al.* prepared chromium, molybdenum and tungsten carbonyl complexes of this ligand (**2.1-2.3**, scheme 2.1). During the reaction, it was observed that the phosphorus atom binds first to the metal center, and chelation through the nitrogen atom occurs afterwards in a second step. Chromium complex **2.2** was crystallographically characterized. It was assumed that there is no electronic communication between the phosphinine ring and the pyridyl group; The length of the internal C-C bond does not change upon complexation compared to bipyridine chromium carbonyl complexes. Thus, it seems that both heterocycles act as isolated ligands.¹



Scheme 2.1 Synthesis of group VI metal complexes with NIPHOS. A: $M(CO)_5(THF)$, r.t., $M = Mo, W$. B: $Mo(CO)_6$, $T = 155\text{ }^\circ\text{C}$, sealed tube

In order to continue exploring the donor properties of NIPHOS, Pt(II) and Pd(II) complexes were prepared. Attempts in obtaining complex $[PtCl_2(NIPHOS)]$ (**2.4**, figure 2.1) from precursors such as $[PtCl_2(MeCN)_2]$, $[PtCl_2(cod)]$ or *cis*- $[PtCl_2(styrene)_2]$ were not successful. When using platinum dimers such as $[Pt_2Cl_4L_2]$, where L is a phosphine, such as PPh_3 , $PMePh_2$, PMe_2Ph , PMe_3 , *Pn*- Bu_3 , the corresponding complexes $[ClPt(L)(NIPHOS)][PtCl_3L]$ were formed (**2.5-2.9**). All these coordination compounds were too unstable to be isolated; they were only

characterized in solution by means of NMR spectroscopy. $[\text{PdCl}(\text{NIPHOS})(\text{PMe}_3)][\text{PdCl}_3(\text{PMe}_3)]$ (**2.10**) was also synthesized but showed even faster decomposition than its platinum analogue **2.8**. These complexes showed high reactivity towards water and alcohols yielding complexes **2.11-2.17** (figure 2.1). Coordination of NIPHOS to a metal center should increase the positive charge on the P atom, thus leading to nucleophilic attack to the P-C double bond. The addition of the -OH or -OR group of the nucleophile to the phosphorus atom resulted in the formation of a racemic mixture of complexes. This was proven by adding enantiomerically pure isoamyl alcohol to complex **2.5**, which resolves the $^{31}\text{P}\{^1\text{H}\}$ NMR spectrum into two sets of signals for each diastomeric complex. The -OH proton from complex **2.11** was successfully removed after adding 1 equivalent of diisopropylethylamine and could be protonated again after $\text{CF}_3\text{SO}_3\text{H}$ was added to the solution.²

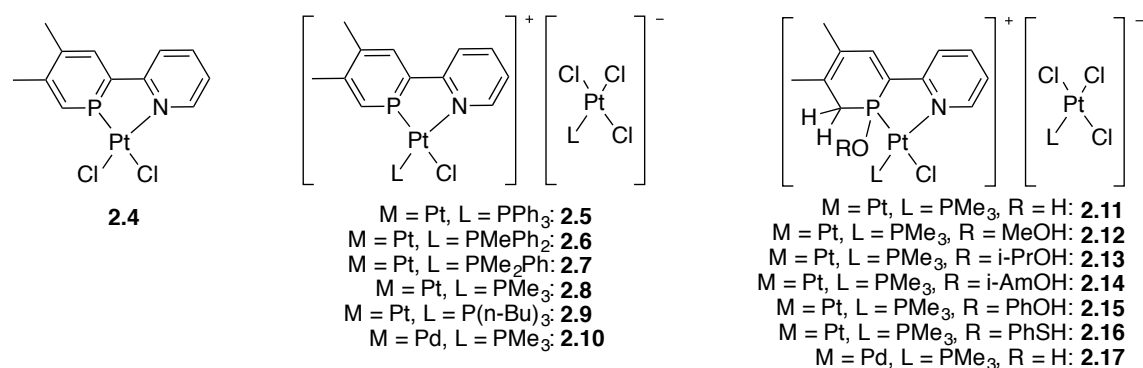
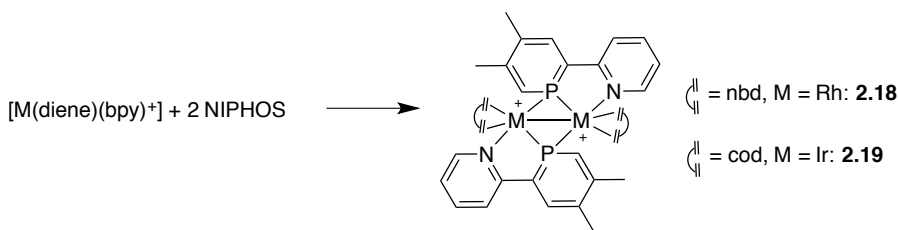


Figure 2.1 Pt and Pd complexes with NIPHOS and their water or alcohol addition products

The coordination chemistry of NIPHOS towards Rh(I) and Ir(I) was also investigated. In the corresponding binuclear cationic complexes (**2.18** and **2.19**, scheme 2.2), the ligand showed a different coordination mode, as the phosphorus atom is acting as a bridging ligand (μ^2 -mode). The formation of the dimer was attributed to the fact that the lone pair of the P atom has a higher *s*-character and is more diffuse and less directional than the corresponding lone pair in pyridine.³



Scheme 2.2 Synthesis of cationic rhodium and iridium dimers with NIPHOS

Interestingly, the 2-(2'-pyridyl)-4,6-diphenylphosphinine ligand (**PN**) behaves quite differently with group VI metal carbonyl complexes than NIPHOS does with the Rh, Ir, Pt and Pd precursors mentioned above. Müller *et. al* reported on air- and moisture-stable **PN**-tetracarbonyl complexes **2.20**, **2.21** and **2.22**, and their 2-(2'-pyridyl)-4,6-diphenylpyridine (**NN**) analogues **2.23-2.25** (figure 2.2), which were obtained by thermal or photochemical treatment of hexacarbonyl complexes of Cr, Mo, or W with the corresponding bidentate ligand. The **PN** ligand turned out to be a much better π -acceptor than its **NN** analogue as proved by structural characterization as well as by the higher IR stretching frequencies of the corresponding carbonyl complexes. Additionally, a less negative reduction processes in CV and the presence of negative solvatochromism was observed.⁴

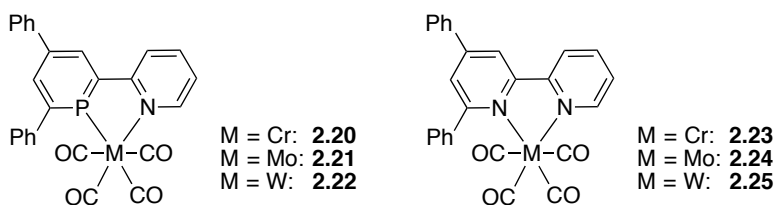


Figure 2.2 Group VI carbonyl metal complexes of **PN** and **NN** ligands

The first crystallographically characterized Pt(II) and Pd(II) complexes of a λ^3 -phosphinine ligand were synthesized by Müller *et al.* using **PN** as a ligand (**2.26** and **2.27**, figure 2.3). Contrary to NIPHOS, the **PN** phosphinine bears a phenyl ring on the 6-position of the heterocyclic ring, which brings kinetic stabilization of the otherwise reactive P-C double bond when coordinated to metal centers. The P-C double bond in the heterocycle is sterically more shielded against addition reactions and thus the complexes do not present decomposition during manipulation, contrary to the case observed for Pt(II) and Pd(II) complexes of NIPHOS. In combination with the chelate effect, this allows the preparation and isolation of complexes with metal centers even in higher oxidation states (*vide infra*). These complexes have the largest C-P-C angles reported so far for phosphinine-metal complexes. This accounts for the disruption of the aromaticity of the phosphinine ring and a higher P-C double bond reactivity towards nucleophiles.

The water-stable $[\text{Cr}(\text{tmbp})(\text{CO})_4]$ (**1.4**, figure 1.4) has a C-P-C angle of 104.3° ; $[\text{Rh}(\text{PN})(\text{cod})]\text{BF}_4$ (**2.30**, figure 2.4) has a value of 105.25° and has not been reported to be extremely sensitive to water or alcohols. In the Ru(II) complex *cis*- $[\text{Ru}(\text{tmbp})(\text{dmsO})_2\text{Cl}_2]$ the C-P-C angle is 106.08° , making the complex already much less stable towards nucleophilic attack. Methanol addition to complexes **2.26** and **2.27** (figure 2.3), however, was achieved at $T = 65^\circ\text{C}$

for overnight. The product shows *syn* addition of CH₃OH to one of the P–C double bonds, unambiguously demonstrated by single crystal X-ray diffraction of the products [MCl₂(PNH·OCH₃)] (**2.28** and **2.29**, figure 2.3). The regioselectivity of the product is explained if a concerted mechanism is assumed and not a 2-step process as proposed by Venanzi *et al.*, which would lead to the *anti* product, and probably disfavored by steric reasons. Surprisingly, when [PdCl₂(PNH·OCH₃)] (**2.29**) is mixed with a slight excess of the diphosphine DPEphos, regeneration of the **PN** ligand is observed after methanol elimination.⁵

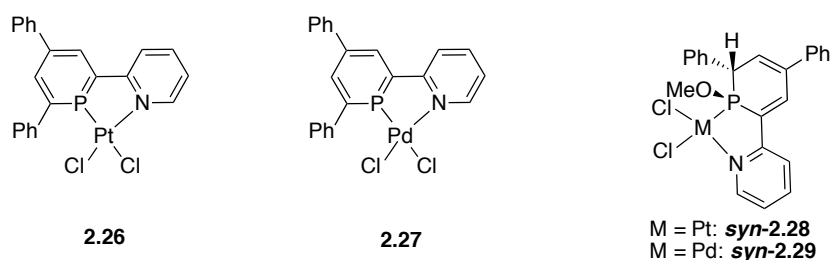


Figure 2.3 Pt and Pd complexes of **PN** and their methanol addition products

Contrary to NIPHOS, the **PN** ligand forms the mononuclear square planar [(cod)Rh(**PN**)]BF₄ complex (**2.30**, figure 2.4), which was compared to its bipyridine analogue [(cod)Rh(**NN**)] (**2.31**). From the distribution and atomic orbital coefficients, DFT calculations of the **PN** ligand demonstrate, that the LUMO enables the phosphinine moiety to act as a strong π -acceptor upon coordination, while the pyridine moiety has a larger coefficient on the carbocyclic part, just as expected for the weak π -accepting bipyridine. The HOMO contributes to π -donation from the ligand and the HOMO-3 represent the lone pairs of P and N, the former being less directional and more diffuse than the latter, which shows a pronounced σ -donating ability.⁶

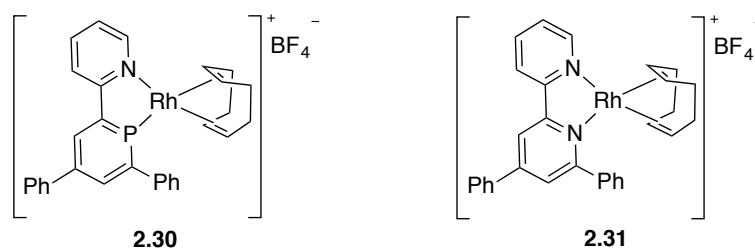


Figure 2.4 Rhodium complexes of **PN** and **NN** ligands

Inspired by the success of the chelating **PN** ligand to stabilize metal centers also in higher oxidation states, coordination of **PN** to Rh(III) and Ir(III) was also investigated. Monomeric complexes **2.32** and **2.33** (figure 2.5) were characterized by means of X-ray diffraction. They

show C-P-C angles of 106.6° and 106.7°, respectively and thus are expected to react with nucleophiles. Indeed, the reaction with water leads quantitatively and regio- and diastereoselectively to an *anti*-addition of H₂O to the external P=C double bond, as confirmed unambiguously by X-ray crystal structure determination (**2.34** and **2.35**, figure 2.5). Additionally, hydrogen bonding between the –OH hydrogen atom and the Cl[–] counteranion was observed.⁷

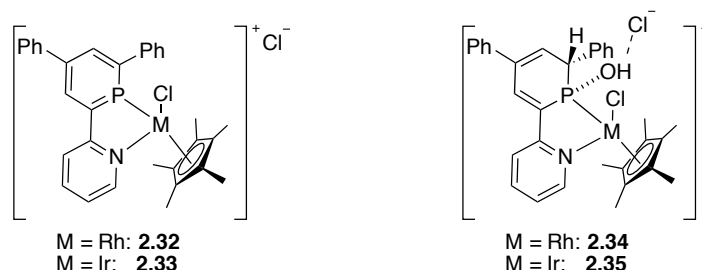


Figure 2.5 Rhodium and iridium complexes of **PN** and their water addition products

Complex [(PNH·OH)Cp*IrCl]Cl (**2.35**) was treated with NEt₃ to form the new zwitterionic coordination compound [(PNH·O)Cp*IrCl] (**2.36**, figure 2.6) after HCl elimination (pK_a of the complex is similar to the one of the pyridinium ion, which is 5.25). In the case of [(PNH·OH)Cp*RhCl]Cl (**2.34**), the addition of NEt₃ does not only lead to the zwitterionic species; in the solid state, [(PN·OH)Cp*RhCl] (**2.37**) is obtained as a tautomeric form of the zwitterionic compound. In order to conclude if the driving force of the proton abstraction by means of HCl elimination was permitted because of the hydrogen bond between the H from the –OH group and the Cl counterion, [PNCp*IrCl]Cl (**2.33**) was reacted with methanol to obtain [(PNH·OCH₃)Cp*IrCl] (**2.38**, figure 2.6). **2.38** further reacted with NEt₃ yielding [(PN·OCH₃)Cp*IrCl] (**2.39**), regardless of the absence of an –OH group. The reactivity of these complexes shows an elegant route to complexes containing λ⁴σ⁴-phosphorus heterocycles.⁸

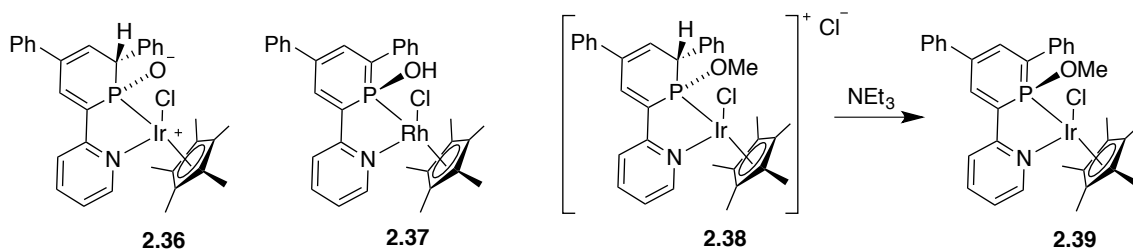


Figure 2.6 Deprotonation products of [(PNH·OH)Cp*IrCl]Cl and [(PNH·OH)Cp*RhCl]Cl with NEt₃ and reaction product of [PNCp*IrCl]Cl with methanol and consecutive reaction with NEt₃

The reduced π -retrodonation ability of metals in higher oxidation states such as Rh(III) and Ir(III) could be also correlated to the reactivity of these complexes towards nucleophiles. Müller *et al.* have described the coordination chemistry of the **PN** ligand with Ru(II), which in general is more electron-rich metal center than the ones mentioned previously. Complex **2.40** (figure, 2.7) was crystallographically characterized and shows a C-P-C angle of 103.7° , the lowest value reported so far for the **PN** ligand. Indeed, the complex is stable towards water and methanol even when refluxed in THF. $[\text{RuCp}^*\text{Cl}(\text{tmbp})]$, a stable diphosphinine complex similar to **2.40**, shows a slightly larger C-P-C angle of 104.7° .⁹ This means that the pyridyl ring contributes to the formation and stabilization of phosphinine-based complex **2.40**. Cationic complexes could be obtained by abstraction of a Cl^- from the coordination sphere with $\text{AgOSO}_2\text{CF}_3$ or by coordinating the **PN** phosphinine to the cationic precursor $[\text{Ru}(\text{MeCN})_3\text{Cp}^*]\text{PF}_6$. Surprisingly, these cationic complexes also do not react with water.

$[\text{RuCl}_2(\text{dmsO})(\text{PN})]$ (**2.41**) and *cis*- Δ - $[\text{RuCl}_2(\text{PN})_2]$ (**2.42**) were also synthesized and structurally characterized. From the reaction mixture of *cis*- $[\text{RuCl}_2(\text{dmsO})_2]$ and 2 equivalents of the **PN** phosphinine, two products are obtained: *cis*- Δ - $[\text{RuCl}_2(\text{PN})]$ (**2.42**) and *trans*- Δ - $[\text{RuCl}_2(\text{PN})]$. They can serve as starting materials for the synthesis of phosphinine-based Ru(II) analogues of the well-known bipyridine-based Ru(II) complexes, such as $[\text{Ru}(\text{bpy})_3]^{2+}$ and *cis*- $[\text{Ru}(\text{NCS})_2\text{L}_2]$ (L = 2,2'-bipyridyl-4,4'-dicarboxylic acid), which are used for solar energy conversion.¹⁰⁻¹⁶ $[\text{RuCl}_2(\text{dmsO})(\text{PN})]$ (**2.42**) reacts with water at the external P=C bond, leading exclusively to the *anti*-addition product. With methanol, the reaction appears reversible and can be directed by changing the temperature. The coordination of three **PN** ligands to a Ru(II) center proved to be impossible. Nevertheless, $[\text{Ru}(\text{bpy})_2\text{PN}]\text{X}_2$ complexes (**2.43-2.46**, figure 2.7) were prepared and compared to the well-known triple emitter $[\text{Ru}(\text{bpy})_3]^{2+}$. The HOMO of complex **2.43** is fully conjugated from the metal center to one of the exocyclic phenyl rings, which makes it a good candidate for electron transfer processes in future studies.

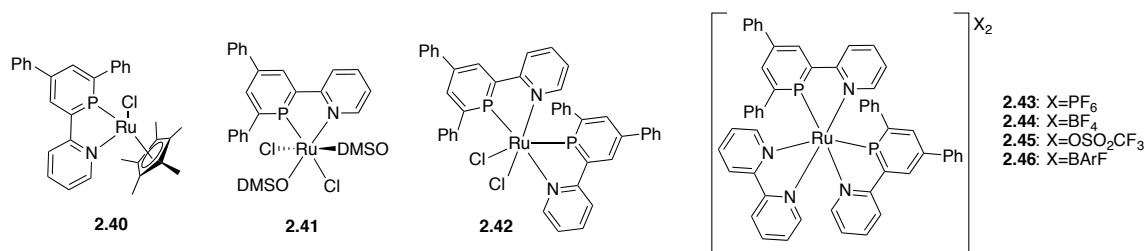


Figure 2.7 Ruthenium complexes of **PN** ligand

The reaction of these complexes towards water depends on the counter ion; BARF^- (**2.46**) gives a more stable complex, whereas BF_4^- (**2.44**) and CF_3SO_3^- (**2.45**) lead to complexes that show reversible water-addition reactions, the addition product being the preferred one at room temperature.¹⁷

From the molecular orbitals of the unsubstituted phosphinine (**1.16**, figure 1.9), the weak σ -donor (energetically low-lying HOMO-2), but rather strong π -acceptor (energetically low-lying LUMO) properties of the ligand have been acknowledged and discussed in literature.¹⁸ HOMO and HOMO-1 are believed to participate in the formation of η^6 -metal complexes, but the potentially π -donor properties had neither been considered, nor discussed in literature until recently. Müller *et al.* performed a systematic investigation on the influence of substituents on the electronic properties of the PN ligand by means of the IR frequencies of the CO stretching bands of the corresponding tungsten carbonyl complexes (**2.47-2.50**, figure 2.8). For the complex with the F-substituted ligand (**2.48**), only a slight $-I$ effect was noticed, which can be attributed to the $+M$ effect that this substituent has. This balances the overall electronic effect. For complex **2.49** with the CF_3 -substituted ligand, an almost pure $-I$ effect can be noticed, but for complex **2.50** with the donating CH_3S substituted ligand, an inverse effect was observed: the CO stretching bands shift to even higher wave numbers even though a shift to lower wave numbers was expected under the assumption that a stronger donor would enhance π -back-donation from the metal to the C-O anti-bonding orbital. DFT calculations were carried out, which showed that donor substituents at the *para*-position of the phosphinine ring increase the π -donating properties by conjugative interactions through the HOMO, making the latter higher in energy. Moreover, the HOMO and LUMO have large coefficients at the phosphorus atom, they have similar shapes and point in the same direction, which leads to interaction with the same *d*-metal orbitals in octahedral complexes.

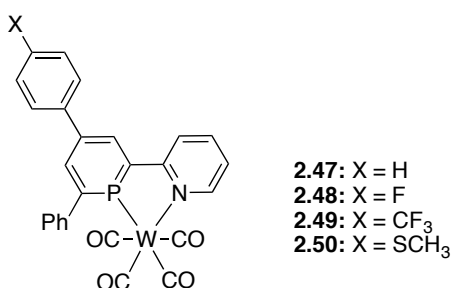


Figure 2.8 Tungsten complexes of functionalized PN ligands

This might lead to repulsion and net weakening of the P-M bond, which explains the shift of the C-O stretching bands for complex **2.45** to higher wave numbers in the IR spectrum. This study shows that the electronic properties of phosphinines can be modulated systematically by introducing substituents into specific position of the heterocycle.¹⁹

2.2 Results and discussion

It is the aim of this work to continue exploring the coordination chemistry of the very versatile **PN** ligand, therefore the results obtained throughout this research will be presented and discussed in this section. The studies on the coordination reactions of the **PN** ligand with metal centers have been divided according to transition metal groups in the periodic table. The NMR assignment for the ligand signals follows the numbering depicted in figure 2.9.

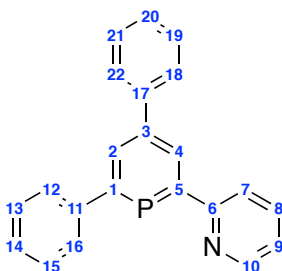


Figure 2.9 Numbering for the NMR signal assignment

Hydrogen atoms have the same numbers as the carbon atoms attached to them. The atoms that constitute the heteroatomic rings give the most valuable and interesting information about the coordination chemistry and the discussion will mainly evolve around this subject.

Group XI metal complexes

Copper

Several very interesting copper complexes containing phosphinine ligands have been described in literature (figure 2.10). The synthesis and spectroscopic properties of complex **2.51** were reported by Kanter and Dimroth.²⁰ Complex **2.52** was obtained by mixing CuI with 2-phenyl-3,4-dimethylphosphinine, from which an infinite stepped straight structure was characterized in the solid state.²¹ On the other hand, a monomeric species (complex **2.53**) was obtained by Le Floch and Mathey by reacting **TMBP** and $[\text{Cu}(\text{MeCN})_4]\text{BF}_4$. In the presence of one equivalent of bipyridine, the formation of an infinite helical polymeric structure was observed.²²

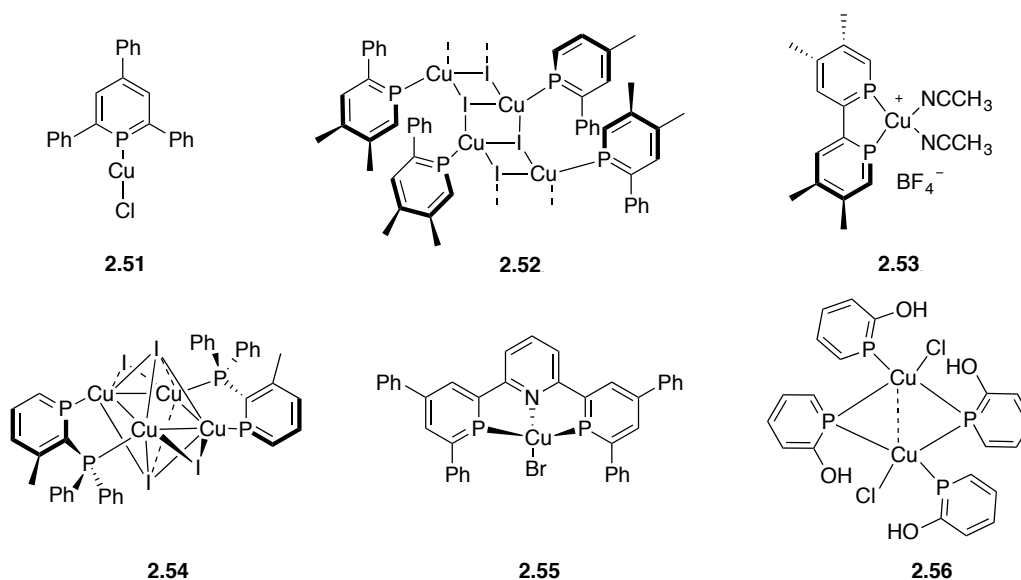


Figure 2.10 Copper complexes with phosphinine ligands

The same group discussed on the tetranuclear cluster **2.54**. It consists of a $[\text{CuI}]_4$ core containing two chelating 2-diphenylphosphino-3-methylphosphinine ligands.²³ Müller *et. al* reported on a monomeric copper complex formed by a phosphinine derivative of terpyridine and $\text{CuBr} \cdot \text{SMe}_2$ (**2.55**). This complex shows a distorted tetrahedral coordination geometry around the Cu(I) center.²⁴ Mathey described a dimeric structure (**2.56**), where two molecules of 2-phosphaphenol are coordinated in an η^1 -fashion to two different Cu centers. The metal atoms are bridged *via* two molecules of 2-phosphaphenol coordinated in a μ^2 -fashion, forming a diamond core structure.²⁵

Müller *et al.* reported on the first heterocubane-type cluster: a tetrameric Cu(I) cluster containing an aromatic phosphorus heterocycle (**2.57**, figure 2.11). This compound exhibits an intense orange luminescence (λ_{max} 640 nm) at room temperature when irradiated with UV light in the solid state. DFT calculations showed that the excitations observed correspond to charge transfers from the $[\text{Cu}_4\text{Br}_4]$ core to the phosphinine ligand.²⁶

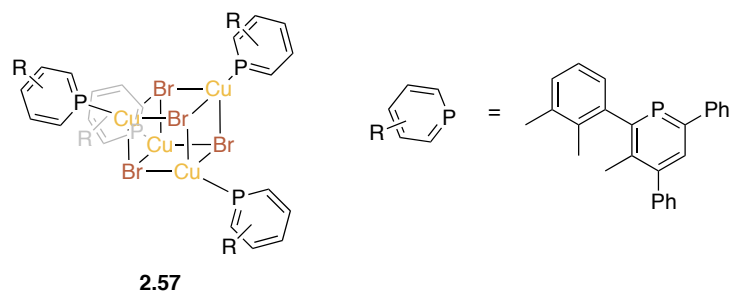


Figure 2.11 Copper cluster of the type $\text{Cu}_4\text{Br}_4\text{L}_4$

The coordination chemistry of the **PN** ligand to copper(I) precursors was studied with awareness that coordination of phosphinines to Cu cannot be so easily predicted as confirmed by the literature reports described above.

Different Cu(I) salts were used to synthesize Cu(I) complexes with **PN** as ligand. In general, the solubility played an important role. Some Cu(I) precursors are poorly soluble in common organic solvents such as MeCN, toluene, THF, DCM, diethyl ether, *etc.* Below, a table with the different copper precursors used is shown, along with the corresponding chemical shifts of the signals observed in the $^{31}\text{P}\{^1\text{H}\}$ NMR spectrum for the reaction mixtures.

Table 2.1 $^{31}\text{P}\{^1\text{H}\}$ NMR data of different Cu-**PN** complexes synthesized

Compound	Precursor	M:L	$^{31}\text{P}\{^1\text{H}\}$ NMR	Observations
1	$[\text{Cu}(\text{MeCN})_4]\text{BF}_4$	1:1	133.1 ppm (DMF)	Insoluble orange solid
2	$[\text{CuBr}\cdot\text{SMe}_2]$	1:1	none	Insoluble orange solid
3	$[(\text{cod})\text{CuCl}]_2$	1:1	129.9, 30.5, -23.5 ppm (DMSO)	Red solid
4	$[\text{Cu}(\text{CF}_3\text{SO}_3)_2]\cdot\text{Tol}$	1:1	33.2, 19.6(br), 9.3(br) ppm (DCM)	Partially soluble
5	$[\text{Cu}(\text{MeCN})_4]\text{PF}_6$	1:1	131.5 ppm (DCM) 130.6 ppm (DCM) 136.4 ppm (DCM) 150.6 ppm (MeCN)	Yellow solution
6	$[\text{Cu}(\text{MeCN})_4]\text{PF}_6$	1:2	142.2 ppm (DCM) 146.6 ppm (DCM) 152.3 ppm (DCM) 154.0 ppm (MeCN)	Yellow solution

$[\text{Cu}(\text{MeCN})_4]\text{PF}_6$ seemed to form fairly soluble complexes when mixed with the **PN** phosphinine in DCM or MeCN. It was noticed that in every attempt, either with a M:L ratio of 1:1 or 1:2, the chemical shift of the product changes by several ppm, even when measured in the same solvent. This has been observed earlier for Cu-phosphinine complexes. Compounds **5** and **6** crystallized easily as very fine yellow needles, which most of the times were not suitable for X-ray diffraction. From compound **5**, a picture of the molecular structure of the complex could be obtained, and thus the very interesting connectivity can be shown. Before the crystallization attempt, the reaction mixture showed a very broad signal at $\delta = 136.4$ ppm in the $^{31}\text{P}\{^1\text{H}\}$ NMR spectrum. In order to assign the molecular structure in the crystal to its corresponding species in solution, a $^{31}\text{P}\{^1\text{H}\}$ NMR spectrum was recorded, but no signal could be detected, probably due to a low concentration of the complex in the sample solution and the low signal intensities that this type of complexes give. Figure 2.12 shows the molecular structure of **5** in the crystal. The PF_6^- anions and the phenyl rings of the **PN** ligand have been omitted for clarity.

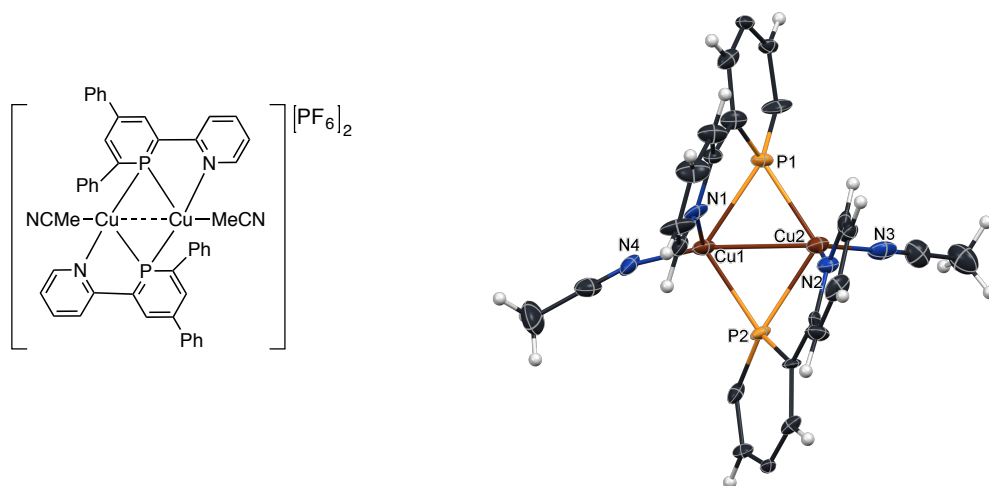


Figure 2.12 Schematic structure of **5** (left). Molecular structure of **5** in the crystal (right). Ellipsoids are scaled to enclose 50% of the electron density. Part of the molecule has been omitted for clarity purposes. Only the core structure is shown

The complex shows two copper centers, which are bridged *via* the phosphorus atoms forming a core diamond structure. Moreover, each nitrogen atom of the pyridyl ring is also coordinated to a metal center and there are two molecules of MeCN in the coordination sphere, resulting in a distorted tetrahedral geometry around each copper center. The short distance between the two coppers (approximately 2.56 Å) suggests a Cu-Cu bond, similar to the Cu-Cu distance 2.5487(5)

Å observed for complex **2.56**, in which the phosphinine ligand also adopts a μ^2 - and a η^1 -coordination. The chelating nature of the **PN** ligand should not be the only factor that influences the ligand to adopt the μ^2 -coordination. If it were so, a mononuclear cationic complex would be expected as in the case of complex **2.53**. The electronic properties of the pyridyl substituent might play a role on this preferred coordination mode.

This diamond-core shape results very interesting for applications such as catalytic oxidation processes, organic light-emitting diodes and low molecular weight model complexes for copper containing enzymes.^{27–34} It is worth mentioning that the DCM solution of this complex neither shows fluorescence under long nor short wavelength of UV light (with the naked eye).

Silver

Silver complexes with phosphorus ligands have been a subject area of interest, due to their versatile ability of forming mononuclear, dinuclear, and polynuclear complexes with different characteristics. It has been shown for diphosphines of the type dppm, dppe, and dppp, that the nuclearity of the complexes varies. Dppm (bite angle of 71.7°) forms with silver only dinuclear complexes of the type M_2L_2 , where dppm is acting as a bridging ligand rather than as a chelating one (figure 2.13). For dppe and dppp (85.0° and 91.1° , respectively) a mixture of mononuclear and polynuclear complexes are formed, where the ligands act as chelating ligands and/or bridging ligands. The most stable complexes result when the ligands act as bridging ligands (figure 2.13).^{35–39}

Even though the electronic properties of phosphinines differ from those of phosphines, the bite angle of bidentate ligands plays an important role in the type of complexes formed. The **PN** ligand has a bite angle of around 82° , which is in between the given value for dppm and dppp.

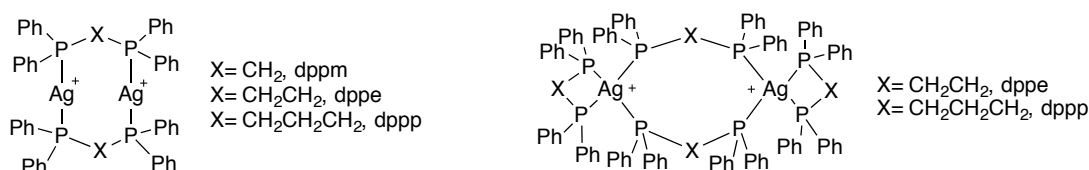
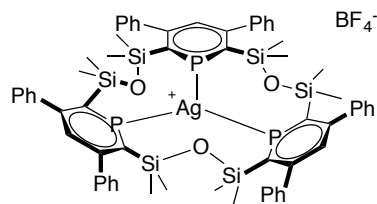


Figure 2.13 Cationic dinuclear silver complexes with diphosphines

Le Floch published complex **2.58** (figure 2.14), the only reported example of a phosphinine-silver complex so far. The ligand in this complex is an extended silacalix-[3]-phosphinine which forms a planar complex with $AgBF_4$ according to NMR spectroscopic analyses.⁴⁰



2.58

Figure 2.14 Silver complex of a silacalix-[3]-phosphinine.

The coordination chemistry of the **PN** ligand towards different silver salts has already been studied in the group of Müller.⁴¹ Unfortunately, no clear proof of the geometry or type of complex was elucidated before. Single crystals suitable for X-ray diffraction of these coordination reactions results somewhat difficult to obtain due to decomposition, which can be noticed already after few minutes in the $^{31}\text{P}\{^1\text{H}\}$ NMR spectra of the reaction solutions. It was detected, however, that silver tosylate showed less decomposition products and longer life-time in solution.

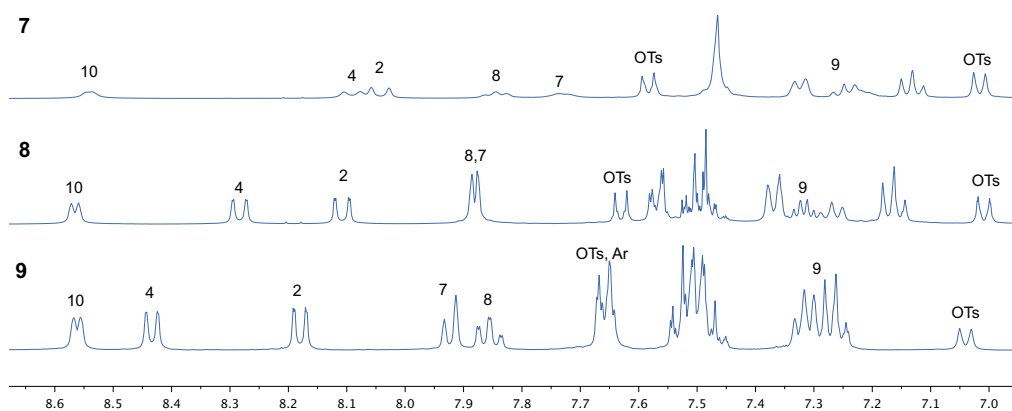
The coordination chemistry of the **PN** phosphinine with silver tosylate (AgOTs) was therefore studied in more detail. AgOTs was mixed with the **PN** ligand in a 1:1 ratio in DCM. After letting the solution stir thoroughly for some hours, no suspended solid could be seen in the yellow solution formed (AgOTs is barely soluble in DCM). The mixture was then characterized by means of NMR spectroscopy. The only signal obtained in the $^{31}\text{P}\{^1\text{H}\}$ NMR spectrum, with a chemical shift of $\delta = 135.7$ ppm, suggests coordination of the **PN** ligand to silver (complex 7). Based on the large $^{31}\text{P}\{^1\text{H}\}$ shift difference in comparison to the free ligand ($\Delta\delta$: 51.8 ppm), the phosphorus atom is expected to be directly bound to the metal center. The ^1H NMR shows a set of signals, where especially H10, H4 and H2 are strongly shifted to high field compared to the free ligand. Moreover, the $^3J_{\text{P-H}}$ coupling constants of H2 and H4 increase from approximately 6 Hz in the free ligand to 11 Hz in the complex (table 2.2). It seems that the P atom as well as the N atom are coordinated to a silver center, but whether the coordination mode is chelating or bridging remains undefined.

It was noticed that there were silver mirror spots inside the crystallization vials every time. As DCM is a non-coordinating solvent, the reaction was performed also in acetonitrile, to see if this would bring more stability to the complex formed, and to avoid precipitation of silver. After the solids were mixed and the solvent added, a $^{31}\text{P}\{^1\text{H}\}$ NMR spectrum was recorded. It showed a very broad signal at $\delta = 142.2$ ppm, but silver mirror spots were still formed immediately.

Table 2.2 $^{31}\text{P}\{^1\text{H}\}$ and ^1H NMR selected data for silver-phosphinine complexes with different M:L ratios

Expected complex	M:L	solvent	$^{31}\text{P}\{^1\text{H}\}$	^1H (ppm), $^3J_{\text{H-P}}$ (Hz)			
				H10	H4	H2	H9
7 [Ag(PN)]OTs	1:1	DCM	135.7 ppm	8.54	8.08, 11.3	8.04, 12.2	7.24
7 [Ag(PN)]OTs	1:1	MeCN	142.2 ppm				
8 [Ag(PN) ₂]OTs	1:2	DCM	155.6 ppm	8.55	8.27, 9.2	8.10, 9.8	7.31
8 [Ag(PN) ₂]OTs	1:2	MeCN	168.3 ppm				
9 [Ag(PN) ₃]OTs	1:3	DCM	168.5 ppm	8.56	8.43, 7.8	8.18, 8.3	7.04
9 [Ag(PN) ₃]OTs	1:3	MeCN	162.1 ppm				
PN		DCM	187.8 ppm	8.73	8.73, n.d.	8.25, 6.0	7.29

The reaction was performed again with two equivalents of ligand this time (complex **8**). The $^{31}\text{P}\{^1\text{H}\}$ NMR spectrum of the mixture in DCM shows a signal at $\delta = 155.6$ ppm. In the ^1H NMR spectrum a high field shift is again observed for all signals except for H9, which shifts slightly to lower field. The $^3J_{\text{P-H}}$ coupling constants of H2 and H4 are larger for complex **8** than for complex **7** (see table 2.2). After some hours, dark solid precipitated again from the solution, but the $^{31}\text{P}\{^1\text{H}\}$ NMR spectrum still showed the same signal and no free ligand. This suggested that a 1:3 M:L ratio might yield more stable products.

**Figure 2.15** ^1H NMR spectra with signal assignment for complexes **7-9**

Three equivalents of ligand were mixed with one equivalent of AgOTs in DCM (complex **9**). The yellow solution gives a signal in the $^{31}\text{P}\{^1\text{H}\}$ NMR at $\delta = 168.5$ ppm. In the ^1H NMR spectrum there is one set of signals for the coordinated PN ligand, that are shifted to high field but to a less extent compared to complexes **7** and **8** (see figure 2.15).

Unfortunately, crystals suitable for X-ray diffraction could not be obtained even after several crystallization attempts. In all cases, whether using DCM or MeCN as a solvent the formation of silver mirror spots or black solid was observed.

Three different types of silver complexes containing the **PN** phosphinine have been synthesized. From their $^{31}\text{P}\{^1\text{H}\}$ and ^1H NMR spectra, it is obvious that the electronic situation is fairly different in each case. It is worth to highlight the shift of H2 and H4 signals from high to low field and the decrease in their $^3J_{\text{P-H}}$ coupling constants when going from complex **7** to **9**. It is reasonable to propose a μ^2 -P coordination mode for complex **7**, going to a P-N bridging-mode in complex **9**, judged by the NMR data obtained.

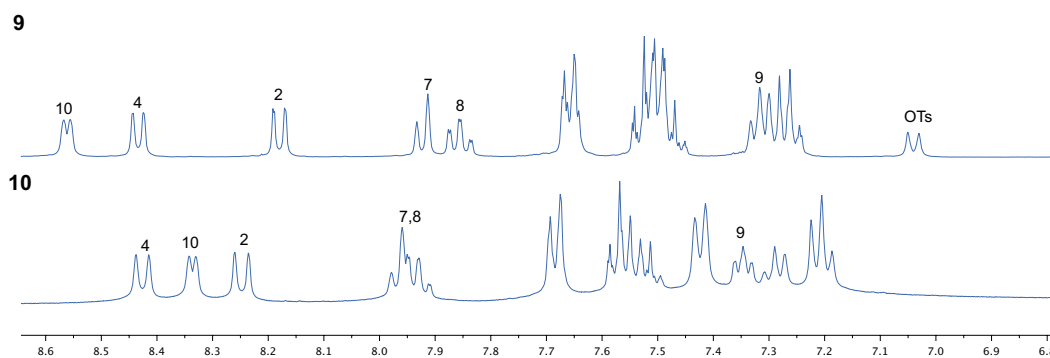


Figure 2.16 Comparison of the ^1H NMR spectra of complexes **9** and **10**

In order to compare the results with cases where other silver precursors were used, the analogous reaction for complex **9** was conducted starting with silver triflate (AgOTf). Three equivalents of **PN** were weighed together with one equivalent of AgOTf and dissolved in DCM (complex **10**). The mixture gives a $^{31}\text{P}\{^1\text{H}\}$ NMR signal at $\delta = 156.3$ ppm and the ^1H NMR spectrum looks different than that observed for **9** (see figure 2.16).

In the case of complex **10**, H10 is electronically much more shielded than the corresponding signal in complex **9**, and the $^3J_{\text{P-H}}$ coupling constants for H2 and H4 are larger in **10** (9.9 and 9.2 Hz, respectively) than in **9** (7.8 and 8.3 Hz, respectively). Obviously, the anion plays a role in these complexes. Unfortunately, crystals suitable for X-ray diffraction could not be obtained for complex **10**. The structures of these four silver complexes remain open for elucidation.

Gold

Some Au(I)-phosphinine complexes have been reported in literature.⁴²⁻⁴⁶ In the most recent publication Moussa and Amouri discuss the molecular structure of 2,6-diphenyl-4-methylphosphinine gold chloride.⁴⁷ The bond lengths and angles in the crystal show similar values to those of the gold complexes reported previously (see table 2.3). Nevertheless, none of these complexes contain an hetero-donor functionality, therefore, it was interesting to study the coordination chemistry of the **PN** ligand to gold.

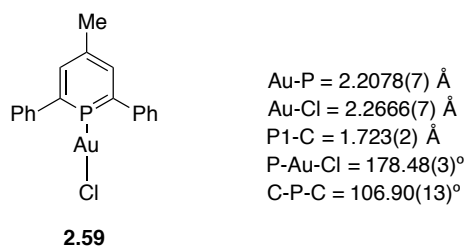
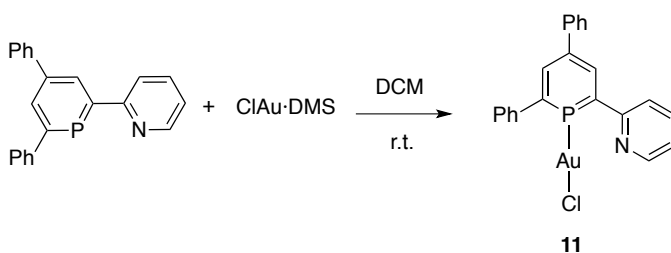


Figure 2.17 2,6-diphenyl-4-methylphosphinine gold chloride and selected bond lengths and angles from the molecular structure in the crystal

It is known that gold in its oxidation state +1 prefers to form linear complexes. For this reason, we expected the **PN** ligand to coordinate to the metal center only *via* the phosphorus atom and not as a chelating ligand. To get evidence for this, [AuCl·SMe₂] was mixed with one equivalent of **PN** ligand in DCM (scheme 2.3).



Scheme 2.3 Reaction between [AuCl·SMe₂] and **PN** ligand

Immediately, the solution turns light yellow. The ³¹P{¹H} NMR spectrum of the reaction mixture shows a singlet at δ = 158.3 ppm (Δδ = 29.5 ppm). The ligand signals in the ¹H NMR spectrum barely change compared to the ¹H NMR spectrum of the free ligand, except that H2 and H4 are slightly shifted toward low field and the ³J_{P-H} coupling constants increase dramatically from approximately 6 Hz in the free ligand to 21 Hz in the complex. Indeed, the σ-

coordination mode *via* the P atom was confirmed by X-ray diffraction of crystals obtained by slow evaporation of DCM. Figure 2.18 shows the ORTEP plot of complex **11**.

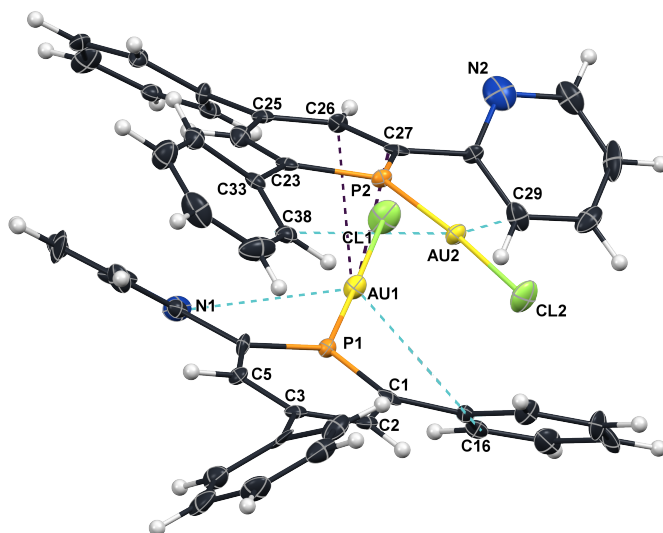
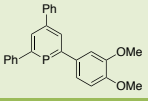
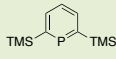
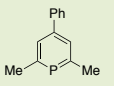
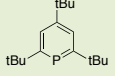
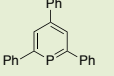
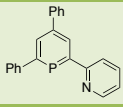


Figure 2.18 Molecular structure of complex **11** in the crystal. Ellipsoids are scaled to enclose 50% of the electron density

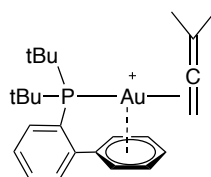
Two independent molecules are present in the asymmetric unit of the crystal. Linear gold complexes have shown to normally form parallel, antiparallel or crossed arrangements in the solid state. In this case, the complexes form a crossed arrangement between each other. The torsion angle between Cl(1)-Au(1)-Au(1)-Cl(2) is 119° (ideally, a crossed arrangement would have a torsion angle of 90°). Each independent molecule has a slightly distorted linear geometry: P(1)-Au(1)-Cl(1) and P(2)-Au(2)-Cl(2) angles are 176.22°(11) and 175.27°(11), respectively. P(1)-Au(1) and P(2)-Au(2) bond lengths (2.209(3) Å and 2.203(9) Å, respectively) are very similar to those reported by Le Floch, Nixon, Goudat and Siemeling, while the P-C double bonds are slightly longer in this case compared to literature cases (see table 2.3).

An interesting feature of this structure is that Au-C_{arene} inter- and intramolecular interactions are present (see Figure 2.15). These types of interactions have been acknowledged in recent years, especially for playing a role in gold catalysis.⁴⁸⁻⁵⁰ Some interactions have shown to be of the same magnitude as Au-Au interactions. The Au-C_{arene} interactions are considered important when the distance between the gold atom and the arene centroid is shorter than 4.0 Å, based on crystal structure data and van der Waals radii considerations. Intermolecular interactions of different types (Au-Au, Au-Cl, Au-C_{arene}) can stabilize the complex by building supramolecular arrays.⁵¹⁻⁵³

Table 2.3 Selected data from the crystal structures of gold-phosphinine complexes reported in literature and from **11**

Au(L)Cl bonds (Å), angles (°) and interactions (Å) from the crystal structures						
L=						
P-Au-Cl	175.9(1)	175.36(7)	175.70(10)	177.76(6)	177	176.22(11)
Au-P	2.206(1)	2.211(2)	2.234(3)	2.2194(15)	2.22	2.209(3)
Au-Cl	2.277(1)	2.281(2)	2.298(3)	2.2654(17)	2.28	2.283(3)
P-C		1.710(6) 1.702(7)	1.681(12) 1.723(10)	1.726(4)		1.730(10) 1.724(10)
C-P-C		110.4(3) ^o		108.0(3)		106.9(5)
Au-Au	-	-	3.60	-	-	5.797
Au-C _{arene}	-	-	-	-	3.32(3) (η ¹) 3.39(3)/3.44(3) (η ²)	3.164 (η ¹) 3.327/3.466 (η ²)
Au...Cl	3.387	-	crossed	-	-	-
motif	parallel	-	crossed	-	crossed	crossed
ref	Gudat ⁴³	Le Floch ⁴⁵	Siemeling ⁴⁶	Nixon ⁴²	Siemeling ⁴⁶	This work

Ligands for gold complexes have been carefully designed, in which an arene functionality attached to the skeleton of the ligand acts as a π -ligand and form intramolecular Au-C_{arene} interactions (figure 2.19).

**Figure 2.19** Cationic gold complex, where intramolecular C_{arene}-Au interactions are found

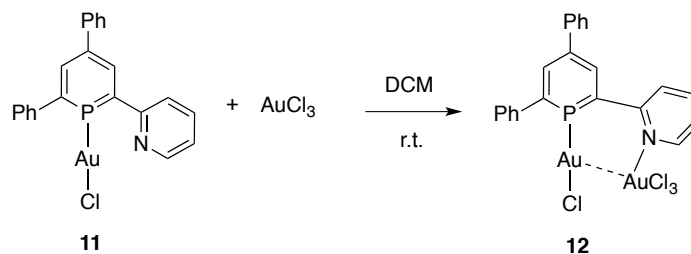
These features are especially important in linear cationic gold complexes for enhancing the stabilization of intermediate species formed during the catalytic cycle to obviate the need for silver co-catalysts, which help eliminate the halides to form the cationic active species.^{54–57}

Table 2.4 shows the inter- and intramolecular interactions observed in the molecular structure in the crystal of compound **11** (purple and blue dotted lines, respectively).

Table 2.4 Inter- and intramolecular interactions found in the crystal structure of **11**

Intermolecular (Å)	Intramolecular (Å)
Au1-N1 =3.271	Au1-C26 =3.327
Au1-C16 =3.472	Au1-C27 =3.466
Au2-C29 =3.661	Au1-C25 =3.976
Au2-C38 =3.164	Au2-C2 =3.935
Au2-C33 =3.698	

Distances as short as 3.164 Å are found for Au(2)-C(38) and 3.271 Å for Au(1)-N(1). The interaction that holds the molecules together is basically a Au-C_{arene} interaction between Au(1) and C(26) and C(27) (3.327 Å and 3.466 Å, respectively). This interaction can be considered a η²-interaction; the distances between Au(1) and C(25) and the rest of the ring are somewhat longer and already on the limit of the accepted value to be assigned as Au-C_{arene} interactions. The free pyridine ring in this complex leaves open the possibility to coordinate a second metal fragment to complex **11**. Based on the HSAB principle, the hard Au(III) should coordinate to the N atom, while the softer Au(I) should coordinate to the P atom. Also, Au(I)-Au(III) interactions could be an extra feature to form a highly stable complex. After adding 1 equivalent of AuCl₃ to a DCM solution of complex **11** and stirring for several hours a yellow solution was obtained (Scheme 2.4).



Scheme 2.4 Reaction of **11** with AuCl₃ to form proposed complex **12**

The ³¹P{¹H} NMR spectrum of the reaction mixture shows a signal at δ = 23.6 ppm (Δδ= 164 ppm). A smaller shift of the ³¹P{¹H} signal was expected if it was assumed that only the pyridyl ring would coordinate to Au(III) and the P atom would remain attached to Au(I). Unfortunately, crystals suitable for X-ray diffraction could not be obtained in order to show what type of complex is formed. There is more than one situation that explains the NMR data obtained, for example, that the P atom is bridging the two Au centers or that the ligand decoordinates from the AuCl fragment and coordinates only to AuCl₃. Of course, attempts to form a dinuclear complex with other metals and complex **11** should be made, for such complexes have enormous interest for catalysis and material sciences.

Group X metal complexes

Nickel

Nickel(0) complexes containing phosphinines have been reported before in literature and a selection of these are shown in figure 2.20. Complexes **2.60** and **2.61** were synthesized from $[\text{Ni}(\text{cod})_2]$ and the corresponding phosphinine. With more sterically demanding phosphinines, for example with *t*Bu groups in 2- and 4-positions, no complexes were formed.⁵⁸ The same group reported on tetrasubstituted Ni-(2-halophosphinine) complexes,⁵⁹ which are analogues to complex **2.62**, described by Elschenbroich. The tetrahedral coordination compound proved to be more stable than its pyridine or arsabenzene analogues.⁶⁰ Mathey described the structure of complex **2.63**, where the phosphine-phosphinine ligand is bridging two nickel centers forming a dimer. The presence of the strong π -accepting phosphinine allows the stabilization of the complex, whereas with the 2-phosphinopyridine ligand no nickel complex is formed.²³

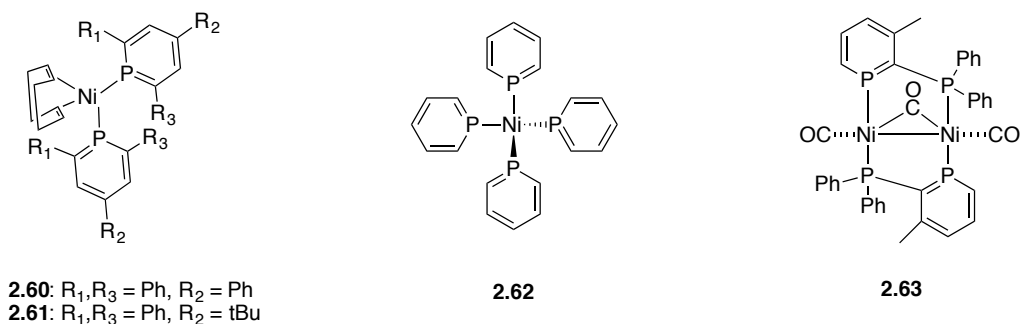


Figure 2.20 Selected Ni(0) complexes with phosphinine ligands reported in literature

The PN phosphinine was reacted with $[\text{Ni}(\text{CO})_4]$ rather than another nickel precursor, due to the valuable information about the electronic properties of the ligand that can be collected by means of IR spectroscopic analysis of the CO stretching bands.

The reaction was conducted by condensing $[\text{Ni}(\text{CO})_4]$ in an NMR tube with a PN solution in THF, which immediately gives a very dark solution. From time to time, the tube was degassed in order to remove CO out of the closed system, and a $^{31}\text{P}\{^1\text{H}\}$ NMR spectrum was recorded. The course of the reaction is shown in figure 2.21.

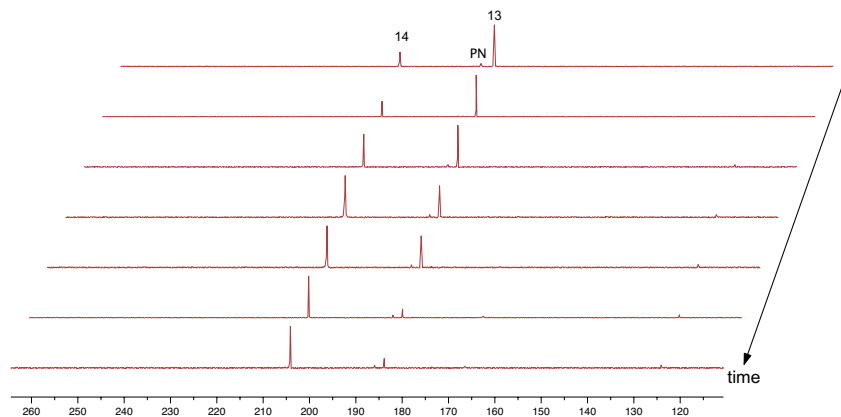


Figure 2.21 Time dependent $^{31}\text{P}\{^1\text{H}\}$ NMR spectra from the conversion of **PN** with $\text{Ni}(\text{CO})_4$. Each spectrum was recorded after degassing the solution

In the first spectrum shown above, three signals are observed. The minor one at $\delta = 186.7$ ppm corresponds to the free **PN** ligand. At higher field, a signal at $\delta = 183.8$ ppm (**13**) seems to be the first species formed, which in time slowly converts to **14** with a shift of $\delta = 204.2$ ppm. After degassing the solution several times almost only **14** remains in solution. The interpretation of the spectra is that compound **13** is $[\text{Ni}(\eta^1\text{-PN})(\text{CO})_3]$, which would be supported by the observations made by Mathey.¹ In this case, NIPHOS coordinates to $[\text{W}(\text{CO})_6]$ first only *via* the P atom to the metal center, while after dissociation of another CO molecule the signal undergoes a high field shift compared to the signal of the free ligand. Once the pyridyl ring is coordinated, the complex gives a signal at lower field shift. Following this logic, it is believed that **14** is the chelate complex $[\text{Ni}(\text{PN})(\text{CO})_2]$. Unfortunately, an IR spectrum of the solution could not be recorded to corroborate these assumptions, due to the high toxicity of $[\text{Ni}(\text{CO})_4]$ that remains in solution. Consequently, all volatiles were removed under vacuum to isolate the product. Interestingly, the new species **15** is formed, which shows a $^{31}\text{P}\{^1\text{H}\}$ NMR shift at $\delta = 166.2$ ppm ($\Delta\delta = 17.2$ ppm). The IR spectrum of the dark powder obtained shows two CO stretching bands at $\tilde{\nu} = 2035$ cm^{-1} and $\tilde{\nu} = 1987$ cm^{-1} . There are no signals present in the area where bridging CO frequencies appear. Moreover, most of the $^{13}\text{C}\{^1\text{H}\}$ NMR signals of compound **15** are split into pseudotriplets, which means that there are two inequivalent, but very similar P atoms in the molecule. The ^1H NMR spectrum gives one set of broad signals that corresponds to the **PN** ligand, which supports the observation from the $^{31}\text{P}\{^1\text{H}\}$ NMR spectrum that both ligands in the complex are very similar but not equivalent. Compared to the ^1H NMR spectrum of the **PN** ligand, all signals are fairly high-field shifted. H2 and H4 overlap and give a pseudotriplet with a coupling constant of approximately 7.3 Hz. The pyridyl ring protons undergo a high-field shift,

especially H10, which normally undergoes a downfield-shift in mononuclear complexes where the **PN** ligand is coordinated in a chelating fashion. Unfortunately, crystals suitable for X-ray diffraction could not be obtained and the structure of this complex remains unknown. From the IR and NMR spectra a dimeric structure is proposed for complex **15** (figure 2.22), where two **PN** ligands are involved and no CO-bridging ligands are present.

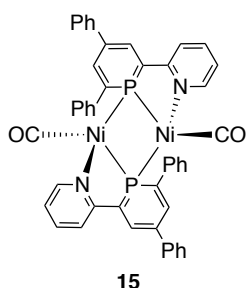
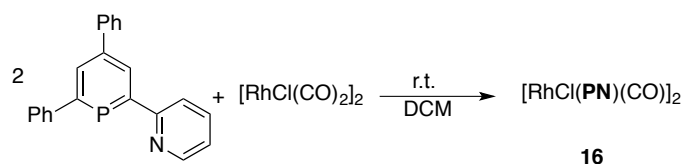


Figure 2.22 Proposed structure for complex **15**

Group IX metal complexes

Rhodium

Rhodium complexes with the **PN** ligand have been synthesized and structurally characterized previously in the group of Müller (**2.30** and **2.32** from figure 2.4 and 2.5, respectively).^{6,7} In order to further investigate the coordination chemistry of the **PN** ligand with other precursors and for comparison purposes with other **PN**-derived ligands (see chapter 4), $[\text{RhCl}(\text{CO})_2]_2$ was mixed with 0.5 equivalents of **PN** in DCM (scheme 2.5).



Scheme 2.5 Coordination reaction between **PN** and $[\text{RhCl}(\text{CO})_2]_2$ to form complex **16**

A black powder is formed immediately. This black solid is insoluble in almost every common organic solvent, and the compound could not be analyzed by means of NMR spectroscopic techniques.

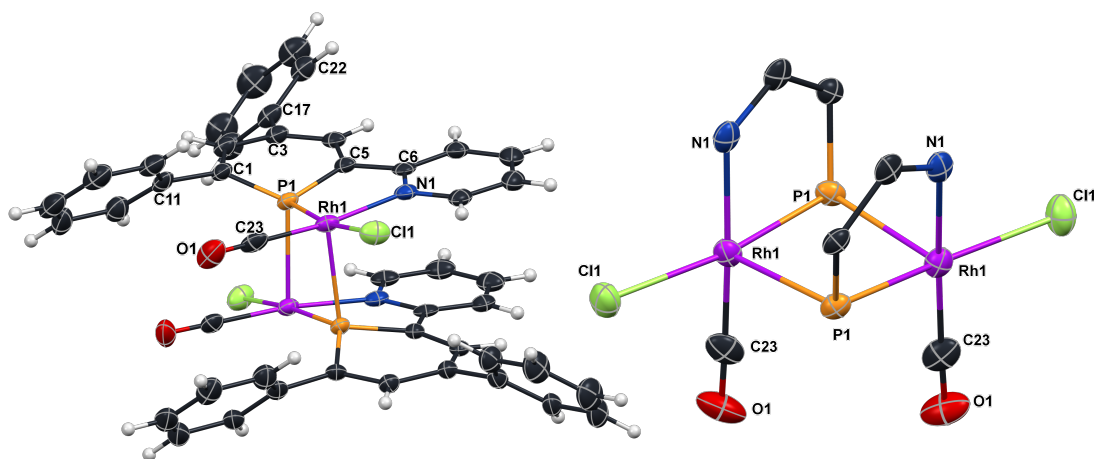


Figure 2.23 Molecular structure of complex **16** in the crystal (left). Core structure of the dimer (right). Ellipsoids are scaled to enclose 50% of the electron density

Fortunately, crystals suitable for X-ray diffraction were obtained by slowly diffusing a solution of the ligand into the solution of the precursor. Figure 2.23 shows the molecular structure in the crystal for complex **16**. Selected angles and bond distances are shown in table 2.5. The structure corresponds to the neutral binuclear complex **16**. It can be pictured as two chelate complexes, which are bound together *via* the phosphorus atoms. The Rh1-P1 bond has a bond distance of 2.2295(14) Å but the Rh2-P1 distance is somewhat longer, 2.4764(13) Å. These four atoms are approximately coplanar (Rh1-P1-Rh2-P2 torsion angle is 8.23°) and the geometry around each metal center is slightly distorted square pyramidal.

Table 2.5 Selected bond lengths and angles in complex **16**

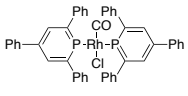
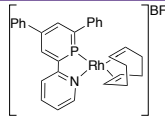
Bonds	Distance in Å	Angles	Degrees
Rh1-Cl1	2.4021(14)	C1-P1-C5	104.5(2)
Rh1-P1	2.4764(13)	P1-Rh1-P1	85.36(5)
Rh1-P1	2.2295(14)	N1-Rh1-Cl1	93.93(13)
Rh1-N1	2.125(5)	N1-Rh1-P1	81.12(12)
Rh1-C23	1.872(7)	C23-Rh1-Cl1	87.8(2)
O1-C23	1.128(7)	C10-N1-C6	118.3(5)
P1-C5	1.743(5)	P1-C1-C2-C3	10.3(8)
P1-C1	1.740(5)	P1-C1-C11-C16	56.7(7)
N1-C6	1.375(7)	P1-C5-C6-N1	9.5(6)
N1-C10	1.353(7)	C2-C3-C17-C18	44.3(7)

Venanzi and Mathey obtained cationic dinuclear complexes with the NIPHOS ligand and [Ir(cod)Cl]₂ and [Rh(nbd)Cl]₂. After an anion exchange, more stable complexes were formed,

which allowed their isolation and structural characterization.³ Only the iridium complex could be structurally characterized by means of X-ray diffraction, thus the molecular structure of the dirhodium complex cannot be compared to the one of **16**.

Müller showed the coordination reaction of $[\text{Rh}(\text{cod})_2]\text{BF}_4$ and the **PN** ligand, which leads to the monomeric complex $[\text{Rh}(\text{cod})\text{PN}]\text{BF}_4$ (**2.30**).⁶ Breit and coworkers prepared several *trans*-(phosphinine)₂Rh(CO)Cl complexes such as **2.64**, and compared their IR CO-stretching frequencies arriving to the conclusion that the electronic properties of phosphinines are closer to those of phosphites than to phosphines.⁶¹ A summary of selected bond lengths and angles of these rhodium complexes is listed in table 2.6 for comparison purposes with the structure of **16**.

Table 2.6 Selected bond lengths and angles of Rh-phosphinine complexes reported in literature

	 2.64	 2.30	Complex 16
P-Rh	2.2805(12) Å 2.2724(12) Å	2.2250(8) Å	2.2295(14) Å
N-Rh	-	2.159(2) Å	2.125(5) Å
C-P-C	105.8(21)°	105.24(14)°	104.5(2)°
P-Rh-N	-	79.77°	81.12(12)°
P-C	1.716(4) Å 1.723(5) Å	1.729(3) Å 1.721(3) Å	1.743(5) Å 1.740(5) Å
Ref.	Breit ⁶¹	Müller ⁶	This work

The Rh-P and Rh-N bond lengths are very similar to those present in $[(\text{PN})\text{Rh}(\text{cod})]\text{BF}_4$ (**2.30**). The P-C bond is slightly longer and the C-P-C angle does not differ substantially from the cationic monomer.

Due to the nature of the chelating ligand, in complex **16** the chloride and carbonyl ligands are forced to be in *cis*-position with respect to each other. CO is *trans* to the N atom of the pyridyl ring (strong σ donor), while in the case of complex **2.64** a Cl atom is in *trans*-position to the CO ligand (see table 2.6). This, of course influences the IR stretching frequencies of the CO ligands. Two CO stretching bands are detected for complex **16** ($\tilde{\nu} = 2064$ and $\tilde{\nu} = 1987$ cm^{-1}), the one at higher wave numbers is considerably shifted from the one obtained for **2.64** ($\tilde{\nu} = 1999$ cm^{-1}). The overall effect can be explained by the fact that in complex **16** there is more electron density on the metal center (from the pyridyl ring) and less π -accepting ligands (2 phosphinines and one CO in the case of complex **2.64**), resulting in higher CO stretching wave numbers.

Complex **16** demonstrates that the PN ligand can bind to Rh(I) also in a μ^2 -mode, depending on the precursor used. The μ^2 -mode consists of one phosphorus atom bridging two Rh(I) centers.

Group VIII metal complexes

Iron

The Iron-phosphinine complexes depicted in figure 2.24 have been reported in literature.

Homoleptic η^1 -phosphinine complex **2.65** was obtained from open ferrocene ($2,4\text{-Me}_2\text{-}\eta^5\text{-C}_5\text{H}_5\text{)}_2\text{Fe}$ and an excess of phosphinine, which forms a trigonal bipyramidal Fe(0) complex.⁶²

Complex **2.66** is an air stable η^6 -phosphinine iron complex, which was used as a catalyst for the [2+2+2] cycloaddition reaction of one molecule of butyronitrile with two molecules of methyl propargyl ether giving up to 160 mol of pyridine derivatives/mol.⁶³

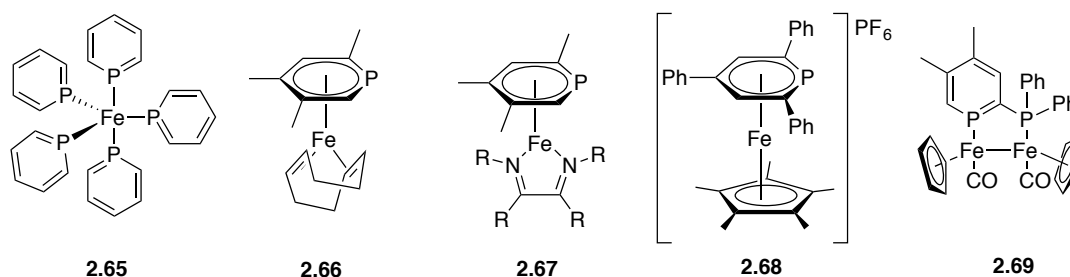
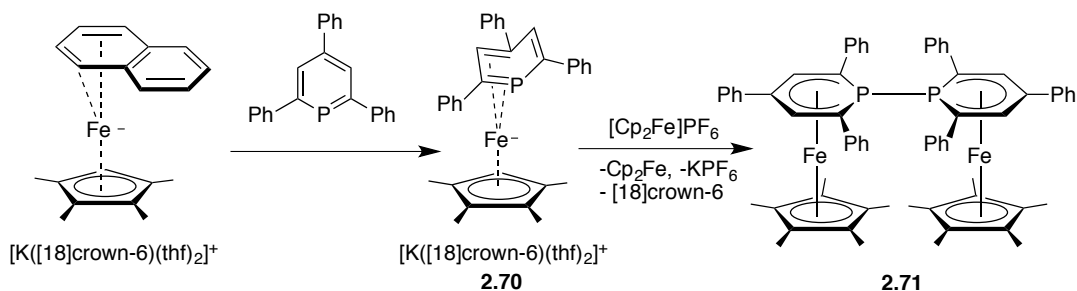


Figure 2.24 Iron-phosphinine complexes reported in literature

Complex **2.67** was synthesized by Le Floch from complex **2.66** and different diazadienes, which showed to be more robust than similar complexes bearing pyridines instead of the phosphinine ligand.⁶⁴ The sandwich complex **2.68** contains a neutral η^6 -coordinated 2,4,6-triphenylphosphinine ligand as well as an anionic cyclopentadienyl ligand.⁶⁵ Complex **2.69** shows a diiron η^1 -phosphinine- η^1 -phosphine complex, which bridges both iron centers. Cyclopentadienyl ligands as well as carbonyl ligands are also present in the complex, where each iron center has an unusual oxidation state of +1.⁶⁶

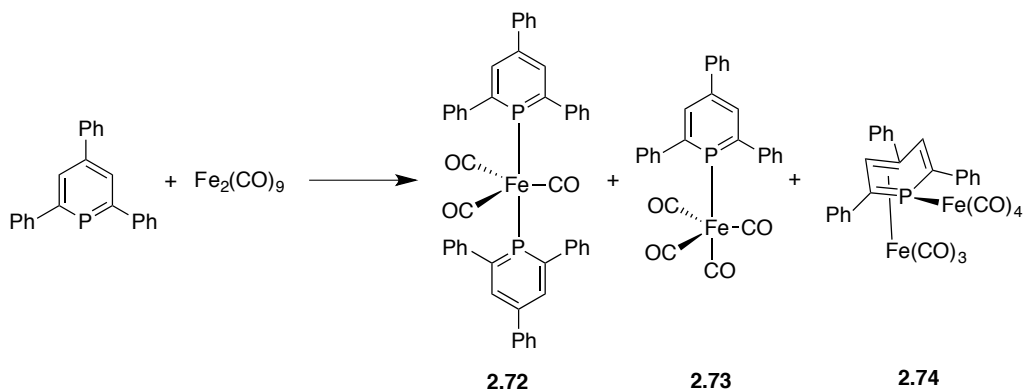
Wolf and Müller recently reported on the first anionic iron complex with a π -coordinated phosphinine (**2.70**, scheme 2.6). The phosphinine ligand in this complex is coordinated in the unusual η^4 -fashion. This coordination compound is extremely water sensitive and reacts with it to form the ionic complex $[\text{K}[18]\text{-crown-6}]\{\text{Cp}^*\text{Fe}(\eta^4\text{-}2,4,6\text{-triphenyl-}2,3\text{-dihydrophosphinine}$

1-oxide}. On the other hand, complex **2.70** can be chemically oxidized with ferrocenium leading to complex **2.71**, a P–P bonded dimer.⁶⁷



Scheme 2.6 Synthesis of complex **2.70** and its oxidation to form complex **2.71**

The coordination chemistry of phosphinines with Fe(0)-carbonyl complexes has been barely explored. To the extent of our knowledge the few examples of Fe(0) phosphinine-carbonyl complexes were reported in the PhD thesis of Eggers (scheme 2.7).⁶⁸



Scheme 2.7 Reaction of 2,4,6-triphenylphosphinine with $\text{Fe}_2(\text{CO})_9$

The preparation of these complexes is not straightforward. When reacting triphenylphosphinine with $\text{Fe}_2(\text{CO})_9$ a mixture of products **2.72-2.74** is obtained in different ratios depending on the reaction conditions. Complexes **2.73** and **2.74** were structurally characterized and the interesting η^4 -coordination of the ligand in complex **2.74** could be unequivocally described, where the heterocycle bends 46.4° across an imaginary line, which would connect the phosphorus atom with the C3 of the ring.

Looking at the chemistry of the related bipyridine ligands, heteroleptic carbonyl-bipyridine complexes have been prepared and show to have potential applications in synthesis and catalysis.⁶⁹ Bipyridines belong to the 1,4-diaza-1,3-diene ligand class (figure 2.24). The carbonyliron complexes of this class of ligands catalyze the dimerization or oligomerization of unsaturated organic molecules. It is important to elucidate the coordination modes of these substrates to the metal center, and investigate the reaction mechanisms in order to gain understanding in these processes. The group of Frühauf has reported on the coordination of dienes (with η^4 -coordination modes) to precursors of the type [(1,4-diaza-1,3-diene)Fe(CO)₃], and they have observed an interesting dependence between the ligand arrangement and the π -acidity of the diene ligand.

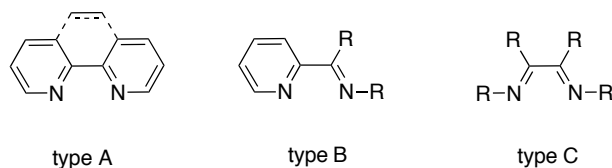


Figure 2.25 Different types of 1,4-diaza-1,3-diene ligands

When dienes with pronounced π -accepting properties, such as diethyl muconate, are coordinated to the metal center, the 1,4-diaza-1,3-diene ligand adopts a basal/apical position in the square pyramidal [(1,4-diaza-1,3-diene)Fe(η^4 -diene)(CO)] complex formed (**2.75**, figure 2.25). When the dienes are not π -acidic enough (for example 2,3-dimethylbutadiene), the coordination of the diaza-ligand results in unreactive complexes of C_s -symmetry, where the latter ligands adopt a basal/basal position (**2.76**, figure 2.25).

The most stable complexes were obtained with strong donating 1,4-diaza-1,3-diene and strong accepting diene ligands, nevertheless, the complexes are not active catalysts. Lability of the ligands is a necessary aspect for catalytic processes. The substitutional lability of the ligands in such complexes increases with increasing acceptor properties of the diaza-ligands. It is worth to mention that from the three types of 1,4-diaza-1,3-diene ligands shown in figure 2.24, bipyridines are the weakest π -acceptors of all.^{70–73}

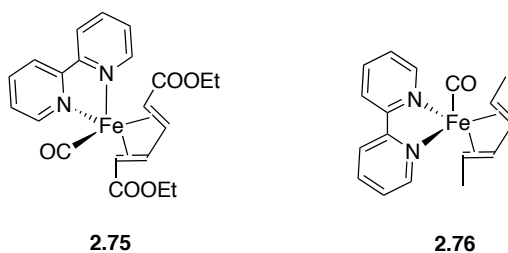


Figure 2.26 basal/equatorial and basal/basal complexes of the type [(1,4-diaza-1,3-diene)(1,3-diene)Fe(CO)]

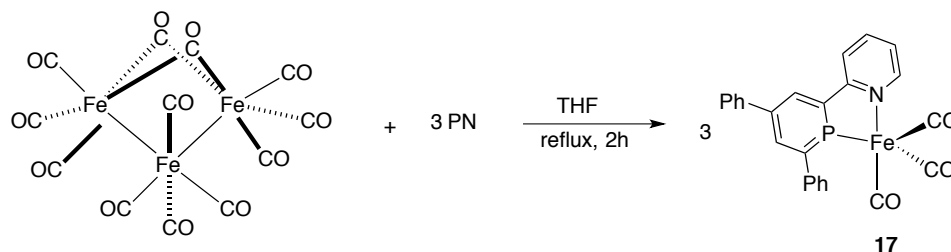
When reacting the readily available $[\text{Fe}_3(\text{CO})_{12}]$, $[\text{Fe}_2(\text{CO})_9]$ or $[\text{Fe}(\text{CO})_5]$ with bipyridines, slow reactions give a mixture of products in low yields, which mainly correspond to $[\text{Fe}_2\text{CO}_7(\text{bpy})]$ as the major product and $[\text{Fe}(\text{CO})_3(\text{bpy})]$ as the minor product. These two products can be separated by column chromatography. Triiron complex $[\text{Fe}_3(\text{CO})_{10}(\text{bpy})]$ could not be obtained even when mixing it with $[\text{Fe}_3(\text{CO})_{12}]$ at very low temperatures to avoid trimer dissociation. Even when starting from $[\text{Fe}(\text{CO})_5]$, the dimeric species $[\text{Fe}_2(\text{CO})_7(\text{bpy})]$ was obtained.

CO dissociation can happen thermally (refluxing the solution), photolytically (under UV light) or chemically (with trimethyl-*N*-oxide). Regardless of the procedure used, the reactions are not completely clean; they have low yields and hence need further purification. The monomeric $[\text{Fe}(\text{CO})_3(\text{bpy})]$ complex can be obtained in moderate yields (approximately 50%) starting from $[\text{Fe}(\text{CO})_3(\text{bda})]$ (bda= benzylideneacetone) and refluxing it with the corresponding bipyridine in THF or toluene.^{45–50}

It seemed plausible that **PN** could be a good candidate as ligand in iron carbonyl chemistry for the replacement of the diaza-ligand according to its good π -accepting ability. Because of that and the few carbonyl-phosphinine iron complexes reported, it was decided to synthesize the heteroleptic iron-carbonyl complex with the **PN** ligand and investigate its properties.

Thus, the synthetic routes described for bipyridine-iron carbonyl complexes were followed. Contrary to bipyridines, the formation of the monomer $[\text{Fe}(\text{CO})_3\text{PN}]$ (**17**) was straightforward. After 2 hours of refluxing $[\text{Fe}_3(\text{CO})_{12}]$ and three equivalents of the **PN** ligand in THF, the reaction turned to completion (scheme 2.8). The $^{31}\text{P}\{^1\text{H}\}$ NMR spectrum of the reaction mixture shows only one singlet at $\delta = 224.3$ ppm. The ^1H NMR spectrum shows the corresponding signals for the coordinated **PN** ligand. The pyridyl ring protons H10 and H7, undergo a downfield shift upon coordination, whereas H9 shifts to higher field. The phosphinine ring

protons H2 and H4 undergo a slight downfield shift and their $^3J_{P-H}$ coupling constants increase from 5.7 and 6.0 Hz, in the free ligand to 17.7 and 14.1 Hz, respectively in the iron complex.



Scheme 2.8 Synthesis of complex 16 from $[\text{Fe}_3(\text{CO})_{12}]$ and PN

The $^{13}\text{C}\{^1\text{H}\}$ NMR spectrum shows two doublets for the carbonyl ligands at $\delta = 170.7$ ($^2J_{P-C} = 50.6$ Hz) and $\delta = 172.7$ ($^2J_{P-C} = 50.9$ Hz). The chemical shifts of the signals and the large $^3J_{P-H}$ and $^2J_{P-C}$ coupling constants suggest that the ligand is coordinated to the iron center in a chelating fashion. To prove this, the product was recrystallized from MeCN and crystals suitable for X-ray diffraction were obtained. Figure 2.27 depicts the molecular structure of **17**, which consists of a mononuclear iron carbonyl complex.

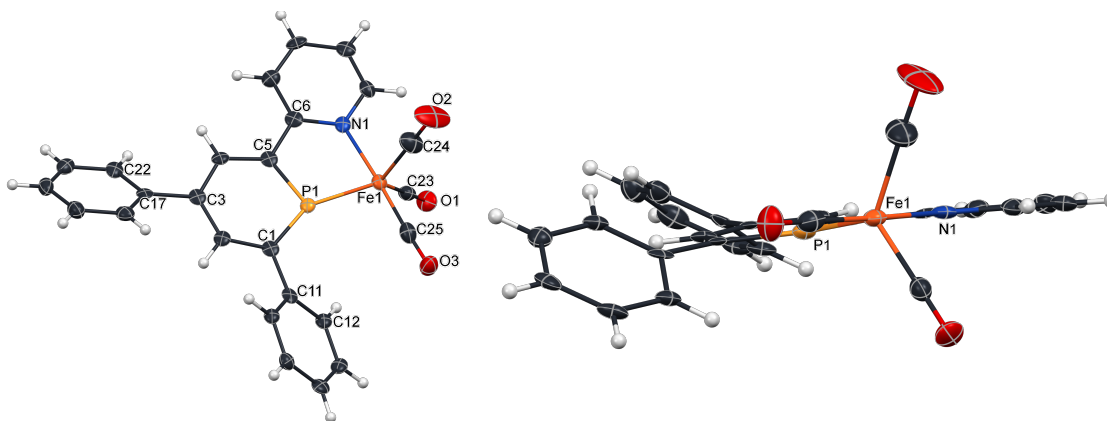


Figure 2.27 Molecular structure of **17** in the crystal. View from the top (left) and view from the side (right). Displacement ellipsoids are shown at the 50% probability level

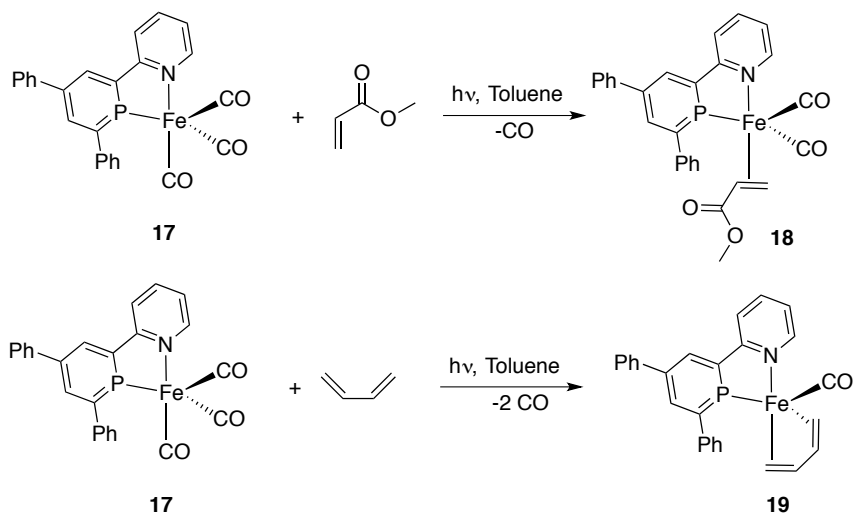
The central iron(0) atom is bound to three CO molecules and one PN ligand, which acts as a bidentate ligand. The angles between the ligands and the metal center point to a trigonal bipyramidal geometry, where the P atom occupies an equatorial position and the N atom an axial position. Table 2.7 lists a selection of bond lengths and angles for complex **17**, $[\text{Fe}(\text{CO})_3(\text{bpy})]$ and $[\text{Fe}(\text{CO})_4(\text{triphenylphosphinine})]$ (**2.73**, scheme 2.7), for comparison purposes. The P-Fe

bond in $[\text{Fe}(\text{CO})_3\text{PN}]$ is shorter than in complex **2.73**, which is expected due to the increased overall electron density in the complex. This can be explained due to the presence of a strong σ -donor N in pyridine ring, which allows an extended π -retrodonation of the π -accepting ligands phosphinine and CO (see corresponding entries in table 2.7). The shortest Fe-C bond is the Fe-C25, which is *trans* to the N atom (1.753(5) Å vs. 1.795(8) Å and 1.816(9) Å in **2.73**). In the case of $[\text{Fe}(\text{CO})_3(\text{bpy})]$ this trend is opposite, due to two strong σ -donating ligands (bpy) present instead of two strong π -accepting ligands. The *trans*-influence of the N and P atoms in **PN** can be proved as expected: Fe1-C25 is shorter than Fe1-C24 and Fe1-C23, thus C25-O3 is longer than C24-O2 and C23-O1, while the opposite effect is seen for the CO ligands that are located on the same plane as the π -accepting P atom. This of course is reflected in the IR spectrum, where three CO stretching bands at $\tilde{\nu} = 1999, 1949,$ and 1904 cm^{-1} are obtained for complex **17**; $\tilde{\nu} = 2066, 1992$ (with a shoulder), and 1959 cm^{-1} for complex **2.73**; and $\tilde{\nu} = 1968, 1897, 1862 \text{ cm}^{-1}$ for $[\text{Fe}(\text{CO})_3(\text{bpy})]$. This can be explained on the basis of the number of σ -donating ligands and π -accepting ligands in each complex. The more σ -donating ligands, the higher the wave number values of the CO stretching bands.

Table 2.7 Selected bond lengths and angles of Fe-phosphinine complexes and **17**

[Fe(CO) ₄ PN] (17)		[Fe(CO) ₃ (bpy)]		[Fe(CO) ₄ P] (2.73)	
P1-Fe1	2.1419(14)Å	Neq-Fe1	1.995(3) Å	P1-Fe1	2.189(2) Å
N1-Fe1	2.032(4) Å	Nax-Fe1	1.974(3) Å		
C25-O3	1.162(6) Å	Cax-O	1.154(5) Å		
C24-O2	1.144(7) Å	Ceq-O	1.152(5) Å		
C23-O1	1.158(6) Å	Ceq-O	1.152(5) Å	Fe1-Cax	1.795(8) Å
Fe1-C25	1.753(5) Å	Fe1-Cax	1.757(4) Å	Fe1-Cax	1.816(9) Å
Fe1-C24	1.793(6) Å	Fe1-Ceq	1.777(4) Å	Fe1-Ceq	1.794(10) Å
Fe1-C23	1.784(6) Å	Fe1-Ceq	1.773(4) Å	Fe1-Ceq	1.787(9) Å
C5-C6	1.465(7) Å	C5-C6	1.457(5) Å		-
P1-Fe1-N1	81.34(12)°	Nax-Fe1-Neq	79.64(12)°		-
P1-Fe1-C23	122.8(2)°	Neq-Fe1-Ceq	120.07(15)°	P1-Fe1-Ceq	117.6(3)°
P1-Fe1-C24	121.1(2)°	Neq-Fe1-Ceq	125.26(16)°	P1-Fe1-Ceq	118.0(3)°
C24-Fe1-N1	88.8(2)°	Ceq-Fe1-Nax	91.49(15)°	Ceq-Fe1-Cax	89.2(4)°
C1-P1-C5	103.9(2)°	C1-P1-C5	-	C-P1-C	102.9(3)°
P1-Fe1-C25	95.5(2)°	Neq-Fe1-Cax	95.62(15)°	P1-Fe1-Cax	91.8(2)°
N1-Fe1-C25	176.6(2)°	Nax-Fe1-Cax	174.97(15)°	Cax-Fe1-Cax	176.9(4)°
P1-C1-C11-C12	40.7(7)°	-	-	P1-C-Car-ar2	54.8°
C4-C3-C17-C22	34.9(7)°	-	-	Car-Car-Car-Car	38.6°

The easy synthetic access of $[\text{Fe}(\text{CO})_3(\text{PN})]$ (**17**) compared to $[\text{Fe}(\text{CO})_3(\text{bpy})]$ and $[\text{Fe}(\text{CO})_4(\text{triphenylphosphinine})]$ (**2.73**) makes the former complex a very interesting candidate as catalyst for processes where $[\text{Fe}(\text{CO})_3(\text{bpy})]$ has been investigated. Thus, some preliminary tests on the coordination of alkenes to complex **17** were performed.



Scheme 2.9 Coordination reaction of methylacrylate (top) and 1,3-butadiene(bottom) to **17**

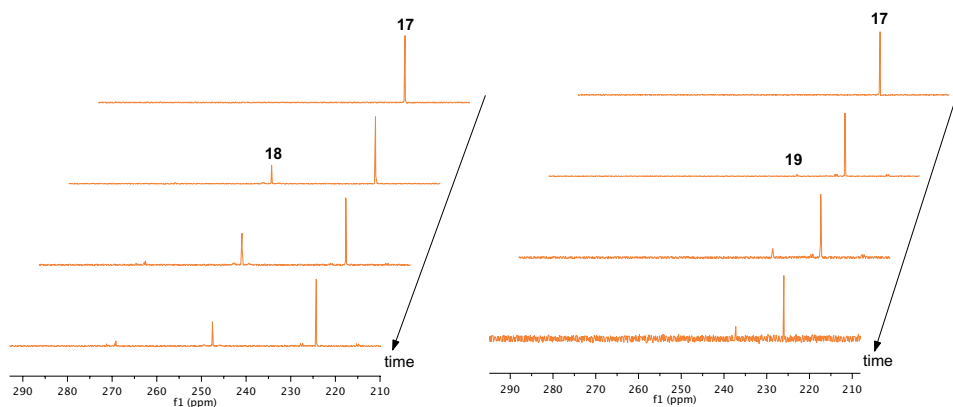


Figure 2.28 Time dependent $^{31}\text{P}\{^1\text{H}\}$ NMR spectra of **17** with methylacrylate (left) and 1,3-butadiene (right).

Methylacrylate and 1,3-butadiene are readily available and were used as depicted in scheme 2.9. Complex **17** was weighed in a *J*-Young NMR tube, where a toluene solution of an approximately ten-fold excess of methylacrylate was condensed in. Figure 2.28 shows the $^{31}\text{P}\{^1\text{H}\}$ NMR spectrum of the reaction mixture (left spectrum, top).

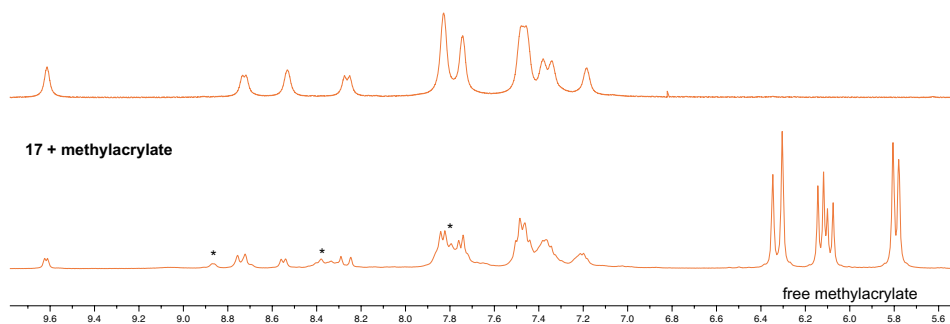


Figure 2.29 ^1H NMR spectra of complex **16** (top) and the reaction mixture of **16** and methylacrylate (bottom)

After two hours under UV light, a new singlet appears at $\delta = 247.5$ ppm (**18**). The tube was shortly opened to remove the CO overpressure. Afterwards, irradiation with UV light was continued. The reaction appears to reach equilibrium when the ratio between **17** and **18** is approximately 60:40.

A ^1H NMR spectrum of the reaction mixture was taken, which is shown in figure 2.29. The top spectrum corresponds to the starting material, **17**. On the bottom spectrum, the reaction mixture of complex **17** and methylacrylate is shown. The broad signals that are marked with a star should belong to the coordinated methylacrylate in complex **18**, which are expected to undergo a downfield shift upon coordination. Unfortunately, attempts to isolate the product were unsuccessful. After evaporating the solvent, the only species remaining was the starting material, **17**. Apparently, methylacrylate as ligand can easily be removed under vacuum. Separation of the product and crystallization attempts of the reaction mixture were unsuccessful.

The reaction of **17** with 1,3-butadiene was carried out according to a similar procedure. Figure 2.28 (right) shows the $^{31}\text{P}\{^1\text{H}\}$ NMR spectrum of **17** before irradiation with UV light, where only the precursor signal is observed. Upon irradiation, a new signal appears at $\delta = 235.5$ ppm (complex **19**). In this case the reaction stops when the ratio between complex **17** and complex **19** is approximately 80:20. It seems that complex **17** is capable of binding alkenes upon CO dissociation. The next step would be to test complex **17** in the dimerization or oligomerization of alkenes and to continue the investigations on the active species formed during the catalytic cycle. Unfortunately, these experiments could not be carried out within the duration of this project.

Iron(II)

The chemistry of Iron(II) has a myriad of interesting applications.⁸⁰⁻⁸³ In this work the diiron complex $[\mu\text{-(pdt)Fe}_2(\text{CO})_6]$ (pdt = propanedithiolate) will be discussed. This complex has served as a model for the investigation of structure and activity of hydrogenases, which are important biological enzymes. On the quest for renewable energies, these compounds are in sight because they can both break and form H_2 catalytically. A lot of effort has been made to structurally characterize these enzymes in living cells, as is of interest for biomimetics in areas such as biochemistry, bioinorganic, inorganic or organometallic chemistry. The analysis of several crystal structure determinations obtained from different organisms with similar enzymes has allowed to partially determine the structure of some catalytic sites, but some issues remain still unclear. Figure 2.30 depicts a general structure of Fe-Fe hydrogenase models.

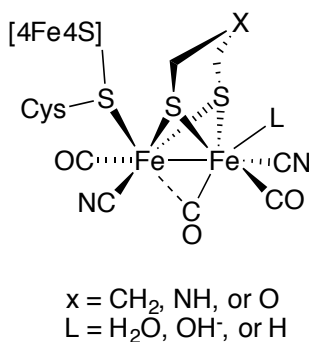


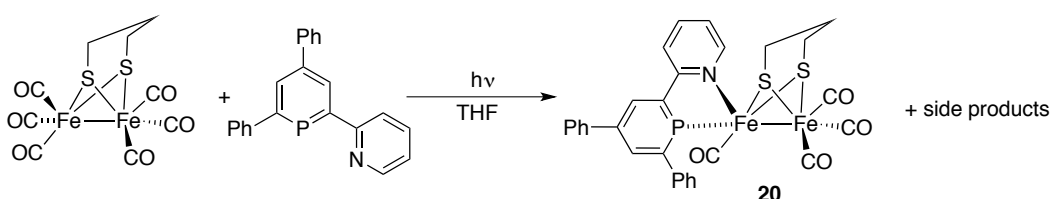
Figure 2.30 General structure of Fe-Fe hydrogenase models

The model consists of two iron(II) centers which are bound to each other, a dithiolate unit that bridges both iron centers and three asymmetrically bound CO or CN ligands on each metal center. Many groups have investigated the role of the bridge between the two iron centers, for example changing the chain length, or inserting heteroatoms (depicted as X in figure 2.30). The nature of the ligand depicted as L is still being discussed. It could be a hydrogen atom or H_2O , for example, and it could potentially be the initiator of H_2 evolution. The fact that a CO ligand bridges the two metal centers might allow the coordination of another ligand (H or H_2O) while changing its coordination mode to terminal, thus making a coordination site available. When the catalyst finds no more substrate, a possible resting state could be stabilized by the CO ligand going back to a bridging-coordination mode. Last but not least, one of the iron centers is bound to a sulfur atom of a cysteine that binds to a $[\text{Fe}_4\text{S}_4]$ cluster. This operates as the electron transfer

chain for delivering electrons to the active site of the enzyme. A large amount of publications can be found in literature, where all these questions have been separately addressed, hoping to come to a better understanding of this interesting system.^{80–136} Considering the aspects just mentioned, a lot of research groups have focused on the synthesis and characterization of this type of complexes bearing a hydride ligand. It has been demonstrated that the electronic situation of the metal centers determines the formation and selectivity of the hydride complex; the metal has to be basic enough to undergo protonation. $[\mu\text{-(pdt)Fe}_2(\text{CO})_6]$ does not form a stable conjugated acid, but if two CO ligands are replaced by two CN^- or PMe_3 ligands, the complex undergoes protonation with HCl , forming a $[(\mu\text{-H})\text{Fe}_2]$ complex. These synthetic models of the type $[\text{Fe}_2(\text{SR})_2(\mu\text{-H})\text{L}_2(\text{CO})_4]_z$ produce H_2 by electrocatalytic reduction of protons ($\text{L}=\text{CN}^-$, PMe_3). Such $[\text{Fe}_2(\mu\text{-H})]$ species, however, exhibit no inherent reactivity toward protons.¹²⁸

First of all, it was of interest to study the coordination chemistry of the **PN** ligand with $[\mu\text{-(pdt)Fe}_2(\text{CO})_6]$ and then to explore its reactivity towards proton sources, taking into account that the electronic properties of CO and CN ligands resemble those of phosphinine ligands.

One equivalent of **PN** was mixed with one equivalent of $[\mu\text{-(pdt)Fe}_2(\text{CO})_6]$ in THF and the mixture was irradiated with UV light for 2 hours (scheme 2.10). A $^{31}\text{P}\{^1\text{H}\}$ NMR spectrum was recorded and a mixture of three species was observed ($\delta = 248.8$ (7%), $\delta = 243.4$ (8%), and $\delta = 240.7$ (85%).



Scheme 2.10 Coordination reaction of **PN** with $[\mu\text{-(pdt)Fe}_2(\text{CO})_6]$ and formation of complex **20**

After a small silica column with toluene as eluent, the pure main product **20** ($\delta = 240.7$ ppm) was obtained as a dark red solid. The ^1H NMR spectrum shows characteristic resonances for the propanedithiolate bridge and for the chelating **PN** ligand.

A ^1H NMR spectrum of complex **20** was recorded and is depicted in figure 2.31. Resonances for H10, H4 and H7 shift to lower field compared to the free ligand, and H2 and H9 to higher field, which confirms the chelating coordination mode of the ligand. Also, the $^3J_{\text{P-H}}$ coupling constants between H2 and H4 with P increase upon coordination (17.0 and 15.1 Hz, respectively vs. 5.7 and 6.0 Hz, in the free ligand). In the $^{13}\text{C}\{^1\text{H}\}$ NMR spectrum, three signals for CO are observed at $\delta = 216.2$ ppm, $\delta = 211.9$ ppm (intensity almost as twice as the other ones), and $\delta = 209.1$ ppm, from which the first one is split into a doublet ($^2J_{\text{P-C}} = 5.9$ Hz), due to coupling to phosphorus.

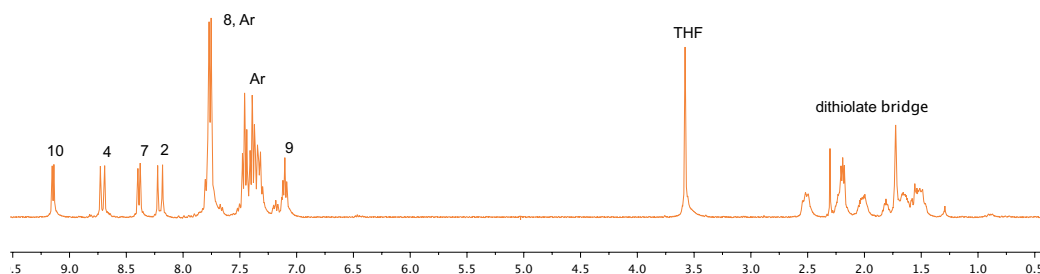


Figure 2.31 ^1H NMR spectrum of complex **20**

The IR spectrum of **20** shows six CO stretching bands for the complex: $\tilde{\nu} = 2072, 2032, 2021, 1990, 1953, \text{ and } 1920 \text{ cm}^{-1}$. When compared to the CO stretching bands of $[\mu\text{-(pdt)Fe}_2(\text{CO})_6]$, a general shift to lower wave numbers is observed, while when compared to $[\mu\text{-(pdt)Fe}_2(\text{CO})_4(\text{CN})_2]^{2-}$, a shift to higher wave numbers is noticed, especially considering the lowest band (table 2.8). It can be concluded that the basicity of complex **20** is somewhat in the middle between $[\mu\text{-(pdt)Fe}_2(\text{CO})_6]$ and $[\mu\text{-(pdt)Fe}_2(\text{CO})_4(\text{CN})_2]^{2-}$ previously reported in literature.¹²⁵

Table 2.8 IR CO-stretching bands for complexes of the type $[\mu\text{-(pdt)Fe}_2(\text{CO})_4\text{L}_2]$

Compound	IR stretching bands for CO
$[\mu\text{-(pdt)Fe}_2(\text{CO})_6]$	2074, 2036, 1995 cm^{-1}
$[\mu\text{-(pdt)Fe}_2(\text{CO})_4(\text{CN})_2]^{2-}$	1964, 1924, 1885 cm^{-1}
$[\mu\text{-(pdt)Fe}_2(\text{CO})_4(\text{PN})]$ (20)	2073, 2032, 2022, 1990, 1954, 1921 cm^{-1}

The molecular structure of the complex was confirmed by X-ray diffraction as crystals could be obtained from a THF solution of **20** after slow evaporation of the solvent. Figure 2.32 shows two

molecules of a diiron complex in the asymmetric unit. A THF molecule has been omitted from the Ortep plot for clarity reasons.

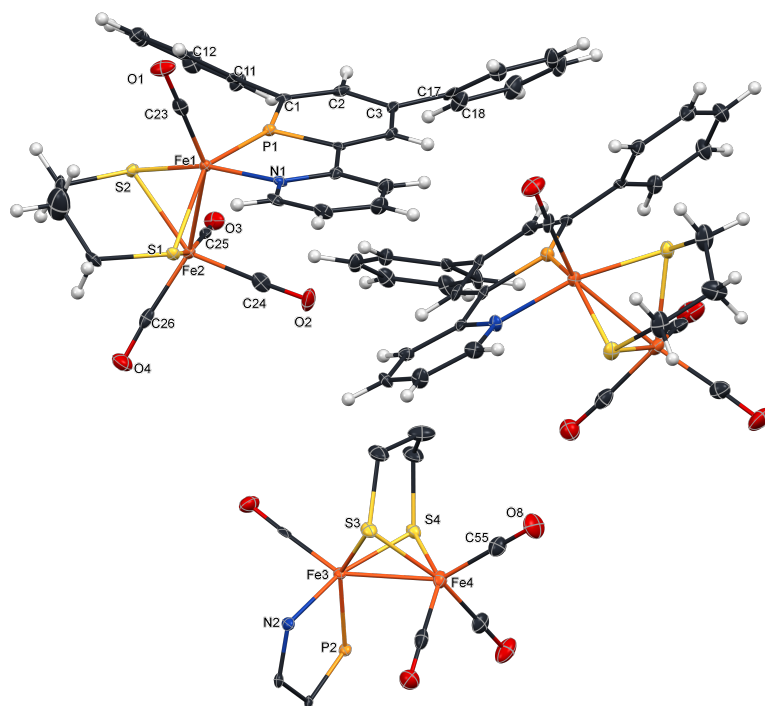


Figure 2.32 Molecular structure of **20** in the crystal (top), core structure (bottom). Displacement ellipsoids are shown at the 50% probability level

Table 2.9 Selected bond lengths and angles from the crystal structure of complex **20**

Bonds	Distance (Å)	Bonds	Angle (°)
Fe1-P1	2.148(1)	P1-Fe1-N1	81.1(1)
Fe1-N1	2.043(3)	P1-Fe1-C23	107.1(2)
Fe1-Fe2	2.5283(9)	C23-Fe1-N1	95.6(2)
Fe1-C23	1.763(5)	P1-Fe1-Fe2	90.25(4)
C23-O1	1.151(6)	S2-Fe1-P1	139.0(1)
Fe1-S1	2.236(1)	S1-Fe1-P1	139.0(6)
Fe1-S2	2.227(1)	S2-Fe1-S1	85.24(5)
P1-C1	1.738(5)	S1-Fe1-N1	87.4(1)
P1-C5	1.728(5)	P1-C1-C11-C16	34.8(2)
Fe2-C25	1.789(5)	C2-C3-C17-C18	41.2(7)
C25-O3	1.146(6)	P1-C5-C6-N1	1.1(5)
Fe2-C24	1.779(5)	Fe1-C23-O1	178.7(4)
C24-O2	1.145(6)	Fe2-C26-O4	174.6(4)
Fe2-C26	1.792(5)	Fe2-C24-O2	176.7(4)
C26-O4	1.145(6)	Fe2-C25-O3	178.4(4)
Fe2-S1	2.263(1)		
Fe2-S2	2.261(1)		

The two molecules shown are enantiomers. The analysis of the structure will refer to the molecule on the left side of the picture. Table 2.9 lists selected bond lengths and angles for complex **20**. For comparison purposes, selected crystal data from $[\mu\text{-(pdt)Fe}_2(\text{CO})_4(\text{dppv})]^{98}$ (**2.77**, figure 2.33) and $[\mu\text{-(pdt)Fe}_2(\text{CO})_4(\text{dppm})]^{137}$ (**2.78**) are shown in table 2.10. In all three cases (**2.77**, **2.78**, and **20**) the corresponding phosphorus ligand is coordinated to one iron center in a chelating mode. The iron atoms are bound by a single bond, where one of them connects to three terminal CO ligands and the other iron center only to one terminal CO molecule.

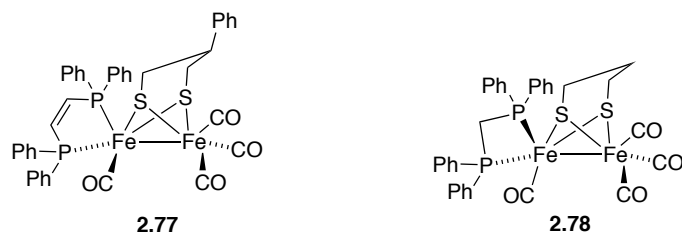


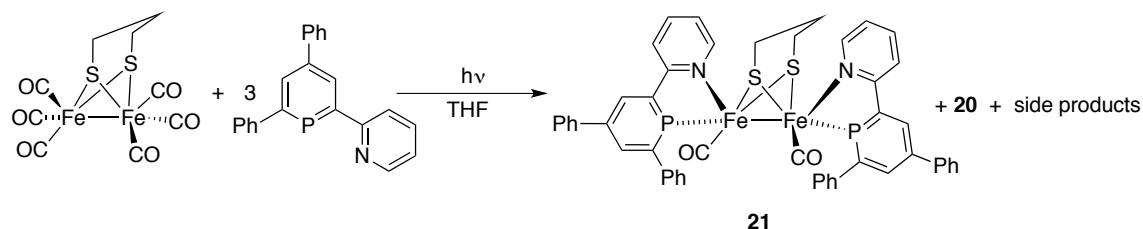
Figure 2.33 $[\mu\text{-(pdt)Fe}_2(\text{CO})_4(\text{dppv})]$ and $[\mu\text{-(pdt)Fe}_2(\text{CO})_4(\text{dppm})]$; (dppv = *cis*-1,2-bis(diphenylphosphine)ethylene, dppm = bisdiphenylphosphinomethane)

For complex **20** and **2.78** the phosphorus ligands adopt a basal/basal configuration, whereas in complex **2.77**, the ligand occupies apical/basal sites, even though the bite angle is quite small for **2.78** and for **20** ($74.55(4)^\circ$ and $81.1(1)^\circ$, respectively). For monophosphine ligands, the preferred coordination site is the apical one. The Fe-P bond is the longest for complex **2.78** (with dppm as ligand), and decreases going to **2.77** (where dppv is coordinated) and has the shortest for complex **20** (where PN acts as a ligand). The π -accepting properties of these three ligands increase in the same order as their Fe-P bonds decrease, which explains the trend. The Fe-Fe bond distance in complex **2.77** and **2.78** is close to those found in the reduced active site of Fe-Fe-hydrogenases¹³⁸ but in complex **20**, the distance is somewhat shorter ($2.5283(9)$ Å vs. 2.55 Å and 2.61 Å in hydrogenases found in *DesulfoVibrio desulfuricans*).

Table 2.10 Selected data from the crystal structures of **2.77**, **2.78**, and **20**

$\mu\text{-(pdt)Fe}_2(\text{CO})_4\text{L}$	L = dppv (2.77)	L = dppm (2.78)	L = PN (20)
Fe-P (Å)	2.1797(7)	2.2123(11)	2.148(1)
Fe-Fe (Å)	2.5517(5)	2.5671(5)	2.5283(9)
Coordination	apical/basal	basal/basal	basal/basal
Bite angle ($^\circ$)	87.83(5)	74.55(4)	81.1(1)
Reference	95	134	This work

Attempts on isolating the minor products formed during the synthesis of **20** were performed (scheme 2.11). It was noticed that with ligand excess and longer reaction times, the signal at $\delta = 243.4$ ppm in the $^{31}\text{P}\{^1\text{H}\}$ NMR spectrum increased until it became the major product (46% based on signal integration).



Scheme 2.11 Reaction of $[\mu\text{-(pdt)Fe}_2(\text{CO})_6]$ with an excess **PN** ligand to form **21**

This product precipitates from THF and after filtering the solid over celite and washing with THF and pentane, it was redissolved in DCM. After slow evaporation of the solvent black needles suitable for X-ray diffraction were obtained. Unfortunately, due to the poor quality of the crystals, bond lengths and angles cannot be properly discussed. Figure 2.34 shows the molecular structure of complex **21**. Two **PN** ligands are coordinated to a different iron center. Both metals are bound to each other and bridged *via* the dithiolate ligand, as in complex **20**. The ligands are pointing towards the same direction and are parallel to each other but not right on top of each other, instead a slipped arrangement can be noticed.

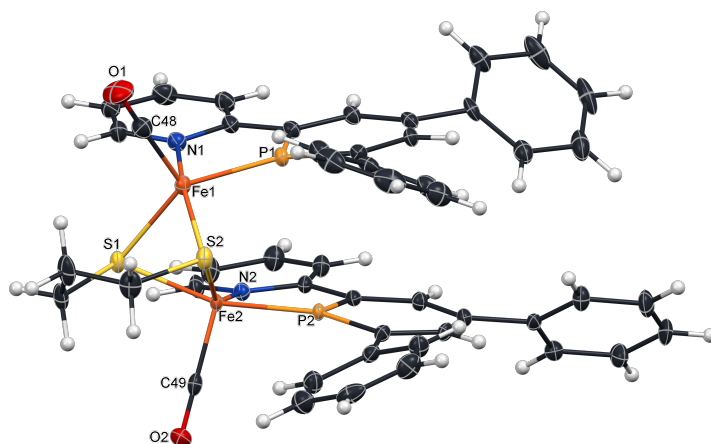


Figure 2.34 Molecular structure of **21** in the crystal. Displacement ellipsoids are shown at the 50% probability level

The IR spectrum of compound **21** shows four CO stretching bands at $\tilde{\nu} = 2015, 1948, 1899$ and 1884 cm^{-1} . These are considerably shifted to lower wavenumbers compared to **20**, which is in accordance to the overall higher electron density that is expected for such a complex. There are more donating ligands and less π -acceptors in complex **21** than in **20**; this leads to an enhanced π -backdonation into the C-O *anti*-bonding orbitals of the carbonyl ligands.

To get more information on the reactivity of these molecular hydrogenase models, complex **20** was reacted with different acids, expecting the formation of a hydride complex. Acids with different pK_a values were added and the reactions were performed in different solvents as summarized in table 2.11.

Table 2.11 Summary of the reaction with **20** and different acids

acid	CF ₃ SO ₃ H	CF ₃ SO ₃ H	HBF ₄ ·Et ₂ O	HBF ₄ ·Et ₂ O	HCl
solvent	THF	DCM	MeCN	DCM	DCM
observations	Orange solution formed, ³¹ P{ ¹ H} NMR signal at ca. 192 ppm (depending on the solvent), corresponds to PNH ⁺				

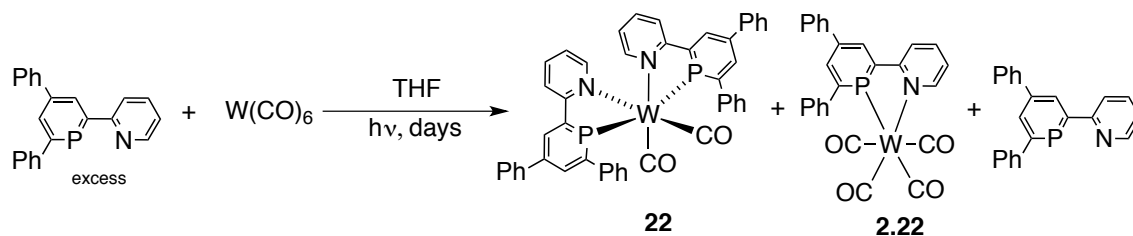
Surprisingly, an orange solution was obtained in every attempt, while a ³¹P{¹H} NMR signal at $\delta = 192.0 \text{ ppm}$ (among other minor signals, including the starting material) was observed. This signal corresponds to the protonated PNH⁺ ligand, which has been reported elsewhere.¹⁴⁰ This was confirmed also by X-ray analysis of crystals formed in the reaction mixture of **20** and CF₃SO₃H in DCM. After filtering the crystals, an IR spectrum of the remaining reaction mixture was recorded and three CO stretching bands were obtained at $\tilde{\nu} = 2072, 2030$ and 1988 cm^{-1} , which are very close to those reported for [μ -(pdt)Fe₂(CO)₆] (see table 2.8). Even though it is coordinated, the N atom of the pyridine ring is the most basic site in complex **20** and no hydride complex with the PN ligand could be obtained.

Group VI metal complexes

Tungsten

A series of group VI carbonyl complexes with substituted and unsubstituted **PN** ligands has been reported before by the group of Müller.^{4,19} In further attempts to completely substitute an octahedral complex with three **PN** ligand units, a tungsten precursor was chosen as the starting material, due to the larger P-W bond present for complex **2.22** compared to the shorter P-Ru bond of complex **2.40**, where the coordination of three **PN** molecules proved to be unsuccessful. Therefore, an excess of **PN** ligand was mixed with $[\text{W}(\text{CO})_6]$ in THF and irradiated with UV light, releasing CO overpressure from time to time (scheme 2.12).

After a couple of hours, a small signal for the intermediate complex (ligand only bound *via* phosphorus) and a second signal for the mono-substituted complex **2.22** were observed in the $^{31}\text{P}\{^1\text{H}\}$ NMR spectrum along with free **PN** ligand, as observed before by Mathey and Müller for NIPHOS and **PN** coordination to group VI metal complexes.^{1,4}



Scheme 2.12 Reaction between $[\text{W}(\text{CO})_6]$ and the **PN** ligand under UV irradiation

After several more hours a second, somewhat broader signal with tungsten satellites ($^1J_{\text{W-P}} = 370.8$ Hz) appeared at higher field ($\delta = 209.2$ ppm), which continues to increase while the others decrease (complex **22**). Figure 2.35 shows the course of the reaction within 2 weeks. After this time, the solvent was evaporated and the mixture was separated into its three components by means of column chromatography. The **PN**-disubstituted carbonyl tungsten complex **22** was obtained as a dark brown solid.

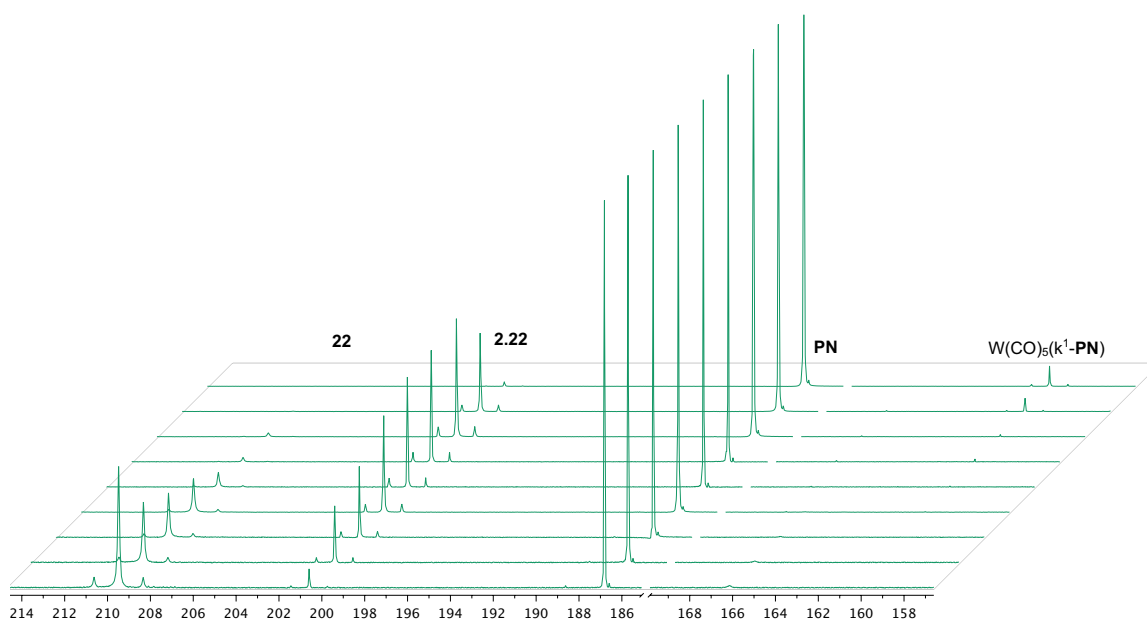


Figure 2.35 Time dependent $^{31}\text{P}\{^1\text{H}\}$ NMR spectra from the conversion of an excess of PN with $[\text{W}(\text{CO})_6]$

Crystals suitable for X-ray diffraction were obtained by slow diffusion of pentane into a THF solution of **22**. Figure 2.36 shows the molecular structure of the bis-chelate carbonyl complex **22**, where two CO ligands are in *cis*-position.

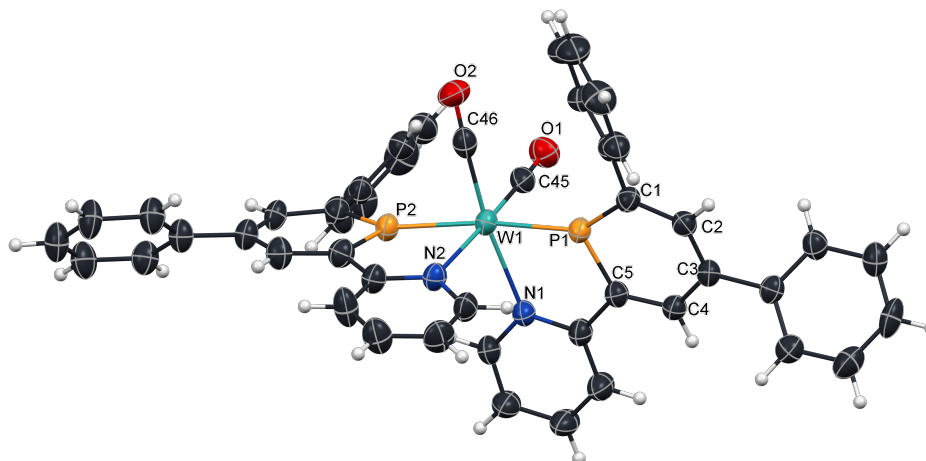


Figure 2.36 Molecular structure of **22** in the crystal. Displacement ellipsoids are shown at the 50% probability level. Selected bond lengths [\AA] and angles [$^\circ$]: P1-W1: 2.358(1); P2-W1: 2.363(1); N1-W1: 2.289(4); N2-W1: 2.290(4); C46-W1: 1.953(6); C45-W1: 1.946(6); C46-O2: 1.171(7); C45-O1: 1.176(7); C27-P2: 1.743(6); C23-P2: 1.740(6); C28-N2: 1.368(7); C32-N2: 1.365(7); C10-N1: 1.348(7); C6-N1: 1.369(7); C1-P1: 1.739(6); C5-P1: 1.741(6); P1-W1-P2: 169.84(5); C1-P1-W1: 146.3(2); N2-W1-P1: 95.78(11); N1-W1-P1: 74.25(12); C45-W1-P1: 90.4(2); C46-W1-P1: 98.3(2); C46-W1-P2: 85.3(2); N2-W1-P2: 74.22(11); N1-W1-N2: 84.1(2); C46-W1-N1: 172.3(2); C45-W1-N2: 172.8(2); N1-W1-P2: 102.42(12); C45-W1-C46: 84.0(2); P2-C27-C28-C29: 6.6(5); P2-C27-C28-N2: 2.6(7); P1-C5-C6-C7: 2.2(5); P1-C5-C6-N1: 0.3(7); P2-C23-C33-C34: 7.8(4); P1-C1-C11-C12: 48.5(7); C24-C25-C39-C40: 44.5(8); C2-C3-C17-C18: 43.2(6)

The geometry of the complex shows a distorted octahedral complex ($P1-W1-P2 = 169.84(5)^\circ$, $C46-W1-N1 = 172.3(2)^\circ$ and $C45-W1-N2 = 172.8(2)^\circ$). The *trans*-influence is demonstrated by the fact that the better σ -donating N atoms are *trans* to the π -accepting CO ligands and that the P atoms are *trans* to each other. Even though the W-P bond is larger in the mono chelate complex **2.22** than in **21** (2.3579(14) Å and 2.3626(15) Å), the C-P-C angle is shorter in **21** than in **2.22** (103.24° and 103.46° and 104.84° , respectively). The exocyclic phenyl rings of the **PN** ligands are tilted between 40.8° and 51.0° , more than in the monochelate W complex, where the torsion angles are between 34.9° and 38.4° , probably because of steric reasons. The three CO stretching bands that are observed in the IR spectrum ($\tilde{\nu} = 1935, 1866$ and 1805 cm^{-1}) are very similar to those of **2.22** ($\tilde{\nu} = 1934, 1871, \text{ and } 1819\text{ cm}^{-1}$), but slightly shifted to lower wavenumbers. The overall effect is in agreement with having more electron density in the ligand to retrodonate to the CO ligands and the fact that there are less of them than in $[(\mathbf{PN})\text{W}(\text{CO})_4]$.

2.3 Conclusions

The results presented in this work sum up to the literature reports on the coordination chemistry of the **PN** ligand, to show that this compound offers many possibilities for the design and synthesis of new compounds with interesting potential applications. Several transition metals complexes such as copper, silver, gold, nickel, rhodium, iron and tungsten in oxidation states ranging from 0 to II have been synthesized. Most of them account for the first reported complexes with a pyridyl-substituted ligand. **PN**, as a ligand, can adopt different coordination modes such as the classical chelating mode (iron complexes **17**, **20** and **21**), a κ^1 -**PN** mode (gold complex **11**), μ^2 -P- η^1 -N mode (copper complex **5**, rhodium complex **16**, probably nickel complex **15**, and most likely a P-N bridging mode in silver complexes. Also, the potential access to heterobimetallic complexes is obvious from these results. The detailed work on the exploration of the coordination chemistry of this functionalized phosphinine gives a better understanding for the design of complexes based on low-coordinate phosphorus species with uncommon and tailored properties. Moreover, some preliminary tests on the reactivity of the iron complexes have been shown, which point the complexes to be promising catalysts. Further exploration of the coordination chemistry of the **PN** ligand is, no doubt, awaiting interesting new discoveries that can lead to exciting results and applications.

2.4 Experimental

General remarks

All reactions were performed under argon by using Schlenk and glovebox techniques. All glassware was dried prior to use. All metal precursors were commercially available and used without further purification. **PN** ligand¹⁴¹ and $[\mu\text{-(pdt)Fe}_2(\text{CO})_6]$ ¹²¹ were synthesized according to literature procedures. All common solvents and chemicals were commercially available. Dry solvents were prepared by using custom-made solvent purification columns filled with Al_2O_3 from Braun Solvent systems. THF and diethyl ether were distilled under argon from potassium/benzophenone prior to use. NMR spectra were recorded with a *JEOL ECP 500* (^1H NMR 500.00 MHz), a *JEOL ECX400*, *JEOL ECAII 400* NMR Spectrometer (^1H NMR 399.74 MHz, $^{13}\text{C}\{^1\text{H}\}$ NMR 100.51 MHz, $^{31}\text{P}\{^1\text{H}\}$ NMR 161.82 MHz) or a *Brucker AVANCE III 700* NMR Spectrometer (^1H NMR 700.0 MHz); ^1H and ^{13}C chemical shifts are given relative to tetramethylsilane (TMS), and the residual solvent peaks were used as the reference signal; the ^{31}P chemical shifts are referenced to an 85% aqueous solution of H_3PO_4 . IR spectra were measured on a Nicolet iS 10 FTIR-ATR spectrometer by Thermo Scientific. For reactions under UV irradiation, a UVP High intensity 100 Watt B-100AP Mercury Vapor Lamp without filter was used.

$[(\text{PN})\text{Cu}(\text{MeCN})]_2[\text{PF}_6]_2$ (5)

PN (50 mg, 0.154 mmol) and tetrakis(acetonitrile)copper(I)-hexafluorophosphate (57.3 mg, 0.154 mmol) were dissolved separately in 1 mL dichloromethane each. The copper solution was dropped slowly into the phosphinine solution while stirring. The brown orange solution obtained was stirred for ten more minutes. The solvent was evaporated and dried under vacuum. Crystals were obtained by slow evaporation of DCM. Note: different NMR data were obtained for different attempts using the same procedure. The following information is for one of these attempts.

^1H NMR (400 MHz, CD_3CN): δ = 1.94 (s, 6H, MeCN), 7.38 (s, 14H), 7.43-7.59 (m, 4H), 7.71 (m, 2H), 8.02 (t, J = 7.9 Hz, 2H), 8.22 (d, J = 8.3 Hz, 2H), 8.26 (d, J = 11.9 Hz, 2H), 8.53-8.64 (m, 4H).

$^{13}\text{C}\{^1\text{H}\}$ NMR (100.5 MHz, CD_3CN): δ = 1.7 (d, J = 3.3 Hz, CH_3CN), 118.3, 121.5 (d, J = 7.1 Hz), 126.5 (d, J = 4.3 Hz), 128.5 (d, J = 13.2 Hz), 128.8 (d, J = 2.2 Hz), 129.6, 129.9 (d, J = 1.9 Hz), 130.1, 132.7 (d, J = 12.7 Hz), 136.2 (d, J = 13.3 Hz), 140.3, 141.4 (d, J = 20.0 Hz), 141.6

(d, $J = 4.3$ Hz), 144.8 (d, $J = 18.2$ Hz), 151.2 (d, $J = 3.1$ Hz), 156.3 (d, $J = 14.6$ Hz), 161.4 (d, $J = 17.4$ Hz), 161.7 ppm.

$^{31}\text{P}\{^1\text{H}\}$ NMR (161.8 MHz, CD_3CN): $\delta = -144.0$ (sep, PF_6^-), 150.0 (s) ppm.

$[(\text{PN})_2\text{Cu}][\text{PF}_6]$ (6)

PN (44.9 mg, 0.138 mmol) and tetrakis(acetonitrile)copper(I)-hexafluorophosphate (25.7 mg, 0.069 mmol) were dissolved separately in 1 mL dichloromethane. The copper solution was dropped slowly into the phosphinine solution while stirring. The brown orange solution obtained was stirred for ten more minutes. The solvent was evaporated and dried under vacuum. Note: different NMR data were obtained for different attempts using the same procedure. The following information is for one of these attempts.

^1H NMR (400 MHz, DCM-d_2): $\delta = 7.22$ -7.38 (m, 7H), 7.49-7.58 (m, 7H), 7.58-7.65 (m, 6H), 7.76-7.85 (m, 4H), 8.16-8.28 (m, 2H), 8.42-8.48 (m, 4H), 8.52 (d, $J = 4.5$ Hz, 2H), 8.76-8.86 (m, 2H).

$^{13}\text{C}\{^1\text{H}\}$ NMR (100.5 MHz, DCM-d_2): $\delta = 121.2$ (d, $J = 3.8$ Hz), 126.6, 127.7 (d, $J = 11.2$ Hz), 128.4, 129.6 (d, $J = 11.8$ Hz), 129.9 (d, $J = 20.6$ Hz), 132.4 (d, $J = 10.5$ Hz), 136.5 (d, $J = 11.1$ Hz), 140.5 (d, $J = 17.9$ Hz), 140.8, 141.4, 146.1 (d, $J = 16.8$ Hz), 151.4, 156.6 (d, $J = 12.7$ Hz), 161.8, 162.5 ppm.

$^{31}\text{P}\{^1\text{H}\}$ NMR (161.8 MHz, DCM-d_2): $\delta = 149.9$ (s), -143.8 (sep, PF_6^-) ppm.

$[\text{Ag}(\text{PN})][\text{OTs}]$ (7)

In a *J*-Young NMR tube covered in aluminum foil to protect it from light, AgOTs (20.5 mg, 0.074 mmol) and **PN** ligand (24.4 mg, 0.075 mmol) were dissolved in 0.5 mL DCM. The mixture was shaken for several hours. A yellow solution was formed. The solution was filtered over celite and left to evaporate slowly in the glovebox.

^1H NMR (400 MHz, DCM-d_2): $\delta = 2.29$ (s, 2H, $\text{CH}_3\text{-PhSO}_3$), 7.02 (d, $J = 8.0$ Hz, 2H, OTs), 7.10-7.17 (m, 2H, H_{ar}), 7.18-7.28 (m, 2H, H9, H_{ar}), 7.29-7.35 (m, 2H, H_{ar}), 7.43-7.50 (m, 4H, H_{ar}), 7.58 (d, $J = 8.2$ Hz, 2H, OTs), 7.69-7.77 (m, 1H, H7), 7.79-7.90 (m, 1H, H8), 8.04 (d, $J = 12.2$ Hz, 1H, H2), 8.09 (d, $J = 11.2$ Hz 1H, H4), 8.51-8.58 (m, 1H, H10) ppm.

$^{13}\text{C}\{^1\text{H}\}$ NMR (100.5 MHz, DCM-d_2): $\delta = 21.5$, 121.8-122.2 (m), 125.0-125.2 (m), 126.6, 128.0 (d, $J = 13.9$ Hz), 128.1 (d, $J = 2.6$ Hz), 129.1, 129.6 (d, $J = 3.7$ Hz), 129.7 (d, $J = 17.6$ Hz), 133.8 (d, $J = 14.1$ Hz), 135.4 (d, $J = 13.9$ Hz), 139.4-139.9 (m), 140.4, 140.6, 140.6, 142.8, 145.6 (d, $J = 18.6$ Hz), 151.7-152.9 (m), 155.5-156.7 (m), 166.6 (d, $J = 20.9$ Hz) ppm.

$^{31}\text{P}\{^1\text{H}\}$ NMR (161.8 MHz, DCM- d_2): $\delta = 135.7$ (s) ppm.

[Ag(PN) $_2$][OTs] (**8**)

In a *J*-Young NMR tube covered in aluminum foil to protect it from light, AgOTs (4.6 mg, 0.016 mmol) and PN ligand (16.0 mg, 0.049 mmol) were dissolved in 0.5 mL DCM- d_2 . The mixture was shaken for some minutes. A dark yellow solution was formed. The solution was filtered over celite and let evaporate slowly in the glovebox.

^1H NMR (400 MHz, DCM- d_2): $\delta = 2.26$ (s, 3H, CH_3 -PhSO $_3$), 6.99-7.04 (m, 2H, OTs), 7.12-7.20 (m, 4H, H $_{ar}$), 7.24-7.30 (m, 2H, H $_{ar}$), 7.30-7.34 (m, 2H, H $_9$), 7.34-7.40 (m, 4H, H $_{ar}$), 7.44-7.54 (m, 6H, H $_{ar}$), 7.54-7.60 (m, 4H, H $_{ar}$), 7.61-7.66 (m, 2H, OTs), 7.85-7.91 (m, 4H, H7/H8), 8.11 (d, $J = 9.7$ Hz, 2H, H2), 8.28 (d, $J = 9.1$ Hz, 2H, H4), 8.52-8.60 (m, 2H, H10) ppm.

$^{13}\text{C}\{^1\text{H}\}$ NMR (100.5 MHz, DCM- d_2): $\delta = 21.5$, 121.6 (d, $J = 6.6$ Hz), 124.8 (d, $J = 3.0$ Hz), 126.4, 127.9 (d, $J = 13.2$ Hz), 128.2 (d, $J = 2.0$ Hz), 128.9, 129.2 (d, $J = 1.9$ Hz), 129.3, 129.4, 129.7, 132.9 (d, $J = 13.2$ Hz), 134.8 (d, $J = 13.0$ Hz), 139.3, 139.5, 141.2 (d, $J = 3.9$ Hz), 141.5 (d, $J = 21.8$ Hz), 144.5, 145.3 (d, $J = 16.7$ Hz), 151.2, 157.0 (d, $J = 14.4$ Hz), 165.9 (d, $J = 22.9$ Hz), 168.2 (d, $J = 32.8$ Hz) ppm.

$^{31}\text{P}\{^1\text{H}\}$ NMR (161.8 MHz, DCM- d_2): $\delta = 155.6$ (s) ppm.

[Ag(PN) $_3$][OTs] (**9**)

In a *J*-Young NMR tube covered in aluminum foil to protect it from light, AgOTs (5.8 mg, 0.021 mmol) and PN ligand (20.0 mg, 0.062 mmol) were dissolved in 0.5 mL DCM- d_2 . The mixture was shaken for some minutes. A yellow solution was formed. The solution was filtered over celite and layered with pentane in the glovebox.

^1H NMR (401 MHz, DCM- d_2): $\delta = 2.27$ (s, 3H, Me -PhSO $_3$), 7.04 (d, $J = 7.9$ Hz, 2H, MePhSO $_3$), 7.20-7.37 (m, 12H, H $_9$ /H $_{ar}$), 7.43-7.57 (m, 15H, H $_{ar}$), 7.61, 7.70 (m, 6H, H $_{ar}$ /MePhSO $_3$), 7.86 (m, 3H, H8), 7.92 (m, 3H, H7), 8.18 (dd, $J = 8.3$, 1.3 Hz, 3H, H2), 8.43 (dd, $J = 7.8$, 1.3 Hz, 3H, H4), 8.52-8.61 (m, 3H, H10) ppm.

$^{13}\text{C}\{^1\text{H}\}$ NMR (101 MHz, DCM- d_2): $\delta = 201.0$, 121.2 (d, $J = 9.1$ Hz), 123.9 (d, $J = 2.5$ Hz), 126.0, 127.6 (d, $J = 12.9$ Hz), 127.7 (d, $J = 1.9$ Hz), 128.3-128.5 (m), 128.6, 128.9, 129.2, 132.2 (d, $J = 13.2$ Hz), 133.9 (d, $J = 12.4$ Hz), 138.2-138.5 (m), 138.8, 141.2 (d, $J = 3.6$ Hz), 141.9 (d, $J = 22.9$ Hz), 144.7 (d, $J = 15.5$ Hz), 145.0, 157.4 (d, $J = 18.0$ Hz), 165.8-166.6 (m), 168.8-169.8 (m) ppm.

$^{31}\text{P}\{^1\text{H}\}$ NMR (161.8 MHz, DCM- d_2): $\delta = 168.5$ (s) ppm.

[Ag(PN)₃][OTf] (10)

In a *J*-Young NMR tube covered in aluminum foil to protect it from light, AgOTf (5.3 mg, 0.021 mmol) and PN ligand (20.0 mg, 0.062 mmol) were dissolved in 0.5 mL DCM-*d*₂. The mixture was shaken for some minutes. A yellow solution was formed. The solution was filtered over celite and layered with pentane in the glovebox.

¹H NMR (401 MHz, DCM-*d*₂): δ = 7.21 (t, *J* = 7.6 Hz, 6H, H_{ar}), 7.25-7.32 (m, 3H, H_{ar}), 7.32-7.38 (m, 3H, H9), 7.39-7.45 (m, 6H, H_{ar}), 7.48-7.61 (m, 10H, H_{ar}), 7.65-7.73 (m, 5H, H_{ar}), 7.88-8.00 (m, 6H, H7/H8), 8.25 (d, *J* = 9.9 Hz, 3H, H2), 8.34 (d, *J* = 5.1 Hz, 3H, H10), 8.43 (d, *J* = 9.2 Hz, 3H, H4) ppm.

¹³C{¹H} NMR (101 MHz, DCM-*d*₂): δ = 121.3 (t, *J* = 4.9 Hz), 124.6-125.2 (m), 127.6 (d, *J* = 13.0 Hz), 127.8 (d, *J* = 2.1 Hz), 128.9, 129.2 (d, *J* = 33.9 Hz), 132.3-132.9 (m), 134.9 (d, *J* = 13.9 Hz), 139.3 (d, *J* = 5.9 Hz), 140.8 (d, *J* = 3.6 Hz), 140.9 (d, *J* = 22.0 Hz), 145.7 (d, *J* = 17.6 Hz), 150.1, 156.1-157.2 (m), 165.2 (dd, *J* = 20.3, 4.9 Hz), 167.9-169.3 (m) ppm.

³¹P{¹H} NMR (161.8 MHz, DCM-*d*₂): δ = 156.3 (s) ppm.

[Au(PN)Cl] (11)

In a *J*-Young NMR tube protected from light with aluminum foil, PN (15.0 mg, 0.031 mmol) and AuCl·DMS (9.1 mg, 0.031 mmol) were dissolved in 0.5 mL DCM-*d*₂. The mixture was shaken for some minutes. A clear yellow solution was formed. Crystals suitable for X-ray diffraction were obtained by slow evaporation of DCM in the glovebox.

¹H NMR (401 MHz, DCM-*d*₂): δ = 7.41-7.46 (m, 1H, H9), 7.47-7.58 (m, 6H, H_{ar}), 7.69-7.74 (m, 2H, H18/H22), 7.76-7.82 (m, 2H, H12/H16), 7.85-7.93 (m, 1H, H8), 8.01-8.10 (m, 1H, H7), 8.46 (dd, ³*J*_{P-H} = 22.0, ⁴*J*_{H-H} = 1.7 Hz, 1H, H2), 8.71-8.75 (m, 1H, H10), 8.80 (dd, ³*J*_{P-H} = 22.1, ⁴*J*_{H-H} = 1.7 Hz, 1H, H4) ppm.

¹³C{¹H} NMR (101 MHz, DCM-*d*₂): δ = 122.4 (d, ³*J*_{C-P} = 9.7 Hz, C7), 124.8 (d, ⁵*J*_{C-P} = 2.4 Hz, C9), 128.4 (d, *J* = 3.3 Hz, C_{ar}), 129.1 (s, C_{ar}), 129.2 (s, C_{ar}), 129.5 (d, *J* = 1.4 Hz, C_{ar}), 129.8 (d, *J* = 0.9 Hz, C_{ar}), 129.8 (d, *J* = 0.8 Hz, C_{ar}), 130.0 (d, *J* = 2.4 Hz, C_{ar}), 136.5 (d, ²*J*_{C-P} = 12.6 Hz, C4), 138.0 (d, ²*J*_{C-P} = 11.6 Hz, C2), 138.2 (s, C8), 139.7 (d, ²*J*_{C-P} = 12.8 Hz, C11), 140.9 (d, ³*J*_{C-P} = 5.7 Hz, C17), 144.1 (d, ⁴*J*_{CP} = 26.6 Hz, C3), 150.5 (s, C10), 155.6 (d, ²*J*_{C-P} = 10.6 Hz, C6), 157.5 (d, ¹*J*_{C-P} = 38.7 Hz, C1), 160.7 (d, ¹*J*_{C-P} = 32.3 Hz, C5) ppm.

³¹P{¹H} NMR (162 MHz, DCM-*d*₂): δ = 158.3 (s) ppm.

Au(I)-Au(III)(μ -PN)Cl₄] (12)

In an NMR tube, complex **11** (25.6 mg, 0.046 mmol) and AuCl₃ (13.9, 0.046 mmol) were weighed together and dissolved in 0.5 mL DCM-*d*₂. A yellow solution was formed. The solution was filtered over celite and layered with ether to crystallize.

³¹P{¹H} NMR (162 MHz, DCM-*d*₂): δ = 23.6 (s) ppm.

[Ni(PN)CO]₂ (15)

In a Schlenk flask equipped with a PTFE high-vacuum valve, **PN** (75.0 mg, 0.231 mmol) was dissolved in THF. The solution was frozen and [Ni(CO)₄] (approximately 25 mbar, 10-fold excess) was condensed in. The reaction mixture was stirred and degassed 10 times every 2 hours. Volatiles were evaporated and a black powder was obtained. The powder was redissolved in DCM and filtered over celite. The solvent was evaporated and the black powder obtained was dried under vacuum. Yield: 83%, 81 mg.

¹H NMR (401 MHz, THF-*d*₈): δ = 6.61-6.70 (m, 1H, H₉), 7.29-7.38 (m, 1H, H_{ar}), 7.38-7.46 (m, 4H, H₈/H_{ar}), 7.52-7.59 (m, 2H, H_{ar}), 7.70-7.80 (m, 3H, H₇/H_{ar}), 7.87-7.92 (m, 1H, H_{ar}), 7.95 (m, 1H, H₁₀), 8.06-8.18 (m, 2H, H₂/H₄) ppm.

¹³C{¹H} NMR (101 MHz, THF-*d*₈): δ = 120.9 (t, *J* = 3.6 Hz, C₇), 122.2 (s, C₉), 127.5 (s, C_{ar}), 127.8 (s, C_{ar}), 128.1 (s, C_{ar}), 129.1 (t, *J* = 5.7 Hz, C_{ar}), 129.4 (s, C_{ar}), 129.8 (s, C_{ar}), 132.3 (t, *J* = 5.0 Hz, C₂), 135.7 (t, *J* = 8.1 Hz, C₁₁), 136.2 (s, C₈), 136.7 (t, *J* = 4.5 Hz, C₄), 144.0-144.35 (m, C₃/C₁₇), 149.4 (t, *J* = 6.6 Hz, C₁), 150.8 (t, *J* = 6.6 Hz, C₅), 151.5 (t, *J* = 3.6 Hz, C₁₀), 160.4 (t, *J* = 9.1 Hz, C₆), 198.6 (t, *J* = 8.3 Hz, CO) ppm.

³¹P{¹H} NMR (162 MHz, THF-*d*₈): δ = 166.1 (s) ppm.

IR(ATR) $\tilde{\nu}_{\text{CO}}$: 2035 and 1987 cm⁻¹

[Rh(PN)Cl(CO)]₂ (16)

4 mL of a DCM solution of [RhCl(CO)₂]₂ (15 mg, 0.038 mmol) was dropped into 1 mL of a DCM solution of **PN** ligand (25 mg, 0.077 mmol). A black precipitate formed immediately. The solution was decanted, washed with DCM and pentane and dried under vacuum. Dark blue needles suitable for X-Ray diffraction were obtained layering a DCM ligand solution on top of a DCM solution of the rhodium precursor. Yield: 96%, 36 mg.

IR(ATR) $\tilde{\nu}_{\text{CO}}$: 2064 and 1987 cm^{-1}

[Fe(PN)(CO)₃] (17)

In a Schlenk flask, [Fe₃(CO)₁₂] (19.3 mg, 0.038 mmol) and **PN** ligand (37.4 mg, 0.115 mmol) were dissolved in THF and stirred at $T = 70^\circ \text{C}$ for 2 h. The solvent was evaporated and a dark red powder obtained. The solid was washed with ether and dried under vacuum. Crystals suitable for X-ray diffraction were obtained by recrystallization from acetonitrile. Yield: 70%, 37 mg.

¹H NMR (401 MHz, THF-*d*₈) $\delta = 7.16\text{-}7.25$ (m, 1H, H9), 7.29-7.41 (m, 2H, H_{ar}), 7.43-7.54 (m, 4H, H_{ar}), 7.72-7.78 (m, 2H, H_{ar}), 7.80-7.89 (m, 3H, H8, H_{ar}), 8.27 (dd, ³*J*_{H-P} = 17.7, ⁴*J*_{H-H} = 1.3 Hz, 1H, H2), 8.54 (d, ⁴*J*_{H-P} = 8.2 Hz, 1H, H7), 8.73 (dd, 1H, ³*J*_{H-P} = 14.1, ⁴*J*_{H-H} = 1.3 Hz, 1H, H4), 9.62 (d, ⁵*J*_{H-P} = 5.9 Hz, 1H, H10) ppm.

¹³C {¹H} NMR (101 MHz, THF-*d*₈): $\delta = 121.2$ (s, C9), 121.9 (d, ³*J*_{C-P} = 13.5 Hz, C7), 127.9 (s, C_{ar}), 128.2 (s, C_{ar}), 128.7 (d, *J*_{C-P} = 1.5 Hz, C_{ar}), 129.7 (d, *J*_{C-P} = 8.7 Hz, C_{ar}), 129.8 (s, C_{ar}), 129.8 (s, C_{ar}), 130.8 (d, ²*J*_{C-P} = 9.5 Hz, C4), 135.0 (d, ²*J*_{C-P} = 15.5 Hz, C11), 135.6 (s, C8), 139.3 (d, ²*J*_{C-P} = 7.6 Hz, C2), 142.4 (d, ³*J*_{C-P} = 16.4 Hz, C3), 143.5 (d, ³*J*_{C-P} = 3.1 Hz, C17), 146.8 (d, ¹*J*_{C-P} = 9.8 Hz, C1), 152.4 (d, ¹*J*_{C-P} = 10.3 Hz, C5), 158.9 (s, C10), 162.6 (d, ²*J*_{C-P} = 26.6 Hz, C6), 217.4 (d, ²*J*_{C-P} = 3.5 Hz, CO) ppm.

³¹P {¹H} NMR (162 MHz, THF-*d*₈): $\delta = 224.3$ (s) ppm.

IR(ATR) $\tilde{\nu}_{\text{CO}}$: 1999, 1949 and 1904 cm^{-1}

[Fe(PN)(η^2 -methylacrylate)(CO)₂] (18)

Complex **17** (20 mg, 0.043 mmol) was weighed in a *J*-Young NMR tube. The tube was evacuated and 0.6 mL of toluene with methylacrylate (0.35 ml, 3.86 mmol) were condensed in. The tube was irradiated with UV-light for several hours, opening the cap shortly from time to time until the reaction came to equilibrium. Attempts on doing the reaction under argon flow and in other solvents like acetone, were unsuccessful. No product could be isolated.

[Fe(PN)(η^2 -(1,3-butadiene))(CO)₂] (19)

Complex **16** (24 mg, 0.052 mmol) was weighed in a *J*-Young NMR tube. The tube was evacuated and 0.5 mL of toluene with 15% w 1,3-butadiene (0.5 mL, 0.10 mmol) were

condensed in. The tube was irradiated with UV-light for several hours, opening the cap shortly from time to time until the reaction came to an equilibrium. No product could be isolated.

$[\mu\text{-(pdt)Fe}_2\text{(PN)(CO)}_4]$ (20)

In a *J*-Young NMR tube, **PN** ligand (30.0 mg, 0.09 mmol) and $[\mu\text{-(dpt)-Fe}_2\text{(CO)}_6]$ (35.6 mg, 0.09 mmol) were dissolved in 0.6 mL THF and let stir under UV-light for 1 h. A dark red solution was formed. The solvent was evaporated and the brown solid was fixed on silica. A short column was run with toluene. The first fraction (red) was collected, the solvent was evaporated and the red powder was dried under vacuum. Crystals were formed by slow diffusion of pentane into a THF solution. Yield: 74%, 45 mg.

^1H NMR (700 MHz, THF- d_8): δ = 1.53-1.45 (m, 1H, P-Fe-SCH₂CH₂), 1.62-1.53 (m, 1H, P-Fe-SCH₂CH₂), 1.68-1.62 (m, 1H, CH₂-S), 2.05-1.97 (m, 1H, CH₂-S), 2.27-2.20 (m, 1H, P-Fe-SCH₂), 2.56-2.47 (m, 1H, P-Fe-SCH₂), 7.11 (m, 1H, H₉), 7.36-7.30 (m, 2H, H_{ar}), 7.39 (m, 2H, H_{ar}), 7.48-7.44 (m, 2H, H_{ar}), 7.71-7.83 (m, 5H, H₈/H_{ar}), 8.20 (d, $^3J_{\text{P-H}}$ = 17.0 Hz, 1H, H₂), 8.39 (d, $^4J_{\text{P-H}}$ = 8.2 Hz, 1H, H₇), 8.71 (d, $^3J_{\text{P-H}}$ = 15.1 Hz, 1H, H₄), 9.15 (ddd, J = 6.0, 1.6, 0.7 Hz, 1H, H₁₀) ppm.

$^{13}\text{C}\{^1\text{H}\}$ NMR (176 MHz, THF- d_8): δ = 24.4 (d, $^4J_{\text{P-C}}$ = 7.7 Hz, P-Fe-SCH₂CH₂), 25.9 (d, $^3J_{\text{P-C}}$ = 20.3 Hz, P-Fe-SCH₂), 31.3 (s, SCH₂), 120.5 (d, $^3J_{\text{P-C}}$ = 12.3 Hz, C₇), 121.2 (s, C₉), 128.2 (s, C_{ar}), 128.4 (s, C_{ar}), 128.8 (s, C_{ar}), 129.4 (s, C_{ar}), 129.6 (d, J = 8.1 Hz, C_{ar}), 129.8 (s, C_{ar}), 130.7 (d, $^2J_{\text{P-C}}$ = 10.7 Hz, C₄), 135.9 (s, C₈), 137.5 (d, $^2J_{\text{P-C}}$ = 18.6 Hz, C₁₁), 138.9 (d, $^2J_{\text{P-C}}$ = 9.6 Hz, C₂), 141.3 (d, $^4J_{\text{P-C}}$ = 14.6 Hz, C₁₇), 143.2 (d, $^3J_{\text{P-C}}$ = 3.2 Hz, C₃), 151.2 (d, $^1J_{\text{P-C}}$ = 16.3 Hz, C₅), 156.8 (s, C₁₀), 158.8 (d, $^1J_{\text{P-C}}$ = 8.3 Hz, C₁), 163.3 (d, $^2J_{\text{P-C}}$ = 19.3 Hz, C₆), 209.1 (s, CO), 211.9 (s, CO), 216.2 (d, $^2J_{\text{P-C}}$ = 5.9 Hz, CO) ppm.

$^{31}\text{P}\{^1\text{H}\}$ NMR (162 MHz, THF- d_8) δ = 240.7 ppm.

IR(ATR) $\tilde{\nu}_{\text{CO}}$: 2073, 2032, 2022, 1990, 1954, 1921 cm^{-1}

$[\mu\text{-(pdt)Fe}_2\text{(PN)}_2\text{(CO)}_2]$ (21)

In a *J*-Young NMR tube, **PN** ligand (20.0 mg, 0.06 mmol) and $[\mu\text{-(dpt)-Fe}_2\text{(CO)}_6]$ (12.5 mg, 0.03 mmol) were dissolved in 0.6 mL THF and stirred under UV-light for 1 h, then the CO overpressure was released. This was repeated six times until the $^{31}\text{P}\{^1\text{H}\}$ NMR signal at δ = 243 ppm did not increase anymore. A black precipitate was formed. The powder was filtered over celite, washed with THF and pentane and redissolved in DCM. Volatiles were evaporated, and

the product was dried under vacuum. Crystals were formed by slow evaporation of a DCM solution. Yield, 44%, 14 mg.

$^{31}\text{P}\{^1\text{H}\}$ NMR (162 MHz, DCM- d_2): $\delta = 243.3$ (s) ppm.

IR(ATR) $\tilde{\nu}_{\text{CO}}$: 2015, 1948, 1899 and 1884 cm^{-1}

[W(PN) $_2$ (CO) $_2$] (22)

In a *J*-Young NMR-tube PN ligand (113.0 mg, 0.35 mmol) and [W(CO) $_6$] (52.0 mg, 0.15 mmol) were weighed together and 0.7 mL of dry THF- d_8 were added. The tube was remained under UV-light for two weeks, opening the cap shortly from time to time to release the CO overpressure in the solution. The dark brown solution was transferred to a Schlenk flask. The solvent was evaporated and the black powder was fixed on silica. A 9 cm high column (fritt) was prepared under argon and run with EtOAc:P.Eth 1:1. The last fraction (dark brown) was collected, the solvent was evaporated and a black shiny powder was obtained. Yield: 21%, 28 mg.

^1H NMR (401 MHz, THF- d_8): $\delta = 6.70$ - 6.77 (m, 1H, H9), 7.22 - 7.34 (m, 2H, H18/H22), 7.34 - 7.48 (m, 5H, H13/15/19/21), 7.64 - 7.71 (m, 1H, H8), 7.72 - 7.78 (m, 2H, H14/H20), 8.00 - 8.06 (m, 2H, H12/16), 8.14 - 8.23 (m, 1H, H2), 8.36 - 8.45 (m, 1H, H7), 8.64 - 8.67 (m, 1H, H4), 8.70 - 8.72 (m, 1H, H10) ppm.

$^{13}\text{C}\{^1\text{H}\}$ NMR (101 MHz, THF- d_8): $\delta = 119.0$ (t, $J = 5.0$ Hz), 122.7, 126.5, 126.7, 127.2, 128.1 (t, $J = 4.2$ Hz), 128.7 (d, $J = 7.6$ Hz), 131.1 (t, $J = 3.4$ Hz), 132.4 (t, $J = 6.9$ Hz), 136.6, 137.8, 141.4 (t, $J = 8.2$ Hz), 142.7, 147.0, 149.7 (t, $J = 11.4$ Hz), 156.1 (d, $J = 8.9$ Hz), 161.3 (t, $J = 9.7$ Hz), 208.8 (d, $J = 9.6$ Hz) ppm.

$^{31}\text{P}\{^1\text{H}\}$ NMR (162 MHz, THF- d_8): $\delta = 209.4$ (s, $^1J_{\text{P-W}} = 369.3$ Hz) ppm.

IR(ATR) $\tilde{\nu}_{\text{CO}}$: 1935, 1866 and 1805 cm^{-1}

X-ray crystal structure determinations

Compound 5: C $_{48}$ H $_{38}$ Cu $_2$ F $_{12}$ N $_4$ P $_4$, Fw = 1149.80, yellow needle, $0.60 \times 0.05 \times 0.05$ mm 3 , monoclinic, P2 $_1$ /n, a = 13.7840(1), b = 12.5322(1), c = 28.0620(3) Å, $\alpha = 90$, $\beta = 93.294(1)$, $\gamma = 90$, V = 4839.53(7) Å 3 , Z = 4, D $_x = 1.578$ g/cm 3 , $\mu = 3.097$ mm $^{-1}$. 53855 reflections were measured by using a Bruker Photon CMOS detector with a rotating anode (CuK α radiation; $\lambda = 1.54178$ Å) at a temperature of 100(2) K up to a resolution were $\theta_{\text{max}} = 67.896$. 8123 reflections were unique ($R_{\text{int}} = 0.080$). The structures were solved with SHELXL-2013 142 by using direct methods and refined with SHELXL-2013 142 on F^2 for all reflections. Non-hydrogen atoms were

refined with anisotropic displacement parameters. 633 parameters were refined without restraints. $R_1 = 0.1601$ for 7062 reflections with $I > 2s(I)$ $e\text{\AA}^3$, and $wR_2 = 0.3508$ for 8123 reflections, $S = 1.248$. Geometry calculations and checks for higher symmetry were performed with the PLATON program.¹⁴³

Compound 11: $C_{22}H_{16}AuClNP$, Fw = 557.75, red block, $0.31 \times 0.09 \times 0.08$ mm^3 , orthorhombic, $P2_12_1$, $a = 7.4160(5)$, $b = 19.3611(15)$, $c = 26.242(2)$ \AA , $\alpha = 90$, $\beta = 90$, $\gamma = 90$, $V = 3767.9(5)\text{\AA}^3$, $Z = 8$, $D_x = 1.966$ g/cm^3 , $\mu = 8.041$ mm^{-1} . 26543 reflections were measured by using a Bruker Photon CMOS Detector, D8 Venture diffractometer with a rotating anode (MoK α radiation; $\lambda = 0.71073$ \AA) at a temperature of 100(2) K up to a resolution were $\theta_{\text{max}} = 25.31$. 6826 reflections were unique ($R_{\text{int}} = 0.0410$). The structures were solved with SHELXL-2014/7¹⁴² by using direct methods and refined with SHELXL-2014/7¹⁴² on F^2 for all reflections. Non-hydrogen atoms were refined with anisotropic displacement parameters. 422 parameters were refined without restraints. $R_1 = 0.0329$ for 6380 reflections with $I > 2s(I)$ $e\text{\AA}^3$, and $wR_2 = 0.065$ for 6826 reflections, $S = 1.218$. Geometry calculations and checks for higher symmetry were performed with the PLATON program.¹⁴³

Compound 16: $C_{48}H_{36}N_2O_2P_2Rh_2Cl_6$, Fw = 1153.25, blue needle, $0.36 \times 0.03 \times 0.03$ mm^3 , monoclinic, $C 1 2/c 1$, $a = 18.5521(8)$, $b = 18.8373(8)$, $c = 13.0069(5)$ \AA , $\alpha = 90$, $\beta = 97.2910(19)$, $\gamma = 90$, $V = 4508.8(3)$ \AA^3 , $Z = 4$, $D_x = 1.699$ g/cm^3 , $\mu = 1.202$ mm^{-1} . 20347 reflections were measured by using a Bruker Photon CMOS detector with a rotating anode (MoK α radiation; $\lambda = 0.71073$ \AA) at a temperature of 100.04 K up to a resolution were $\theta_{\text{max}} = 25.12$. 4024 reflections were unique ($R_{\text{int}} = 0.048$). The structures were solved with SHELXL-2014/6¹⁴² by using direct methods and refined with SHELXL-2014/6¹⁴² on F^2 for all reflections. Non-hydrogen atoms were refined with anisotropic displacement parameters. 280 parameters were refined without restraints. $R_1 = 0.048$ for 3186 reflections with $I > 2s(I)$ $e\text{\AA}^3$, and $wR_2 = 0.136$ for 4024 reflections, $S = 1.080$. Geometry calculations and checks for higher symmetry were performed with the PLATON program.¹⁴³

Compound 17: $C_{25}H_{16}O_3NPFe$, Fw = 465.21, red platlet, $0.53 \times 0.08 \times 0.07$ mm^3 , monoclinic, $C2/c$, $a = 44.5179(17)$, $b = 13.1217(5)$, $c = 7.2157(3)$ \AA , $\alpha = 90$, $\beta = 95.209(2)$, $\gamma = 90$, $V = 4197.7(3)$ \AA^3 , $Z = 8$, $D_x = 1.472$ g/cm^3 , $\mu = 0.822$ mm^{-1} . 17015 reflections were measured by using a D8 Venture Bruker Photon CMOS detector with a rotating anode (MoK α radiation; $\lambda = 0.71073$ \AA) at a temperature of 100(2) K up to a resolution were $\theta_{\text{max}} = 26.468$. 4322 reflections were unique ($R_{\text{int}} = 0.108$). The structures were solved with SHELXL-2014/7¹⁴² by using direct methods and refined with SHELXL-2014/7¹⁴² on F^2 for all reflections. Non-hydrogen atoms were refined with anisotropic displacement parameters. 268 parameters were refined without restraints. $R_1 = 0.074$ for 2946 reflections with $I > 2s(I)$ $e\text{\AA}^3$, and $wR_2 = 0.172$ for 4322 reflections, $S = 1.093$. Geometry calculations and checks for higher symmetry were performed with the PLATON program.¹⁴³

Compound 20: $C_{62}H_{52}Fe_4N_2P_2O_9S_4$, Fw = 1382.64, Brown needle, $0.46 \times 0.02 \times 0.02$ mm^3 , triclinic, $P-1$, $a = 7.6186(2)$, $b = 15.8628(4)$, $c = 24.7357(7)$ \AA , $\alpha = 99.0281(1)$, $\beta = 93.6936(8)$, $\gamma = 99.1003(9)$, $V = 2913.41(13)$ \AA^3 , $Z = 2$, $D_x = 1.576$ g/cm^3 , $\mu = 1.235$ mm^{-1} . 49559 reflections were measured by using a D8 Venture Bruker Photon CMOS detector with a rotating anode (MoK α radiation; $\lambda = 0.71073$ \AA) at a temperature of 100(2) K up to a resolution were $\theta_{\text{max}} = 25.09^\circ$. 10320 reflections were unique ($R_{\text{int}} = 0.117$). The structures were solved with SHELXL-2014/7¹⁴² by using direct methods and refined with SHELXL-2014/7¹⁴² on F^2 for all reflections. Non-hydrogen atoms were refined with anisotropic displacement parameters. 736 parameters were refined without restraints. $R_1 = 0.0550$ for 7281 reflections with $I > 2s(I)$ $e\text{\AA}^3$, and $wR_2 = 0.1125$ for 10320 reflections, $S = 1.047$. Geometry calculations and checks for higher symmetry were performed with the PLATON program.¹⁴³

Compound 21: $C_{50}H_{40}Cl_2Fe_2N_2P_2O_2$, Fw = 1009.50, brown chunk, $0.41 \times 0.23 \times 0.13$ mm^3 , triclinic, $P-1$, $a = 10.8470(2)$, $b = 14.2551(3)$, $c = 14.6866(3)$ \AA , $\alpha = 100.815(1)$, $\beta = 14.2551(3)$,

$\gamma = 94.899(1)$, $V = 2219.71(8) \text{ \AA}^3$, $Z = 2$, $D_x = 1.510 \text{ g/cm}^3$, $\mu = 0.984 \text{ mm}^{-1}$. 41770 reflections were measured by using a D8 Venture Bruker Photon CMOS detector with a rotating anode (MoK α radiation; $\lambda = 0.71073 \text{ \AA}$) at a temperature of 100(2) K up to a resolution were $\theta_{\max} = 26.44$. 9121 reflections were unique ($R_{\text{int}} = 0.040$). The structures were solved with SHELXL-2014/7¹⁴² by using direct methods and refined with SHELXL-2014/7¹⁴² on F^2 for all reflections. Non-hydrogen atoms were refined with anisotropic displacement parameters. 559 parameters were refined without restraints. $R_1 = 0.054$ for 7886 reflections with $I > 2s(I) \text{ e\AA}^3$, and $wR_2 = 0.1368$ for 9121 reflections, $S = 1.042$. Geometry calculations and checks for higher symmetry were performed with the PLATON program.¹⁴³

Compound 22: $C_{47}H_{34}Cl_2N_2P_2O_2W$, Fw = 975.44, red rod, $0.21 \times 0.13 \times 0.09 \text{ mm}^3$, monoclinic, $P2_1/n$, $a = 11.0705(7)$, $b = 14.1569(7)$, $c = 26.7727(19) \text{ \AA}$, $\alpha = 90$, $\beta = 92.663(6)$, $\gamma = 90$, $V = 4191.4(4) \text{ \AA}^3$, $Z = 4$, $D_x = 1.546 \text{ g/cm}^3$, $\mu = 3.001 \text{ mm}^{-1}$. 30394 reflections were measured by using a Stoe IPDS 2T detector with a rotating anode (MoK α radiation; $\lambda = 0.71073 \text{ \AA}$) at a temperature of 200(2) K up to a resolution were $\theta_{\max} = 29.22$. 11222 reflections were unique ($R_{\text{int}} = 0.083$). The structures were solved with SHELXL-2013¹⁴² by using direct methods and refined with SHELXL-2013¹⁴² on F^2 for all reflections. Non-hydrogen atoms were refined with anisotropic displacement parameters. 506 parameters were refined without restraints. $R_1 = 0.046$ for 6451 reflections with $I > 2s(I) \text{ e\AA}^3$, and $wR_2 = 0.1057$ for 11222 reflections, $S = 0.861$. Geometry calculations and checks for higher symmetry were performed with the PLATON program.¹⁴³

2.5 References

- (1) Brèque, A.; Santini, C. C.; Mathey, F.; Fischer, J.; Mitschler, A. *Inorg. Chem.* **1984**, *23*, 3463.
- (2) Schmid, B.; Venanzi, L. M.; Albinati, A.; Mathey, F. *Inorg. Chem.* **1991**, *30* (25), 4693.
- (3) Schmid, B.; Venanzi, L. M.; Gerfin, T.; Gramlich, V.; Mathey, F. *Inorg. Chem.* **1992**, *31*, 5117.
- (4) de Krom, I.; Lutz, M.; Müller, C. *Dalton Trans.* **2015**, *44* (22), 10304.
- (5) Campos-Carrasco, A.; Broeckx, L. E. E.; Weemers, J. J. M.; Pidko, E. A.; Lutz, M.; Masdeu-Bultó, A. M.; Vogt, D.; Müller, C. *Chem. Eur. J.* **2011**, *17* (8), 2510.
- (6) Campos-Carrasco, A.; Pidko, E. A.; Masdeu-Bultó, A. M.; Lutz, M.; Spek, A. L.; Vogt, D.; Müller, C. *New J. Chem.* **2010**, *34* (8), 1547.
- (7) de Krom, I.; Broeckx, L. E. E.; Lutz, M.; Müller, C. *Chem. Eur. J.* **2013**, *19*, 3676.
- (8) De Krom, I.; Pidko, E. A.; Lutz, M.; Müller, C. *Chem. Eur. J.* **2013**, *19* (23), 7523.
- (9) Le Floch, P.; Mansuy, S.; Ricard, L.; Mathey, F.; Jutand, A.; Amatore, C. *Organometallics* **1996**, *15* (15), 3267.
- (10) Grätzel, M. *Inorg. Chem.* **2005**, *44* (20), 6841.
- (11) O'Regan, B.; Grätzel, M. *Nature* **1991**, *353* (6346), 737.
- (12) Balzani, V.; Juris, A. *Coord. Chem. Rev.* **2001**, *211* (1), 97.
- (13) Kober, E. M.; Meyer, T. J. *Inorg. Chem.* **1982**, *21* (11), 3967.
- (14) Juris, A.; Balzani, V.; Barigelletti, F.; Campagna, S.; Belser, P.; von Zelewsky, A. *Coord. Chem. Rev.* **1988**, *84*, 85.
- (15) Nazeeruddin, M. K.; Kay, A.; Rodicio, I.; Humphry-Baker, R.; Mueller, E.; Liska, P.; Vlachopoulos, N.; Graetzel, M. *J. Am. Chem. Soc.* **1993**, *115* (14), 6382.
- (16) Grätzel, M. *Acc. Chem. Res.* **2009**, *42* (11), 1788.
- (17) de Krom, I. 2-(2'-Pyridyl)-4,6-diphenylphosphinine: Synthesis, characterization, and reactivity of novel transition metal complexes based on aromatic phosphorus heterocycles. Ph.D. Dissertation, Technische Universiteit Eindhoven, 2015.
- (18) Müller, C.; Broeckx, L. E. E.; de Krom, I.; Weemers, J. J. M. *Eur. J. Inorg. Chem.* **2013**, *2013* (2), 187.
- (19) Loibl, A.; de Krom, I.; Pidko, E. A.; Weber, M.; Wiecko, J.; Müller, C. *Chem. Commun.* **2014**, *50* (64), 8842.
- (20) Kanter, H.; Dimroth, K. *Tetrahedron Lett.* **1975**, *16* (8), 541.
- (21) Shiotsuka, M.; Matsuda, Y. *Chem. Lett.* **1994**, (2), 351.
- (22) Le Floch, P.; Ricard, L.; Mathey, F. *Bull. Soc. Chim. Fr.* **1996**, *133*, 691.
- (23) Mézailles, N.; Le Floch, P.; Waschbüsch, K.; Ricard, L.; Mathey, F.; Kubiak, C. P. *J. Organomet. Chem.* **1997**, *541* (1-2), 277.
- (24) Müller, C.; Pidko, E. A.; Lutz, M.; Spek, A. L.; Vogt, D. *Chem. Eur. J.* **2008**, *14* (29), 8803.
- (25) Mao, Y.; Lim, K. M. H.; Li, Y.; Ganguly, R.; Mathey, F. *Organometallics* **2013**, *32* (12), 3562.
- (26) Roesch, P.; Nitsch, J.; Lutz, M.; Wiecko, J.; Steffen, A.; Müller, C. *Inorg. Chem.* **2014**, *53* (18), 9855.
- (27) Alemany, P.; Alvarez, S. *Inorg. Chem.* **1992**, *31* (21), 4266.
- (28) Fleischmann, M.; Welsch, S.; Peresyphkina, E. V.; Virovets, A. V.; Scheer, M. *Chem. eur. J.* **2015**, *21* (41), 14332.
- (29) Ghalib, M.; Jones, P. G.; Schulzke, C.; Sziebert, D.; Nyulászi, L.; Heinicke, J. W. *Inorg. Chem.* **2015**, *54* (5), 2117.
- (30) Greiser, T.; Weiss, E. *Chem. Ber.* **1978**, *111* (2), 516.
- (31) Heindl, C.; Peresyphkina, E. V.; Virovets, A. V.; Komarov, V. Y.; Scheer, M. *Dalton*

- Trans.* **2015**, *44* (22), 10245.
- (32) Mankad, N. P.; Harkins, S. B.; Antholine, W. E.; Peters, J. C. *Inorg. Chem.* **2009**, *48* (15), 7026.
- (33) Mankad, N. P.; Rivard, E.; Harkins, S. B.; Peters, J. C. *J. Am. Chem. Soc.* **2005**, *127* (46), 16032.
- (34) Rhee, Y. M.; Head-Gordon, M. *J. Am. Chem. Soc.* **2008**, *130* (12), 3878.
- (35) Perreault, D.; Drouin, M.; Michel, A.; Miskowski, V. M.; Schaefer, W. P.; Harvey, P. D. *Inorg. Chem.* **1992**, *31* (4), 695.
- (36) Dean, P. A. W.; Vittal, J. J.; Srivastava, R. S. *Can. J. Chem.* **1987**, *65*, 2628.
- (37) Del Zotto, A.; Di Bernardo, P.; Tolazzi, M.; Tomat, G.; Zanonato, P. *J. Chem. Soc. Dalton Trans.* **1993**, (20), 3009.
- (38) Di Bernardo, P.; Dolcetti, G.; Portanova, R.; Tolazzi, M.; Tomat, G.; Zanonato, P. *Inorg. Chem.* **1990**, *29* (15), 2859.
- (39) Saboonchian, V.; Wilkinson, G.; Hussain-Bates, B.; Hursthouse, M. B. *Polyhedron* **1991**, *10* (7), 737.
- (40) Moores, A.; Mezailles, N.; Maigrot, N.; Ricard, L.; Mathey, F.; le Floch, P. *Eur. J. Inorg. Chem.* **2002**, 2034.
- (41) Adjedje, V. Coordination Chemistry of 2-(2-Pyridyl)-4,6-diphenyl- λ^3 -Phosphinine with Gold (I) and Silver (I), Bachelor thesis, Freie Universität Berlin, Berlin, 2015.
- (42) Clendenning, S. B.; Hitchcock, P. B.; Lawless, G. a.; Nixon, J. F.; Tate, C. W. *J. Organomet. Chem.* **2010**, *695* (5), 717.
- (43) Mallissery, S. K.; Nieger, M.; Gudat, D. *Z. Anorg. Allg. Chem.* **636** (7), 1354.
- (44) Mézailles, N.; Avarvari, N.; Maigrot, N.; Ricard, L.; Mathey, F.; Le Floch, P.; Cataldo, L.; Berclaz, T.; Geoffroy, M. *Angew. Chem. Int. Ed.* **1999**, *38* (21), 3194.
- (45) Mézailles, N.; Ricard, L.; Mathey, F.; Le Floch, P. *Eur. J. Inorg. Chem.* **1999**, *1999* (12), 2233.
- (46) Stott, J.; Bruhn, C.; Siemeling, U. *Z. Naturforsch. B* **2013**, *68* (8), 2.
- (47) Moussa, J.; Chamoreau, L. M.; Amouri, H. *RSC Adv.* **2014**, *4* (23), 11539.
- (48) Fürstner, A.; Davies, P. W. *Angew. Chem. Int. Ed.* **2007**, *46* (19), 3410.
- (49) Rudolph, M.; Hashmi, A. S. K. *Chem. Soc. Rev.* **2012**, *41* (6), 2448.
- (50) Teller, H.; Corbet, M.; Mantilli, L.; Gopakumar, G.; Goddard, R.; Thiel, W.; Fürstner, A. *J. Am. Chem. Soc.* **2012**, *134* (37), 15331.
- (51) Caracelli, I.; Zukerman-Schpector, J.; Tiekink, E. R. T. *Gold Bull.* **2013**, *46* (2), 81.
- (52) Leznoff, D. B.; Xue, B. Y.; Batchelor, R. J.; Einstein, F. W.; Patrick, B. O. *Inorg. Chem.* **2001**, *40* (23), 6026.
- (53) *Modern Supramolecular Gold Chemistry: Gold-Metal Interactions and Applications*; Laguna, A., Ed.; Wiley-VCH, 2008.
- (54) Herrero-Gómez, E.; Nieto-Oberhuber, C.; López, S.; Benet-Buchholz, J.; Echavarren, A. M. *Angew. Chem. Int. Ed.* **2006**, *45* (33), 5455.
- (55) Lavallo, V.; Frey, G. D.; Kousar, S.; Donnadiou, B.; Bertrand, G. *PNAS.* **2007**, *104* (34), 13569.
- (56) Ni, Q.-L.; Jiang, X.-F.; Huang, T.-H.; Wang, X.-J.; Gui, L.-C.; Yang, K.-G. *Organometallics* **2012**, *31* (6), 2343.
- (57) Tiekink, E. R. T.; Zukerman-Schpector, J. *CrystEngComm* **2009**, *11* (7), 1176.
- (58) Lehmkuhl, H.; Paul, R.; Mynott, R. *Liebigs Ann.* **1981**, *1981* (6), 1139.
- (59) Trauner, H.; Le Floch, P.; Lefour, J.-M.; Ricard, L.; Mathey, F. *Synthesis* **1995**, *1995* (06), 717.
- (60) Elschenbroich, C.; Nowotny, M.; Behrendt, A.; Massa, W.; Wocadlo, S. *Angew. Chem.* **1992**, *104* (10), 1388.
- (61) Breit, B.; Winde, R.; Mackewitz, T.; Paciello, R.; Harms, K. *Chem. Eur. J.* **2001**, *7* (14), 3106.

- (62) Elschenbroich, C.; Nowotny, M.; Behrendt, A.; Harms, K.; Wocadlo, S.; Pebler, J. *J. Am. Chem. Soc.* **1994**, *116* (14), 6217.
- (63) Knoch, F.; Kremer, F.; Schmidt, U.; Zenneck, U.; Le Floch, P.; Mathey, F. *Organometallics* **1996**, *15*, 2713.
- (64) Le Floch, P.; Knoch, F.; Kremer, F.; Mathey, F.; Scholz, J.; Scholz, W.; Thiele, K.-H.; Zenneck, U. *Eur. J. Inorg. Chem.* **1998**, *1998* (1), 119.
- (65) Nief, F.; Fischer, J. *Organometallics* **1986**, *5* (5), 877.
- (66) Waschbüch, K.; Le Floch, P.; Ricard, L.; Mathey, F. *Chem. Ber.* **1997**, *130* (7), 843.
- (67) Rezaei Rad, B.; Chakraborty, U.; Mühlendorf, B.; Sklorz, J. A. W.; Bodensteiner, M.; Müller, C.; Wolf, R. *Organometallics* **2015**, *34* (3), 622.
- (68) Eggers, K. Darstellung, Reaktivität und Elektrochemie von Phosphinin- und Triphosphininmetall- π -Komplexen. Ph. D. Dissertation, Friedrich-Alexander-Universität Erlangen-Nürnberg, 2000.
- (69) Bolm, C.; Legros, J.; Le Pailh, J.; Zani, L. *Chem. Rev.* **2004**, *104* (12), 6217.
- (70) Frühauf, H.-W.; Grevels, F.-W.; Landers, A. *J. Organomet. Chem.* **1979**, *178*, 349.
- (71) Frühauf, H.-W.; Gotthelf, W. *Chem. Ber.* **1982**, *115*, 1070.
- (72) Frühauf, H.-W.; Seils, F.; Romao, M. J.; Goddard, R. *J. Angew. Chem.* **1983**, *12*, 1014.
- (73) Frühauf, H. W.; Pein, I.; Seils, F. *Organometallics* **1987**, *6* (8), 1613.
- (74) Calderazzo, F.; Falaschi, S.; Marchetti, F.; Pampaloni, G. *J. Organomet. Chem.* **2002**, *662*.
- (75) Cotton, F. A.; Troup, J. M. *J. Am. Chem. Soc.* **1974**, *96* (4), 1233.
- (76) Dela Varga, M.; Costa, R.; Reina, R.; Nuñez, A.; Ángel Maestro, M.; Mahía, J. J. *Organomet. Chem.* **2003**, *677* (1-2), 101.
- (77) van Dijk, H. K.; Stufkens, D. J.; Oskam, A. *J. Org. Chem.* **1988**, *340*, 227.
- (78) Frühauf, H.-W. *J. Chem. Res.* **1983**, 218.
- (79) Frühauf, H.-W. *J. Chem. Res.* **1983**, 216.
- (80) Bauer, I.; Knölker, H.-J. *Chem. Rev.* **2015**, *115* (9), 3170.
- (81) Güttlich, P.; Hauser, A.; Spiering, H. *Angew. Chem. Int. Ed.* **1994**, *33* (20), 2024.
- (82) Létard, J.-F. *J. Mater. Chem.* **2006**, *16* (26), 2550.
- (83) Yu, S.; Chow, G. M. *J. Mater. Chem.* **2004**, *14* (18), 2781.
- (84) Borg, S. J.; Behrsing, T.; Best, S. P.; Razavet, M.; Liu, X.; Pickett, C. J. *J. Am. Chem. Soc.* **2004**, *126* (51), 16988.
- (85) Boyke, C. A.; Rauchfuss, T. B.; Wilson, S. R.; Rohmer, M.; Be, M.; Pasteur, L. *J. Am. Chem. Soc.* **2004**, *126*, 15151.
- (86) Cheah, M. H.; Best, S. P. *Eur. J. Inorg. Chem.* **2011**, *2011* (7), 1128.
- (87) Cloirec, A. Le; Davies, S. C.; Evans, D. J.; Hughes, D. L.; Pickett, C. J.; Best, S. P.; Borg, S. *Chem. Commun.* **1999**, *22*, 2285.
- (88) Darensbourg, M. Y.; Weigand, W. *Eur. J. Inorg. Chem.* **2011**, 917.
- (89) Darensbourg, M. Y.; Weigand, W. *Eur. J. Inorg. Chem.* **2011**, *7*, 994.
- (90) Derossi, S.; Becker, R.; Li, P.; Hartl, F.; Reek, J. N. H. *Dalton Trans.* **2014**, *43*, 8363.
- (91) DuBois, D. L.; Morris Bullock, R. *Eur. J. Inorg. Chem.* **2011**, 1017.
- (92) Filippi, G.; Arrigoni, F.; Bertini, L.; De Gioia, L.; Zampella, G. *Inorg. Chem.* **2015**, *54*, 9529.
- (93) Galinato, M. G. I.; Whaley, C. M.; Roberts, D.; Wang, P.; Lehnert, N. *Eur. J. Inorg. Chem.* **2011**, *2011* (7), 1147.
- (94) Gloaguen, F.; Lawrence, J. D.; Schmidt, M.; Wilson, S. R.; Rauchfuss, T. B. *J. Am. Chem. Soc.* **2001**, *123* (50), 12518.
- (95) Harb, M. K.; Apfel, U.-P.; Sakamoto, T.; El-khateeb, M.; Weigand, W. *Eur. J. Inorg. Chem.* **2011**, *2011* (7), 986.
- (96) Koray, A. R.; L. Ziegler, M. *J. Organomet. Chem.* **1979**, *169* (3), C34.
- (97) Lansing, J. C.; Camara, J. M.; Gray, D. E.; Rauchfuss, T. B. *Organometallics* **2014**, *33*,

- 5897.
- (98) Li, C.-G.; Li, Y.-F.; Shang, J.-Y.; Lou, T.-J. *Transition Met. Chem.* **2014**, *39* (4), 373.
- (99) Li, C.-G.; Xue, F.; Cui, M.-J.; Shang, J.-Y. *J. Coord. Chem.* **2015**, *68* (9), 1559.
- (100) Li, C.-G.; Xue, F.; Cui, M.-J.; Shang, J.-Y. *J. Cluster. Sci.* **2014**, *25* (6), 1641.
- (101) Li, C.-G.; Xue, F.; Cui, M.-J.; Shang, J.-Y.; Lou, T.-J. *Transition Met. Chem.* **2015**, *40* (1), 47.
- (102) Liu, C.; Peck, J. N. T.; Wright, J. a.; Pickett, C. J.; Hall, M. B. *Eur. J. Inorg. Chem.* **2011**, 1080.
- (103) Liu, Y.-C.; Lee, C.-H.; Lee, G.-H.; Chiang, M.-H. *Eur. J. Inorg. Chem.* **2011**, *2011* (7), 1155.
- (104) Lounissi, S.; Capon, J.-F.; Gloaguen, F.; Matoussi, F.; Pétilion, F. Y.; Schollhammer, P.; Talarmin, J. *Chem. Commun.* **2011**, *47* (3), 878.
- (105) Lyon, E.; Georgakaki, I.; Reibenspies, J.; Darensbourg, M. *Angew. Chem. Int. Ed.* **1999**, *38* (21), 3178.
- (106) Matthews, S. L.; Heinekey, D. M. *Inorg. Chem.* **2011**, *50* (17), 7925.
- (107) Mejia-Rodriguez, R.; Chong, D.; Reibenspies, J. H.; Soriaga, M. P.; Darensbourg, M. Y. *J. Am. Chem. Soc.* **2004**, *126* (38), 12004.
- (108) Onoda, A.; Hayashi, T. *Curr. Opin. Chem. Biol.* **2015**, *25*, 133.
- (109) Petro, B. J. Preparation And Characterization of Hydrogenase Enzyme Active Site-inspired Catalysts: The effects of Alkyl Bulk and Conformer Strains as Studied by Photoelectron Spectroscopy, Electrochemistry, and Computational Methods. Ph. D. Dissertation, University of Arizona, Tucson, 2009.
- (110) Reisner, E. *Eur. J. Inorg. Chem.* **2011**, *7*, 1005.
- (111) Roy, S.; Nguyen, T.-A. D.; Gan, L.; Jones, A. K. *Dalton Trans.* **2015**, *44* (33), 14865.
- (112) Schmidt, M.; Contakes, S. M.; Rauchfuss, T. B. *J. Am. Chem. Soc.* **1999**, *121* (41), 9736.
- (113) Seyferth, D.; Henderson, R. S.; Song, L. C. *Organometallics* **1982**, *1* (1), 125.
- (114) Seyferth, D.; Henderson, R. S.; Song, L.-C. *J. Organomet. Chem.* **1980**, *192* (1), C1.
- (115) Stiebritz, M. T.; Finkelman, A. R.; Reiher, M. *Eur. J. Inorg. Chem.* **2011**, *2011*, 1163.
- (116) Streich, D.; Karnahl, M.; Astuti, Y.; Cady, C. W.; Hammarström, L.; Lomoth, R.; Ott, S. *Eur. J. Inorg. Chem.* **2011**, *2*, 1106.
- (117) Thauer, R. K. *Eur. J. Inorg. Chem.* **2011**, *2011* (7), 919.
- (118) Vashi, P. *Eur. J. Inorg. Chem.* **2011**, 915.
- (119) Wang, W.; Rauchfuss, T. B.; Zhu, L.; Zampella, G. *J. Am. Chem. Soc.* **2014**, *136* (15), 5773.
- (120) Winter, A.; Zsolnai, L.; Huttner, G. *Z. Naturforsch. B* **1982**, *37b*, 1430.
- (121) Works, C. F. *J. Chem. Educ.* **2007**, *84* (5), 836.
- (122) Zaffaroni, R.; Rauchfuss, T. B.; Fuller, A.; De Gioia, L.; Zampella, G. *Organometallics* **2013**, *32* (1), 232.
- (123) Zhao, P.; Li, X.; Liu, Y.; Liu, Y. *J. Coord. Chem.* **2014**, *67* (5), 766.
- (124) Zhao, P.-H.; Wang, W.-T.; Liu, Y.-F.; Liu, Y.-Q. *Transition Met. Chem.* **2014**, *39* (5), 501.
- (125) Zhao, X.; Georgakaki, I. P.; Miller, M. L.; Yarbrough, J. C.; Darensbourg, M. Y. *J. Am. Chem. Soc.* **2001**, *123* (39), 9710.
- (126) Zheng, D.; Wang, M.; Wang, N.; Cheng, M.; Sun, L. *Inorg. Chem.* **2015**, *55*(2), 411.
- (127) Zheng, D.; Wang, N.; Wang, M.; Ding, S.; Ma, C.; Darensbourg, M. Y.; Hall, M. B.; Sun, L. *J. Am. Chem. Soc.* **2014**, *136* (48), 16817.
- (128) van der Vlugt, J. I.; Rauchfuss, T. B.; Whaley, C. M.; Wilson, S. R. *J. Am. Chem. Soc.* **2005**, *127* (46), 16012.
- (129) Matthews, S. L.; Heinekey, D. M. *Inorg. Chem.* **2010**, *49* (21), 9746.
- (130) Gao, W.; Sun, J.; Li, M.; Åkermark, T.; Romare, K.; Sun, L.; Åkermark, B. *Eur. J. Inorg. Chem.* **2011**, *2011* (7), 1100.

- (131) Wright, J. A.; Pickett, C. J. *Eur. J. Inorg. Chem.* **2011**, 2011 (7), 1033.
- (132) Wang, W.; Nilges, M. J.; Rauchfuss, T. B.; Stein, M. *J. Am. Chem. Soc.* **2013**, 135 (9), 3633.
- (133) Beaume, L.; Clémancey, M.; Blondin, G.; Greco, C.; Pétillon, F. Y.; Schollhammer, P.; Talarmin, J. *Organometallics* **2014**, 33 (22), 6290.
- (134) Jablonskytė, A.; Webster, L. R.; Simmons, T. R.; Wright, J. a; Pickett, C. J. *J. Am. Chem. Soc.* **2014**, 136 (37), 13038.
- (135) Cui, H.-H.; Wu, N.-N.; Wang, J.-Y.; Hu, M.-Q.; Wen, H.-M.; Chen, C.-N. *J. Organomet. Chem.* **2014**, 767, 46.
- (136) Ghosh, S.; Hogarth, G.; Hollingsworth, N.; Holt, K. B.; Kabir, S. E.; Sanchez, B. E. *Chem. Commun.* **2014**, 50 (8), 945.
- (137) Adam, F. I.; Hogarth, G.; Richards, I. *J. Organomet. Chem.* **2007**, 692 (18), 3957.
- (138) Nicolet, Y.; de Lacey, A. L.; Vernède, X.; Fernandez, V. M.; Hatchikian, E. C.; Fontecilla-Camps, J. C. *J. Am. Chem. Soc.* **2001**, 123 (8), 1596.
- (139) Janiak, C. *J. Chem. Soc. Dalton Trans.* **2000**, 21, 3885.
- (140) Pfeifer, G.; Ribagnac, P.; Le Goff, X.-F.; Wiecko, J.; Mézailles, N.; Müller, C. *Eur. J. Inorg. Chem.* **2015**, 240.
- (141) Müller, C.; Wasserberg, D.; Weemers, J. J. M.; Pidko, E. A.; Hoffmann, S.; Lutz, M.; Spek, A. L.; Meskers, S. C. J.; Janssen, R. A. J.; van Santen, R. A.; Vogt, D. *Chem. Eur. J.* **2007**, 13 (16), 4548.
- (142) Sheldrick, G. M.; *Acta Crystallogr. Sect. A.* **2008**, 64, 112.
- (143) Spek, A. L.; *Acta Crystallogr. Sect. D.* **2009**, 65, 148.

Chapter 3

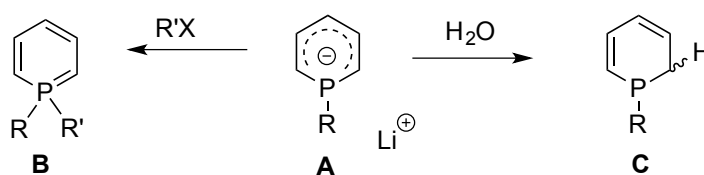
Synthesis, Reactivity and Coordination Chemistry of Pyridyl-Substituted λ^4 -Phosphinines

3	λ^4-Phosphinines	81
3.1	Introduction.....	81
3.2	Coordination chemistry of λ^4-phosphinines.....	83
3.3	Results and discussion	85
3.4	Conclusions	103
3.5	Experimental part.....	104
	General remarks.....	104
	1-Ferrocenyl-(2,6-diphenyl-4-(p-tolyl))-cyclophosphahexadienyllithium (17).....	104
	1-Methyl-4,6-triphenyl-2-(2'pyridyl)-phosphacyclohexadienyllithium (18).....	105
	1,4,6-triphenyl-2-(2'pyridyl)-phosphacyclohexadienyllithium (19)	105
	1-Ferrocenyl- (2-Pyridyl)-4,6-diphenylphosphinine (20)	106
	[(cod)Rh(η^1 -19)] (25)	106
	[(cod)Rh(η^1 -20)] (26)	107
	[(cod)Rh(η^1 -(H)20)] (27)	107
	[(cod) ₂ Rh ₂ (η^1 - η^5 -20)] (28).....	108
	[(cod) ₂ Rh ₂ (η^1 - η^6 -17)] (29).....	108
	X-ray crystal structure determinations.....	109
3.6	References	111

3 λ^4 -Phosphinines

3.1 Introduction

The difference in electronegativity between carbon, phosphorus and nitrogen (Pauling electronegativities: 2.2 for P, 2.5 for C, and 3.0 for N)¹ makes the charge distribution in the phosphinine- and pyridine- heterocycle opposite. Hence, the N atom in pyridines acts as a nucleophile, whereas phosphinines can undergo electrophilic attack *via* the phosphorus atom.² Therefore strong nucleophiles such as Grignard-reagents or organolithium compounds can alkylate or arylate the phosphorus atom of phosphinines, which gives a new class of molecules: λ^4 -phosphinines. Märkl *et al.* prepared λ^4 -1-alkyl- or 1-aryl-2,4,6-triphenylphosphinine anions (A, scheme 3.1) and proved their reactivity towards water and organic halides to give 1-alkyl- or 1-aryl-1,2-dihydrophosphinines (C) or 1,1-disubstituted phosphinines (B), respectively.³⁻⁵



Scheme 3.1 Reactivity of λ^4 -phosphinine anions towards water and organic halides

Ashe III investigated the reaction of MeLi with the unsubstituted phosphinine **1.2**. The ^1H and $^{13}\text{C}\{^1\text{H}\}$ NMR spectroscopic analysis shows that carbons and protons in 2-, 4-, and 6-positions of the ring (figure 3.1) are much more shielded than those in 3- and 5- positions. This implies that structure **3.2** is more realistic than **3.1** to describe the actual electronic situation of these anions with the electron charge largely localized on 2-, 4-, and 6-positions. However, the name λ^4 -phosphinines is used as an easier way to differentiate $\lambda^4\sigma^3$ -phosphinines from $\lambda^3\sigma^2$ - and $\lambda^5\sigma^4$ -phosphinines. Also, the fact that the chemical shifts of carbons and protons 3 and 5 in the anionic structure are very similar to the atoms in the same positions of the conjugate acid (**3.3**), means that the phosphorus lone pair does not interact with the delocalized electrons of the π -system.⁶

In 2003, Le Floch *et al.* discussed the first crystallographic characterization of the λ^4 -phosphinine lithium salt **3.4**, in which the lithium cation is coordinated in an η^5 - fashion, while

the phosphorus atom is strongly pyramidalized, pointing out of the plane formed by the five carbon atoms of the heterocycle (figure 3.2).⁷

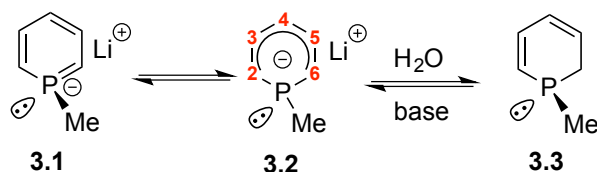


Figure 3.1 Tautomeric forms of 1-methyl-phosphacyclohexadienyl anion and its protonated form **3.3**

An easy way to access a library of anionic phosphinines can be achieved by reacting interesting and more sterically demanding organolithium reagents such as CH_2PyLi or enantiomerically pure lithium mentholate. The latter leads to chiral derivatives of λ^4 -phosphinines.⁸ The preparation of this class of compounds offers a way to fine-tune the steric and electronic properties of sp^3 -hybridized phosphorus species and thus the careful design of ligands for catalytic processes. A short review on the coordination studies of λ^4 -phosphinine anions will be described below (see figure 3.3).

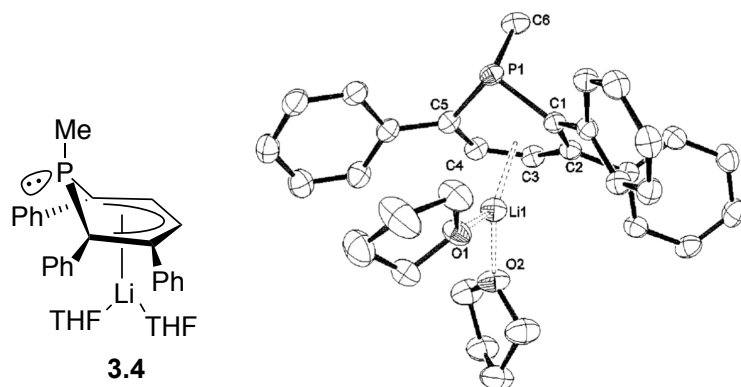


Figure 3.2 Schematic structure (left) and molecular structure in the crystal (right) of 1-methyl-2,5,6-triphenyl-phosphacyclohexadienyl lithium **3.4**

3.2 Coordination chemistry of λ^4 -phosphinines

This class of ligands can potentially coordinate to metal centers in different coordination modes (figure 3.3): *Via* the delocalized π -system of the heterocyclic ring with a hapticity from 2 to 5; directly *via* the phosphorus atom in a σ -coordination mode; and *via* a combination of the latter two, as shown in figure 3.3.

Märkl prepared a ferrocene-like compound starting from FeCl_2 and 1-methyl- (3.5, figure 3.4) or 1-phenyl-2,4,6-triphenylphosphacyclohexadienyl lithium.⁹ Dimroth *et al.* studied these compounds in more detail showing their open ferrocene-like structures and their solubility in water despite of their hydrophobic substituents.¹⁰ The 4-*tert*-butyl analogue was structurally characterized later by Massa *et al.* The molecular structure in the crystal shows a gauche-eclipsed conformation and two phosphinine rings coordinated through 5 carbons each in a η^5 -fashion with a mean Fe-C distance of 2.16 Å, and a Fe-P distance of 2.91 Å. All the C-C distances in the almost planar part of the heterocycle are very similar with a mean value of 1.41 Å.¹¹

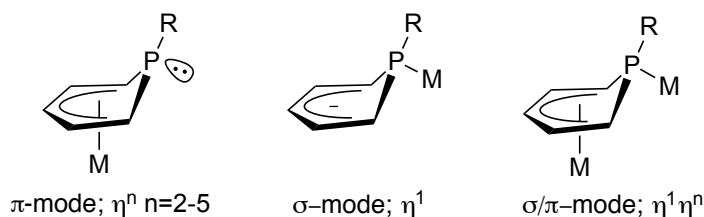


Figure 3.3 Possible coordination modes for λ^4 -phosphinines

Le Floch reported on the η^5 -rhodium complex 3.6. It turned out to be a promising catalyst in the hydroformylation of styrene and cyclohexene, giving high conversion and turnover frequencies under mild conditions with low catalyst loading. The hydroformylation of styrene occurred with a high regioselectivity (93/7) in favor of the branched isomer. The complex also catalyzed the transformation of 2,3-dimethyl-2-butene into 3,4-dimethylpentanal through a tandem isomerization/hydroformylation process.¹² Complexes 3.7 of Pd and Pt were obtained, in which the ligand is coordinated to the $[\text{MCl}(\text{PPh}_3)]$ ($\text{M} = \text{Pd}, \text{Pt}$) fragment through the P-C double bond in an η^2 -fashion.¹³

The same group later reported on phosphinine **3.8**, which bears two phosphine sulfide groups on the C atom in α -position to the P atom of the hetrocycle (SPS).¹⁴ When reacted with $[\text{Pd}(\text{cod})\text{Cl}_2]$, internal attack of a Cl^- to the electrophilic phosphorus atom affords the corresponding λ^4 -phosphinine anion coordinated to the metal fragment, which can then react with methanol to form complex **3.9**.¹⁵ Heterodonor-functionalized SPS λ^4 -phosphinines were also synthesized and they preferentially formed metal complexes, in which the coordination takes place through the phosphorus lone pair and not *via* the π -system. For example, the SPS-Rh^I complex **3.10**, which can activate small molecules such as CO , O_2 , CO_2 , CS_2 , and SO_2 ,¹⁶ or the uranium complex **3.11**.¹⁷ A very interesting feature of SPS anions is their flexibility to stabilize a wide range of geometries in metal complexes, ranging from tetrahedral, square planar to trigonal bipyramidal, to octahedral.¹⁸

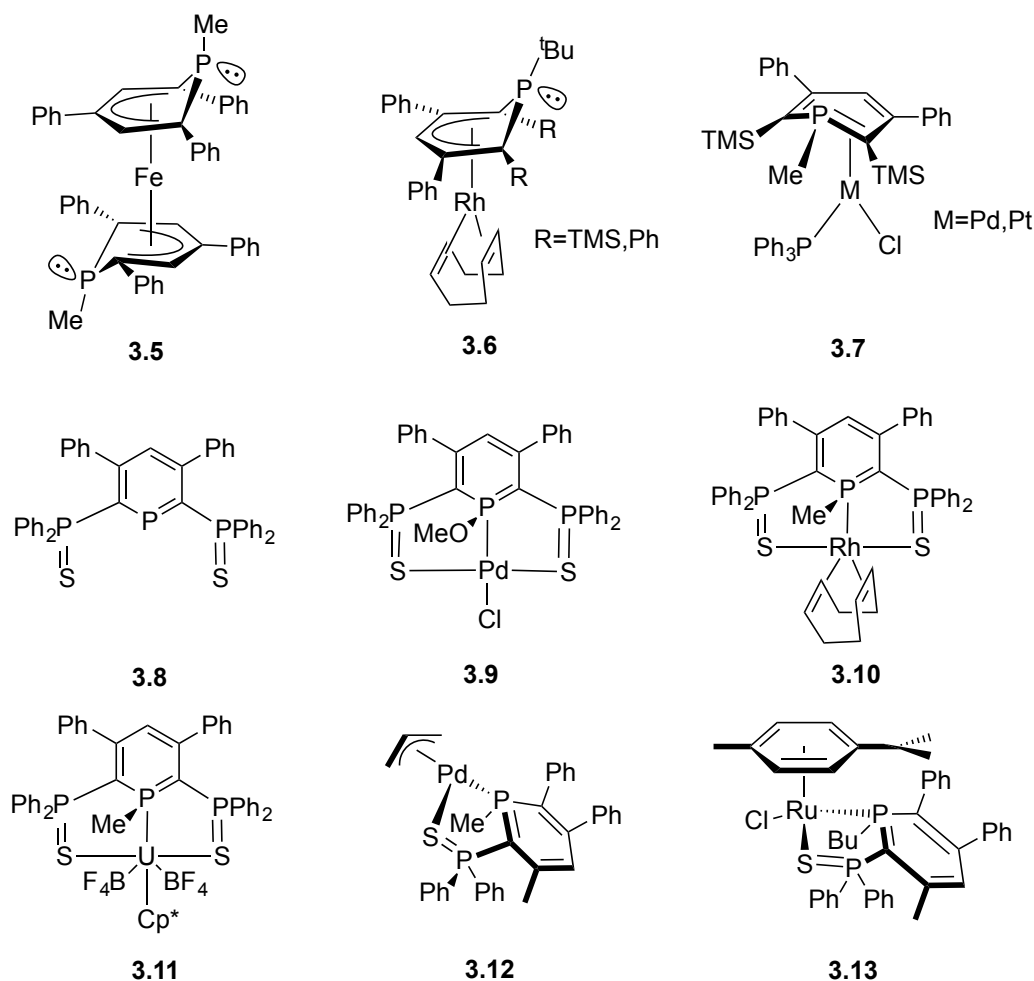


Figure 3.4 λ^4 -phosphinine complexes reported in literature

A *t*Bu-P,S-bidentate phosphinine anion was reported, which upon coordination to $[\text{PdCl}_2(\eta^3\text{-C}_3\text{H}_5)_2]$ affords complex **3.12** as a mixture of diastereoisomers. It was applied as catalyst in the Suzuki–Miyaura cross-coupling reaction between aryl bromides and pinacolborane to yield the corresponding arylboronic esters with a TON of up to 799000. Me-P,S-bidentate phosphinine anion coordinates to ruthenium to afford complex **3.13** also as a mixture of diastereoisomers. The complex shows catalytic activity in hydrogenation reactions of ketones with acceptable conversions albeit long reaction times with TONs of up to 200.¹⁹

3.3 Results and discussion

In this section, the results obtained from the synthesis, reactivity and coordination chemistry of λ^4 -PN phosphinines will be discussed. The NMR assignment for the signals of the ligand, as well as the X-ray analysis follows the numbering scheme depicted in figure 3.5.

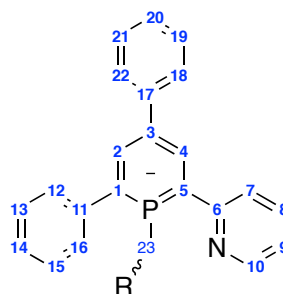


Figure 3.5 Numbering scheme for the NMR signal assignment

The first carbon atom from the alkyl or aryl moiety attached to the P atom is assigned with the number 23. According to the substituent, the numbering follows along the group functionality. Hydrogen atoms have the same numbers as the carbon atoms attached to them. Information obtained from the atoms in the heteroatomic rings is the most valuable and interesting regarding the coordination chemistry and basically the discussion will evolve around these.

So far, there is no example in literature of a pyridyl-substituted λ^4 -phosphinine, so it was of interest to study the reactivity and coordination chemistry of **PN** phosphinine λ^4 -anions. For this purpose 2,4-diphenyl-6-tolyl-phosphinine **16** and the pyridyl functionalized phosphinine **1** were reacted with different organolithium reagents and the obtained lithium salts were coordinated to different transition metals.

Under the general scheme shown below, different λ^4 -phosphinines were prepared. Upon reaction of the neutral ligands **1** or **16** with the corresponding organolithium species in THF an immediate change in color of the solutions occurs from orange to dark green or violet. According to the $^{31}\text{P}\{^1\text{H}\}$ NMR spectra of the reaction mixtures, full conversions were achieved, both at $T = -78\text{ }^\circ\text{C}$ as well as at room temperature, showing one singlet at higher fields at around $\delta = -70\text{ ppm}$ (see figure 3.6). The significant variation in chemical shift from the neutral ligand ($\delta = 187.4\text{ ppm}$ for **1** and $\delta = 182.3\text{ ppm}$ for **16**) is higher than 246 ppm and suggests a disruption of the aromatic system due to a strong pyramidalization of the phosphorus atom. The chemical shifts of the products are more similar to phosphines with a formal sp^3 -hybridization (PMe_3 : $^{31}\text{P}\{^1\text{H}\}$ NMR, $\delta = -60\text{ ppm}$).

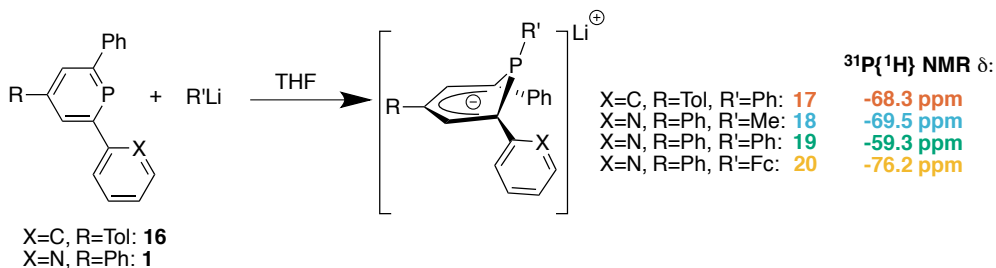


Figure 3.6 Synthesis of lithium salts of λ^4 -phosphinine anions

Although in literature only one signal in the $^{31}\text{P}\{^1\text{H}\}$ NMR spectra of anionic λ^4 -phosphinines was discussed, they can form two different stereoisomers as shown in figure 3.7, which would give two different $^{31}\text{P}\{^1\text{H}\}$ NMR signals. If two groups of chemically equivalent nuclei are exchanged by an intramolecular process, the NMR spectrum is a function of the difference in their resonance frequencies, $\nu_A - \nu_B = \Delta\nu$, and of the rate of exchange, k .²⁰

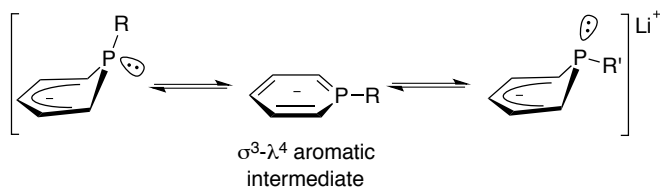


Figure 3.7 Possible configurations of λ^4 -phosphinine anions, interchangeable through inversion at the phosphorus atom

For compound **17** only one sharp signal in the $^{31}\text{P}\{^1\text{H}\}$ NMR spectrum even at $T = -100\text{ }^\circ\text{C}$ was also found, but for **18**, **19**, and **20** the single $^{31}\text{P}\{^1\text{H}\}$ NMR signal at room temperature splits at very low temperatures into two singlets in different ratios (figure 3.8).

The coalescence temperature of these two NMR signals in a 400 MHz NMR spectrometer (162 MHz for ^{31}P) is $T = -94\text{ }^\circ\text{C}$ for **18** (Me-PN), $T = -79\text{ }^\circ\text{C}$ for **19** (Ph-PN), and $T = -81\text{ }^\circ\text{C}$ for **20** (Fc-PN). Following equation 1, K_{T_c} (equilibrium constant at coalescence temperature) was estimated, and with equation 2, the ΔG^\ddagger for the inversion barrier was calculated. The results are shown in table 3.1.

$$K_{T_c} = \frac{\pi}{\sqrt{2}} |v_A - v_B| \quad \text{eq. 1}$$

$$\Delta G^\ddagger = RT_c \cdot \ln \frac{RT_c \sqrt{2}}{\pi N_A h |v_A - v_B|} = RT_c \left[22.96 + \ln \left(\frac{T_c}{\Delta v} \right) \right] \quad \text{eq. 2}$$

The energy barriers for inversion differ slightly from each other. The method used to calculate the data ($^{31}\text{P}\{^1\text{H}\}$ variable temperature NMR) is not accurate enough to explain the observed trend, where $\Delta G^\ddagger(\mathbf{19}) > \Delta G^\ddagger(\mathbf{20}) > \Delta G^\ddagger(\mathbf{18})$. In general, it has been established for phosphines that the bulk of the substituents at phosphorus, as well as the type of substituents (alkyl or aryl) affect the magnitude of the inversion barrier; Bulky substituents and alkyl groups result in higher ΔG^\ddagger .²¹⁻²³ Taking this into account, $\Delta G^\ddagger(\mathbf{20})$ was expected to be higher than $\Delta G^\ddagger(\mathbf{19})$. Nevertheless, the energy barriers are in the same range of those for acyclic phosphines.^{24,25}

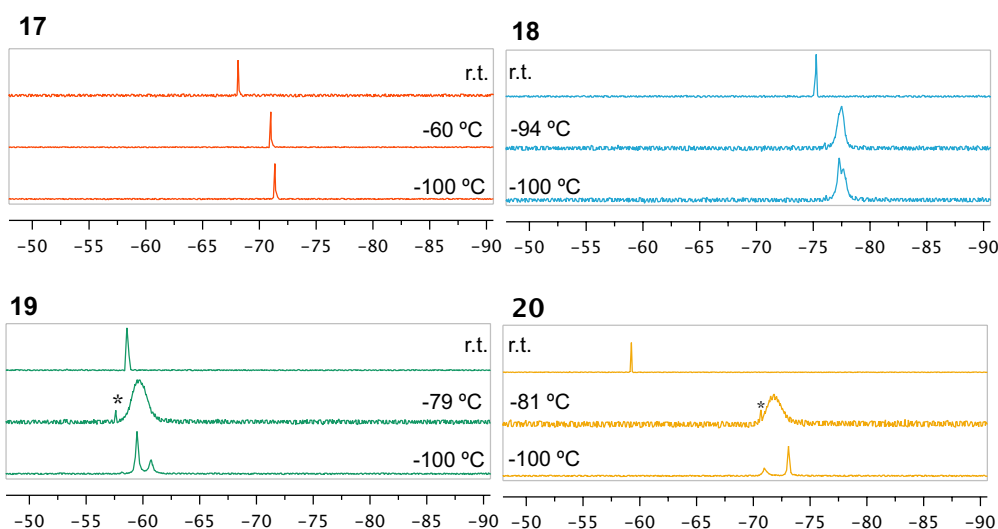


Figure 3.8 Variable temperature $^{31}\text{P}\{^1\text{H}\}$ NMR spectra of **17-20**. Spectra top: room temperature, middle: coalescence temperature, bottom: $T = -100\text{ }^\circ\text{C}$. *impurity

Clearly, the pyridyl substituent in 2-position of the heterocycle increases the inversion barrier in comparison to the non-functionalized anion **17** as only one species is detected even at $T = -100^\circ\text{C}$. The mechanism for the inversion could go through a $\lambda^4\sigma^3$ aromatic system (figure 3.7), which might be more accessible for the pyridyl-substituted ligands by lowering the orbital energies due to the presence of an electronegative atom, such as nitrogen.

Table 3.1 Calculated energy barriers of inversion **18-20**.

Compound	Name	T_c/K	$ v_A - v_B /\text{Hz}$	K_{Tc}	$\Delta G^\ddagger/\text{KJmol}^{-1}$
18	[Me-PN]Li	179.15	93.8556	208.36	35.16
19	[Ph-PN]Li	194.15	199.0386	441.87	37.02
20	[Fc-PN]Li	192.15	346.2948	768.77	35.74

In the ^1H NMR spectrum of each anionic phosphinine, the complete set of signals shows a high-field shift compared to the corresponding neutral compounds, as expected when introducing a negative charge to the system. Especially H4 and H2 of **18-20** (pyridyl-substituted anions) appear more shielded, around 1.2 ppm and 0.7 ppm, respectively compared to their neutral analogues.

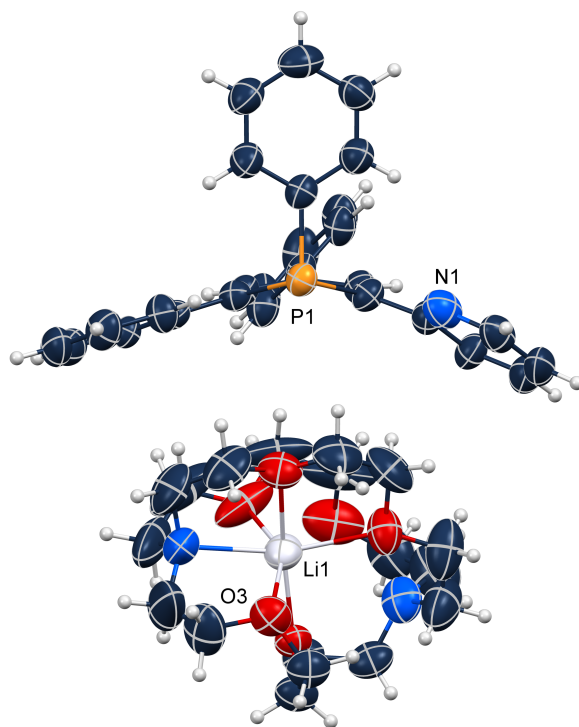
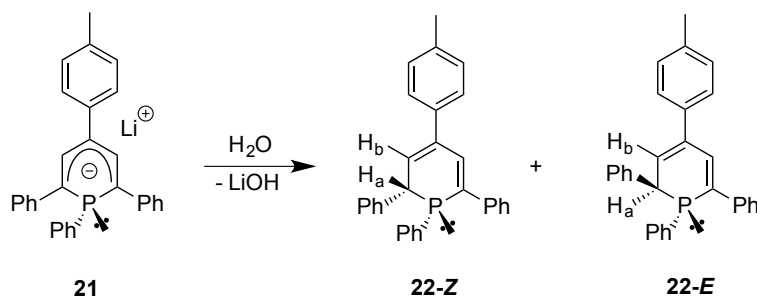


Figure 3.9 Molecular crystal structure of **19** in the crystal. Thermal ellipsoids are shown at the 50% probability level

Based on theoretical calculations and $^{13}\text{C}\{^1\text{H}\}$ NMR data of different phosphinine anions, Le Floch reported in 2003 that the electron density of the heterocycle was mainly localized on the carbons in α -position to phosphorus.⁷ These $^{13}\text{C}\{^1\text{H}\}$ NMR signals showed a significant high-field shift of around 85 ppm compared to their neutral counterparts. Compound **17** shows $^{13}\text{C}\{^1\text{H}\}$ NMR resonances for C1 and C5 at $\delta = 149.9$ ppm ($\Delta\delta = 23.2$ ppm compared to the corresponding neutral phosphinine **16**). On the other hand, the donor-functionalized anions **18-20** show very different chemical shifts for C1 and C5. For the neutral PN ligand **1**, the $^{13}\text{C}\{^1\text{H}\}$ NMR resonances for C1 and C5 are at $\delta = 170.7$ ppm and $\delta = 172.7$ ppm, respectively, while in the anions **18-20** the C1 resonances are shifted to approximately $\delta = 147$ ppm and those for C5 to $\delta = 92$ ppm, suggesting that delocalized electron density on the phosphorus ring is pulled towards the pyridine ring.

The lithium salt of **19** crystallized by slow diffusion of pentane in a THF solution and the molecular structure in the crystal was determined by X-ray diffraction. As expected, the lithium atom is trapped by the 2.2.2. cryptand. Since the quality of the crystals was low, the bond lengths and angles cannot be discussed in detail, but a picture of the molecular structure in the crystal is shown in figure 3.9.

As demonstrated before by Märkl and Ashe III, the reaction of λ^4 -phosphinine anions with H_2O leads quantitatively and selectively to the corresponding 1,2-dihydrophosphinine derivatives.⁵ We decided to further investigate the reactivity of the λ^4 -PN ligand (**19**) with water and to establish similarities and differences to other hetero-functionalized anions reported in literature. For comparison purposes, anion **21** was also reacted with water as described in scheme 3.2. Part of the following results have been obtained in collaboration with Gisa Meißner, especially the synthesis of **16** and the coordination chemistry of **21**.²⁶



Scheme 3.2 Scheme reaction of the λ^4 -phosphinine anion **21** with H_2O

In the case of symmetric phosphinines, four stereoisomers are expected upon protonation as a stereogenic center is formed at the carbon atom at the 2-position of the heterocycle and a second stereogenic center is represented by the P atom. This leads to the presence of a pair of enantiomeric diastereomers, which are distinguished according to the relative location of the phenyl groups at 1- and 2-positions with respect to one another (**22-E** and **22-Z**, scheme 3.2).

After addition of water to a THF-*d*₈ solution of **21**, the characteristic dark color of the solution immediately vanishes to give a clear yellow solution. The ³¹P{¹H} NMR spectrum shows mainly one product (94% based on integration) with a signal at δ = -50.8 ppm, whereas a minor species (6%) is detected at δ = -38.0 ppm. The characteristic ¹H NMR signals for protons H_a and H_b for the major product show chemical shifts at δ = 5.97 ppm for H_b and at δ = 4.23 ppm for H_a (figure 3.10). The signals for the minor product can be observed as traces at δ = 4.02 and δ = 6.08 ppm.

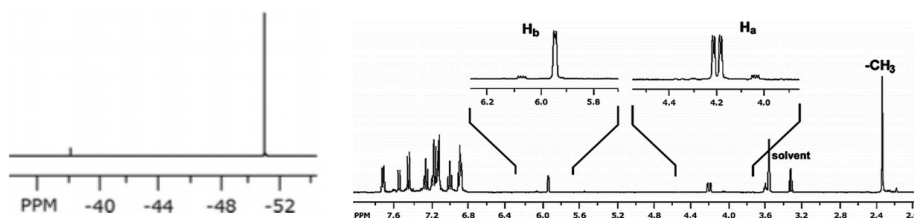


Figure 3.10 ³¹P{¹H} NMR spectrum of reaction mixture of **21** with H₂O (left) and ¹H NMR spectrum of the reaction mixture of **21** with water (right)

An assignment of the exact configuration (*E* or *Z*) of **22** on the basis of the size of the coupling constants appeared, however, to be problematic. Fortunately, crystals of the major product suitable for X-ray diffraction were obtained (as verified by ³¹P{¹H} NMR spectroscopy) after filtering the solution and recrystallizing the product from acetonitrile. The ORTEP plot of **22** shown in figure 3.11 reveals that the molecule has the *Z* configuration. The P–C distances of 1.873(2), 1.827(2), and 1.825(2) Å are much longer than those in **16** (1.757(3) and 1.743(3) Å), and the phosphorus atom is strongly pyramidalized ($\Sigma_{\text{CPCangles}} = 304.5^\circ$), as expected for a formally *sp*³-hybridized phosphorus atom. Consequently, the C–C bond lengths of the heterocycle are consistent with the presence of a C–C single bond [C(1)–C(2)] and a conjugated diene with double bonds between C(2) and C(3) and C(4) and C(5). Therefore, the exact nature of the hydrolysis products of the anions derived from λ⁴-2,6-diphenyl-4-(*p*-tolyl)phosphinine

could be identified for the first time, and this allows for the assignment of the signals observed in the $^{31}\text{P}\{^1\text{H}\}$ NMR spectra: $\delta = -50.8$ ppm as **22-Z** and $\delta = -38.0$ ppm as **22-E** (figure 3.10).

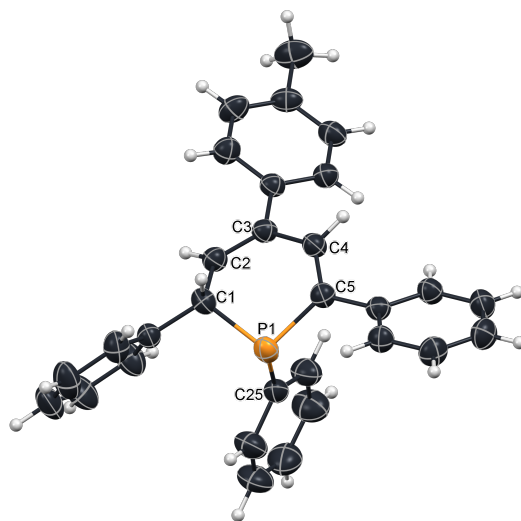
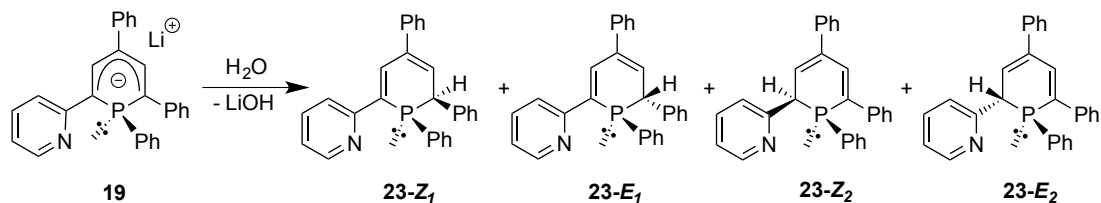


Figure 3.11 Molecular structure of **22-Z** in the crystal. Thermal ellipsoids are shown at the 50% probability level. Selected distances (Å) and bond angles (deg): P1–C1 1.873(2), P1–C5 1.827(2), C1–C2 1.497(2), C2–C3 1.339(2), C3–C4 1.469(2), C4–C5 1.343(2), P1–C25 1.825(2), C1–P1–C5 97.46(8)

Likewise, Ph-PN compound **19** was treated in the same way as **21**. Due to the non-symmetric nature of this compound, another pair of isomers is to be expected since protonation can potentially occur either on the carbon atom at the 2-position of the heterocycle or alternatively, on the one in the 6-position (scheme 3.3).



Scheme 3.3 Reaction of **19** with water and its possible products. Enantiomers are not shown

Indeed the $^{31}\text{P}\{^1\text{H}\}$ NMR spectrum of the reaction mixture shows four signals at $\delta = -40.9$ (1.2% by integration), $\delta = -43.4$ (28.9%), $\delta = -49.6$ (32.7%), and $\delta = -52.6$ ppm (37.2%) (figure 3.12, top). Comparing the chemical shifts and intensities of these signals to those obtained for **22**-*E/Z*, the signals at $\delta = -40.9$ and $\delta = -49.6$ ppm are believed to belong to the isomers protonated at the 2-position, being the latter most likely the *Z*-isomer, as in the case of **22**-*Z*. The signals at $\delta = -43.4$ and $\delta = -52.6$ ppm consequently belong to **23**-*E₂/Z₂*, generated from the protonation of the carbon atom at the 6-position, which is next to the pyridine ring. If this assumptions are correct, the protonation on the pyridyl ring side is much less selective than the protonation at C2, as the integral of the signals assigned as **23**-*E₂* and **23**-*Z₂* are formed in a ratio of approximately 40:60, in contrast to **23**-*E₁* and **23**-*Z₁* with a ratio of 4:96, similar to the ratio obtained for the *E/Z* isomers of **22**. LiOH is formed upon protonation of the λ^4 -phosphinine anions and protonation at C2 and C6 position is reversible. In order to determine if the $\text{p}K_{\text{a}}$ values of the products formed play a role in the reactivity and selectivity of this reaction, the same reactions were performed with methanol instead of water, as LiOCH₃ forms, which is a slightly stronger base than LiOH.

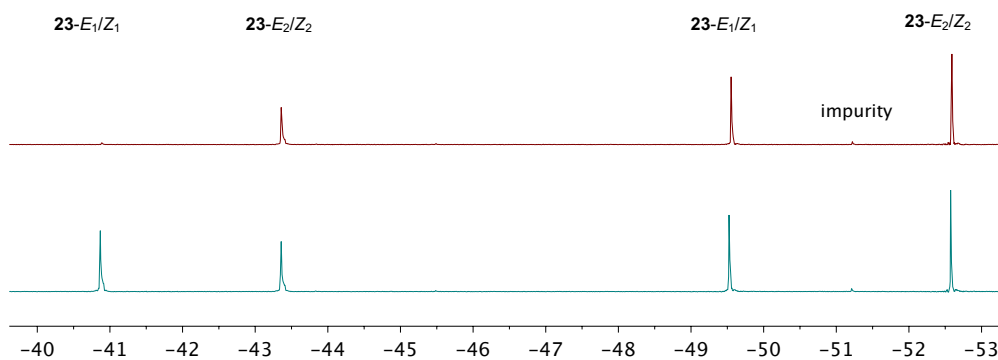


Figure 3.12 $^{31}\text{P}\{^1\text{H}\}$ NMR spectra of the species formed by protonation of **19** with H₂O (top) or MeOH (bottom)

Interestingly, the protonation of **21** and **19** leads to a dramatic change in selectivity. The ratio between *E/Z* isomers of **22** (figure 3.13) changes from 94:6 to almost 50:50 (determined by $^{31}\text{P}\{^1\text{H}\}$ NMR spectrum signal integration).

These changes were also observed in the reaction of **19** with methanol only for the species that were formally assigned as **23**-*E₁/Z₁*, the isomers protonated at C2 (phenyl ring side). The isomers assigned as **23**-*E₂/Z₂* remain in a ratio of 40:60 (figure 3.12, bottom).

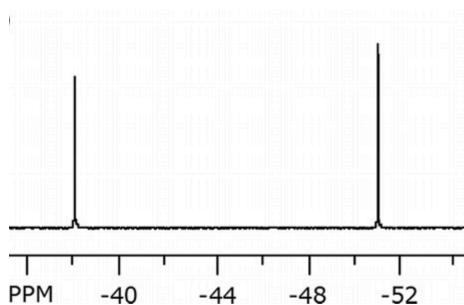
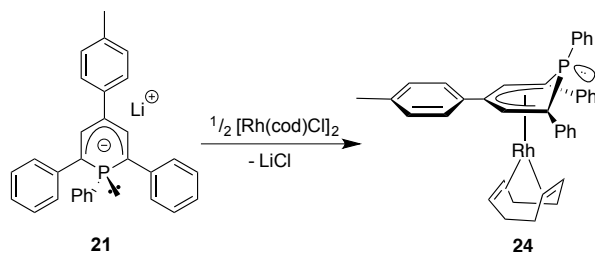


Figure 3.13 $^{31}\text{P}\{^1\text{H}\}$ NMR of the reaction of **21** with MeOH

These results nicely indicate that the assignment in figure 3.12 is most likely correct. Moreover, they show that quenching solutions of λ^4 -phosphinine anions is more complex than previously assumed and that there is a subtle interplay between the $\text{p}K_{\text{a}}$ values of the generated 1,2-dihydrophosphinine species and the $\text{p}K_{\text{b}}$ values of the formed bases. Although quenching of the Li salts with H_2O leads preferentially to the kinetic product (**22-Z** in the case of **21**), the presence of the stronger base LiOCH_3 clearly leads ultimately to the thermodynamic product **22-E**. It can also be concluded that the 1,2-dihydrophosphinine **23-E₂/Z₂** is apparently slightly more acidic than the 1,2-dihydrophosphinine **23-E₁/Z₁**, as the thermodynamic equilibrium between **23-E₂** and **23-Z₂** is already reached with LiOH as a base.

It was also of interest to explore the coordination chemistry of these anionic heterocycles. Rhodium(I) seemed to be a first good choice for this study as the coupling constant between ^{31}P and ^{103}Rh give extra valuable information *via* NMR spectroscopy. Moreover Rh(I) complexes bearing phosphorus ligands have potential applications as catalysts for important transformations such as hydrogenation or hydroformylation reactions.^{12,27} Half an equivalent of $[\text{Rh}(\text{cod})\text{Cl}]_2$ was mixed with **21** in THF and stirred for 5 min at room temperature to quantitatively obtain complex **24** (scheme 3.4).



Scheme 3.4 Reaction of **21** with the Rh^{I} complex $[\text{Rh}(\text{cod})\text{Cl}]_2$

The $^{31}\text{P}\{^1\text{H}\}$ NMR spectrum shows one doublet at $\delta = -58.6$ ppm. It is interesting to note, that only one isomer of the Rh(I) complex is detected, as the lone pair could in principle be oriented either in an axial or equatorial position of the heterocycle. The small $^1J_{\text{P,Rh}}$ coupling constant of 11.1 Hz is indicative of η^5 -coordination of **24** (an η^1 -coordination results in much larger P-Rh coupling constants) and it lies very close to the values obtained by Le Floch for complexes **3.6** (figure 3.4, R = TMS: $^{31}\text{P}\{^1\text{H}\}$ NMR (C_6D_6): $\delta = -17.21$ (d, $^2J_{\text{P,Rh}} = 7.3$ Hz) ppm and R = Ph: $^{31}\text{P}\{^1\text{H}\}$ NMR (CDCl_3): $\delta = -3.53$ (d, $^2J_{\text{P,Rh}} = 9.0$ Hz) ppm).

After removal of LiCl, crystals suitable for X-ray diffraction could be obtained from a diethyl ether solution at $T = -10^\circ\text{C}$. Figure 3.14 shows the molecular structure of **24** in the crystal, along with selected bond lengths, distances, and angles.

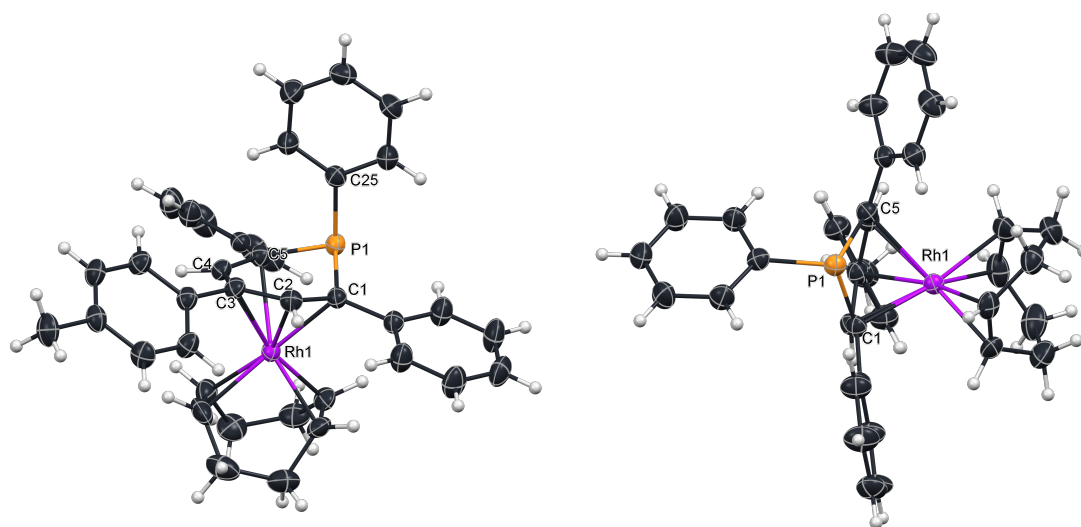
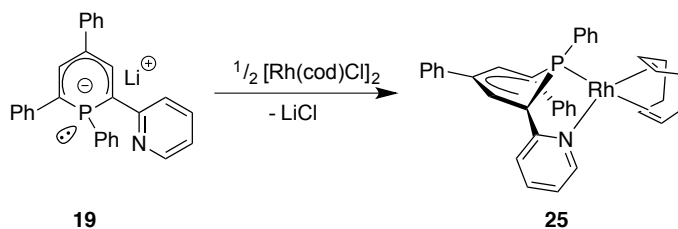


Figure 3.14 Molecular structure of **24** in the crystal. View from the top (left) and from the side (right). Thermal ellipsoids are shown at the 50% probability level. Selected distances (Å) and bond angles (deg): P1–C1 1.842(3), P1–C5 1.822(3), C1–C2 1.434(3), C2–C3 1.409(3), C3–C4 1.440(4), C4–C5 1.392(4), P1–C25 1.848(3), C1–C12 1.499(3), C5–C18 1.493(4), Rh1–C31 2.164(3), Rh1–C32 2.159(3), Rh1–C35 2.115(3), Rh1–C36 2.114(3), C1–P1–C5 94.70(11)

The crystallographic data of the complex indeed confirms that the phosphorus heterocycle coordinates in an η^5 -fashion to the Rh(I) atom with the phenyl group in axial position. The phosphorus atom is clearly located above the plane of the five carbon atoms and is strongly pyramidalized, as expected for a formally sp^3 -hybridized phosphorus atom ($\Sigma\text{angles} = 301.4^\circ$). The C–C bond lengths in the carbocyclic fragment (1.392(4)–1.440(4) Å) are very similar to the ones from the neutral phosphinine **16** (1.384(4)–1.407(4) Å). On the other hand, significant

lengthening of the P1–C1 and the P1–C5 bonds is observed for **24** compared to **16**. The corresponding values increase from the neutral λ^3 -phosphinine [P1–C1 1.757(3), P1–C5 1.743(3) Å] to the complexed anionic λ^4 -phosphinine [P1–C1 1.842(3), P1–C5 1.822(3) Å] and reflect the transition of a C(sp^2)–P(sp^2) to a C(sp^2)–P(sp^3) system upon reaction with PhLi and subsequent coordination. These data are also comparable to the crystallographic data obtained for **3.6** by Le Floch.¹²

Compound **19** was then also reacted with 0.5 equivalents of [Rh(cod)Cl]₂ to obtain complex **25** in quantitative yield according to ³¹P{¹H} NMR spectroscopy (scheme 3.5), which shows only one doublet at $\delta = 13.0$ ppm with a ¹J_{P,Rh} coupling constant of 152.2 Hz. This accounts for coordination to rhodium *via* the P lone pair. Moreover, the typical signals for cod-containing metal complexes could be detected in the ¹H NMR spectrum. These results are in agreement with previous findings that donor-functionalized λ^4 -phosphinine anions preferentially coordinate through the phosphorus lone pair in a η^1 -fashion towards a metal center as shown also by Le Floch for other heterodonor-functionalized ligands (compounds **3.8-3.13** figure 3.4).



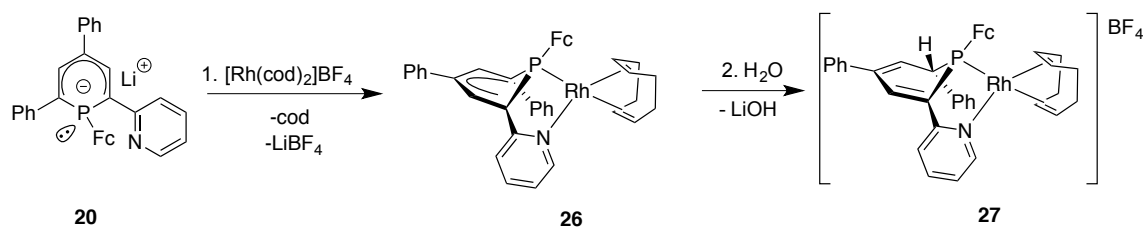
Scheme 3.5 Coordination of **19** to [Rh(cod)Cl]₂

Inspired by these results, a Rh-cod complex with the ferrocenyl substituted pyridyl-functionalized anion was prepared, which is a more sterically demanding substituent at the phosphorus atom. [Rh(cod)₂]BF₄ was mixed with **17** or **20** in THF in a 1:1 ratio. While the reaction of **17** always gave a mixture of products in the ³¹P{¹H} NMR spectrum, the reaction with **20** affords complex **26** (scheme 3.6) as a black solution (very similar to **25**). The ³¹P{¹H} NMR of the reaction mixture shows a doublet at $\delta = 3.53$ ppm with a ¹J_{P,Rh} = 150.0 Hz which suggests coordination *via* the phosphorus lone pair. Compared to **25**, the signal undergoes a low-field shift of 10 ppm, as expected by substituting the phenyl group with a more electron donating one on the phosphorus atom. Nevertheless, the P,Rh coupling constants are very similar.

Complex **26** is very sensitive towards proton sources, such as water. All attempts to isolate this compound gave complex **27** as a dark purple solution which shows a doublet at $\delta = -2.43$ ppm

with a $^1J_{P,Rh} = 156.5$ Hz in the $^{31}P\{^1H\}$ NMR spectrum. It is believed that the proton comes from traces of water from the solvents used (DCM or pentane) or from the glass wall.

The 1H NMR spectrum of **27** (figure 3.15) shows the characteristic signal for the proton that has been added to C1, which is a doublet of doublets at $\delta = 4.34$ ppm, with a large coupling constant of $^2J_{P-H} = 9.3$ Hz and a smaller one of $^3J_{H-H} = 3.2$ Hz. Protons H2 and H4 also have large $^2J_{P-H}$ coupling constants of 8.6 Hz and 18.9 Hz, respectively. Their chemical shifts are in agreement with an aromatic H4 ($\delta = 7.87$ ppm) and an alkenyl H2 ($\delta = 5.98$ ppm). Moreover, the resonances for the ferrocenyl moiety as well as for the typical isignals for coordinated cod can be observed in the spectrum.



Scheme 3.6 Reaction of **20** with $[Rh(cod)_2]BF_4$ and its one-pot protonation with water

It was possible to assign the $-CH$ proton signals of the cod ligand in *cis* position to the phosphorus atom by means of a ^{31}P - 1H HMBC NMR experiment (the given coupling constant was 20 Hz). Cross peaks of these two nuclei are obtained with the signals at $\delta = 4.68$ and $\delta = 5.58$ ppm. As $^3J_{P-H}$ coupling constants are known to have a Karplus-like dependance on the dihedral angle Θ , coupling constants smaller than 20 Hz should correspond to protons with larger dihedral angles and no cross peaks with these nuclei should be obtained in the spectrum.

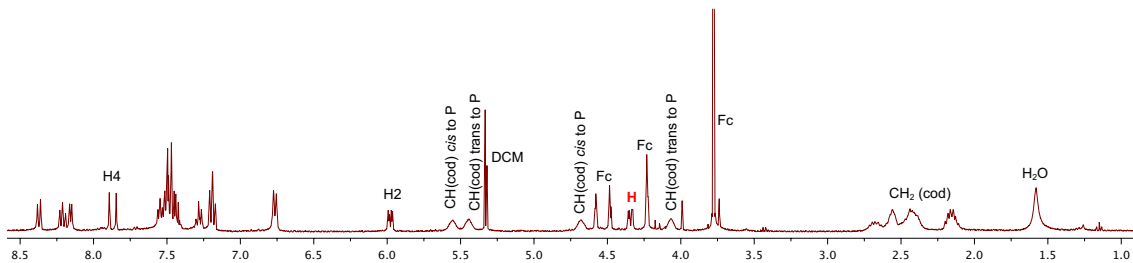


Figure 3.15 1H NMR spectrum of complex **27**

Crystals suitable for X-ray diffraction were obtained from slow diffusion of diethylether into a DCM solution of **26**. However, the Ortep plot shown in figure 3.16 shows again that the cationic rhodium complex **27** has been formed. The chelate complex has been selectively protonated at C1 leading to a preferred equatorial position of the sterically demanding phenyl substituent. It is interesting that protonation of the pyridyl-substituted λ^4 -phosphinine anions is selective when the ligand is coordinated to Rh(cod) fragments.

The isomer obtained corresponds to the Z_1 -isomer according to the free ligand assignment (**23**, figure 3.12). Moreover, P1-C5 and P1-C23 bond lengths are approximately equal (1.808(5) Å and 1.855(5) Å, respectively) and are in agreement with typical $C(sp^2)$ – $P(sp^3)$ bond lengths. The C1-P1-C5 angle (99.58°(22)) is in the order of classical λ^4 -phosphinines.⁷

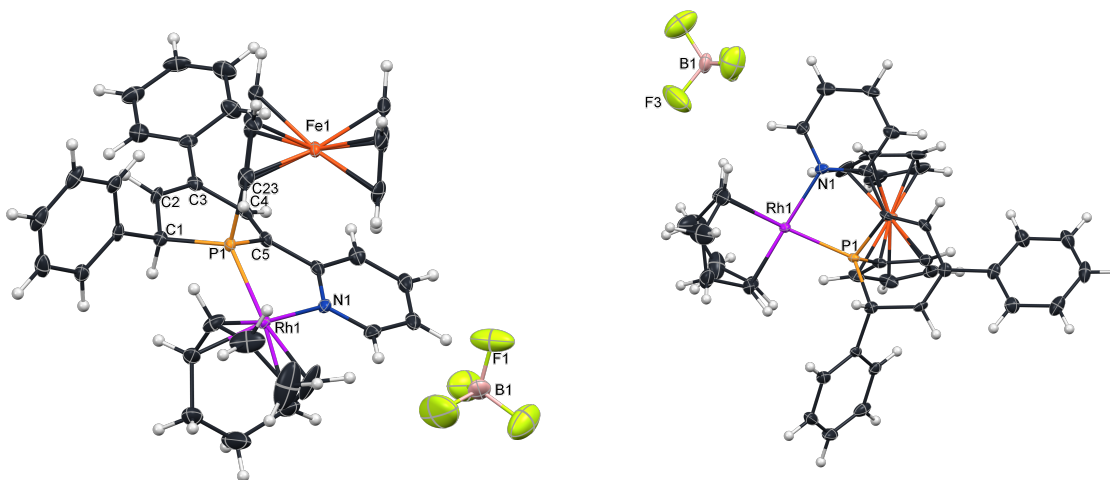


Figure 3.16 Molecular structure of **27** in the crystal. View from the side (left) and from the top (right). Ellipsoids are scaled to enclose 50% of the electron density. Selected distances (Å) and bond angles (deg): P1-Rh1, 2.2621; N1-Rh1, 2.119(4); P1-C1, 1.8555; P1-C5, 1.808(5); P1-C23, 1.808(5); C1-C11, 1.521(6); C5-C6, 1.473(7); C1-C2, 1.511(7); C2-C3, 1.342(7); C3-C4, 1.460(7); C4-C5, 1.342(7); Rh1-C38, 2.142(5); Rh1-C37, 2.148(5); Rh1-C33, 2.236(6); Rh1-C34, 2.226(6); C1-P1-C5, 99.58(22); C5-P1-C23, 104.74(21); C23-P1-C1, 106.50(22); P1-Rh1-N1, 82.39(11)

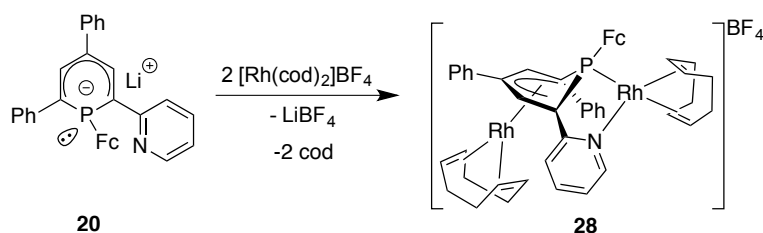
The P atom is strongly pyramidalized (Σ angles = 311°) as in free λ^4 -phosphinine anions. The angle between the two heteroatoms (P1 and N1) and rhodium is 82.39°. The P1-Rh1 bond (2.262(1) Å) in **27** is longer than the one in $[\text{Rh}(\text{cod})(\mathbf{1})][\text{BF}_4]$ (P1-Rh1, 2.2250(8) Å), which denotes the difference between the π -accepting properties of a $\lambda^3\sigma^2$ -phosphinine and a $\lambda^4\sigma^3$ -phosphinine, being the latter almost only a σ -donor. Analyzing the *trans*-effect between the heteroatoms and the cod ligand, the electronic properties of P and N in the PN ligand can be

compared. Rh1-C33 and Rh1-C34 (2.236(6) Å and 2.228(6) Å, respectively), the carbon atoms trans to P, are longer than Rh1-C37 and Rh1-C38 (2.148(5) and 2.142(5) Å, respectively), the carbon atoms trans to N. This indicates that the N atom is a better σ -donor than the P atom in this ligand. Torsion angles between P1-Rh1-C37-H37 and P1-Rh1-C38-H38 (atoms in *cis* position to phosphorus) have values of 10.99° and 21.38°, respectively, whereas P1-Rh1-C33-H33 and P1-Rh1-C34-H34 (atoms in trans position to the P atom) have values of 61.78° and 60.20°, respectively.

Based on the structural characterization of **27** it is assumed that complex **26** is the neutral complex depicted in scheme 3.6, which upon addition of water to the reaction mixture leads to complex **27**.

Since the first reports on λ^4 -phosphinine anions, their ambivalent nature has been recognized and discussed. However, to the best of our knowledge there are no examples of structural characterizations of such complexes. Therefore, it was decided to mix two equivalents of $[\text{Rh}(\text{cod})][\text{BF}_4]$ with one equivalent of **20** to obtain a ligand coordinated to a rhodium center *via* the P lone pair and to a second one *via* the delocalized π -system of the heterocyclic ring (**28**, scheme 3.7).

Indeed, the $^{31}\text{P}\{^1\text{H}\}$ NMR spectrum of the reaction mixture in THF shows a doublet of doublets at $\delta = 10.8$ ppm with a large coupling constant of $^1J_{\text{P,Rh}} = 163.1$ Hz and a smaller one of $^2J_{\text{P,Rh}} = 9.8$ Hz, suggesting the formation of a dirhodium complex, as expected. To gain more knowledge about the structure, crystals were grown by slow diffusion of pentane into a THF solution and were analyzed by means of X-ray diffraction. The molecular structure of **28** in the crystal is shown in figure 3.16.



Scheme 3.7 Synthesis of complex **28** from **20** and $[\text{Rh}(\text{cod})_2]\text{BF}_4$

Compound **28** shows the ferrocenyl- λ^4 -phosphinine anion bound to a cationic Rh(cod) fragment (Rh1) *via* the P and N lone pairs, and to a neutral Rh(cod) fragment (Rh2) *via* the anionic π -system, assuming that the latter bears the negative charge of the anion. Unfortunately, bond lengths and angles cannot be discussed, due to the poor quality of the crystals.

In order to determine whether **17** could also act as a bidentate ligand, without having the second donor functionality that enforces the coordination mode *via* the phosphorus lone pair, ligand **17** was mixed with two equivalents of [Rh(cod)]BF₄ in THF as reported for complex **28** (scheme 3.8).

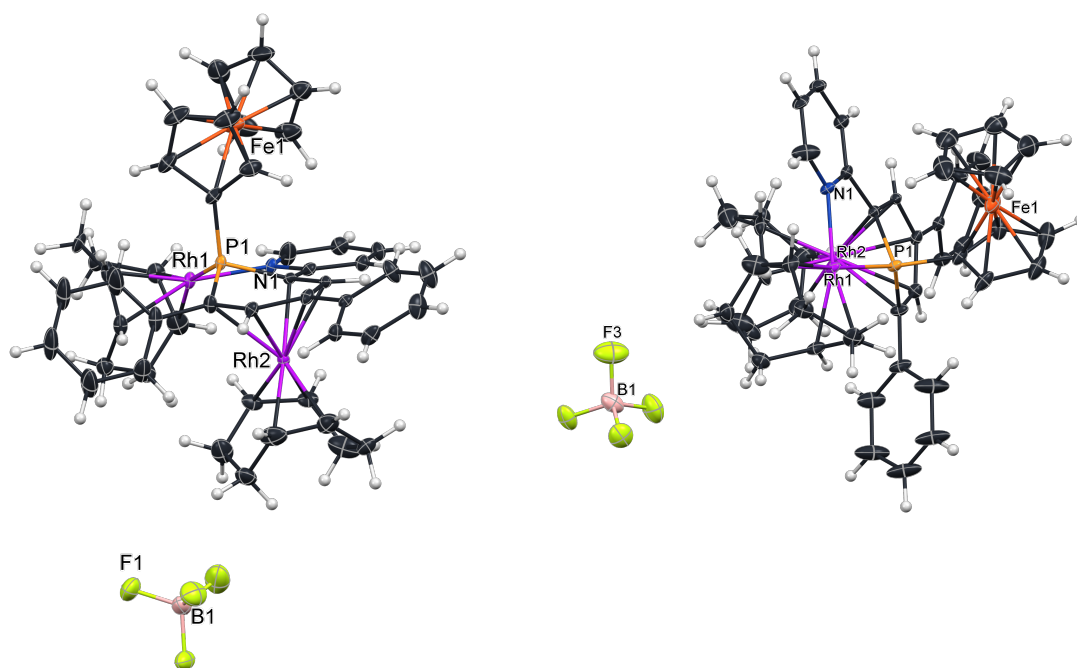
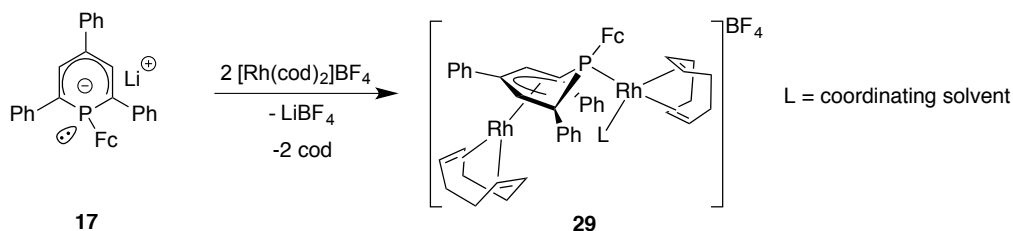


Figure 3.17 Molecular structure of **28** in the crystal. View from the side (left) and from the top (right). Ellipsoids are scaled to enclose 50% of the electron density

The $^{31}\text{P}\{^1\text{H}\}$ NMR spectrum shows a major doublet at $\delta = -58.7$ with a coupling constant of $J = 11.8$ Hz and a minor doublet of doublets at $\delta = 13.8$ ppm with a large coupling constant of 180.3 Hz and a small one of 11.6 Hz. Over a couple of days, the doublet of doublets turns into the major signal and a precipitate starts to form inside the NMR tube. The orange solid was filtered off, washed with pentane and redissolved in DCM- d_2 . The $^{31}\text{P}\{^1\text{H}\}$ NMR spectrum of this solution shows only the doublet of doublets at $\delta = 13.8$ ppm ($J = 180.3, 11.6$ Hz). Unfortunately,

crystals suitable for X-ray diffraction could not be obtained to prove the structure of the complex. From the chemical shift and the coupling constants (similar to **28**) it is suggested that the structure of **29** is most likely the one depicted in scheme 3.8.



Scheme 3.8 Synthesis of complex **29** from **17** and $[\text{Rh}(\text{cod})]\text{BF}_4$

The formation of a dirhodium complex is faster and more selective with the donor-functionalized ligand **20** than with **17**, most likely because the resulting complex **28** is stabilized by the chelate complex formation. In contrast, the structure proposed for **29** would only be stabilized, for instance, by the presence of coordinating solvents or external donor ligands.

Ferrocenyl moieties are known to play an important role as substituents or ancillary ligands due to their redox properties. When attached to a coordinated ligand, they can potentially control the reactivity at the metal center by switching its oxidation state.²⁸ Investigations on the electrochemical properties of **28** using cyclic voltammetry were performed. Starting with a positive step, the voltammogram recorded in THF (figure 3.18) shows three redox events in the oxidation cycle. The first is quasi-reversible ($E^{\circ}_{\text{pc,pa}} = 0.51 \text{ V vs. [Fc/Fc}^+]$) and has been assigned to the oxidation process from the ferrocenyl moiety (Fe(II)/Fe(III)) by comparison to other ferrocenyl-substituted ligands in literature.²⁹ The third oxidation wave shows an irreversible process at $E^{\circ} = 1.25 \text{ V vs. [Fc/Fc}^+]$ and could be assigned to the oxidation from Rh(I) to Rh(III), also based on similar complexes reported in literature.³⁰ With the data obtained so far, it is not possible to determine which of the Rh centers takes part in the process.

Most likely, the second irreversible oxidation process at $E^{\circ} = 0.74 \text{ V vs. [Fc/Fc}^+]$ belongs to the oxidation of the ligand. There are also four reduction events that were not assigned. One should belong to the pyridyl ring reduction and another might be due to reduction of Rh^{I} to Rh^0 , as these are plausible processes of the system. The experiment was repeated in MeCN (figure 3.19), which allows a scan with broader range of potentials. Moreover, a fourth irreversible oxidation

event ($E^\circ = 2.24$ V vs. [Fc/Fc⁺]) can be noticed, which could belong to the oxidation of the second Rh(I) atom going to Rh(III).

In the reduction area there are two more irreversible reduction processes at lower potentials that could not be detected when measuring in THF, which could also belong, for example, to reduction events such as Rh^I to Rh⁰. With these preliminary results it is concluded that the system neither undergo reversible oxidation nor reduction processes through the whole potential window in THF and MeCN. In order to determine if the ferrocenyl moiety is indeed communicating electronically with the Rh centers in any way, more data are needed. A chemical reduction of the complex followed by characterization of the product would lead to a better insight into these systems, also with respect to applications.

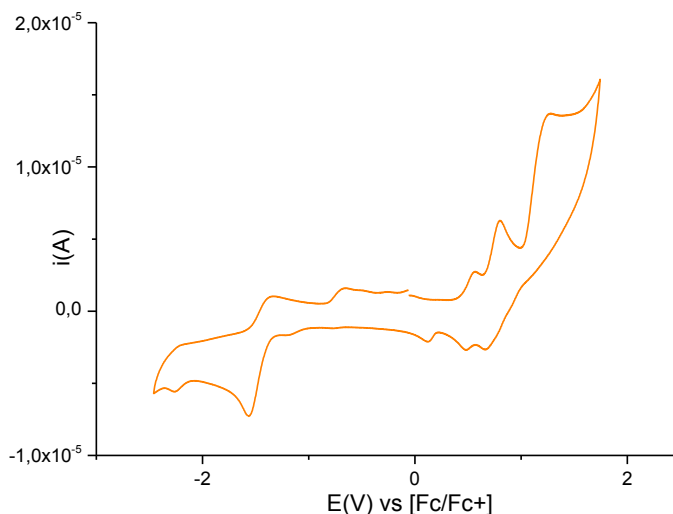


Figure 3.18 Cyclic Voltammogram of complex **28**: 1.8 mM in THF with *n*Bu₄PF₆ (0.1 M) at a scan rate of 0.1 V·s⁻¹

Other attempts to explore the coordination chemistry of this unique λ^4 -phosphinine ligands were performed. Below, a table with a summary of all attempts is depicted. According to the ³¹P{¹H} NMR spectra, the latter experiments led quantitatively to the corresponding metal complex of the λ^4 -phosphinine anion. Unfortunately, crystallization attempts of these products have not been yet successful.

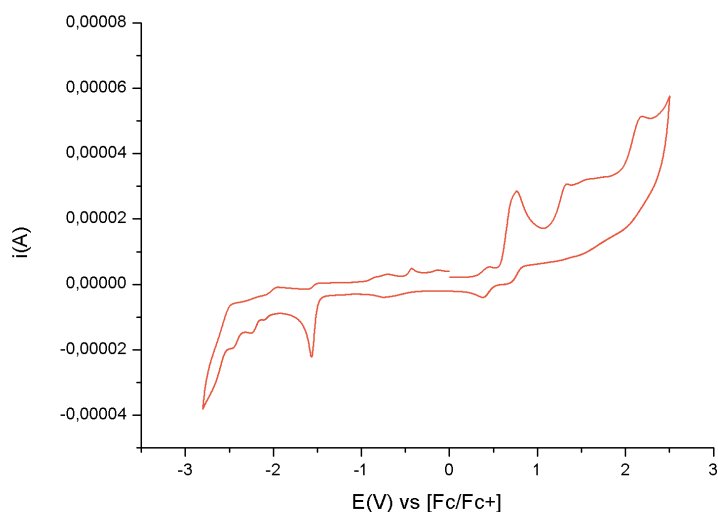


Figure 3.19 Cyclic voltammogram of complex **28**: 1.8 mM in MeCN with $n\text{Bu}_4\text{NBF}_4$ (0.1 M) at a scan rate of $0.1 \text{ V}\cdot\text{s}^{-1}$

Table 3.2 Coordination reactions **18-20** with different metal precursors

Ligand	Precursor	L:M	Solvent	$^{31}\text{P}\{^1\text{H}\}$ NMR δ :
18	$[\text{Rh}(\text{cod})\text{Cl}]_2$	2:1	CD_2Cl_2	1.04 (d, $J=149.0$ Hz) ppm
18	$[\text{IrCl}_2\text{Cp}^*]_2$	1:1	CH_2Cl_2	-8.85 (s) ppm
19	$[\text{IrCl}_2\text{Cp}^*]_2$	1:1	CD_2Cl_2	-5.28 (s) ppm
19	$[\text{AuCl}\cdot\text{SMe}_2]$	1:1	CH_2Cl_2	5.91 (s) ppm
19	$[\text{Fe}(\text{OAc})_2]$	1:1	THF	No reaction
19	$[\text{FeCl}_2]$	1:1	THF	Several signals
20	$[\text{Pt}(\text{cod})\text{Cl}_2]$	1:1	THF	Several signals
20	$[\text{Ir}(\text{cod})\text{Cl}]_2$	1:1	THF	-1.50 (s) ppm

Entries 5-7 in table 3.2 did not give clean reactions; $[\text{Fe}(\text{OAc})_2]$ did not react at all, probably due to the poor solubility of the precursor in THF. $[\text{FeCl}_2]$ and $[\text{Pt}(\text{cod})\text{Cl}_2]$, showed several signals in the $^{31}\text{P}\{^1\text{H}\}$ NMR spectrum when mixed with one equivalent of an anionic λ^4 -phosphinine. For these M(+II) precursors, a L:M ratio of 2:1 might lead to less species in solution, by

substituting the Cl ligands with the anionic phosphinines. On the other hand, clean reactions were observed with other metal precursors, where the metal has an oxidation state of +1 or +3, such as $[M(\text{cod})\text{Cl}]_2$ ($M = \text{Rh}$ or Ir), $[\text{AuCl}\cdot\text{SMe}_2]$, or $[\text{IrCl}_2\text{Cp}^*]_2$.

3.4 Conclusions

With this study, the successful synthesis of four new λ^4 -phosphinine salts has been shown. Three of them are potential chelating ligands due to the presence of a second donor functionality (the pyridine group) (**18-20**). These compounds can undergo inversion at the P atom, leading to two pairs of diastereoisomers, which can be detected by means of NMR techniques. The energy barriers of the pyramidal inversion at phosphorus have been calculated, being approximately of the same magnitude as repeated for other acyclic $\lambda^3\sigma^3$ -phosphines. The anionic phosphinines are reactive towards protons sources such as water or methanol. The formation of the kinetic or the thermodynamic product depends on the $\text{p}K_a$ of the corresponding 1,2-dihydrophosphinine obtained and the $\text{p}K_b$ values of the base formed (LiOH or LiOMe). The coordination chemistry towards $[\text{Rh}(\text{I})(\text{cod})]$ precursors was investigated and showed that donor-functionalized λ^4 -phosphinines coordinate preferably *via* the P lone pair, leading to chelated complexes. If there is no second donor-functionality, the coordination happens preferentially through the anionic π -system. In the case of **25** it was found that the P-Cl bond can add protons selectively to form a cationic complex. It was also proven that this type of anions can act as bidentate ligands (*via* the P lone pair and the anionic π -system) leading to dirhodium complexes, which are stable towards water. Cyclic voltammetry of **28** shows that the complex does not undergo reversible oxidation processes, but most likely quickly reacts to form other products, which have to be further characterized.

3.5 Experimental part

General remarks

All reactions were performed under argon by using Schlenk and glovebox techniques. All glassware was dried prior to use. $[\text{Rh}(\text{cod})_2]\text{BF}_4$ and $[\text{Rh}(\text{cod})\text{Cl}]_2$ were purchased from Aldrich and used without further purification. Ferrocenyl lithium³¹, compound **1**³², **16**, **21**, and **24**²⁶ were prepared according to literature procedures. All common solvents and chemicals were commercially available. Dry solvents were prepared by using custom-made solvent purification columns filled with Al_2O_3 from Braun Solvent systems. THF and Et_2O were distilled under argon from potassium/benzophenone prior to use. All common solvents and chemicals were commercially available. NMR spectra were recorded with a Jeol ECP 500 (^1H NMR 500.00 MHz), a JEOL ECX400 or JEOL ECAII 400 NMR Spectrometer (^1H NMR 399.74 MHz, $^{13}\text{C}\{^1\text{H}\}$ NMR 100.51 MHz, $^{31}\text{P}\{^1\text{H}\}$ NMR 161.82 MHz); The ^1H and ^{13}C chemical shifts are given relative to tetramethylsilane (TMS), and the residual solvent peaks were used as the reference signal; the ^{31}P chemical shifts are referenced to an 85% aqueous solution of H_3PO_4 . Cyclic Voltammetry measurements were performed with AUtolab PGSTAT 302N AUT84884 and a three-electrode system with a Glassy-Carbon working electrode, platinum sheet counter electrode, and a leak-free Ag/AgCl as reference electrode. Conducting salt tetrabutylammonium hexafluorophosphate (NBu_4PF_6 , Aldrich $\geq 99.0\%$) was used for electrochemical analysis. As reference, ferrocene (98%, Aldrich) was used.

1-Ferrocenyl-(2,6-diphenyl-4-(p-tolyl))-cyclophosphahexadienyllithium (17)

Under an argon atmosphere at room temperature, ferrocenyl lithium (0.0062 g, 0.0326 mmol, 1.1 eq.) and **16** (10.0 mg, 0.03 mmol, 1 eq) were mixed in 0.5 mL dry THF in a *J*-Young-tube. The solution immediately turned dark green. The solvent was evaporated and a dark green to orange oil was obtained. The product formed quantitatively according to $^{31}\text{P}\{^1\text{H}\}$ NMR spectroscopy.

^1H NMR (500 MHz, THF-d_8): δ = 7.82 (m, 4H, H7/H11/H13/H17), 7.50 (d, $^3J_{\text{H,P}} = 6.7$ Hz, 2H, H2/H4), 7.27 (d, $J = 8.3$ Hz, 2H, H19/H23), 7.06 – 7.00 (m, 4H, H8/H10/H14/H16), 6.84 (d, $J = 8.1$ Hz, 2H, H20/H22), 6.61 (m, 2H, H9/H15), 4.12 (s, 5H, H30-34), 4.00 (m, 2H, H26/H29), 3.75 (t, $J = 1.8$ Hz, 2H, H27/H28), 2.20 (s, 3H, H24) ppm.

$^{13}\text{C}\{^1\text{H}\}$ NMR (101 MHz, THF- d_8): δ = 149.86 (d, $^1J_{\text{C,P}}$ = 30.4 Hz, C1/C5), 144.89 (s, C3), 130.70 (d, $^2J_{\text{C,P}}$ = 5.0 Hz, C2/C4), 129.26 (s, C20/C22), 128.22 (d, $^4J_{\text{C,P}}$ = 2.0 Hz, C8/C10/C14/C16), 127.96 (s, C21), 124.89 (d, $^3J_{\text{C,P}}$ = 19.1 Hz, C7/C11/C13/C17), 122.41 (s, C19/C23), 119.84 (d, $^5J_{\text{C,P}}$ = 2.0 Hz, C9/C15), 112.88 (s, C18), 100.42 (d, $^2J_{\text{C,P}}$ = 6.4 Hz, C6/C12), 72.08 (d, $^2J_{\text{C,P}}$ = 12.0 Hz, C26/C29), 68.70 (s, C30-34), 68.05 (d, $^3J_{\text{C,P}}$ = 1.8 Hz, C27/C28), 21.12 (s, C24).

$^{31}\text{P}\{^1\text{H}\}$ NMR (162 MHz, THF- d_8): δ = -68.35 ppm.

1-Methyl-4,6-triphenyl-2-(2'pyridyl)-phosphacyclohexadienyllithium (18)

Under an argon atmosphere at room temperature, methyl lithium (0.03 mL, 0.05 mmol) was added to a solution of **1** (15.0 mg, 0.05 mmol) in 0.5 mL dry THF in a *J*-Young-tube. The solvent was evaporated and a dark red oil was obtained. The product formed quantitatively according to $^{31}\text{P}\{^1\text{H}\}$ NMR spectroscopy.

^1H NMR (401 MHz, THF- d_8): δ = 7.75 (dd, J = 5.3, 1.8 Hz, 1H, H10), 7.60 – 7.56 (m, 2H, H12/H16), 7.53 (d, $^3J_{\text{H,P}}$ = 7.6 Hz, 1H, H4), 7.48 (d, $^3J_{\text{H,P}}$ = 9.2 Hz, 1H, H2), 7.43 – 7.35 (m, 3H, H7/H18/H22), 7.18 – 7.05 (m, 5H, H8/H13/H15/H19/H21), 6.85 (t, J = 7.3 Hz, 1H, H14), 6.79 (t, J = 7.3 Hz, 1H, H20), 6.26 (t, J = 6.0 Hz, 1H, H9), 0.62 (s, 3H, H23) ppm.

$^{13}\text{C}\{^1\text{H}\}$ NMR (101 MHz, THF- d_8): δ = 165.70 (d, $^2J_{\text{C,P}}$ = 24.2 Hz, C6), 146.97 (d, $^4J_{\text{C,P}}$ = 2.3 Hz, C10), 145.81 (d, $^1J_{\text{C,P}}$ = 26.3 Hz, C1), 145.71 (d, $^3J_{\text{C,P}}$ = 0.8 Hz, C3), 135.60 (d, $^4J_{\text{C,P}}$ = 2.1 Hz, C8), 132.21 (d, $^2J_{\text{C,P}}$ = 4.9 Hz, C2), 129.61 (d, $^2J_{\text{C,P}}$ = 4.7 Hz, C4), 127.93 (s, C19/C21), 127.79 (d, $^4J_{\text{C,P}}$ = 1.6 Hz, C13/C15), 124.95 (d, $^3J_{\text{C,P}}$ = 15.6 Hz, C12/C16), 123.37 (s, C18/C22), 122.56 (d, $^5J_{\text{C,P}}$ = 1.4 Hz, C14), 121.54 (s, C20), 116.97 (d, $^3J_{\text{C,P}}$ = 6.7 Hz, C7), 116.48 (d, $^4J_{\text{C,P}}$ = 2.9 Hz, C17), 111.91 (d, $^5J_{\text{C,P}}$ = 1.7 Hz, C9), 106.61 (d, $^2J_{\text{C,P}}$ = 20.9 Hz, C11), 91.06 (d, $^1J_{\text{C,P}}$ = 22.3 Hz, C5), 10.66 (d, $^1J_{\text{C,P}}$ = 12.7 Hz, C23) ppm.

$^{31}\text{P}\{^1\text{H}\}$ NMR (162 MHz, THF- d_8): δ = -76.21 ppm.

1,4,6-triphenyl-2-(2'pyridyl)-phosphacyclohexadienyllithium (19)

Under an argon atmosphere at room temperature, phenyl lithium (0.05 mL, 0.08 mmol) was added to a solution of **1** (26.0 mg, 0.08 mmol, 1 eq) in 0.5 mL dry THF in a *J*-Young-tube. The color turned deep blue. The solvent was evaporated and a dark red oil was obtained. The product formed quantitatively according to $^{31}\text{P}\{^1\text{H}\}$ NMR spectroscopy.

^1H NMR (401 MHz, THF- d_8): δ = 7.88 (m, 2H, H24/H28), 7.84 (m, 1H, H10), 7.71 (m, 2H, H12/H16), 7.67 (d, $^3J_{\text{P,H}}$ = 9.9 Hz, 1H, H2), 7.64 (d, $^3J_{\text{P,H}}$ = 8.3 Hz, 1H, H4), 7.51 (d, J = 8.6 Hz, 1H, H7), 7.32 (m, 2H, H18/H22), 7.25 (m, 1H, H8), 7.16 (dd, J = 8.3, 7.2 Hz, 2H, H13/H15), 7.05 (dd, J = 8.3, 7.3 Hz, 2H, H19/H21), 6.90 (m, 1H, H14), 6.83 (m, 2H, H25/H27), 6.77 (m, 1H, H20), 6.73 (m, 1H, H26), 6.38 (m, 1H, H9) ppm.

$^{13}\text{C}\{^1\text{H}\}$ NMR (101 MHz, THF- d_8): δ = 167.09 (d, $^2J_{\text{C,P}}$ = 25.4 Hz, C6), 147.99 (d, $^4J_{\text{C,P}}$ = 2.6 Hz, C10), 147.36 (d, $^1J_{\text{C,P}}$ = 14.6 Hz, C23), 147.14 (d, $^1J_{\text{C,P}}$ = 24.6 Hz, C1), 146.37 (d, $^3J_{\text{C,P}}$ = 0.6 Hz, C3), 144.30 (s, C24/C28), 136.67 (d, $^4J_{\text{C,P}}$ = 2.7 Hz, C8), 134.52 (t, $^2J_{\text{C,P}}$ = 4.2 Hz, C2), 132.04 (d, $^2J_{\text{C,P}}$ = 5.1 Hz, C4), 128.71 (d, $^4J_{\text{C,P}}$ = 2.0 Hz, C13/C15), 128.63 (s, C19/C21), 125.92 (d, $^3J_{\text{C,P}}$ = 15.5 Hz, C12/C16), 125.04 (s, C25/C27), 124.36 (s, C18/C22), 123.42 (d, $^5J_{\text{C,P}}$ = 1.4 Hz, C14), 123.01 (d, $^5J_{\text{C,P}}$ = 1.4 Hz, C26), 122.51 (s, C20), 118.42 (d, $^4J_{\text{C,P}}$ = 3.1 Hz, C17), 117.84 (d, $^3J_{\text{C,P}}$ = 7.8 Hz, C7), 113.49 (d, $^5J_{\text{C,P}}$ = 1.8 Hz, C9), 104.95 (d, $^2J_{\text{C,P}}$ = 22.7 Hz, C11), 91.81 (d, $^1J_{\text{C,P}}$ = 23.4 Hz, C5) ppm.

$^{31}\text{P}\{^1\text{H}\}$ NMR (162 MHz, THF- d_8): δ = -59.25 ppm.

1-Ferrocenyl- (2-Pyridyl)-4,6-diphenylphosphinine (20)

Under an argon atmosphere at room temperature, ferrocenyl lithium (13.6 mg, 0.07 mmol, 1.15 eq.) and **1** (20 mg, 0.06 mmol, 1 eq.) were mixed in 0.5 mL dry THF in a *J*-Young-tube. The solution turned deep blue. Solvent was evaporated and a black oil was obtained. The product formed quantitatively according to $^{31}\text{P}\{^1\text{H}\}$ NMR spectroscopy.

^1H NMR (401 MHz, THF- d_8): δ = 7.90 (d, J = 5.1 Hz, 1H, H10), 7.74 (d, J = 8.2 Hz, 2H, H12/H16), 7.69 (d, $^3J_{\text{H,P}}$ = 7.9 Hz, 1H, H4), 7.61 (d, J = 8.7 Hz, 1H, H7), 7.53 (d, $^3J_{\text{H,P}}$ = 9.5 Hz, 1H, H2), 7.45 (d, J = 6.8 Hz, 2H, H18/H22), 7.27 (t, J = 7.7 Hz, 1H, H8), 7.20 – 7.09 (m, 4H, H13/H15/H19/H21), 6.89 (t, J = 7.3 Hz, 1H, H14), 6.83 (t, J = 7.2 Hz, 1H, H20), 6.36 (t, J = 6.0 Hz, 1H, H9), 4.10 (d, J = 6.5 Hz, 2H, H24/H27), 3.91 (d, J = 11.4 Hz, 2H, H25/H26), 3.79 (s, 5H, H28-H32) ppm.

$^{13}\text{C}\{^1\text{H}\}$ NMR (101 MHz, THF- d_8): δ = 167.70 (d, $^2J_{\text{C,P}}$ = 25.3 Hz, C6), 147.87 (d, $^4J_{\text{C,P}}$ = 2.5 Hz, C10), 147.17 (d, $^1J_{\text{C,P}}$ = 27.0 Hz, C1), 146.45 (C3), 136.66 (d, $^4J_{\text{C,P}}$ = 2.5 Hz, C8), 133.71 (d, $^2J_{\text{C,P}}$ = 5.5 Hz, C2), 131.79 (d, $^2J_{\text{C,P}}$ = 5.1 Hz, C4), 128.70 (C19/C21), 128.47 (d, $^4J_{\text{C,P}}$ = 2.2 Hz, C13/C15), 125.94 (d, $^3J_{\text{C,P}}$ = 15.9 Hz, C12/C16), 124.08 (s, C18/C22), 123.14 (d, $^5J_{\text{C,P}}$ = 2.0 Hz, C14), 122.18 (s, 20), 118.47 (d, $^3J_{\text{C,P}}$ = 8.1 Hz, C7), 117.40 (d, $^4J_{\text{C,P}}$ = 3.6 Hz, C17), 113.22 (d, $^5J_{\text{C,P}}$ = 2.7 Hz, C9), 107.59 (d, $^2J_{\text{C,P}}$ = 22.7 Hz, C11), 93.02 (d, $^1J_{\text{C,P}}$ = 23.7 Hz, C5) ppm.

$^{31}\text{P}\{^1\text{H}\}$ NMR (162 MHz, THF- d_8): δ = -69.51 ppm.

[(cod)Rh(η^1 -19)] (25)

Compound **19** (58.5 mg, 0.18 mmol) was dissolved in 0.5 mL THF. 3 mL of a THF solution of $[\text{Rh}(\text{cod})\text{Cl}]_2$ (44.38 mg, 0.09 mmol) was added dropwise at room temperature. The solvent was evaporated. Dichloromethane was added, and the solution was filtered through Celite. The

solvent was evaporated, and a black shiny powder was obtained. The product formed quantitatively according to $^{31}\text{P}\{^1\text{H}\}$ NMR spectroscopy.

^1H NMR (401 MHz, THF- d_8): δ = 1.73 (br s, 4 H, Hcod), 2.33 (br s, 4 H, Hcod), 4.03 (br. s, 4 H, Hcod), 6.88 (tt, d, $J_{\text{H,H}} = 7.3$, $J_{\text{H,H}} = 1.2$ Hz, 1 H, Har), 7.01–7.15 (m, 10 H, Har), 7.26–7.33 (m, 8 H, Har), 8.08–8.13 (m, 2 H, Har) ppm.

$^{13}\text{C}\{^1\text{H}\}$ NMR (101 MHz, THF- d_8): δ = 26.2 (s), 31.6 (s), 76.9 (br s), 114.0 (s), 118.8 (d, $J_{\text{C,P}} = 11.5$ Hz), 123.5 (s), 124.2 (s), 126.2 (d, $J_{\text{C,P}} = 0.9$ Hz), 127.5 (s), 127.8 (d, $J_{\text{C,P}} = 5.9$ Hz), 128.4 (s), 128.5 (d, $J_{\text{C,P}} = 22.7$ Hz), 128.9 (d, $J_{\text{C,P}} = 2.4$ Hz), 129.0 (s), 129.2 (d, $J_{\text{C,P}} = 2.6$ Hz), 129.31 (s), 130.1 (d, $J_{\text{C,P}} = 2.3$ Hz), 132.4 (d, $J_{\text{C,P}} = 13.66$ Hz), 136.8 (s), 140.6 (s), 144.5 (s), 144.7 (d, $J_{\text{C,P}} = 3.0$ Hz), 144.5 (s) ppm.

$^{31}\text{P}\{^1\text{H}\}$ NMR (161.9 MHz, THF- d_8): δ = -13.0 (d, $J_{\text{Rh,P}} = 152.2$ Hz) ppm.

[(cod)Rh(η^1 -20)] (26)

To 1 mL of a THF solution of **20** (31.8 mg, 0.06 mmol) prepared *in situ*, $[\text{Rh}(\text{cod})_2]\text{BF}_4$ (23.6 mg, 0.06 mmol) was added as a solid in the glovebox. The solution color changes to black. The solvent was evaporated and a red oil was obtained. When DCM or Pentane was added to purify it, **26** led immediately to **27**.

$^{31}\text{P}\{^1\text{H}\}$ NMR (162 MHz, THF- d_8): δ = 3.5 (d, $^1J_{\text{Rh,P}} = 150.0$ Hz) ppm.

[(cod)Rh(η^1 -(H)20)] (27)

To 1 mL of a THF solution of **26** two drops of water were added. The solvent was evaporated and DCM was added, filtered, washed with 1x5 mL ether and 3x5 mL pentane and dried under vacuum. A dark orange powder was obtained in 87% yield.

^1H NMR (401 MHz, DCM- d_2): δ = 2.08 – 2.22 (m, 2H, CH_2 -cod), 2.35 – 2.51 (m, 3H, CH_2 -cod), 2.51 – 2.61 (m, 2H, CH_2 -cod), 2.62 – 2.74 (m, 1H, CH_2 -cod), 3.78 (s, 5H, Fc), 4.04 – 4.10 (m, 1H, CH-cod), 4.20 – 4.26 (m, 2H, Fc), 4.34 (dd, $J = 9.5$, 3.1 Hz, 1H, P-Csp³-H), 4.46 – 4.51 (m, 1H, Fc), 4.56 – 4.61 (m, 1H, Fc), 4.63 – 4.74 (m, 1H, CH-cod), 5.40 – 5.50 (m, 1H, CH-cod), 5.50 – 5.61 (m, 1H, CH-cod), 5.98 (dd, $J = 8.6$, 3.1 Hz, 1H, H2), 6.73 – 6.82 (m, 2H, Har), 7.15 – 7.22 (m, 2H, Har), 7.24 – 7.32 (m, 1H, Har), 7.40 – 7.59 (m, 6H, Har), 7.87 (d, $J = 18.9$ Hz, 1H, Har), 8.13 – 8.18 (m, 1H, Har), 8.18 – 8.24 (m, 1H, Har), 8.33 – 8.41 (m, 1H, Har).

$^{31}\text{P}\{^1\text{H}\}$ NMR (162 MHz, DCM- d_2): δ = -2.4 (d, $^1J_{\text{Rh,P}} = 156.5$ Hz) ppm.

$^{31}\text{P}\{^1\text{H}\}$ NMR (161.9 MHz, THF- d_8): δ = -2.7 (d, $J_{\text{Rh,P}} = 156.5$ Hz) ppm.

[(cod)₂Rh₂(η¹-η⁵-20)] (28)

To 1 mL of a THF solution of **20** (31.8 mg, 0.06 mmol) prepared *in situ*, [Rh(cod)₂]BF₄ (48.0 mg, 0.12 mmol) was added as a solid in the glovebox. The solution color changed to orange. The solvent was evaporated, DCM added and filtered and washed with 1x2mL ether and 3x10 mL of pentane. The product was dried under vacuum and an orange powder was obtained in 92% yield. Crystals were obtained by slow diffusion of ether into a saturated DCM solution.

¹H NMR(401 MHz, THF-d₈): δ = 1.76-2.90 (m, 16H, CH₂-COD), 3.60-3.65 (m, 2H, Fc), 3.78 (s, 5H, Fc), 4.14 (s, 1H, CH-COD), 4.16-4.19 (m, 1H, Fc), 4.40 (m, 1H, Fc), 4.41-4.46 (m, 1H, CH-COD), 4.54 (m, 2H, CH-COD), 4.77 (m, 1H, CH-COD), 5.15 (m, 1H, CH-COD), 5.50 (s, 1H, CH-COD), 5.67 (m, 1H, CH-COD), 5.76 (d, 1H, *J*=13.7 Hz, Har), 7.27 (m, 3H, Har), 7.34-7.44 (m, 4H, Har), 7.49 (m, 2H, Har), 7.71 (d, 1H, *J*=8.0 Hz, Har), 7.95-7.99 (m, 2H, Har), 8.12 (m, 2H, Har), 8.56 (d, 1H, *J*=8.4 Hz, Har) ppm

³¹P{¹H} NMR (162 MHz, DCM-d₂): δ = 10.73 (dd, ¹*J*_{Rh,P} = 163.0, ²*J*_{Rh,P} = 9.9 Hz) ppm.

[(cod)₂Rh₂(η¹-η⁶-17)] (29)

To 1 mL of a THF solution of **17** (31.8 mg, 0.06 mmol) prepared *in situ*, [Rh(cod)₂]BF₄ (48.0 mg, 0.12 mmol) was added as a solid in the glovebox. The solution color changed to orange. After 2 days an orange solid precipitated. The solid was filtered and washed with 3x10 mL of pentane and was subsequently dried under vacuum. An orange powder was obtained.

³¹P{¹H} NMR (162 MHz, DCM-d₂): δ = 13.96 (dd, *J* = 180.3, 11.6 Hz) ppm.

X-ray crystal structure determinations

Compound 19: $C_{46}H_{57}LiN_3O_6P$, Fw = 785.86, red plate, $0.42 \times 0.21 \times 0.12 \text{ mm}^3$, triclinic, P-1, $a = 11.8298(13)$, $b = 12.2214(13)$, $c = 15.8150(16) \text{ \AA}$, $\alpha = 102.609(8)$, $\beta = 92.630(8)$, $\gamma = 110.278(8)$, $V = 2074.5(4) \text{ \AA}^3$, $Z = 2$, $D_x = 1.258 \text{ g/cm}^3$, $\mu = 0.119 \text{ mm}^{-1}$. 24526 reflections were measured by using a Stoe IPDS 2T diffractometer with a rotating anode (MoK α radiation; $\lambda = 0.71073 \text{ \AA}$) at a temperature of 200(2) K up to a resolution were $\theta_{\text{max}} = 29.29$. 11105 reflections were unique ($R_{\text{int}} = 0.095$). The structures were solved with SHELXL-2013³³ by using direct methods and refined with SHELXL-2013³³ on F^2 for all reflections. Non-hydrogen atoms were refined with anisotropic displacement parameters. 515 parameters were refined without restraints. $R_1 = 0.091$ for 4855 reflections with $I > 2s(I) \text{ e\AA}^3$, and $wR_2 = 0.2873$ for 11105 reflections, $S = 0.953$. Geometry calculations and checks for higher symmetry were performed with the PLATON program.³⁴

Compound 22: $C_{30}H_{25}P$, Fw = 416.47, colorless block, $0.43 \times 0.30 \times 0.21 \text{ mm}^3$, triclinic, P-1, $a = 10.347(2)$, $b = 11.003(2)$, $c = 11.191(2) \text{ \AA}$, $\alpha = 97.92(3)$, $\beta = 94.78(3)$, $\gamma = 112.51(3)$, $V = 1152.8(5) \text{ \AA}^3$, $Z = 2$, $D_x = 1.200 \text{ g/cm}^3$, $\mu = 0.134 \text{ mm}^{-1}$. 12916 reflections were measured by using a Stoe IPDS 2T diffractometer with a rotating anode (MoK α radiation; $\lambda = 0.71073 \text{ \AA}$) at a temperature of 210 K up to a resolution were $\theta_{\text{max}} = 29.32$. 6163 reflections were unique ($R_{\text{int}} = 0.055$). The structures were solved with SHELXS-97³³ by using direct methods and refined with SHELXL-97³³ on F^2 for all reflections. Non-hydrogen atoms were refined with anisotropic displacement parameters. The positions of the hydrogen atoms were calculated for idealized positions. 284 parameters were refined without restraints. $R_1 = 0.046$ for 6163 reflections with $I > 2s(I) \text{ e\AA}^3$, and $wR_2 = 0.100$ for 6163 reflections, $S = 0.837$. Geometry calculations and checks for higher symmetry were performed with the PLATON program.³⁴

Compound 24: $C_{38}H_{36}PRh$, Fw = 626.6, orange block, $0.20 \times 0.19 \times 0.18 \text{ mm}^3$, triclinic, P-1, $a = 11.4403(8)$, $b = 11.7642(9)$, $c = 12.3651(16) \text{ \AA}$, $\alpha = 72.295(6)$, $\beta = 69.699(6)$, $\gamma = 70.685(6)$, $V = 1438.8(2) \text{ \AA}^3$, $Z = 2$, $D_x = 1.446 \text{ g/cm}^3$, $\mu = 6.75 \text{ mm}^{-1}$. 14088 reflections were measured by using a Stoe IPDS 2T diffractometer with a rotating anode (MoK α radiation; $\lambda = 0.71073 \text{ \AA}$) at a temperature of 200(2) K up to a resolution were $\theta_{\text{max}} = 29.18$. 7725 reflections were unique ($R_{\text{int}} = 0.062$). The structures were solved with SHELXS-97³³ by using direct methods and refined with SHELXS-97³³ on F^2 for all reflections. Non-hydrogen atoms were refined with anisotropic displacement parameters. 363 parameters were refined without restraints. $R_1 = 0.038$ for 5844 reflections with $I > 2s(I) \text{ e\AA}^3$, and $wR_2 = 0.096$ for 7725 reflections, $S = 0.915$. Geometry calculations and checks for higher symmetry were performed with the PLATON program.³⁴

Compound 27: $C_{40}H_{38}BF_4FeNPRh$, Fw = 809.25, red needle, $0.29 \times 0.04 \times 0.02 \text{ mm}^3$, monoclinic, $P2_1/c$, $a = 10.3832(3)$, $b = 21.5159(5)$, $c = 16.4841(4) \text{ \AA}$, $\alpha = 90$, $\beta = 97.098(1)$, $\gamma = 90$, $V = 3654.39(16) \text{ \AA}^3$, $Z = 4$, $D_x = 1.471 \text{ g/cm}^3$, $\mu = 0.942 \text{ mm}^{-1}$. 27058 reflections were measured by using a Bruker Photon CMOS Detector, D8 Venture diffractometer with a rotating anode (MoK α radiation; $\lambda = 0.71073 \text{ \AA}$) at a temperature of 100(2) K up to a resolution were $\theta_{\text{max}} = 25.38$. 6699 reflections were unique ($R_{\text{int}} = 0.080$). The structures were solved with SHELXL-2014/7³³ by using direct methods and refined with SHELXL-2014/7³³ on F^2 for all reflections. Non-hydrogen atoms were refined with anisotropic displacement parameters. 442 parameters were refined without restraints. $R_1 = 0.098$ for 5117 reflections with $I > 2s(I) \text{ e\AA}^3$, and $wR_2 = 0.1177$ for 6699 reflections, $S = 1.031$. Geometry calculations and checks for higher symmetry were performed with the PLATON program.³⁴

Compound 28: $C_{48}H_{49}BF_4FeNPRh_2$, Fw = 1019.33, orange block, $0.21 \times 0.11 \times 0.09 \text{ mm}^3$, triclinic, P-1, $a = 10.4551(2)$, $b = 12.5271(3)$, $c = 17.5007(3) \text{ \AA}$, $\alpha = 86.2630(8)$, $\beta = 79.0888(7)$, $\gamma = 72.6954(7)$, $V = 2182.66(8) \text{ \AA}^3$, $Z = 2$, $D_x = 1.551 \text{ g/cm}^3$, $\mu = 1.163 \text{ mm}^{-1}$. 41109 reflections were measured by using a Bruker Photon CMOS Detector D8 Venture diffractometer with a rotating anode (MoK α radiation; $\lambda = 0.71073 \text{ \AA}$) at a temperature of 200(2) K up to a resolution were $\theta_{\text{max}} = 29.29$. 11105 reflections were unique ($R_{\text{int}} = 0.057$). The structures were solved with SHELXL-2014/7³³ by using direct methods and refined with SHELXL-2014/7³³ on F^2 for all reflections. Non-hydrogen atoms were refined with anisotropic displacement parameters. 470 parameters were refined without restraints. $R_1 = 0.050$ for 7403 reflections with $I > 2s(I) \text{ e\AA}^3$, and $wR_2 = 0.1193$ for 8962 reflections, $S = 1.048$. Geometry calculations and checks for higher symmetry were performed with the PLATON program.³⁴

3.6 References

- (1) IUPAC Gold Book - electronegativity <http://goldbook.iupac.org/E01990.html> (accessed Jan 24, 2016).
- (2) Mézailles, N.; Mathey, F.; Le Floch, P. *Prog. Inorg. Chem.* **2001**, *49*, 455.
- (3) Märkl, G.; Lieb, F.; Merz, A. *Angew. Chem.* **1967**, *79* (1), 59.
- (4) Märkl, G.; Merz, A. *Tetrahedron Lett.* **1968**, *9* (32), 3611.
- (5) Märkl, G.; Martin, C.; Weber, W. *Tetrahedron Lett.* **1981**, *22* (13), 1207.
- (6) Ashe III, A. J.; Smith, T. W. *Tetrahedron Lett.* **1977**, *18* (5), 407.
- (7) Moores, A.; Ricard, L.; Le Floch, P.; Mézailles, N. *Organometallics* **2003**, *22* (9), 1960.
- (8) Doux, M.; Thue, P.; Blug, M.; Ricard, L.; Le Floch, P. *Organometallics* **2007**, *26* (9), 5643.
- (9) Märkl, G.; Martin, C. *Angew. Chem. Int. Ed.* **1974**, *13* (6), 408.
- (10) Dave, T.; Berger, S.; Edgar, B.; Kaletsch, H.; Pebler, J. J.; Knecht, J.; Dimroth, K.; Bilger, E.; Kaletsch, H.; Pebler, J. J.; Knecht, J.; Dimroth, K. *Organometallics* **1985**, *4* (4), 1565.
- (11) Baum, G.; Massa, W. *Organometallics* **1985**, No. 4, 1572.
- (12) Moores, A.; Mézailles, N.; Ricard, L.; Le Floch, P. *Organometallics* **2005**, *24*, 508.
- (13) Moores, A.; Mézailles, N.; Ricard, L.; Jean, Y.; Le Floch, P. *Organometallics* **2004**, *23*, 2870.
- (14) Doux, M.; Mézailles, N.; Melaimi, M.; Ricard, L.; Le Floch, P. *Chem. Commun.* **2002**, No. 15, 1566.
- (15) Doux, M.; Bouet, C.; Mézailles, N.; Ricard, L.; Le Floch, P. *Organometallics* **2002**, *21* (13), 2785.
- (16) Doux, M.; Mézailles, N.; Ricard, L.; Le Floch, P. *Organometallics* **2003**, *22* (23), 4624.
- (17) Arliguie, T.; Blug, M.; Le Floch, P.; Mézailles, N.; Thuéry, P.; Ephritikhine, M. *Organometallics* **2008**, *27* (16), 4158.
- (18) Doux, M.; Ricard, L.; Le Floch, P.; Mézailles, N. *Dalton Trans.* **2004**, *16*, 2593.
- (19) Dochnahl, M.; Doux, M.; Faillard, E.; Ricard, L.; Le Floch, P. *Eur. J. Inorg. Chem.* **2005**, *1*, 125.
- (20) Lamberta, J. B.; Mazzola, E. P. *Nuclear Magnetic Resonance Spectroscopy*; Prentice Hall: New Jersey, 1995.
- (21) Baechler, R. D.; Mislow, K. *J. Am. Chem. Soc.* **1970**, *92* (10), 3090.
- (22) Reichl, K. D.; Ess, D. H.; Radosevich, A. T. *J. Am. Chem. Soc.* **2013**, *135* (25), 9354.

- (23) Baechler, R. D.; Mislow, K. *J. Am. Chem. Soc.* **1970**, *92* (15), 4758.
- (24) Mislow, K.; Egan, W. *J. Am. Chem. Soc.* **1971**, *93* (7), 1805.
- (25) Kesanli, B.; Mattamana, S. P.; Danis, J.; Eichhorn, B. *Inorg. Chim. Acta* **2005**, *358* (11), 3145.
- (26) Meißner, G. Synthese, Reaktivität und Koordinationsverhalten von λ^4 -und λ^5 -Phosphininen. Master Thesis, Freie Universität Berlin, Berlin, 2013.
- (27) Müller, C.; Vogt, D. Phosphinine-Based Ligands in Homogeneous Catalysis: State of the Art and Future Perspectives. In *Phosphorus Compounds*; Peruzzini, M., Gonsalvi, L., Eds.; Springer: Netherlands, 2011; pp 151.
- (28) Atkinson, R. C. J.; Long, N. J. Monodentate Ferrocene Donor Ligands. In *Ferrocenes: Ligands, Materials and Biomolecules*; Stepnicka, P., Ed.; John Wiley & Sons: West Sussex, 2008; p 1.
- (29) Barrière, F.; Kirss, R. U.; Geiger, W. E. *Organometallics* **2005**, *24* (1), 48.
- (30) Labande, A.; Debono, N.; Sournia-Saquet, A.; Daran, J.-C.; Poli, R. *Dalton Trans.* **2013**, *42* (18), 6531.
- (31) Hedberg, F. L.; Rosenberg, H. *Tetrahedron Lett.* **1969**, *10* (46), 4011.
- (32) Müller, C.; Wasserberg, D.; Weemers, J. J. M.; Pidko, E. A.; Hoffmann, S.; Lutz, M.; Spek, A. L.; Meskers, S. C. J.; Janssen, R. A. J.; van Santen, R. A.; Vogt, D. *Chem. Eur. J.* **2007**, *13*, 4548.
- (33) Sheldrick, G. M.; *Acta Crystallogr. Sect. A.* **2008**, *64*, 112.
- (34) Spek, A. L.; *Acta Crystallogr. Sect. D.* **2009**, *65*, 148.

Chapter 4

Synthesis of the First Pyridyl-Substituted
Phosphabarrelene, its Coordination
Chemistry and Photochemical Reactivity

4	Phosphabarrelenes	115
4.1	Introduction	115
4.2	Results and discussion	121
4.3	Conclusions	140
4.4	Experimental	140
	General remarks.....	140
	Phosphabarrelene (1)	141
	[Au(1)Cl] (2).....	142
	[[1,5-cyclooctadiene](1)rhodium tetrafluoroborate] (3)	142
	[[CO]ClRh(1)] (4)	143
	[[CO] ₄ W(1)] (5).....	144
	[[CO] ₃ Fe(1)] (6)	144
	[[CO]ClRh(phosphasemibullvalene)] (7).....	145
	[[CO] ₄ W(phosphasemibullvalene)] (8)	145
	X-ray crystal structure determinations	145
4.5	References	148

4 Phosphabarrelenes

4.1 Introduction

In the quest for phosphorus ligands with particular electronic and steric properties, phosphorus-containing molecular cages step on stage as a new class of ligands, which are able to create steric bulk in every direction in space. Bulky phosphorus compounds are especially interesting as ligands in specific processes such as Rh-catalyzed hydroformylation of di- and trisubstituted alkenes,¹⁻³ and Pd-catalyzed cross-coupling reactions.⁴⁻⁶ Even though they do not always form very stable complexes with transition metals, they account for a kinetic stabilization of very active catalytic species towards otherwise unreactive substrates.⁷⁻⁹

Phosphabarrelenes belong to this class of compounds; they consist of two fused six-membered rings, where one or more carbon atoms are replaced by a phosphorus atom. Figure 4.1 shows some examples of this class of ligands; the 1-phosphabarrelene, the 1,4-diphosphabarrelene and the 2-phosphabarrelene.

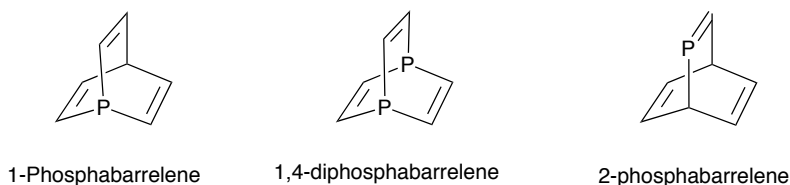
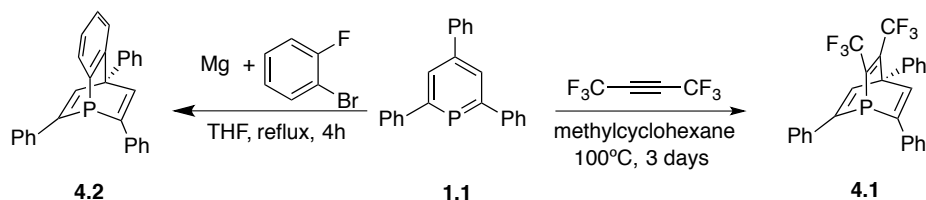


Figure 4.1 Different types of phosphabarrelenes

To the best of our knowledge, there is only one example of a 1,4-diphosphabarrelene¹⁰ (related to diphosphatriptycenes), and one report on 2-phosphabarrelenes,¹¹ whereas 1-phosphabarrelenes have been studied to a greater extent. In this chapter, the synthesis, coordination chemistry and reactivity of 1-phosphabarrelenes will be discussed.

1-phosphabarrelenes can be prepared via a [4+2] Diels-Alder reaction between phosphinines and alkynes, where the former acts as a diene and the latter as a dienophile. In most cases, highly reactive alkynes have to be used for the reaction to take place. As reported by Märkl and Lieb, 2,4,6-triphenylphosphinine does not react with maleic anhydride or Acetylenedicarboxylic acid diethyl ester to form the corresponding phosphabarrelenes. Nevertheless, the more reactive hexafluoro-2-butyne achieves the desired product in approximately 50% yield (**4.1**, scheme

4.1).^{12,13} Also, Märkl and Breit prepared phosphabarrelene **4.2** by reacting *in situ* generated benzyne and phosphinine **1.1** in THF.^{14,15}



Scheme 4.1 Synthesis of phosphabarrelenes **4.1** and **4.2**

Another strategy to access phosphabarrelenes from a variety of alkynes is to activate the phosphorus to make it more electrophilic. This can be achieved *via* pre-coordination of the phosphinine to a metal center. Märkl, Mathey, and Le Floch have used this strategy to obtain phosphabarrelene complexes **4.3-4.5** using moderate-activated alkynes and the corresponding phosphinine-metal complex (figure 4.2).¹⁶⁻¹⁸

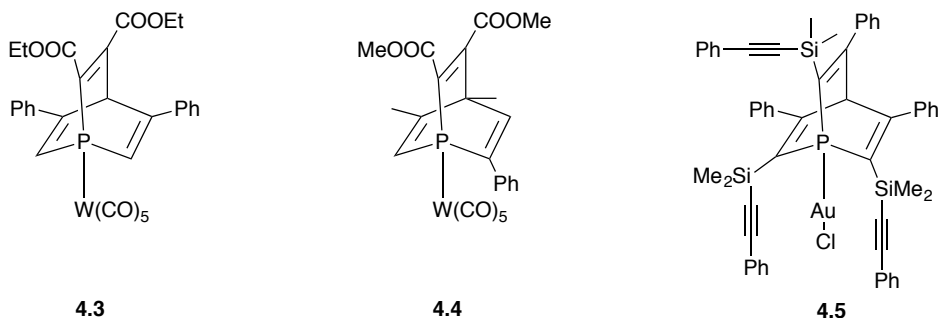


Figure 4.2 Phosphabarrelenes obtained from the corresponding phosphinine metal complexes and the corresponding alkyne

The electronic and steric properties of phosphabarrelenes can be described according to the same parameters with which phosphines and phosphites are described. These are the Tolman's electronic parameter χ , and the cone angle θ . The parameter χ is determined using the symmetric CO stretching frequency of nickel complexes of the general formula $\text{NiL}(\text{CO})_3$, where L is the phosphorus ligand investigated. $\text{P}(t\text{-Bu})_3$ has been set as the reference value, therefore its χ value is 0. For other ligands, the electronic parameter can be calculated by determining the difference in the IR symmetric CO-frequencies of the two complexes; the larger the value, the weaker σ -donating the ligand.

The cone angle θ can be calculated by constructing a cone that opens from the nickel center located at 2.28 Å from the phosphorus atom in the appropriate direction, which embraces all the

atoms of the substituents on the phosphorus atom in CPK models; the larger the angle, the bulkier the phosphine or phosphite (figure 4.3).¹⁹

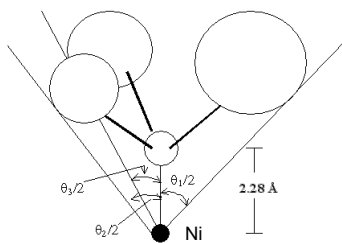


Figure 4.3 Representation of Tolman's cone angle

Phosphabarrelenes **4.6** and **4.7** (figure 4.4), with cone angles of 161° and 181°, respectively were determined from the molecular structure in the crystal of their *trans*-[L₂RhCl(CO)] complexes.²⁰ These values are comparable to those obtained for the bulky phosphines P(*t*Bu)₃ (cone angle of 182°) and P(Cy)₃ (cone angle = 170°).¹⁹ On the other hand, the cone angle for phosphabarrelene **4.7** was calculated from two other metal complexes, [(η⁵-Me₃SiCp)Fe(CO)₂L]PF₆ and [(cym)RuCl₂L], and gave cone angles of 141.4° and 145.3°, respectively.²¹ These values are closer to those reported for P(Ph)₃ (cone angle = 145°) but differ substantially from those obtained for **4.7** in the rhodium complex. Most cone angles reported for phosphabarrelenes have been calculated from X-ray diffraction studies of different metal complexes, which of course makes a direct comparison difficult and shows a strong dependence of the cone angle value to the metal fragment they are coordinated to. In contrast to phosphines, phosphabarrelenes can adapt to have different cone angles regardless of their rigidity. The former can distort more easily and also rotate, which broadens the range of cone angles they can adopt in different coordination environments.

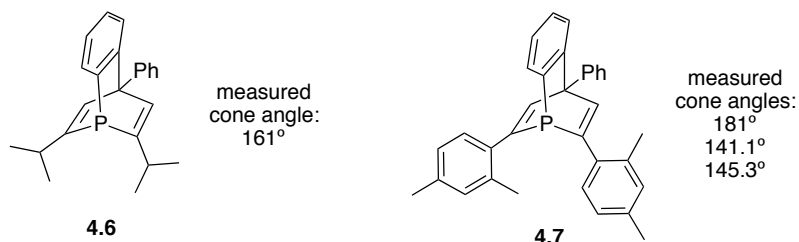


Figure 4.4 Calculated cone angles for phosphabarrelenes **4.6** and **4.7**

The electronic properties of phosphabarrelene **4.7** were studied for different transition metal complexes by means of IR analysis of the CO-stretching frequencies, NMR data (coupling

constants to W or Pt, for example), and bond lengths and angles.²¹ Jones *et. al* came to the conclusion that phosphabarrelene **4.7** is as good σ -donating as P(Ph)₃. The calculated cone angles for **4.7** in different complexes are smaller than those of triphenylphosphine coordination compounds, hence making this phosphabarrelene a less sterically demanding ligand than the former.

The degree of phosphorus pyramidalization in compound **4.2** ($\Sigma_{\text{CPCangles}} = 283^\circ$ vs. 308° for P(Ph)₃) suggests a more pronounced *s*-character of the P lone pair, which provokes mostly a weaker σ -donating character and moderate π -accepting properties of the ligand, due to low lying σ^* orbitals of the P-C bond.²² The lower the sum of the CPC angles, the higher the *s*-character of the P lone pair and thus the less σ -donating the ligand.

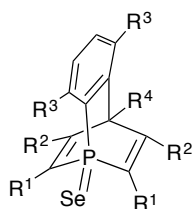
Breit analyzed the electronic properties of ligands **4.2**, **4.6** and **4.7** in the *trans*-[L₂RhCl(CO)] complexes. Phosphabarrelene **4.6** turned out to be the strongest donor followed by **4.7** and **4.2**, which gave the same CO frequencies in the IR spectrum of their respective rhodium complexes. In comparison to these three phosphabarrelenes, P(Ph)₃ is a better σ -donor while triphenylphosphine is a better π -acceptor (table 4.1). In conclusion, it can be said that the coordination properties of these phosphabarrelenes are in between phosphines and phosphinines or phosphites.²³

Table 4.1 IR CO-stretching frequencies of *trans*-[L₂RhCl(CO)] complexes

Ligand	ν [cm ⁻¹]	Ref
P(Ph) ₃	1965	Moloy ²⁴
4.6	1971	Breit ²⁰
4.2	1993	Breit ²⁰
4.7	1993	Breit ²⁰
triphenylphosphine	1999	Breit ²⁵
P[O(2- <i>tert</i> -BuC ₆ H ₄)] ₃	2013	Fernández ²⁶

Contrary to phosphinines, phosphabarrelenes can be more easily oxidized with oxygen, sulfur or selenium. The ³¹P{¹H} NMR data, especially the ¹J_{P-Se} coupling constants of phosphabarrelenes selenides, can contribute to the understanding of their electronic properties.²⁷ It is known that only *s*-orbitals have non-zero electron density at the nucleus and thus can affect neighboring nuclear spin states through the Fermi mechanism; the larger the coupling constant, the higher the

s-character of the phosphorus-selenium bond.²⁸ Some examples of phosphabarrelene selenides have been reported (figure 4.5).^{29,30}



- 4.8:** R¹= Ph, R²= H, R³= H, R⁴= Ph
4.9: R¹= SiMe₂^tBu, R²= Ph, R³= H, R⁴= H
4.10: R¹= SiMe₃, R²= H, R³= H, R⁴= H
4.11: R¹= SiMe₂Ph, R²= Me, R³= H, R⁴= H
4.12: R¹= SiMe₃, R²= Me, R³= H, R⁴= H
4.13: R¹= SiMe₃, R²= Me, R³= Me, R⁴= H

Figure 4.5 Phosphabarrelene selenides reported in literature

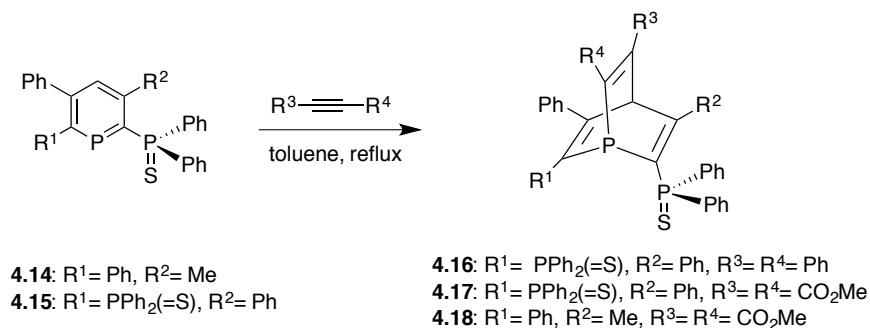
Table 4.2 summarizes the values of $^1J_{\text{P-Se}}$ for compounds **4.8-4.13**. The value given for phosphabarrelene **4.8** outstands from the rest of the compounds. In all the other compounds, more electron donating silyl groups are substituents in the R¹ position. This reflects in the lowering of the $^1J_{\text{P-Se}}$ coupling constant, probably because the C-P-C angles has to open to some extent due to steric demand of the substituents, affecting the hybridization of the P atom. The substitution of the R² and R³ groups also affects the *s*-character of the phosphorus lone pair in phosphabarrelenes. This is interesting for the design of ligands with desired electronic properties. In comparison with some phosphine selenides (see three last entries on table 4.2), phosphabarrelenes can be considered, as compounds, in which the P lone pair has a higher *s*-character. This explains the weaker σ -donation character compared to phosphines that is generally observed in the transition metal complexes discussed above.

Table 4.2 ^{31}P - ^{77}Se coupling constants of selected phosphabarrelene selenides and phosphine selenides

Compound	R ¹	R ²	R ³	R ⁴	$\delta(^{31}\text{P})$ ppm	$^1J_{^{31}\text{P}-^{77}\text{Se}}$ Hz	Ref
4.8	Ph	H	H	Ph	6.6	840	Müller ²⁹
4.9	SiMe ₂ ^t Bu	Ph	H	H	9.2	791	Blug ³⁰
4.10	SiMe ₃	H	H	H	-2.7	787	Blug ³⁰
4.11	SiMe ₂ Ph	Me	H	H	4.8	776	Blug ³⁰
4.12	SiMe ₃	Me	Me	H	4.3	772	Blug ³⁰
4.13	SiMe ₃	Me	Me	H	1.0	756	Blug ³⁰
SePPh ₃					35.9	732	Dean ³¹
SePCy ₃						703	Dean ³¹
SeP(^t Bu) ₃						536	Dean ³²

Donor functionalized phosphabarrelenes **4.16-4.18** (scheme 4.2) have been synthesized by Le Floch from phosphinines **4.14** and **4.15** and diphenylacetylene and dimethylacetylene dicarboxylate. The PPh₂(=S) groups in 1- and 5-position of the phosphinines have shown to

increase the electrophilicity of the phosphorus atom.³³ Taking advantage of this feature, non-activated dienophiles were reacted with such phosphinines to successfully yield the corresponding phosphabarrelenes, especially for the case of the electron poor dimethylacetylene dicarboxylate in comparison with diphenylacetylene (even though reactions times were long).



Scheme 4.2 Synthesis of heterodonor phosphabarrelenes

Palladium complex [Pd(η^3 -C₃H₅)Cl(L)]OTf, L = **4.18**, showed to be a promising catalyst in the allylation of secondary amines in the Suzuki-Miyaura cross-coupling reaction. Other phosphabarrelene complexes have shown interesting catalytic activity in a variety of catalytic processes.³⁴ Phosphabarrelene **4.7** was proven a successful ligand for the Rh-catalyzed hydroformylation of internal alkenes showing no alkene isomerization.^{20,35} Chiral phosphabarrelenes **4.19-4.21** were obtained as a racemic mixture from the reaction of the corresponding phosphinine and *in situ* generated benzyne. Ether cleavage of **4.20** and **4.21** was performed to yield the corresponding hydroxyphenyl-substituted phosphabarrelenes, which after separation of the enantiomers by preparative HPLC, were further functionalized to access enantiomerically pure bidentate phosphabarrelenes **4.22** and **4.23**. Rhodium complexes of both ligands show activity in catalyzed asymmetric hydrogenations of itaconic ester and acetamidoacrylates, giving good *ee* values of up to 90% for the complex with **4.23** as ligand.³⁶

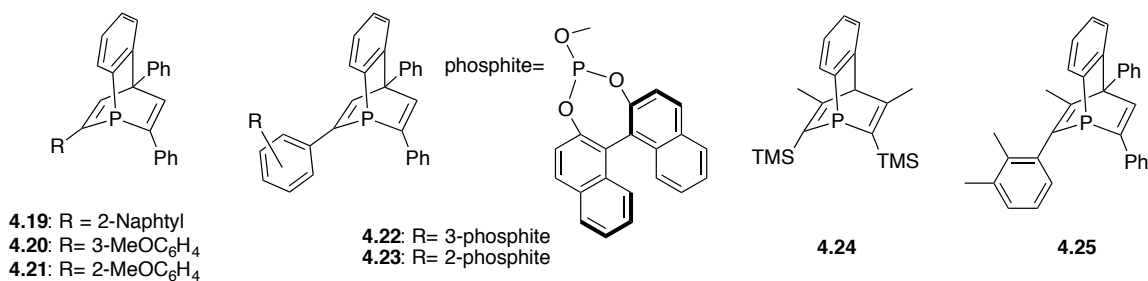


Figure 4.6 Phosphabarrelenes tested as ligands in homogeneous catalysis

Palladium complexes of phosphabarrelene **4.24** have shown promising activity in Pd-catalyzed Negishi-type coupling reactions between a wide range of bromoarenes and aryl zinc derivatives,³⁷ hydrosilylation of alkynes with high regioselectivities under mild conditions,³⁸ and Suzuki-Miyaura cross-coupling reactions of chloroarenes at room temperature.³⁹ The one-pot hydroformylation-cyclization tandem process for the synthesis of bicyclic imidazole derivatives has been successful when using a rhodium precatalyst with **4.25** as ligand.⁴⁰

4.2 Results and discussion

In this section, the results obtained from the synthesis, coordination chemistry and reactivity of the pyridyl-substituted phosphabarrelene **1** will be discussed. The NMR assignment for the signals of the ligand, as well as the X-ray analysis follows the numbering scheme depicted in figure 4.7.

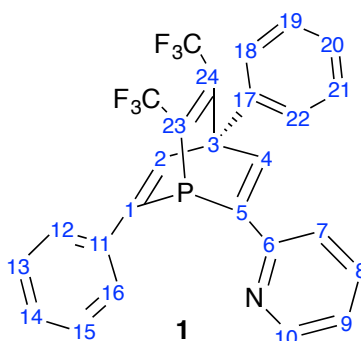
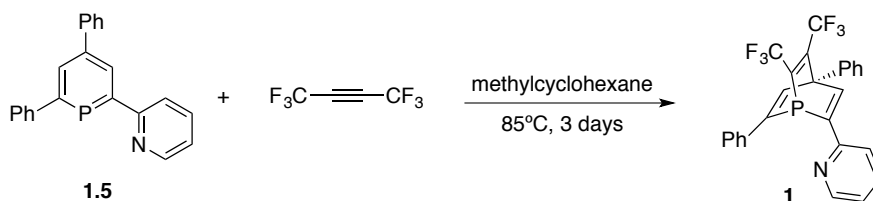


Figure 4.7 Numbering scheme for the NMR signal assignment

As described above, phosphabarrelenes have proven to be promising ligands in catalysis. Thus, the synthesis of a phosphabarrelene starting from the **PN** ligand to obtain a pyridyl-functionalized phosphabarrelene appeared interesting, as it would be the first hetero-functionalized phosphabarrelene with soft-hard characteristics according to the HSAB principle.

Unfortunately, the [4+2] cycloaddition reaction of the **PN** ligand with *in situ* generated benzyne or diethyl acetylenedicarboxylate maleic anhydride was not successful. Interestingly, hexafluoro-2-butyne yielded the desired product **1** under similar conditions to the ones reported by Märkl and Lieb in 1968 (scheme 4.3).¹² The $^{31}\text{P}\{^1\text{H}\}$ NMR spectrum shows a quartet at δ : -68.2 ppm with a $^3J_{\text{P-F}}$ coupling constant of 38.9 Hz. The difference in chemical shift ($\Delta\delta$: 257 ppm) compared to the starting phosphinine clearly accounts for the formation of a $\sigma^3\lambda^3$ -phosphorus compound, more

similar to a phosphine (PMe_3 : $^{31}\text{P}\{^1\text{H}\}$ NMR, $\delta = -60$ ppm). The $^{19}\text{F}\{^1\text{H}\}$ NMR spectrum shows two overlapped multiplets that correspond to the chemically inequivalent CF_3 groups.



Scheme 4.3 Synthesis of phosphabarrelene **1**

While performing attempts to optimize the synthesis and workup of phosphabarrelene **1**, it was noticed that the reaction is reversible when heating the mixture in toluene at temperatures higher than $T = 90^\circ\text{C}$. Crystals suitable for X-ray diffraction were obtained by recrystallization from ethanol and water. The molecular structure depicted in figure 4.8 shows the expected 1-phosphabarrelene. The strong pyramidalization at the phosphorus atom is revealed by the sum of the C-P-C angles with a value of 281.51° , very similar to that of phosphabarrelene **4.2** ($\sum_{\text{CPCangles}} = 283^\circ$).¹⁴

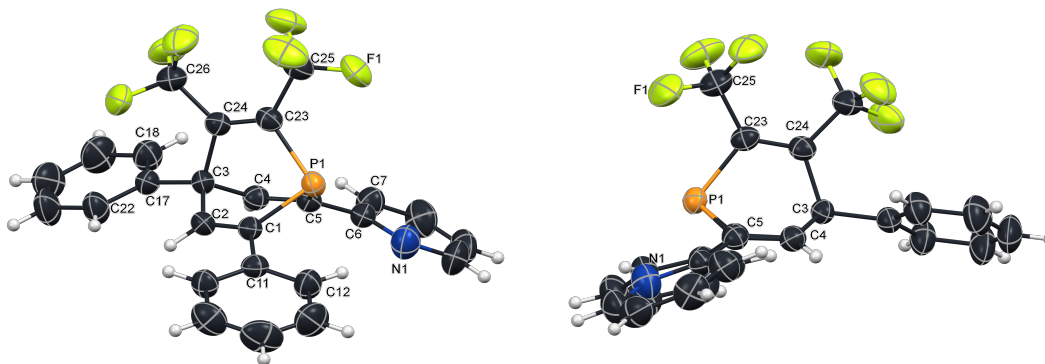


Figure 4.8 Molecular structure of **1** in the crystal. View from the front (left) and view from the side (right). Displacement ellipsoids are shown at the 50% probability level. Selected bond lengths [Å] and angles [$^\circ$]: P1-C1: 1.856(2); P1-C5: 1.954(2); P1-C23: 1.866(3); C1-C2: 1.325(3); C2-C3: 1.532(3); C3-C4: 1.540(3); C4-C5: 1.325(3); C23-C24: 1.328(3); C1-P1-C5: 95.18(10); C1-P1-C23: 94.43(10); C5-P1-C23: 91.86(10)

In contrast to phosphabarrelene **4.2**, there are two stereocenters present in **1**: one located at the C3 atom and another one at the phosphorus atom. As the latter cannot undergo inversion, only one pair of enantiomers can be obtained.

To confirm the formation of a racemic mixture, enantiomerically pure (1*S*)-(+)-10-camphorsulphonic acid was added to a benzene solution of phosphabarrelene **1** to obtain the corresponding pair of diastereoisomers of the protonated phosphabarrelene. In the $^{31}\text{P}\{^1\text{H}\}$ NMR spectrum of the product, the signals split into two quartets in a 1:1 ratio (figure 4.9).

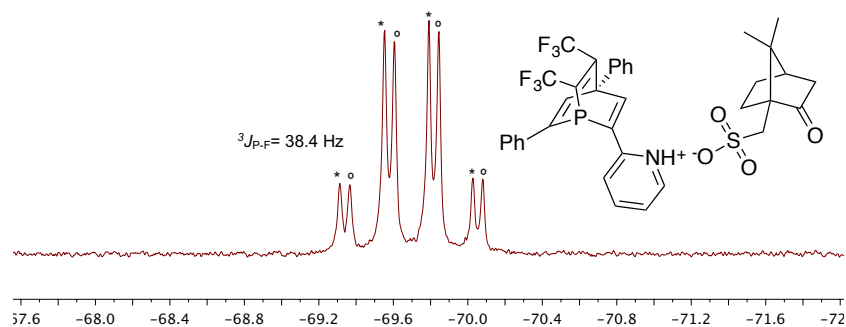


Figure 4.9 $^{31}\text{P}\{^1\text{H}\}$ NMR spectrum of the racemic mixture of **1** protonated by an enantiomerically pure acid

With the new pyridyl-functionalized phosphabarrelene in hand and its potential application in catalysis as a chelating ligand, investigations on its electronic properties were started. Attempts to oxidize the ligand with selenium or sulfur were performed in order to obtain information on the *s*-character of the phosphorus lone pair, as analyzed for other phosphabarrelenes (see figure 4.5). Surprisingly, a mixture of **1** and excess of Se or S₈ in toluene did not react, even after several weeks at $T = 115^\circ \text{C}$. Müller *et. al.* reported on the reactivity of phosphinines towards oxidation with sulfur.⁴¹ Triphenylphosphinine sulfide could also not be obtained unless one equivalent of pyridine was added. The **PN** ligand could be oxidized straightforwardly due to the presence of the incorporated pyridyl ring, which helps to activate the very poor nucleophilic phosphorus of this type of compounds. The same reaction was attempted with selenium instead of sulfur with the idea of obtaining in the first place the **PN** selenide and further react it with hexafluorobutyne to form the desired product. Unfortunately, neither the phosphinine selenide nor the phosphabarrelene selenide could be detected in the $^{31}\text{P}\{^1\text{H}\}$ NMR spectra of the reactions mixtures.

DFT calculations were carried out in order to explain these observations. Figure 4.10 shows the relative energy levels of the frontier orbitals of triphenylphosphinine, 2-(2-pyridyl)-4,6-diphenylphosphinine, benzyne-phosphabarrelene **4.2** and **1**. It is observed that phosphabarrelene **4.2** has the LUMO with the highest energy among all the four compounds represented here.

On the other hand, phosphabarrelene **1** has the more energetically accessible LUMO, probably because the fluorine atoms account for the stabilization of this orbital. Also, from the shape of the HOMOs it is clear that the phosphorus lone pair is not represented by these orbitals, which was already known for the case of phosphinines. For phosphabarrelene **4.2**, the P lone pair has its highest coefficient on the HOMO-2, as in the case of **PN**. For phosphabarrelene **1**, the P lone pair is located on the HOMO-2 and HOMO-3, closer to the situation in triphenylphosphinine, where the P lone pair is represented by the HOMO-3. By comparing the relative energies between the orbitals that represent the phosphorus lone pair in every case, it is observed that for phosphabarrelene **1** and triphenylphosphinine the energies are very similar, while for phosphabarrelene **4.2** and **PN** these orbitals are higher in energy and are the ones that account for the reaction with sulfur.

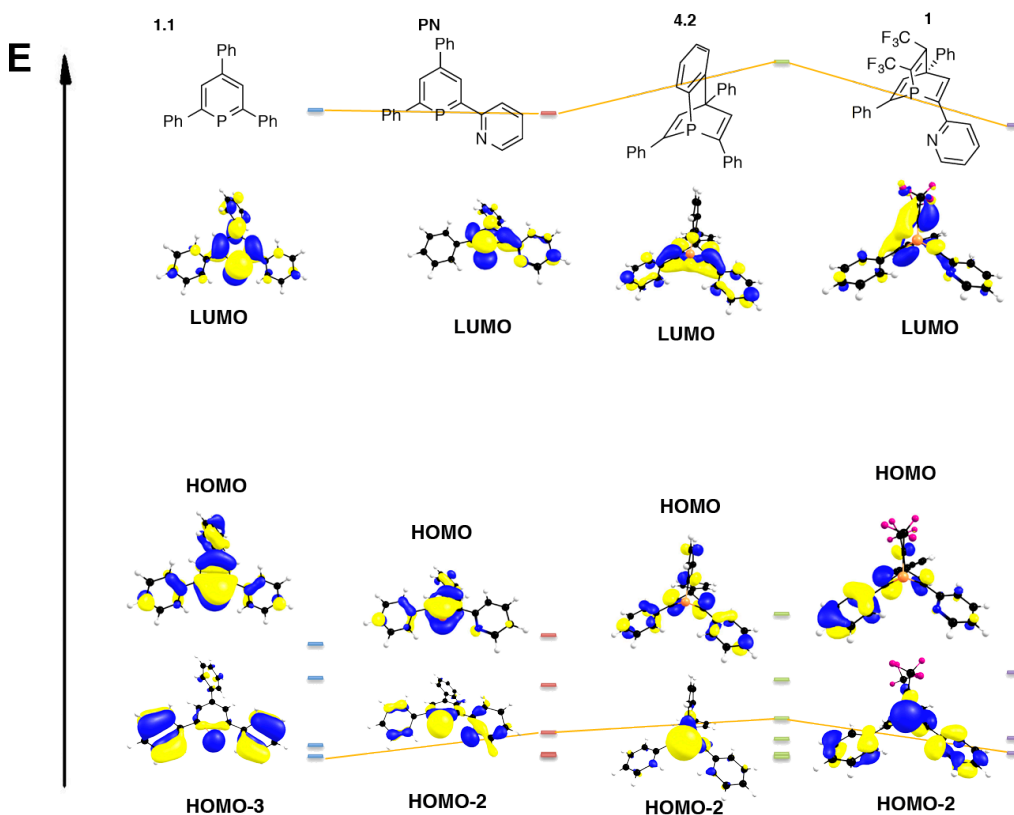
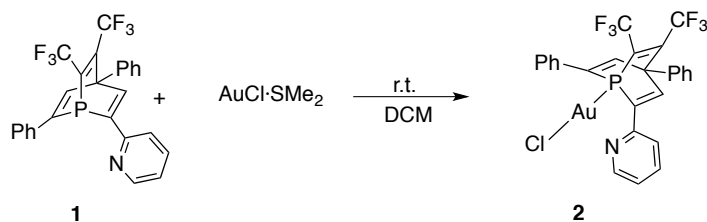


Figure 4.10 Frontier molecular orbitals of phosphinines compared to phosphabarrelenes

Consequently, the P lone pair in the pyridyl-substituted phosphabarrelene **1** is energetically not available to undergo oxidation, nevertheless, it seems that as a ligand it could stabilize metal centers in low oxidation states due to its chelating feature and its low-lying LUMO, which enables it to be a π -acceptor. The coordination chemistry of compound **1** appeared promising and was further explored.



Scheme 4.4 Coordination reaction of **1** with $[\text{AuCl}\cdot(\text{SMe}_2)]$

Phosphabarrelene **1** was first mixed with $[\text{AuCl}\cdot(\text{SMe}_2)]$ in a metal to ligand ratio of 1:1 in dry DCM (scheme 4.4). The solution turns immediately slightly yellow, almost colorless. The $^{31}\text{P}\{^1\text{H}\}$ NMR spectrum shows a signal at $\delta = -9.3$ ppm ($\Delta\delta$: 58.9 ppm compared to the free ligand). The $^3J_{\text{P-F}}$ coupling constant of 21.3 Hz is almost half of that for the free ligand, which is to be expected upon coordination to the metal center *via* the phosphorus lone pair. Crystals suitable for X-ray diffraction were obtained by slow evaporation of a DCM solution (figure 4.11).

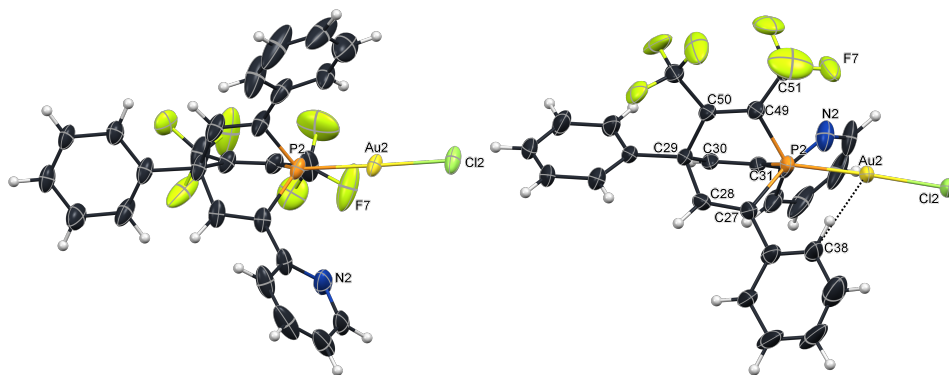
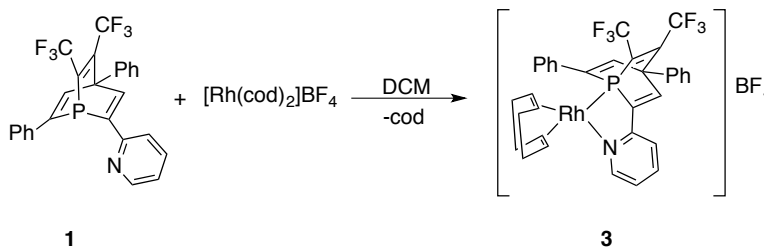


Figure 4.11 Molecular structure of **2** in the crystal. View from the bottom (left) and view from the side (right). Displacement ellipsoids are shown at the 50% probability level. Selected bond lengths [\AA] and angles [$^\circ$]: P2-Au2: 2.214(1); Au2-Cl2: 2.283(2); P2-C27: 1.839(6); P2-C31: 1.825(6); P2-C49: 1.844(6); C50-C49: 1.343(9); C27-C28: 1.328(9); C28-C29: 1.543(7); C29-C30: 1.550(8); C30-C31: 1.325(9); C27-P2-C49: 98.4(3); C49-P2-C31: 96.4(3); C31-P2-C27: 97.4(3); P2-Au2-Cl2: 177.7(4)

Two molecules of complex **2** crystallize in the asymmetric unit, and only one of them is shown for clarity purposes. As in the case of the **PN** ligand, the coordination to gold occurs only *via* the phosphorus atom. Compared to the results obtained by Le Floch and Mathey for complex **4.5**, the P-Au distance of 2.211(1) Å is almost the same as the one for complex **2**, P2-Au2 = 2.214(1) Å. The shortest intramolecular Au-C distance found was the one between Au2-C28, which is 3.128 Å (see chapter 2, complex 11).

Compared to **1**, some differences are worth mentioning. The C-P-C angles become larger in the complex, which has a $\Sigma_{\text{CPCangles}} = 292.2^\circ$, while in the free ligand the value is of only $\Sigma_{\text{CPCangles}} = 283^\circ$. This is expected upon coordination and can be explained by two factors: first, the phosphorus lone pair is now coordinated and generates less electronic repulsions between the substituents in the ligand backbone and itself, especially in 1- and 5-position. Secondly, it is necessary in order to minimize steric hindrance between the metal fragment and the ligand. Moreover, there is a shortening of the P-C bonds, especially the P2-C31, which is 0.127 Å shorter than in the free phosphabarrelene. On the other hand, the distance between the two carbon atoms bearing the CF₃ groups becomes slightly longer.

Attention was then turned to the coordination of **1** towards rhodium(I). Phosphabarrelene **1** and [Rh(cod)₂]BF₄ were mixed in a 1:1 ratio in DCM. The color of the solution changed immediately to orange-red. After evaporating the solvent and washing the orange powder several times with hexane, the product was characterized by means of NMR spectroscopy. The ³¹P{¹H} NMR spectrum shows a doublet of quartets at $\delta = -9.19$ ppm with a large ¹J_{P-Rh} coupling constant of 182.2 Hz and another ³J_{P-F} of 14.2 Hz. The large P-Rh coupling constant is indicative of coordination of the ligand *via* the P lone pair (η^1 -coordination mode).



Scheme 4.5 Reaction of **1** with [Rh(cod)₂]BF₄

The ¹H NMR spectrum of complex **3** was compared with the one of the free ligand **1**; the signals for H2 and H4 do not shift from the ones corresponding to the free ligand, nevertheless the ³J_{P-H}

increases from 6.3 Hz and 5.9 Hz, respectively, to 14.9 Hz and 16.2 Hz, respectively. The ^1H NMR signals of the pyridyl ring (H7-H10) undergo a low-field shift of approximately 0.9 ppm. Moreover, a different signal for each of the cod-protons can be noticed. This reveals that there are no symmetric planes in the molecule. By means of HMBC experiments, each of the cod-protons could be assigned. The π -accepting properties of the P atom in phosphabarrelene **1** leads to a low-field shift of the signals corresponding to the cod-protons *trans* to it ($\delta = 6.0$ ppm and $\delta = 5.7$ ppm) compared to those protons in *trans*-position to the σ -donating nitrogen ($\delta = 4.9$ ppm and $\delta = 3.9$ ppm). Crystals suitable for X-ray diffraction were obtained by slow diffusion of diethyl ether into a DCM solution of **3**.

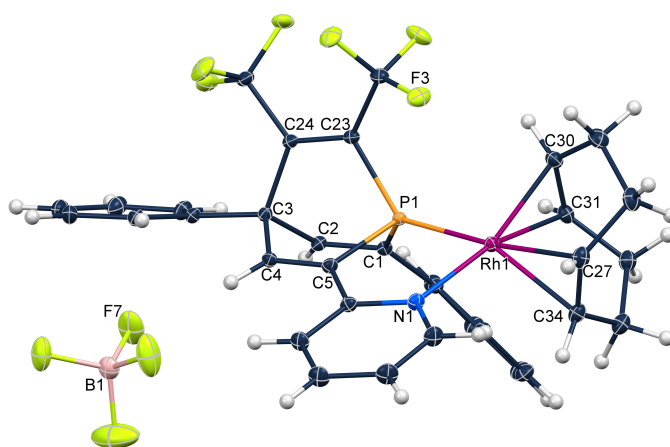


Figure 4.12 Molecular structure of **3** in the crystal. Displacement ellipsoids are shown at the 50% probability level

The molecular structure depicted in figure 4.12 shows the rhodium complex **3** containing a BF_4 anion. One DCM molecule co-crystallizes in the unit cell and has been omitted for clarity. The geometry around the metal center is slightly distorted square planar (P1-Rh1-C27: $172.06(4)^\circ$, P1-Rh1-C34: $152.17(4)^\circ$, N1-Rh1-C30: $159.39(5)^\circ$, N1-Rh1-C31: $162.52(5)^\circ$, C30-Rh1-C27: $80.20(5)^\circ$, C31-Rh1-C34: $81.20(5)^\circ$, P1-Rh1-N1: $81.62(3)^\circ$) and the phosphorus lone pair is not fully directed to rhodium as the metal center is clearly shifted towards the nitrogen atom (see table 4.3). This is a feature that has been observed in phosphinine complexes such as $[\text{Rh}(\text{cod})\text{PN}]\text{BF}_4$,⁴² where the more diffuse lone pair orbital of the phosphorus enables the distortion of the ligand in order to form a chelate complex. Moreover, the C-P-C angles of the phosphabarrelene skeleton become larger compared to those of the free ligand, making the pyramidalization of the phosphorus atom less pronounced ($\Sigma_{\text{CPCangles}} = 290.5^\circ$).

Table 4.3 Selected angles for the molecular structure of **3** in the crystal

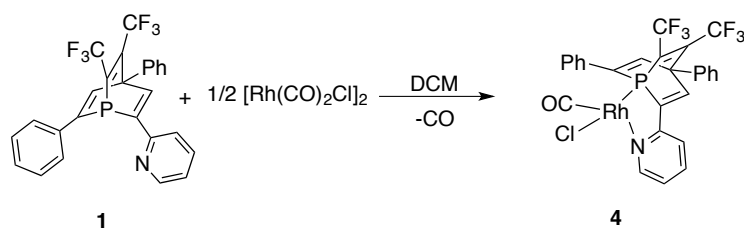
	Complex 3	Phosphabarrelene 1
C1-P1-C5	97.16(5)°	95.18(10)°
C23-P1-C1	98.95(5)°	94.43(10)°
C23-P1-C5	94.39(5)°	91.86(10)°
P1-Rh-N1	81.62(3)°	-
C23-P1-Rh	128.30(4)°	-
C5-P1-Rh	104.51(4)°	-

Another difference with the free ligand is that the P1-C1 and P1-C49 are slightly shorter, while P1-C5 shortens to a greater extent (see table 4.4). The C-C bonds along the ligand framework are, on the other hand, slightly longer. The electronic effects of the ligand follow the same trend discussed in the ¹H NMR spectrum. The C27-C34 bond length suggests that the olefinic cod-carbons *trans* to phosphorus have a higher *sp*² character than that of C30 and C31, the carbon atoms *trans* to N. This difference is caused by the stronger donating nature of the N and the π -accepting ability of the coordinated olefin, which can receive electron density into π^* -orbitals, resulting in the elongation of the C-C bond. On the other hand, the P atom is a weaker donor, thus, this effect is not observed for the olefinic carbons *trans* to the phosphorus.

Table 4.4 Selected bond lengths for the molecular structure of **3** in the crystal

P1-C1	1.832(1) Å	Rh1-C30	2.145(1) Å	<i>trans</i> to N (CF ₃ side)
P1-C5	1.815(1) Å	Rh1-C31	2.170(1) Å	
P1-C49	1.849(1) Å	Rh1-C27	2.277(1) Å	<i>trans</i> to P
P1-Rh1	2.2403(6) Å	Rh1-C34	2.229(1) Å	
N1-Rh1	2.163(1) Å	C30-C31	1.403(2) Å	<i>trans</i> to N
C23-C24	1.344(2) Å	C27-C34	1.380 (2) Å	<i>trans</i> to P
C1-C2	1.339(2) Å			
C2-C3	1.533 (2) Å			
C3-C4	1.556(2) Å			
C4-C5	1.335(2) Å			

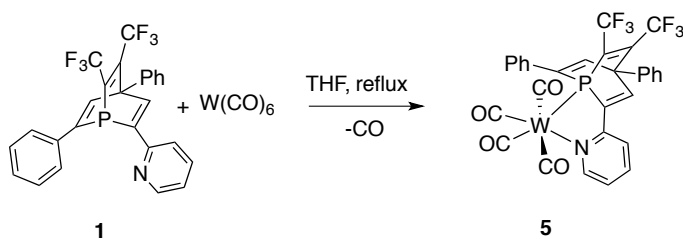
A different rhodium(I) precursor was reacted with phosphabarrelene **1**, in order to get more information on the coordination properties of this new pyridyl-functionalized phosphabarrelene. A 1:1 metal to ligand mixture of [Rh(CO)₂Cl]₂ and **1** was stirred in DCM (scheme 4.6). A brown solution was immediately obtained. The ³¹P{¹H} NMR spectrum shows a doublet of quartets at $\delta = 21.5$ ppm with a large ¹J_{P-Rh} of 198.2 Hz and a smaller ³J_{P-F} of 14.2 Hz. These values are not so different from the ones obtained for complex **3**. When the ¹H NMR spectrum is analyzed, more pronounced differences between **3** and **4** are observed.



Scheme 4.6 Reaction of **1** with $[\text{Rh}(\text{CO})_2\text{Cl}]_2$ in DCM.

The ^1H NMR signal for H4 undergoes a low-field shift of approximately 1 ppm, while the H2 signal appears 0.9 ppm at higher field from the signals of the free ligand. Moreover, the signal for H10 appears now at lower field ($\delta = 9.9$ ppm) compared to **1** and **3**. In the $^{19}\text{F}\{^1\text{H}\}$ NMR spectrum two multiplets are observed; the first one at $\delta = -53.8$ ppm corresponds to the CF_3 group closer to the phosphorus atom. This signal is a quintet, which can be explained by considering that $^5J_{\text{F-F}}$ and the $^4J_{\text{P-F}}$ to be approximately of the same magnitude ($J = 13.5$ Hz). The second one is a quartet at $\delta = -54.4$ ppm with a $^4J_{\text{P-F}}$ of 13.3 Hz. The $^{13}\text{C}\{^1\text{H}\}$ NMR spectrum shows a doublet of doublets at $\delta = 187.3$ ppm, which corresponds to a CO ligand. The larger coupling constant of 67.8 Hz corresponds to the coupling of carbon to rhodium, and the smaller one of 16.9 Hz to the coupling of carbon to phosphorus. The IR spectrum of complex **4** was recorded and a strong absorption band at $\tilde{\nu} = 2014$ cm^{-1} was observed for the asymmetric stretching vibration of coordinated CO. A direct comparison of the IR spectrum of complex **4** with the analogous $[\text{ClRh}(\text{CO})\text{PN}]$ cannot be made, because the reaction of **PN** with $[\text{Rh}(\text{CO})_2\text{Cl}]_2$ leads always to the dimer $[\text{CORh}(\text{PN})\text{Cl}]_2$ (see complex **16** in chapter 2), which shows two CO-stretching bands at $\tilde{\nu} = 2064$ cm^{-1} and 1987 cm^{-1} . Unfortunately, no crystals of **4** suitable for X-ray diffraction could be obtained, but the IR and NMR data strongly support the fact that the structure of complex **4** is the one depicted in scheme 4.6.

For a direct comparison of the electronic properties between a **PN** complex and a phosphabarrelene complex, tungsten complex **5** was synthesized, as $[\text{W}(\text{CO})_4\text{PN}]$ is already known.⁴³



Scheme 4.7 Reaction of **1** with $[\text{W}(\text{CO})_6]$

Phosphabarrelene **1** was dissolved in THF together with $[\text{W}(\text{CO})_6]$. After 1 hour at reflux temperature only one signal can be observed in the $^{31}\text{P}\{^1\text{H}\}$ NMR spectrum at $\delta = -2.4$ ppm with a $^3J_{\text{P-F}} = 17.7$ Hz and tungsten satellites showing a $^1J_{\text{P-W}}$ of 271.5 Hz. The $^{19}\text{F}\{^1\text{H}\}$ NMR shows two multiplets. In this case, the $^3J_{\text{P-F}}$ can be differentiated from the $^4J_{\text{F-F}}$, as the signal results in a doublet of quartets at $\delta = -53.1$ ppm ($^3J_{\text{P-F}} = 17.9$ Hz and $^4J_{\text{F-F}} = 12.8$ Hz), which corresponds to the F atoms in the CF_3 group closest to P. For the distal fluorine atoms the signal is a quartet at $\delta = -54.9$ ppm ($^4J_{\text{F-F}} = 12.8$ Hz). The ^1H NMR spectrum looks very similar to that of the free ligand, except that H4 and H10 signals are more low-field shifted, which suggests the formation of a chelate complex. Indeed, the substitution of two CO ligands is observed in the $^{13}\text{C}\{^1\text{H}\}$ NMR spectrum, where four signals for four CO ligands in complex **5** appear. They all show couplings to P and appear at $\delta = 201.7$ ($^2J_{\text{C-P}} = 6.4$ Hz), $\delta = 204.3$ ($^2J_{\text{C-P}} = 7.9$ Hz), $\delta = 209.6$ ($^2J_{\text{C-P}} = 39.9$ Hz), and $\delta = 210.6$ ($^2J_{\text{C-P}} = 5.3$ Hz) ppm. Crystals suitable for X-ray diffraction were obtained by slow diffusion of pentane into a THF solution of **5** (figure 4.13).

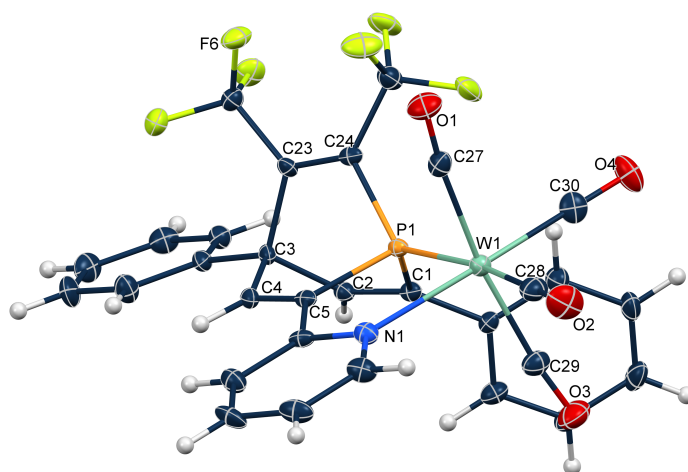


Figure 4.13 Molecular structure of **5** in the crystal. Displacement ellipsoids are shown at the 50% probability level. Two THF molecules have been omitted for clarity

As expected, phosphabarrelene **1** acts as a chelating ligand. As observed for complexes **3** and **4**, the P-C bonds in the ligand backbone are somewhat shorter than in the free ligand, especially P1-C5 (see table 4.5). The C-C bonds are also slightly elongated and the phosphorus pyramidalization is slightly less pronounced than in the free ligand ($\Sigma_{\text{CPCangles}} = 286.7^\circ$).

Table 4.5 Selected bond lengths and angles from the molecular structure of **5**

P1-C1	1.844(4) Å	C2-C3	1.545(6) Å
P1-C5	1.828(5) Å	C3-C4	1.530(5) Å
P1-C24	1.855(4) Å	C4-C5	1.332(6) Å
P1-W1	2.457(1) Å	P1-W1-N1	77.2(1)°
N1-W1	2.300(4) Å	C1-P1-C5	96.7(2)°
C23-C24	1.333(6) Å	C1-P1-C24	94.0(2)°
C1-C2	1.332(6) Å	C5-P1-C24	96.0(2)°

Also in this case, it is evident that the metal center is not in the ideal axis of the phosphorus lone pair (see table 4.6), it is in fact shifted towards the nitrogen atom. Moreover, the carbonyl ligand *trans* to N has a shorter W-C bond and a longer C-O bond compared to the CO ligand *trans* to P. This again indicates the weaker σ -donating properties of the phosphorus compared to N in the phosphabarrelene ligand.

Table 4.6 Selected bond lengths and angles from the molecular structure of **5**

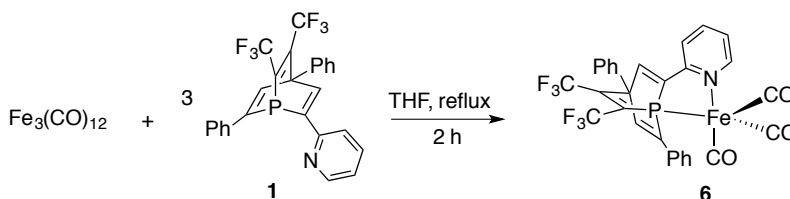
N1-W1-P1	77.2(1)°	W1-C27	2.044(5) Å	axial
C30-W1-P1	97.4(1)°	C27-O1	1.144(6) Å	
C29-W1-N1	94.0(2)°	W1-C28	1.994(5) Å	<i>trans</i> to P
C5-P1-W1	103.8(1)°	C28-O2	1.150(6) Å	
C1-P1-W1	128.9(1)°	W1-C29	2.043(5) Å	axial
C27-W1-P1	93.7(1)°	C29-O3	1.150(6) Å	
C29-W1-N1	94.0(2)°	W1-C30	1.955(5) Å	<i>trans</i> to N
C29-W1-C27	171.7(2)°	C30-O4	1.168(6) Å	

In comparison with the phosphinine complex $[W(CO)_4PN]$, the W-P bond is slightly shorter in **5** (2.4661(4) Å vs. 2.457(1) Å, respectively), while in the case of the W-N bond the trend is opposite (2.2910(17) Å vs. 2.300(4) Å, respectively). According to the C-O bond lengths of the CO ligands in *trans* position to the P atom in the corresponding complex, phosphabarrelene **1** is not as a good π -acceptor as the **PN** ligand. For $[W(CO)_4PN]$, the $C_{transP-O}$ bond is 1.179(9) Å and the $C_{transN-O}$ bond is 1.19(1) Å, while for complex **5**, the $C_{transP-O}$ bond is 1.150(6) Å and the $C_{transN-O}$ bond is 1.168(6) Å.

The IR spectrum of both complexes was also recorded. The CO-stretching frequencies for $[W(CO)_4PN]$: $\tilde{\nu} = 2008, 1893, 1870, \text{ and } 1836 \text{ cm}^{-1}$; are in general at higher wave numbers than those for **5**: $\tilde{\nu} = 2002, 1891(\text{br}), 1846(\text{br}) \text{ cm}^{-1}$. This confirms the trend observed in the bond length analysis of the crystal structures that the **PN** phosphinine is a better π -acceptor.

Another carbonyl complex was chosen in order to compare phosphabarrelene **1** and the **PN** ligand. Scheme 4.8 shows the reaction between $[Fe_3(CO)_{12}]$ and **1**, which yields complex **6**. Two

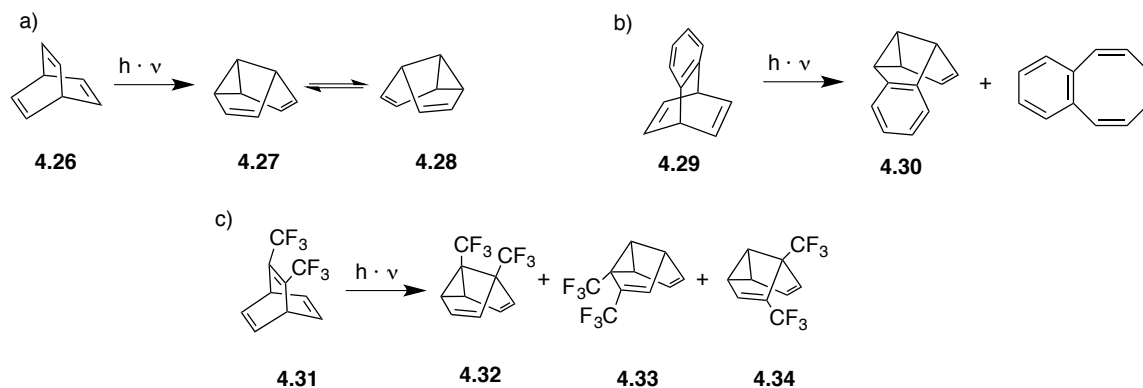
by-products were observed by TLC analysis of the reaction mixture, which do not contain phosphorus (as proven by $^{31}\text{P}\{^1\text{H}\}$ NMR spectroscopy) and are believed to correspond to $[\text{Fe}(\text{CO})_5]$ and $[\text{Fe}_2(\text{CO})_9]$, according to the color of the TLC spots. These observations have been reported in the reaction of $[\text{Fe}_3(\text{CO})_{12}]$ with bipyridines (see complex **16** in chapter 2). Nevertheless, complex **6** could be isolated by means of column chromatography.



Scheme 4.8 Coordination reaction of **1** with $[\text{Fe}_3(\text{CO})_{12}]$

Complex **6** shows a signal in the $^{31}\text{P}\{^1\text{H}\}$ NMR spectrum at $\delta = 27.0$ ppm with a $^3J_{\text{P-F}}$ coupling constant of 15.3 Hz. The ^1H NMR spectrum shows broader signals compared to the ^1H NMR spectra of complexes **3-5**. This might be due to ligand exchange between the CO ligands and the phosphabarrelene. In the $^{13}\text{C}\{^1\text{H}\}$ NMR spectrum there is only one resonance observed for a CO ligand, which supports the idea of dynamic behavior of the complex in solution. It is very interesting that the CO stretching bands in the IR spectrum do not differ very much from the ones obtained for $[\text{Fe}(\text{CO})_3\text{PN}]$ ($\tilde{\nu} = 2001, 1946, 1900 \text{ cm}^{-1}$ vs. $\tilde{\nu} = 1999, 1949, 1904 \text{ cm}^{-1}$, respectively).

Also, some experiments were conducted to explore the reactivity of the phosphabarrelene and the complexes prepared in this work. It is known that barrelenes undergo di- π -methane rearrangement when irradiated with UV light to yield the so-called semibullvalenes (scheme 4.9a).⁴⁴⁻⁵⁴ The photoinduced rearrangement of CF_3 -substituted barrelenes has been reported to yield different isomers of CF_3 -substituted semibullvalenes as depicted in scheme 4.9c. In many other cases, this transformation is also not selective, and formation of byproducts is observed (scheme 4.9b).^{55,56}



Scheme 4.9 a) photochemical rearrangement of barrelene to semibullvalene, b) rearrangement of **4.29** with the formation of by-products, c) non-selective photochemical rearrangement of **4.31** to different semibullvalenes

The phosphorus derivatives of **4.26** and **4.31** are known (**4.2** and **4.1**, respectively), but until very recently only three examples of phosphasemibullvalenes were reported in literature (figure 4.14).

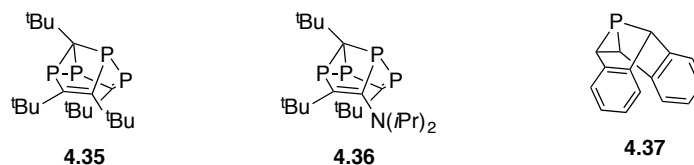
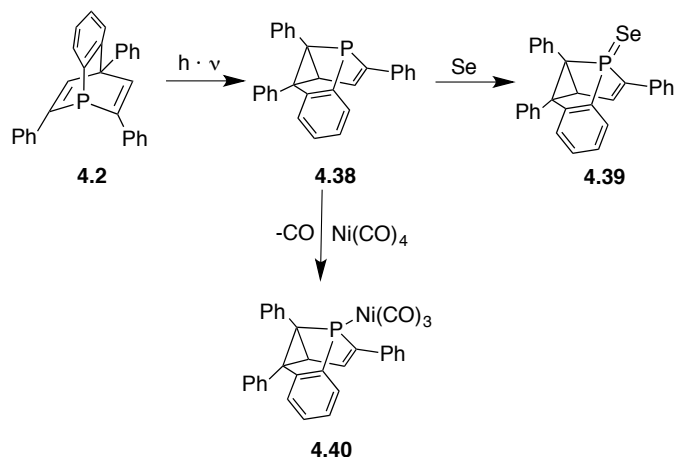


Figure 4.14 Phosphasemibullvalenes reported in literature

Compounds **4.35** and **4.36** were synthesized by Regitz *et al.* during the thermal cyclotetramerization of the corresponding phosphalkyne and by Binger *via* the reaction of 2,4,6-tri-*tert*-butyl-1,3,5-triphosphinine with the diisopropylamino-substituted phosphalkyne, respectively.^{57,58} 1-phosphasemibullvalene **4.37** was synthesized by Grützmacher and co-workers *via* a multistep procedure. This compound resulted thermally unstable and its coordination chemistry has not been further investigated.⁵⁹

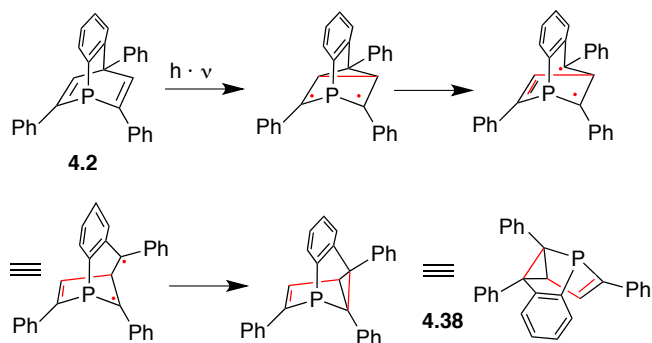
Müller *et al.* reported very recently on the photochemical synthesis and coordination chemistry of phosphasemibullvalene **4.38** derived from phosphabarrelene **4.2** (scheme 4.10).⁶⁰ Upon irradiation of phosphabarrelene **4.2** with UV light, chiral 5-phosphasemibullvalene **4.38** was quantitatively and selectively formed. The product was further oxidized with selenium, which yielded phosphasemibullvalene selenide **4.39**. The latter was crystallographically characterized, which also proved unequivocally the structure of **4.38**.



Scheme 4.10 Photochemical formation of phosphasemibullvalene **4.38** and its further reactivity

Nickel complex **4.40** was synthesized in order to investigate the electronic properties of the 5-phosphasemibullvalene as a ligand. From the observations made, the new phosphorus compound **4.38** can be considered as a slightly stronger net-donor than the corresponding phosphabarrelene **4.2**, while $\text{P}(\text{Ph})_3$ is a much better net-donor.

The proposed mechanism for the rearrangement is in agreement with the one studied by Zimmerman *et al.* for the case of barrelenes. The high selectivity in the case of phosphabarrelene **4.2** is attributed to the fact that the radicals formed in the first step are stabilized by the phenyl-groups in the α -position of the phosphorus heterocycle (scheme 4.11).



Scheme 4.11 Proposed mechanism for the formation of phosphasemibullvalene **4.38** from phosphabarrelene **4.2**

Contrary to the phosphabarrelene **4.2**, phosphabarrelene **1** is chiral, thus the possibility of formation of several more isomers after photolytic rearrangement in principle increases for the case of **1**. While irradiation of the pyridyl-substituted phosphabarrelene with UV light results in several products according to $^{31}\text{P}\{^1\text{H}\}$ NMR spectroscopy, photochemical reactions of complexes of **1** turned out to be much more selective.

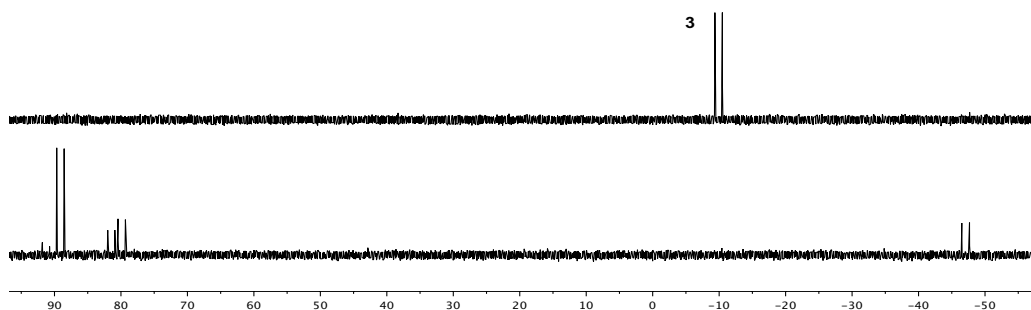


Figure 4.15 $^{31}\text{P}\{^1\text{H}, ^{19}\text{F}\}$ NMR spectrum of **3** (top) and after irradiating the solution with UV light (bottom)

First, a solution of Rh-complex **3** was irradiated with UV light for 2 hours and a $^{31}\text{P}\{^1\text{H}, ^{19}\text{F}\}$ NMR spectrum was recorded. The spectrum reveals that after this time, the starting material has been completely consumed and at least five species have formed. All signals show ^{31}P - ^{103}Rh couplings. One of the signals has a chemical shift of $\delta = -47.1$ ppm, while the rest of them are located in the area between $\delta = 79$ ppm and $\delta = 93$ ppm (figure 4.15). It was noticed that these signals in the $^{31}\text{P}\{^1\text{H}, ^{19}\text{F}\}$ NMR spectrum appear even when the NMR solutions of complexes **3-5** were left standing for one day under normal daylight.

Complexes **4** and **5** were also irradiated and the rearrangement reaction were followed by means of $^{31}\text{P}\{^1\text{H}, ^{19}\text{F}\}$ NMR spectroscopy (figure 4.16). The photochemical rearrangement of ligand **1** is much more selective for complexes **4** and **5** than for **3**. In both cases the formation of a major species and a minor species at low field is observed, with major:minor ratios of approximately 10:1 for both, **7** and **8**.

It turned out that the photochemical rearrangement of ligand **1** is much more selective for complexes **4** and **5** than for **3**. In both cases the formation of a major species and a minor species at low field is observed, with major:minor ratios of approximately 10:1 for both, **7** and **8**.

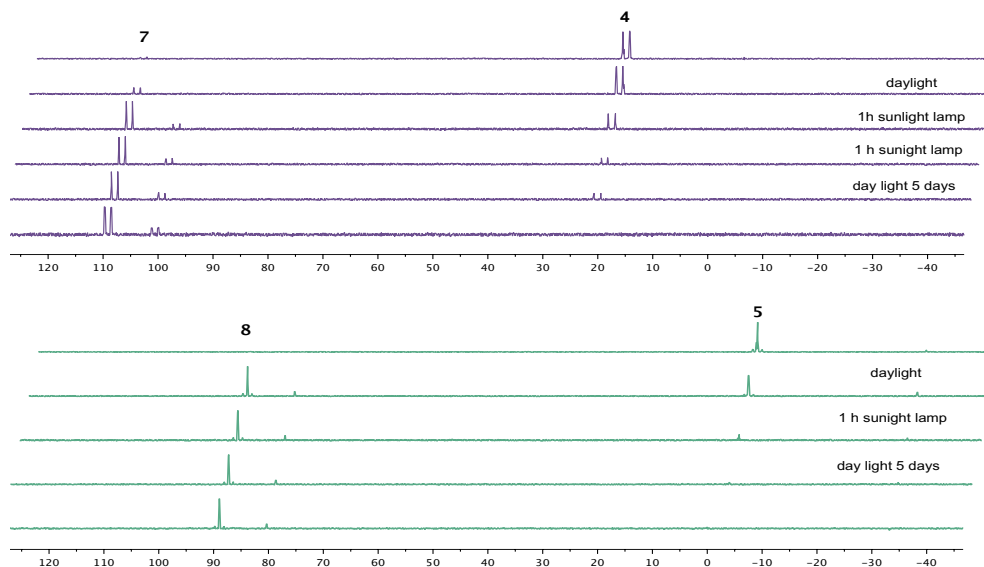


Figure 4.16 Time dependent $^{31}\text{P}\{^1\text{H},^{19}\text{F}\}$ NMR spectra of rearrangement reactions of complex **4** (top) and **5** (bottom) under UV light

For the major species formed from complex **4**, the $^{31}\text{P}\{^1\text{H}\}$ NMR spectrum shows a doublet of quartets at $\delta = 109.2$ with a Rh-P coupling constant of 188.2 Hz and a P-F coupling constant of 7.6 Hz. For the major species formed from tungsten complex **5**, the $^{31}\text{P}\{^1\text{H}\}$ NMR spectrum shows a quartet at $\delta = 88.6$ ppm with tungsten satellites $^1J_{\text{P-W}} = 270.0$ Hz and a $^3J_{\text{P-F}} = 9.3$ Hz. Fortunately, crystals suitable for X-ray diffraction were obtained from the major species (as confirmed by $^{31}\text{P}\{^1\text{H},^{19}\text{F}\}$ NMR spectroscopy) formed in the rearrangement of **4** and **5**.

Two molecules of complex **7** crystallize in the unit cell of the crystal. For clarity purposes only one of them is depicted in figure 4.17 along with selected bond lengths and angles. The rhodium complex contains a chelating phosphasemibullvalene ligand derived from phosphabarrelene **1**. As expected, the CO ligand is *trans* to the pyridine ring, as it is a better σ -donor than the phosphasemibullvalene P atom. The IR spectrum shows a band at $\tilde{\nu} = 2008$ cm^{-1} that corresponds to the asymmetric stretching vibration of the CO ligand. Compared to the CO-stretching frequency of complex **4** at $\tilde{\nu} = 2014$ cm^{-1} , this phosphasemibullvalene ligand can be considered a better σ -donor than phosphabarrelene **1**.

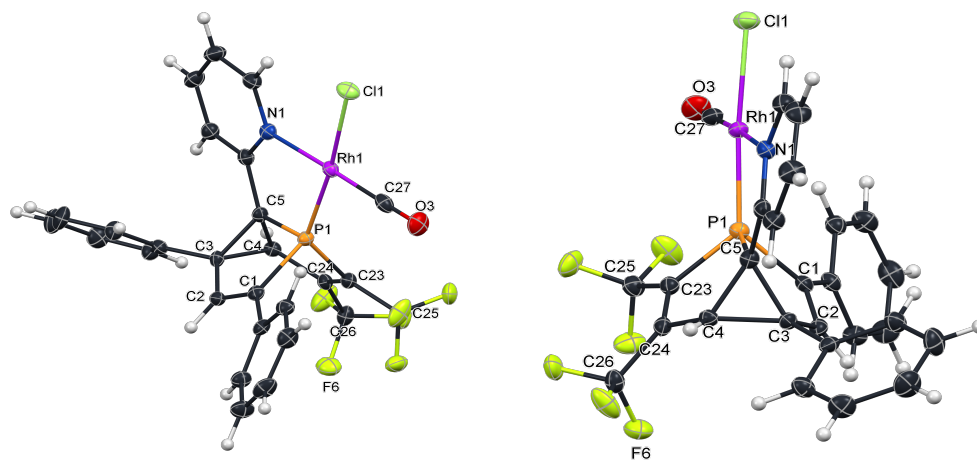


Figure 4.17 Molecular structure of **7** in the crystal. View from the side (left) and view from the back (right). Displacement ellipsoids are shown at the 50% probability level. Selected bond lengths (Å) and angles (°): P1–Rh1: 2.170(4); N1–Rh1: 2.163(1); P1–Cl1: 1.836(4), P1–C23: 1.834(3); P1–C5: 1.823(4); Rh1–Cl1: 2.360(1); Rh1–C27: 1.829(5); C27–O3: 1.144(6); C4–C24: 1.483(4); C24–C23: 1.336(5); C1–C2: 1.349(5); C2–C3: 1.491(5); C3–C5: 1.531(5); C5–C6: 1.480(4); C3–C4: 1.575(4); C1–P1–C23: 93.0(2); C1–P1–C5: 93.5(2); C5–P1–C23: 92.8; P1–Rh1–N1: 81.77(9); Cl1–Rh1–C27: 88.91(1); C27–Rh1–P1: 95.6(1); Cl1–Rh1–N1: 93.78(9).

The mechanism for the rearrangement of ligand **1** in a complex is proposed. Following the scheme depicted in figure 4.18, the formation of a new bond occurs between atoms C2 and C4 (**A**), assuming that the radicals formed in 1- and 5-position should be better stabilized by the phenyl and pyridyl rings, rather than by the CF₃ groups in 23- and 24-position. The homolytic cleavage of the C2–C3 bond and the formation of a double bond between C1 and C2 lead to species **B**. The last step happens when the cyclopropane ring is built by the formation of a single bond between C3 and C5 yielding species **C**.

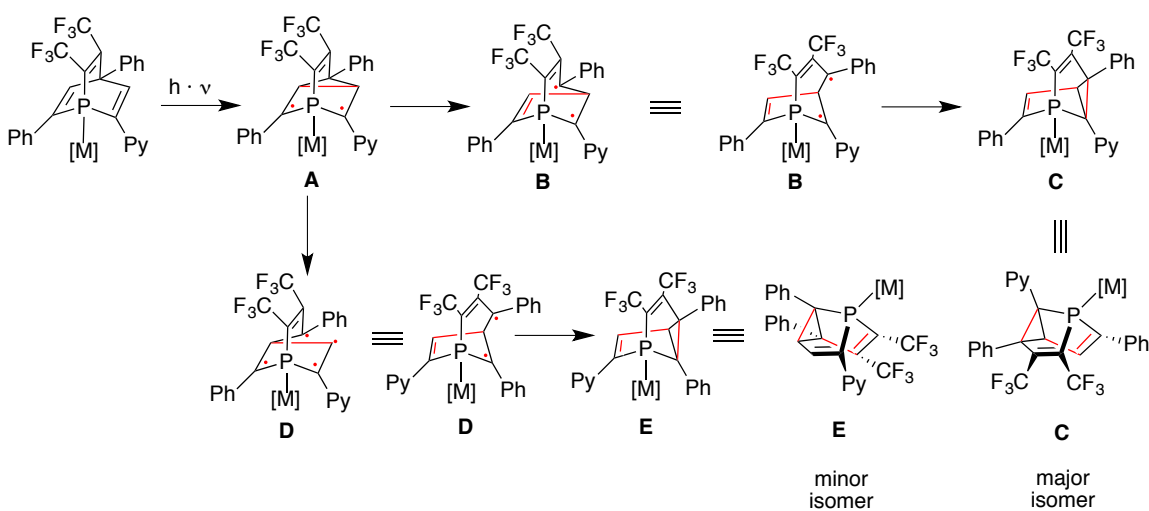


Figure 4.18 Proposed mechanism for the photochemical rearrangement of a given metal complex of phosphabarrelene **1**

At the point where **A** is formed, there is a second possibility: the cleavage of C3-C4 can also occur instead of that of C2-C3, thus yielding **D**. After the formation of the C1-C3 bond, compound **E** is obtained. Molecules **C** and **E** are isomers, and probably the major and minor species detected in the $^{31}\text{P}\{^1\text{H}\}$ NMR spectrum of the irradiated solution of phosphabarrelene complexes. The molecular structure obtained for rhodium complex **7** corresponds to isomer **C**, which, as proven by means of $^{31}\text{P}\{^1\text{H}\}$ NMR, should be assigned as the major species.

Both enantiomers of isomer **C** are observed in the molecular structure in the crystal of tungsten complex **8** (figure 4.19). Two molecules of the complex crystallize together in the unit cell. Each complex bears a different enantiomer of the pyridyl-substituted phosphasemibullvalene. The twinned crystals did not allow the anisotropic refinement of C and N atoms, thus some bond lengths and angles cannot be discussed in detail. The molecular structure in the crystal also corresponds to the major species observed in the $^{31}\text{P}\{^1\text{H}, ^{19}\text{F}\}$ NMR spectrum depicted in figure 4.16 (bottom).

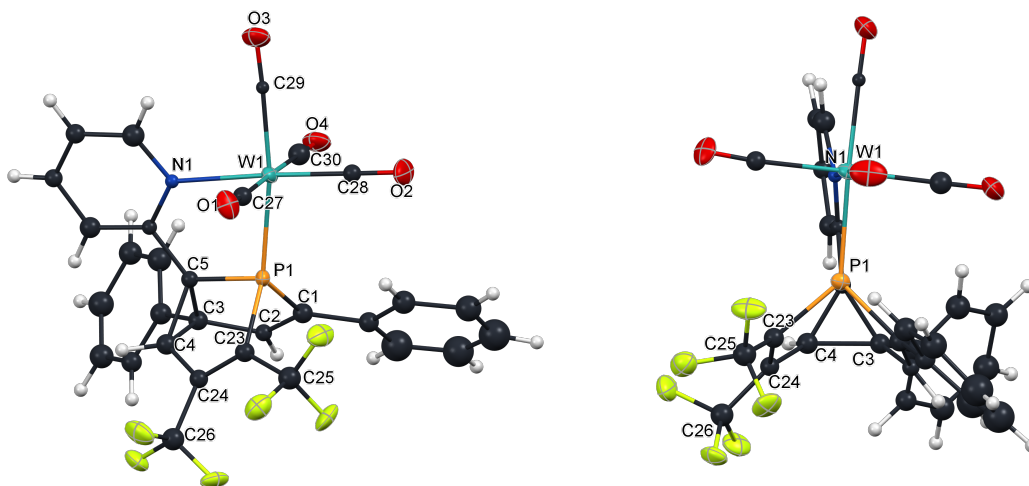


Figure 4.19 Molecular structure of **8** in the crystal. View from side (left) and view from the front (right). Displacement ellipsoids are shown at the 50% probability level.

It is clear that the selectivity of the phosphabarrelene rearrangement has to be metal-mediated, as the photochemical reaction of the free ligand leads to several unidentified products, although the conversion of Rh-complex **3** also leads to more isomers. The radical species **A** (figure 4.18) that forms the major products observed in the case of complexes **7** and **8** and according to the proposed mechanism, could be better stabilized when the metal fragment bears other electron-

withdrawing (π -acceptors), and less labile ligands which could explain the differences in selectivity between complex **3**, **4** and **5**.

With these complexes in hand, a comparison of the electronic properties of the **PN** ligand, the pyridyl-substituted phosphabarrelene **1**, and the pyridyl-phosphasemibullvalene can now be made. Table 4.7 shows the IR CO-stretching frequencies for these three complexes. Judging only from the IR values, it seems that the **PN** phosphinine is the best net donor of all, followed by phosphabarrelene **1** and the corresponding phosphasemibullvalene. This is, however, the opposite trend found in literature as well as in this work as the IR spectra analysis of the rhodium complexes **4** and **7** revealed that the phosphasemibullvalene shows better donating properties than the phosphabarrelene.

Table 4.7 IR values of CO-stretching frequencies of tungsten carbonyl complexes

	[W(CO) ₄ PN]	5	8
IR- $\tilde{\nu}_{\text{CO}}(\text{cm}^{-1})$	2008	2022	2024
	1893	1891	1898
	1870	1846	1861
	1836		

Other effects need to be considered before making a direct comparison. Apparently, the fact that phosphabarrelene and phosphasemibullvalene bear strong electron-withdrawing CF_3 groups, leads to the fact that the **PN** phosphinine, known to be a strong π -acceptor, results in the best net-donor of this series of tungsten complexes. For this reason, only complexes **5** and **8** will be compared. From the molecular structures of the complexes, it is evident that the metal center is not in the direction of the phosphorus lone pair, and this should influence also the donation properties of the ligand. The C-P-W bonds were analyzed for both complexes, where it was observed that phosphasemibullvalene complex **8** is slightly more distorted than complex **5** (C23-P1-W1: 133.1(7) $^\circ$; C5-P1-W1: 102.8(7) $^\circ$; C1-P1-W1: 128.3(7) and C24-P1-W1: 128.7(1) $^\circ$; C5-P1-W1: 103.8(1) $^\circ$; C1-P1-W1: 129.9(1) $^\circ$, respectively). The P1-W1-C_{trans} angles also confirm this observation: for complex **8** this angle has a value of 169.5(5) $^\circ$, whereas for complex **5** the value is 171.7(2) $^\circ$, which is closer to the ideal angle of 180 $^\circ$. It appears that steric factors in the octahedral tungsten complex can lead to a misleading analysis of the electronic properties of bulky phosphorus ligands.

4.3 Conclusions

The first pyridyl-substituted phosphabarrelene has been synthesized, spectroscopically- and structurally characterized. According to DFT-calculations, the phosphorus lone pair in **1** is rather low in energy (HOMO-2) leading to the situation that the compound cannot be oxidized to the corresponding sulfide or selenide. Nevertheless the LUMO is energetically accessible. Five different transition metal complexes (**2-6**) have been synthesized and characterized. In five of them, phosphabarrelene **1** acts as a chelating ligand, whereas with Au(I) coordination occurs only *via* the P lone pair. By means of IR- and crystal structure analysis, the ligand has been assigned as a weaker net donor compared to phosphinines due to the higher *s*-character of the phosphorus lone pair. Although phosphabarrelene **1** yields many different products after irradiation with UV-light, the reactivity of phosphabarrelene complexes upon UV irradiation turned out to be much more selective. In most of the cases, two isomers of the corresponding phosphasemibullvalene are formed after irradiation of a solution of the phosphabarrelene complex and remain coordinated to the metal center. Apparently, the more π -accepting the ancillary ligands in such complexes, the more selective the reaction. For complexes **4** and **5**, only two products are obtained whereas for complex **3** at least five products were detected. The major products of the irradiation reaction of complexes **4** and **5** could be crystallographically characterized as the corresponding complexes bearing a phosphasemibullvalene ligand, which also coordinates as a chelate to the metal center. The proposed mechanism for the photochemical rearrangement of phosphabarrelene **1** assumes that there is stabilization of the radicals formed on the carbon atoms in α position to the phosphorus atom (C1 and C5), which bear a phenyl and a pyridyl substituent respectively. This explains the preferred formation of the observed isomers. Pyridyl-substituted phosphasemibullvalene proves to be a slightly better net-donor in comparison to phosphabarrelene **1**, according to the spectroscopic properties of the corresponding [LRhCOCl] complexes.

4.4 Experimental

General remarks

All reactions were performed under argon by using Schlenk and glovebox techniques. All glassware was dried prior to use. All common solvents and chemicals were commercially available. Dry solvents were prepared by using custom-made solvent purification columns filled with Al₂O₃ from Braun Solvent systems. THF and Et₂O were distilled under argon from

potassium/benzophenone prior to use. All common solvents and chemicals were commercially available. NMR spectra were recorded with a *JEOL ECP500* (^1H NMR 500.00 MHz), a *JEOL ECX400*, a *JEOL ECAII 400* NMR Spectrometer (^1H NMR 399.74 MHz, ^{or a} a *Brucker AVANCE III 700* NMR Spectrometer (^1H NMR 700.0 MHz); The ^1H and ^{13}C chemical shifts are given relative to tetramethylsilane (TMS), and the residual solvent peaks were used as the reference signal; the ^{31}P chemical shifts are referenced to an 85% aqueous solution of H_3PO_4 . The mass characterizations have been performed on an Agilent 6210 ESI-TOF instrument by Agilent Technologies, Santa Clara, CA, USA with standard settings of 5 L/min, 4 kV and 15 psi for ESI-TOF and on a MAT 711 by Varian MAT, Bremen, Germany with an electron energy of 0.8 mA for EI-MS. IR spectra were measured on a Nicolet iS10 FTIR-ATR spectrometer by Thermo Scientific. For reactions under UV radiation a Osram Ultra Vitalux 300W lamp was used. DFT calculations were performed with Gaussian09 program package.⁶¹ For the Geometry optimizations “OPT” B3LYP⁶²⁻⁶⁴ functional was used and the convergence criteria were set to “Direct” and “tight” as SCF=(Direct,Tight). The coupled cluster triple- ζ valence quality basis set (cc-pVTZ)⁶⁵⁻⁶⁹ was applied for all atoms. Integrals were set to FineGrid (Integrals=FineGrid). All molecular orbitals and energies were determined by population analysis (Pop=Full).

Phosphabarrelene (1)

2-pyridyl-4,6-diphenylphosphinine (1030 mg, 2.11 mmol) was weighed in a Schlenk flask. Methylcyclohexane (50 mL) and hexafluorobutylene (700 mbar) were condensed in and a suspension was formed. The mixture was stirred for 3 days at $T = 85^\circ\text{C}$ (higher than this temperature retro Diels-Alder reaction takes place). Volatiles were evaporated; the black powder obtained was passed through column packed with silica gel and eluted with an hexane/diethyl ether 4:1 mixture. The first two fractions (black and yellow) were dismissed and the last dark red fraction was collected. This contained a mixture of the corresponding phosphinine and the product. The latter was recrystallized from an ethanol-water mixture (20:1). White crystals suitable for X-Ray diffraction were obtained. 255mg, 16% yield.

HRESI-MS (+, 200V) m/z : $[\text{M} + \text{H}]^+$ 488.0997 calc. 488.0991.

^1H NMR (700 MHz, CD_2Cl_2): $\delta = 7.22$ (m, 1H, H₉), 7.33 (m, 1H, H_{ar}), 7.40 (m, 2H, H_{ar}), 7.40 (m, 2H, H_{ar}), 7.49 (m, 1H, H_{ar}), 7.57 (m, 1H, H_{ar}), 7.64-7.67 (m, 2H, H_{ar}), 7.70-7.73 (m, 2H,

H8/H7), 7.85 (d, $J=12.0$ Hz, 2H, H_{ar}), 8.05 (m, 1H, H2), 8.61 (d, $J=5.4$ Hz, 2H, H4/H10) ppm.

$^{13}\text{C}\{^1\text{H}\}$ NMR (176 MHz, CD_2Cl_2): $\delta = 67.9$ (d, $J = 6.0$ Hz, C3), 121.7 (d, $J = 11.5$ Hz, C7), 124.1 (s, C9), 127.2 (d, $J = 13.5$ Hz, C_{ar}), 129.5 (s, C_{ar}), 129.7 (d, $J = 1.3$ Hz, C_{ar}), 129.8 (s, C_{ar}), 123.0 (s, C_{ar}), 130.5 (s, C_{ar}), 137.9 (d, $J = 1.8$ Hz, C8), 138.0 (d, $J = 26.5$ Hz, C1), 139.9 (C17), 149.8 (d, $J = 3.3$ Hz, C2), 150.3 (C23), 150.9 (C10), 153.1 – 153.5 (m, C4/C11), 153.9 (d, $J = 17.2$ Hz, C5), 155.7 (d, $J = 26.5$ Hz, C6), 160.1 (q, $J = 30.1$ Hz, C24) ppm.

$^{31}\text{P}\{^1\text{H}\}$ NMR (162 MHz, CD_2Cl_2): $\delta = -68.2$ (q, $^3J_{\text{P-F}} = 38.9$ Hz) ppm.

$^{19}\text{F}\{^1\text{H}\}$ NMR (376 MHz, CD_2Cl_2): $\delta = -54.9$ (m, 3F, $\text{CF}_3\text{-P}$), -54.9 (m, 3F, CF_3) ppm.

[Au(1)Cl] (2)

In a *J*-Young NMR tube, phosphabarrelene **1** (9.1 mg, 0.031 mmol) and AuCl·DMS (15 mg, 0.031 mmol) were dissolved in 0.5 mL DCM under protection of light. A colorless solution was formed. Crystals were obtained by slow evaporation of the DCM solution.

^1H NMR (401 MHz, $\text{DCM-}d_2$): $\delta = 7.78\text{-}7.34$ (m, 1H, H9), 7.43 -7.49 (m, 4H, H_{ar}), 7.51-7.56 (m, 1H, H_{ar}), 7.58-7.63 (m, 3H, H_{ar}), 7.65-7.69 (m, 1H, H7), 7.70-7.74 (m, 2H, H_{ar}), 7.75-7.83 (m, 4H, H_{ar}/H8), 8.16 (d, $J = 21.0$ Hz, 1H, H2), 8.56 (d, $J = 21.1$ Hz, 1H, H4), 8.72-8.66 (m, $J = 4.8, 1.8, 0.9$ Hz, 1H, H10) ppm.

$^{13}\text{C}\{^1\text{H}\}$ NMR (101 MHz, $\text{DCM-}d_2$): $\delta = 64.9$ (d, $J = 17.4$ Hz, C3), 121.6 (d, $J = 5.5$ Hz, C7), 124.8 (d, $J = 1.6$ Hz, C9), 127.9 (d, $J = 8.9$ Hz, C_{ar}), 129.2 (d, $J = 1.9$ Hz, C_{ar}), 129.5 (s, C_{ar}), 129.7 (s, C_{ar}), 129.8 (s, C_{ar}), 130.2 (d, $J = 1.8$ Hz, C_{ar}), 135.1 (d, $J = 15.2$ Hz, C11), 137.5-137.9 (m, C8/C17), 142.9-144.3 (m, C23), 146.5 (d, $J = 12.5$ Hz, C1/C5), 150.0 (s, C10), 151.9 (d, $J = 10.9$ Hz, C6), 152.2 (d, $J = 4.6$ Hz, C2), 153.0 (d, $J = 5.2$ Hz, C4), 159.9-162.1 (m, C24) ppm.

$^{31}\text{P}\{^1\text{H}\}$ NMR (162 MHz, $\text{DCM-}d_2$): $\delta = -9.3$ (q, $^3J_{\text{P-F}} = 21.3$ Hz) ppm.

$^{19}\text{F}\{^1\text{H}\}$ NMR (376 MHz, $\text{DCM-}d_2$): $\delta = -54.5$ (q, $J = 13.5$ Hz, C23F₃), $-54.3 - -54.0$ (m, C24F₃) ppm.

[(1,5-cyclooctadiene)(1)rhodium tetrafluoroborate] (3)

In a Schlenk flask phosphabarrelene **1** (21.6 mg, 0.044 mmol) and $[\text{Rh}(\text{cod})_2]\text{BF}_4$ (18.0 mg, 0.044 mmol) were dissolved in 1 mL DCM and stirred at r.t. for 30 minutes. A dark brown solution was formed. The solvent was evaporated and the solid was washed with 3x5 mL pentane. The yellow powder obtained was dried under vacuum. Crystals suitable for X-ray diffraction were obtained by slow diffusion of ether into a DCM solution.

^1H NMR (500 MHz, DCM- d_2): δ = 1.87-1.98 (m, 1H, cod), 1.99-2.10 (m, 1H, cod), 2.16-2.25 (m, 1H, cod), 2.35-2.44 (m, 1H, cod), 2.44-2.61 (m, 2H, cod), 2.61-2.73 (m, 2H, cod), 3.80-3.95 (m, 1H, cod), 4.82-4.91 (m, 1H, cod), 5.68-5.79 (m, 1H, cod), 5.90-6.08 (m, 1H, cod), 7.47-7.56 (m, 4H, H_{ar}), 7.58-7.66 (m, 5H, H_{ar}), 7.74-7.81 (m, 2H, H_{ar}), 8.00-8.08 (m, 2H, H2/H7), 8.09-8.16 (m, 1H, H8), 8.20 (m, 1H, H10), 8.58 (d, $^3J_{\text{P-H}}$ = 16.1 Hz, 1H, H4) ppm.

$^{13}\text{C}\{^1\text{H}\}$ NMR (101 MHz, DCM- d_2): δ = 27.3 (s, cod), 30.3 (s, cod), 31.4 (s, cod), 33.9 (s, cod), 65.6 (d, $^3J_{\text{P-C}}$ = 11.7 Hz, C3), 80.9 (d, $^2J_{\text{P-C}}$ = 10.8 Hz, cod), 81.6 (d, $^2J_{\text{P-C}}$ = 10.4 Hz, cod), 109.7-110.09 (m, cod), 110.2-110.6 (m, cod), 122.8 (d, $^3J_{\text{P-C}}$ = 10.1 Hz, C7), 127.3 (s, C9), 128.6 (d, $J_{\text{P-C}}$ = 6.1 Hz, C_{ar}), 129.3 (s, C_{ar}), 129.5 (s, C_{ar}), 129.8 (s, C_{ar}), 130.0 (s, C_{ar}), 130.2 (d, $J_{\text{P-C}}$ = 2.1 Hz, C_{ar}), 135.1 (d, $^2J_{\text{P-C}}$ = 16.3 Hz, C11), 137.1 (s, C17), 141.8 (s, C8), 142.4-143.6 (m, C23), 146.2 (d, $^1J_{\text{P-C}}$ = 23.9 Hz, C1), 149.3 (d, $^1J_{\text{P-C}}$ = 30.5 Hz, C5), 151.4 (s, C10), 151.5 (d, $^2J_{\text{P-C}}$ = 5.3 Hz, C2), 155.5 (d, $^2J_{\text{P-C}}$ = 22.1 Hz, C6), 155.9 (d, $^2J_{\text{P-C}}$ = 5.7 Hz, C4), 158.9-160.8 (m, C24) ppm.

$^{31}\text{P}\{^1\text{H}\}$ NMR (162 MHz, DCM- d_2): δ = -9.2 (dq, $^1J_{\text{Rh-P}}$ = 182.2 Hz, $^3J_{\text{P-F}}$ = 14.2 Hz) ppm.

$^{19}\text{F}\{^1\text{H}\}$ NMR (376 MHz, DCM- d_2): δ = -152.8 (s, 1F, BF₃-F), -152.7 (s, 3F, BF-F₃) -54.18 (q, $^3J_{\text{P-F}}$ = 13.0 Hz, C25F₃), -54.0 – -53.8 (m, C26F₃) ppm.

[(CO)CIRh(1)] (4)

In a Schlenk flask phosphabarrelene **1** (28.0 mg, 0.057 mmol) and [Rh(CO)₂Cl]₂ (11.2 mg, 0.029 mmol) were dissolved in 1 mL DCM and stirred at r.t. for 30 minutes. A dark orange solution was formed. The solvent was evaporated and the solid was washed with 3x5 mL pentane. The orange powder obtained was dried under vacuum.

^1H NMR (700 MHz, CD₂Cl₂): δ = 7.38-7.49 (m, 3H, H_{ar}/H9), 7.50-7.58 (m, 1H, H_{ar}), 7.58-7.65 (m, 3H, H_{ar}), 7.81 (s, 5H, H_{ar}/H2/H7), 7.93-7.97 (m, 1H, H8), 8.81 (d, $^3J_{\text{P-H}}$ = 15.9 Hz, 1H, H4), 9.81-9.93 (m, 1H, H10) ppm.

$^{13}\text{C}\{^1\text{H}\}$ NMR (176 MHz, DCM- d_2): δ = 63.8 (d, J = 15.0 Hz, C3), 120.5 (d, J = 10.5 Hz, C7), 125.6 (s, C9), 128.6 (d, J = 7.4 Hz, C_{ar}), 129.1 (s, C_{ar}), 129.2 (s, C_{ar}), 129.6 (s, C_{ar}), 129.8 (s, C_{ar}), 129.9 (s, C_{ar}), 134.8 (d, J = 15.4 Hz, C11), 138.1 (s, C17), 140.1 (s, C8), 142.7 (m, C23), 144.3 (d, J = 34.7 Hz, C1), 148.7 (d, J = 6.8 Hz, C4), 152.2 (s, C10), 152.3 (m, C5), 152.4 (d, J = 3.9 Hz, C2), 154.3 (d, J = 22.6 Hz, C6), 157.8 (m, C24), 187.3 (dd, J = 67.9, 16.9 Hz, CO) ppm.

$^{31}\text{P}\{^1\text{H}\}$ NMR (162 MHz, DCM- d_2): δ = 21.5 (dq, $^1J_{\text{P-Rh}}$ = 198.2, $^3J_{\text{P-F}}$ = 14.2 Hz) ppm.

$^{19}\text{F}\{^1\text{H}\}$ NMR (376 MHz, DCM- d_2): δ = -54.4 (q, $^3J_{\text{P-F}}$ = 13.2 Hz, C24F₃), -53.82 (m, C23F₃) ppm.

IR $\tilde{\nu}_{\text{CO}}$: 2014 cm⁻¹

[(CO)₄W(1)] (5)

In an *J*-Young NMR tube, phosphabarrelene **1** (15 mg, 0.031 mmol) and [W(MeCN)₂(CO)₄] (11.6 mg, 0.031 mmol) were dissolved in 0.5 mL THF and the solution was heated at *T* = 50 °C for one hour. A red-brown solution was formed. The solvent was evaporated and the solid was washed with 2x1 mL pentane. The red-brown powder obtained was dried under vacuum. Crystals suitable for X-ray diffraction were obtained by slow diffusion of pentane into a THF solution of **5**.

¹H NMR (401 MHz, THF-*d*₈) δ = 7.11-7.24 (m, 1H, H9), 7.31-7.43 (m, 3H, H_{ar}), 7.45-7.61 (m, 5H, H_{ar}), 7.76 (d, ³*J*_{P-H} = 17.3, 1H, H2), 7.83-7.94 (m, 1H, H8), 7.96-8.03 (m, 2H, H_{ar}), 8.12-8.20 (m, 1H, H7), 9.10-9.20 (m, 1H, H10), 9.34 (d, ³*J*_{P-H} = 13.2, 1H, H4) ppm.

¹³C{¹H, ¹⁹F} NMR (101 MHz, THF-*d*₈) δ = 66.0 (d, ³*J*_{C-P} = 9.6 Hz, C3), 122.1 (d, ³*J*_{C-P} = 3.7 Hz, C24), 122.1 (d, ³*J*_{C-P} = 7.5 Hz, C7), 123.8-124.2 (m, C23), 125.6 (d, ⁵*J*_{C-P} = 1.6 Hz, C9), 129.1 (d, *J* = 7.3 Hz, C_{ar}), 129.7 (s, C_{ar}), 129.7 (s, C_{ar}), 129.8 (s, C_{ar}), 129.9 (s, C_{ar}), 130.2 (s, C_{ar}), 135.8 (d, ²*J*_{C-P} = 18.2 Hz, C11), 139.0 (s, C17), 139.3 (d, ⁴*J*_{C-P} = 1.4 Hz, C8), 146.1 (d, ¹*J*_{C-P} = 13.3 Hz, C23), 149.5 (d, ¹*J*_{C-P} = 26.2 Hz, C1), 151.4 (d, ²*J*_{C-P} = 5.3 Hz, C4), 153.2 (d, ²*J*_{C-P} = 4.8 Hz, C2), 155.2 (d, ¹*J*_{C-P} = 21.7 Hz, C5), 156.9 (d, ²*J*_{C-P} = 20.9 Hz, C6), 157.8 (d, ⁴*J*_{C-P} = 4.6, C10), 159.7 (d, ²*J*_{C-P} = 6.6 Hz, C24), 201.7 (d, ²*J*_{C-P} = 6.4 Hz, CO), 204.3 (d, ²*J*_{C-P} = 7.9 Hz, CO), 209.6 (d, ²*J*_{C-P} = 39.9 Hz, CO), 210.6 (d, ²*J*_{C-P} = 5.3 Hz, CO) ppm.

³¹P{¹H} NMR (162 MHz, THF-*d*₈) δ = -2.4 (q, ³*J*_{P-F} = 17.7 Hz, ¹*J*_{P-W} = 272.0 Hz) ppm.

¹⁹F{¹H} NMR (376 MHz, THF-*d*₈) δ: = -54.9 (q, ⁵*J*_{F-F} = 12.8 Hz, C24F₃), -53.10 (dq, ³*J*_{P-F} = 17.9 Hz, ⁵*J*_{F-F} = 12.8 Hz, C23F₃) ppm.

IR $\tilde{\nu}_{\text{CO}}$: 2022, 1891, 1846 cm⁻¹

[(CO)₃Fe(1)] (6)

In a Schlenk flask phosphabarrelene **1** (27.0 mg, 0.055 mmol) and [Fe₃(CO)₁₂] (9.0 mg, 0.018 mmol) were dissolved in 1 mL THF and stirred under reflux for 3 hours. A dark brown solution was formed. The solvent was evaporated and the solid was run through a silica column (pipette) and eluted with hexane to separate a green fraction and then with a 4:1 mixture of pentane/diethyl ether to separate a yellow fraction. The last dark brown fraction was collected after eluting only with diethyl ether. The solvent was evaporated and the dark brown solid was dried under vacuum.

¹H NMR (401 MHz, DCM-*d*₂) 6.97-7.06 (m, 1H), 7.25-7.35 (m, 3H), 7.37-7.44 (m, 4H), 7.46-7.50 (m, 2H), 7.50-7.59 (m, 3H), 7.67-7.72 (m, 2H), 8.72 (d, 1H, *J* = 12.0 Hz), 8.87-8.96 (m, 1H) ppm.

$^{31}\text{P}\{^1\text{H}\}$ NMR (162 MHz, DCM- d_2): $\delta = 27.0$ (q, $^3J_{\text{P-F}} = 15.3$ Hz) ppm.

$^{19}\text{F}\{^1\text{H}\}$ NMR (376 MHz, THF- d_8) δ : = -54.7 (q, $^4J_{\text{F-F}} = 12.8$ Hz), -53.9 (dq, $^3J_{\text{P-F}} = 15.5$ Hz, $^4J_{\text{F-F}} = 12.8$ Hz) ppm.

IR $\tilde{\nu}_{\text{CO}}$: 2001, 1946, 1900 cm^{-1}

[(CO)ClRh(phosphasemibullvalene)] (7)

A THF solution of **4** (24.8 mg, 0.031 mmol) was irradiated with UV-light for 6 hours. The solvent was evaporated and the solid obtained washed with 2x1mL pentane. Crystals were obtained by slow diffusion of diethyl ether into a DCM solution of the complex.

^1H NMR (401 MHz, DCM- d_2) $\delta = 4.47$ (dq, 1H, $J = 7.9, 1.3$ Hz), 5.98-6.07 (m, 1H), 6.37 (d, 1H, $J = 27.5$ Hz), 7.28-7.33 (m, 1H), 7.36-7.40 (m, 1H), 7.50-7.56 (m, 1H), 7.73-7.80 (m, 2H), 9.49-9.98 (m, 1H) ppm.

$^{31}\text{P}\{^1\text{H}\}$ NMR (162 MHz, DCM- d_2): $\delta = 109.2$ (dq, $^1J_{\text{P-Rh}} = 188.2$ Hz, $^3J_{\text{P-F}} = 7.6$ Hz) ppm.

$^{19}\text{F}\{^1\text{H}\}$ NMR (376 MHz, THF- d_8) δ : = -62.1 (q, $^3J_{\text{P-F}} = 9.8$ Hz), -53.5 – -53.02 (m) ppm.

IR $\tilde{\nu}_{\text{CO}}$: 2008 cm^{-1}

[(CO) $_4$ W(phosphasemibullvalene)] (8)

A THF solution of **5** (24.8 mg, 0.031 mmol) was irradiated with UV-light for 4 hours. The solvent was evaporated and the solid obtained washed with 2x1mL pentane. Crystals were obtained by slow diffusion of pentane into a THF solution of the complex.

^1H NMR (401 MHz, THF- d_8) $\delta = 4.77$ -4.84 (m, 1H), 6.13-6.21 (m, 1H), 6.79 (d, 1H, $J = 21.8$ Hz), 7.08-7.15 (m, 1H), 7.29-7.48 (m, 6H), 7.48-7.59 (m, 2H), 7.96-8.06 (m, 3H), 9.14-9.24 (m, 1H) ppm.

$^{31}\text{P}\{^1\text{H}\}$ NMR (162 MHz, THF- d_8) $\delta = 88.6$ (q, $^1J_{\text{P-W}} = 269.98$ Hz, $^3J_{\text{P-F}} = 9.3$ Hz) ppm.

$^{19}\text{F}\{^1\text{H}\}$ NMR (376 MHz, THF- d_8) δ : = -62.14 (q, $J = 10.0$ Hz), -54.12 (p, $J = 9.8$ Hz) ppm

IR $\tilde{\nu}_{\text{CO}}$: 2024, 1897, 1861 cm^{-1}

X-ray crystal structure determinations

Compound 1: $\text{C}_{26}\text{H}_{16}\text{F}_6\text{NP}$, Fw = 487.37, colorless rod, $0.40 \times 0.17 \times 0.08$ mm^3 , monoclinic, $P2_1/c$, $a = 10.6473(10)$, $b = 22.6473(19)$, $c = 9.6111(9)$ Å, $\alpha = 90$, $\beta = 108.075(7)$, $\gamma = 90$, $V =$

2203.2(4) Å³, $Z = 4$, $D_x = 1.469 \text{ g/cm}^3$, $\mu = 0.190 \text{ mm}^{-1}$. 16607 reflections were measured by using a Stoe IPDS 2T diffractometer with a rotating anode (MoK α radiation; $\lambda = 0.71073 \text{ \AA}$) at a temperature of 210(2) K up to a resolution were $\theta_{\text{max}} = 29.28$. 5917 reflections were unique ($R_{\text{int}} = 0.070$). The structures were solved with SHELXL-2014/7⁷⁰ by using direct methods and refined with SHELXL-2014/7⁷⁰ on F^2 for all reflections. Non-hydrogen atoms were refined with anisotropic displacement parameters. 307 parameters were refined without restraints. $R_1 = 0.053$ for 2983 reflections with $I > 2s(I) \text{ e\AA}^3$, and $wR_2 = 0.1317$ for 5917 reflections, $S = 0.888$. Geometry calculations and checks for higher symmetry were performed with the PLATON program.⁷¹

Compound 2: C₂₆H₁₆AuClF₆NP, Fw = 719.78, yellow block, 0.230 × 0.190 × 0.090 mm³, triclinic, P-1, $a = 10.0431(2)$, $b = 14.8199(3)$, $c = 18.4254(4) \text{ \AA}$, $\alpha = 83.4879(7)$, $\beta = 86.6308(8)$, $\gamma = 74.1458(7)$, $V = 2619.95(9) \text{ \AA}^3$, $Z = 4$, $D_x = 1.825 \text{ g/cm}^3$, $\mu = 5.836 \text{ mm}^{-1}$. 47477 reflections were measured by using a Bruker Photon CMOS Detector, D8 Venture diffractometer with a rotating anode (MoK α radiation; $\lambda = 0.71073 \text{ \AA}$) at a temperature of 100(2) K up to a resolution were $\theta_{\text{max}} = 26.42$. 10734 reflections were unique ($R_{\text{int}} = 0.0478$). The structures were solved with SHELXL-2014/7⁷⁰ by using direct methods and refined with SHELXL-2014/7⁷⁰ on F^2 for all reflections. Non-hydrogen atoms were refined with anisotropic displacement parameters. 649 parameters were refined without restraints. $R_1 = 0.033$ for 9099 reflections with $I > 2s(I) \text{ e\AA}^3$, and $wR_2 = 0.072$ for 10734 reflections, $S = 1.043$. Geometry calculations and checks for higher symmetry were performed with the PLATON program⁷¹

Compound 3: C₃₅H₃₀F₁₀NPRhBCl₂, Fw = 870.19, yellow block, 0.16 × 0.21 × 0.33 mm³, monoclinic, C 2/c, $a = 16.8592(3)$, $b = 16.8926(2)$, $c = 25.6235(4) \text{ \AA}$, $\alpha = 90$, $\beta = 103.500(1)$, $\gamma = 90$, $V = 7095.83(19) \text{ \AA}^3$, $Z = 8$, $D_x = 1.629 \text{ g/cm}^3$, $\mu = 0.757 \text{ mm}^{-1}$. 17281 reflections were measured by using a Bruker Photon CMOS detector with a rotating anode (MoK α radiation; $\lambda = 0.71073 \text{ \AA}$) at a temperature of 100(2) K up to a resolution were $\theta_{\text{max}} = 36.41$. 15793 reflections were unique ($R_{\text{int}} = 0.046$). The structures were solved with SHELXL-2013⁷⁰ by using direct methods and refined with SHELXL-2013⁷⁰ on F^2 for all reflections. Non-hydrogen atoms were refined with anisotropic displacement parameters. 460 parameters were refined without restraints. $R_1 = 0.036$ for 15793 reflections with $I > 2s(I) \text{ e\AA}^3$, and $wR_2 = 0.091$ for 17281 reflections, $S = 1.041$. Geometry calculations and checks for higher symmetry were performed with the PLATON program.⁷¹

Compound 5: C₃₈H₃₂F₆O₆NPW, Fw = 927.46, orange block, 0.43 × 0.22 × 0.09 mm³, monoclinic, P2₁/c, $a = 13.1326(10)$, $b = 27.046(2)$, $c = 10.9336(8) \text{ \AA}$, $\alpha = 90$, $\beta = 110.364(2)$, $\gamma = 90$, $V = 3640.7(5) \text{ \AA}^3$, $Z = 4$, $D_x = 1.692 \text{ g/cm}^3$, $\mu = 3.295 \text{ mm}^{-1}$. 8119 reflections were measured by using a D8 Venture Bruker Photon CMOS detector with a rotating anode (MoK α radiation; $\lambda = 0.71073 \text{ \AA}$) at a temperature of 100(2) K up to a resolution were $\theta_{\text{max}} = 27.253$. 8119 reflections were unique ($R_{\text{int}} = 0.084$). The structures were solved with SHELXL-2014/7⁷⁰ by using direct methods and refined with SHELXL-2014/7⁷⁰ on F^2 for all reflections. Non-hydrogen atoms were refined with anisotropic displacement parameters. 478 parameters were refined without restraints. $R_1 = 0.036$ for 7310 reflections with $I > 2s(I) \text{ e\AA}^3$, and $wR_2 = 0.084$ for 8119 reflections, $S = 1.240$. Geometry calculations and checks for higher symmetry were performed with the PLATON program.⁷¹

Compound 7: C₂₇H₁₆F₆NPClORh, Fw = 653.74, yellow plate, 0.13 × 0.10 × 0.05 mm³, triclinic, P-1, $a = 10.8376(3)$, $b = 11.1071(3)$, $c = 22.2815(5) \text{ \AA}$, $\alpha = 99.0281(1)$, $\beta = 93.106(1)$, $\gamma = 108.868(1)$, $V = 2490.71(11) \text{ \AA}^3$, $Z = 4$, $D_x = 1.743 \text{ g/cm}^3$, $\mu = 0.925 \text{ mm}^{-1}$. 10209 reflections were measured by using a D8 Venture Bruker Photon CMOS detector with a rotating anode

(MoK α radiation; $\lambda = 0.71073 \text{ \AA}$) at a temperature of 100(2) K up to a resolution were $\theta_{\max} = 26.47$. 10209 reflections were unique ($R_{\text{int}} = 0.056$). The structures were solved with SHELXL-2014/7⁷⁰ by using direct methods and refined with SHELXL-2014/7⁷⁰ on F^2 for all reflections. Non-hydrogen atoms were refined with anisotropic displacement parameters. 686 parameters were refined without restraints. $R_1 = 0.0393$ for 8352 reflections with $I > 2s(I) \text{ e\AA}^3$, and $wR_2 = 0.0817$ for 10209 reflections, $S = 1.062$. Geometry calculations and checks for higher symmetry were performed with the PLATON program.⁷¹

Compound 8: C₃₀H₁₆F₆NPO₄W, Fw = 783.25, yellow platelette, $0.40 \times 0.17 \times 0.08 \text{ mm}^3$, triclinic, P-1, $a = 11.2828(3)$, $b = 14.6442(4)$, $c = 16.8057(5) \text{ \AA}$, $\alpha = 86.598(1)$, $\beta = 89.479(1)$, $\gamma = 81.434(1)$, $V = 2740.95(13) \text{ \AA}^3$, $Z = 4$, $D_x = 1.898 \text{ g/cm}^3$, $\mu = 4.352 \text{ mm}^{-1}$. 10034 reflections were measured by using a D8 Venture Bruker Photon CMOS detector with a rotating anode (MoK α radiation; $\lambda = 0.71073 \text{ \AA}$) at a temperature of 100(2) K up to a resolution were $\theta_{\max} = 25.51$. 10034 reflections were unique ($R_{\text{int}} = 0.161$). The structures were solved with SHELXL-2014/7⁷⁰ by using direct methods and refined with SHELXL-2014/7⁷⁰ on F^2 for all reflections. Non-hydrogen atoms were refined with anisotropic displacement parameters. 454 parameters were refined without restraints. $R_1 = 0.088$ for 6991 reflections with $I > 2s(I) \text{ e\AA}^3$, and $wR_2 = 0.1786$ for 10034 reflections, $S = 1.190$. Geometry calculations and checks for higher symmetry were performed with the PLATON program.⁷¹

4.5 References

- (1) van Leeuwen, P. W. N. M.; Roobeek, C. F. *J. Organomet. Chem.* **1983**, 258 (3), 343.
- (2) van Rooy, A.; Orij, E. N.; Kamer, P. C. J.; van Leeuwen, P. W. N. M. *Organometallics* **1995**, 14 (1), 34.
- (3) Jongsma, T.; Challa, G.; van Leeuwen, P. W. N. *J. Organomet. Chem.* **1991**, 421 (1), 121.
- (4) Littke, A. F.; Dai, C.; Fu, G. C. *J. Am. Chem. Soc.* **2000**, 122 (17), 4020.
- (5) Wolfe, J.; Buchwald, S. *Angew. Chem. Int. Ed.* **1999**, 38 (16), 2413.
- (6) Mann, G.; Incarvito, C.; Rheingold, A. L.; Hartwig, J. F. *J. Am. Chem. Soc.* **1999**, 121 (13), 3224.
- (7) Otsuka, S.; Yoshida, T.; Matsumoto, M.; Nakatsu, K. *J. Am. Chem. Soc.* **1976**, 98 (19), 5850.
- (8) Paul, F.; Patt, J.; Hartwig, J. F. *J. Am. Chem. Soc.* **1994**, 116 (13), 5969.
- (9) Reid, S. M.; Boyle, R. C.; Mague, J. T.; Fink, M. J. *J. Am. Chem. Soc.* **2003**, 125 (26), 7816.
- (10) Kobayashi, Y.; Kumadaki, I.; Ohsawa, A.; Hamana, H. *Tetrahedron Lett.* **1977**, 18 (10), 867.
- (11) Annen, U.; Regitz, M. *Tetrahedron Lett.* **1987**, 28 (43), 5141.
- (12) Märkl, G.; Lieb, F. *Angew. Chemie* **1968**, 17, 702.
- (13) Märkl, G.; Heier, K.-H. *Tetrahedron Lett.* **1974**, 49-50, 4369.
- (14) Breit, B.; Fuchs, E. *Chem. Commun.* **2004**, 6, 694.
- (15) Märkl, G.; Lieb, F.; Martin, C. *Tetrahedron Lett.* **1971**, 12 (17), 1249.
- (16) Märkl, G.; Beckh, H.-J. *Tetrahedron Lett.* **1987**, 28 (30), 3475.
- (17) Alcaraz, J.-M.; Mathey, F. *Tetrahedron Lett.* **1984**, 25 (2), 207.
- (18) Mézailles, N.; Ricard, L.; Mathey, F.; Le Floch, P. *Eur. J. Inorg. Chem.* **1999**, 1999 (12), 2233.
- (19) Tolman, C. A. *Chem. Rev.* **1977**, 77 (3), 313.
- (20) Fuchs, E.; Keller, M.; Breit, B. *Chem. Eur. J.* **2006**, 12 (26), 6930.
- (21) Wallis, C.; Edwards, P. G.; Hanton, M.; Newman, P. D.; Stasch, A.; Jones, C.; Tooze, R. P. *Dalton Trans.* **2009**, 12, 2170.
- (22) Dunne, B. J.; Morris, R. B.; Orpen, A. G. *J. Chem. Soc. Dalton Trans.* **1991**, 653.
- (23) Fuchs, E.; Keller, M.; Breit, B. *Chem. Eur. J.* **2006**, 12 (26), 6930.

- (24) Moloy, K. G.; Petersen, J. L. *J. Am. Chem. Soc.* **1995**, *117* (29), 7696.
- (25) Breit, B.; Winde, R.; Mackewitz, T.; Paciello, R.; Harms, K. *Chem. Eur. J.* **2001**, *7* (14), 3106.
- (26) Fernández, E.; Ruiz, A.; Claver, C.; Castellón, S.; Polo, A.; Piniella, J. F.; Alvarez-Larena, A. *Organometallics* **1998**, *17* (13), 2857.
- (27) Allen, D. W.; Taylor, B. F. *J. Chem. Soc. Dalton Trans.* **1982**, *1*, 51.
- (28) Autschbach, J.; Le Guennic, B. *J. Chem. Educ.* **2007**, *84* (1), 156.
- (29) Rigo, M.; Sklorz, J. A. W.; Hatje, N.; Noack, F.; Weber, M.; Wiecko, J.; Müller, C. *Dalton Trans.* **2016**, *45*, 2218.
- (30) Blug, M. Phosphinines as Precursors for Phosphabarrelenes and Phosphinine Anions : Coordination Chemistry, Catalysis and Stabilisation of Nanoparticles. PhD thesis, Ecole Polytechnique, France, 2010.
- (31) Dean, P. A. W. *Can. J. Chem.* **1979**, *57* (7), 754.
- (32) Dean, Philip A W, Polensek, L. *Can. J. Chem.* **1980**, *58* (16), 1627.
- (33) Doux, M.; Bouet, C.; Mezailles, N.; Ricard, L.; Le Floch, P. *Organometallics* **2002**, *21* (13), 2785.
- (34) Müller, C.; Vogt, D. In *Phosphorus Compounds*; Peruzzini, M., Gonsalvi, L., Eds.; Springer: Netherlands, 2011; pp 151–181.
- (35) Breit, B.; Fuchs, E. *Chem. Commun.* **2004**, *6*, 694.
- (36) Breit, B.; Fuchs, E. *Synthesis* **2006**, *13*, 2121.
- (37) Ribagnac, P.; Blug, M.; Villa-Urbe, J.; Le Goff, X.-F.; Gosmini, C.; Mézailles, N. *Chem. Eur. J.* **2011**, *17* (51), 1438.
- (38) Blug, M.; Le Goff, X.-F.; Mézailles, N.; Le Floch, P. *Organometallics* **2009**, *28* (8), 2360.
- (39) Blug, M.; Guibert, C.; Le Goff, X.-F.; Mézailles, N.; Le Floch, P. *Chem. Commun.* **2009**, *210* (2), 201.
- (40) Bäuerlein, P. S.; Gonzalez, I. A.; Weemers, J. J. M.; Lutz, M.; Spek, A. L.; Vogt, D.; Müller, C. *Chem. Commun.* **2009**, *33*, 4944.
- (41) Pfeifer, G.; Ribagnac, P.; Le Goff, X.-F.; Wiecko, J.; Mézailles, N.; Müller, C. *Eur. J. Inorg. Chem.* **2015**, 240.
- (42) Campos-Carrasco, A.; Pidko, E. A.; Masdeu-Bultó, A. M.; Lutz, M.; Spek, A. L.; Vogt, D.; Müller, C. *New J. Chem.* **2010**, *34* (8), 1547.
- (43) Loibl, A.; de Krom, I.; Pidko, E. A.; Weber, M.; Wiecko, J.; Müller, C. *Chem. Commun.* **2014**, *50* (64), 8842.

- (44) Zimmerman, H. E.; Grunewald, G. L. *J. Am. Chem. Soc.* **1966**, *88* (1), 183.
- (45) Zimmerman, H. E.; Grunewald, G. L.; Paufler, R. M.; Sherwin, M. A. *J. Am. Chem. Soc.* **1969**, *91* (9), 2330.
- (46) Zimmerman, H. E.; Armesto, D. *Chem. Rev.* **1996**, *96* (8), 3065.
- (47) Frutos, L. M.; Sancho, U.; Castaño, O. *Org. Lett.* **2004**, *6* (8), 1229.
- (48) Greve, D. R. *J. Phys. Org. Chem.* **2011**, *24* (3), 222.
- (49) Ramaiah, D.; Sajimon, M. C.; Joseph, J.; George, M. V. *Chem. Soc. Rev.* **2005**, *34* (1), 48.
- (50) Zhang, S.; Zhang, W.-X.; Xi, Z. *Acc. Chem. Res.* **2015**, *48* (7), 1823.
- (51) Hine, J.; Brown, J. A.; Zalkow, L. H.; Gardner, W. E.; Hine, M. *J. Am. Chem. Soc.* **1955**, *77* (3), 594.
- (52) Zimmerman, H. E.; Paufler, R. M. *J. Am. Chem. Soc.* **1960**, *82* (6), 1514.
- (53) Zimmerman, H. E.; Binkley, R. W.; Givens, R. S.; Grunewald, G. L.; Sherwin, M. A. *J. Am. Chem. Soc.* **1969**, *91* (12), 3316.
- (54) Zimmerman, H. E.; Binkley, R. W.; Givens, R. S.; Sherwin, M. A. *J. Am. Chem. Soc.* **1967**, *89* (15), 3932.
- (55) Zimmerman, H. E.; Givens, R. S.; Pagni, R. M. *J. Am. Chem. Soc.* **1968**, *90* (22), 6096.
- (56) Liu, R. S. H. *J. Am. Chem. Soc.* **1968**, *90* (1), 215.
- (57) Binger, P.; Stutzmann, S.; Bruckmann, J.; Krüger, C.; Grobe, J.; Le Van, D.; Pohlmeier, T. *Eur. J. Inorg. Chem.* **1998**, *1998* (12), 2071.
- (58) Mack, A.; Breit, B.; Wettling, T.; Bergsträsser, U.; Leininger, S.; Regitz, M. *Angew. Chemie Int. Ed.* **1997**, *36* (12), 1337.
- (59) Geier, J.; Frison, G.; Grützmacher, H. *Angew. Chem. Int. Ed.* **2003**, *42* (33), 3955.
- (60) Rigo, M.; Weber, M.; Müller, C. *Chem. Commun.* **2016**, *52*, 7090.
- (61) Frisch, M. J.; Trucks, G. W.; Schlegel, H. B.; Scuseria, G. E.; Robb, M. A.; Cheeseman, J. R.; Scalmani, G.; Barone, V.; Mennucci, B.; Petersson, G. A.; Nakatsuji, H.; Caricato, M.; Li, X.; Hratchian, H. P.; Izmaylov, A. F.; Bloino, J.; Zheng, G.; Sonnenberg, J. L.; Hada, M.; Ehara, M.; Toyota, K.; Fukuda, R.; Hasegawa, J.; Ishida, M.; Nakajima, T.; Honda, Y.; Kitao, O.; Nakai, H.; Vreven, T.; Montgomery, J. A. J.; Peralta, J. E.; Ogliaro, F.; Bearpark, M.; Heyd, J. J.; Brothers, E.; Kudin, K. N.; Staroverov, V. N.; Keith, T.; Kobayashi, R.; Normand, J.; Raghavachari, K.; Rendell, A.; Burant, J. C.; Iyengar, S. S.; Tomasi, J.; Cossi, M.; Rega, N.; Millam, J. M.; Klene, M.; Knox, J. E.; Cross, J. B.; Bakken, V.; Adamo, C.; Jaramillo, J.; Gomperts, R.; Stratmann, R. E.; Yazyev, O.; Austin, A. J.; Cammi, R.; Pomelli, C.; Ochterski, J. W.; Martin, R. L.; Morokuma, K.; Zakrzewski, V. G.; Voth, G. A.; Salvador, P.; Dannenberg, J. J.; Dapprich, S.; Daniels, A. D.; Farkas, O.; Foresman, J. B.; Ortiz, J. V.; Cioslowski, J.; Fox, D. J. Gaussian, Inc.:

Wallingford CT 2013.

- (62) Kim, K.; Jordan, K. D. *J. Phys. Chem.* **1994**, *98* (40), 10089.
- (63) Vosko, S. H.; Wilk, L.; Nusair, M. *Can. J. Phys.* **1993**, *98* (7), 5648.
- (64) Stephens, P. J.; Devlin, F. J.; Chabalowsky, C. F.; Frisch, M. J. *J. Phys. Chem.* **1994**, *98* (45), 11623.
- (65) Dunning, T. H. J. *J. Chem. Phys.* **1989**, *90* (2), 1007.
- (66) Kendall, R. A.; Dunning, T. H. J. *J. Chem. Phys.* **1992**, *96* (9), 6796.
- (67) Woon, D. E.; Dunning, T. H. J. *J. Chem. Phys.* **1993**, *98* (2), 1358.
- (68) Peterson, K. A.; Woon, D. E.; Dunning, T. H. J. *J. Chem. Phys.* **1994**, *100* (10), 7410.
- (69) Wilson, A. K.; van Mourik, T.; Dunning, T. H. J. *J. Mol. Struct.* **1996**, *388*, 339.
- (70) Sheldrick, G. M.; *Acta Crystallogr. Sect. A.* **2008**, *64*, 112.
- (71) Spek, A. L.; *Acta Crystallogr. Sect. D.* **2009**, *65*, 148.

Chapter 5

Summary and Conclusions

5 Summary and conclusions

In chapter one, the coordination chemistry of the pyridyl-substituted phosphinine **PN** with different transition metal complexes was studied. With $[\text{Cu}(\text{MeCN})_4]\text{PF}_6$ and **PN** in a 1:1 ratio a dimeric complex is obtained. Its structure was verified by means of single crystal X-ray diffraction and it consists of two copper centers bridged *via* the two phosphorus atoms (μ^2 -coordination mode) forming a core structure with the shape of a diamond. This motif could be interesting for applications such as catalytic oxidations, OLEDS, and as models for copper containing enzymes.

Silver complexes of the type $[\text{Ag}(\text{PN})_x]\text{OTf}$ ($x = 1-3$) were prepared. The products were found to be rather unstable and could not be isolated. However, the $^{31}\text{P}\{^1\text{H}\}$ NMR spectra of the complexes in solution suggest the quantitative formation of only one species in each case.

A gold(I) complex was obtained by reaction of $[\text{AuCl}\cdot\text{SMe}_2]$ with the **PN** phosphinine. The linear coordination compound contains the phosphinine ligand bound *via* the phosphorus atom in a η^1 -mode. The nitrogen atom in the pyridyl ring remains uncoordinated, which allows the possibility of the incorporation of a second metal fragment. This complex was also characterized by means of X-ray diffraction analysis.

According to $^{31}\text{P}\{^1\text{H}\}$ NMR and IR analyses, it appears that $[\text{Ni}(\text{CO})_4]$ reacts with the **PN** ligand to form $[\text{Ni}(\text{CO})_2(\text{PN})]$, which dimerizes rapidly after liberating two CO molecules under UV light and forming $[\text{Ni}(\text{CO})(\text{PN})]_2$. Unfortunately, no structural information could be obtained, but the proposed stoichiometry is based on the molecular structure of a Rh(I) complex obtained from reaction of $[\text{Rh}(\text{CO})_2\text{Cl}]_2$ with two equivalents of the **PN** phosphinine. In that particular case, the molecular structure in the crystal shows two rhodium centers bridged *via* the phosphorus atom in a μ^2 -fashion. Each pyridine ring is coordinated to one rhodium center. This coordination mode to Rh(I) differs from the monomeric Rh-complex known in literature ($[(\text{cod})\text{Rh}(\text{PN})]\text{BF}_4$), where the phosphinine is coordinated in the usual chelating-fashion, *via* both the P and N atom.

Iron carbonyl complexes with the **PN** phosphinine were subsequently investigated. Contrary to bipyridine, the reaction of $[\text{Fe}_3(\text{CO})_{12}]$ and three equivalents of **PN** ligand is selective and straightforward. $[\text{Fe}(\text{CO})_3(\text{PN})]$ is formed, which was also characterized crystallographically. According to NMR analyses, this complex seems to coordinate dienes, such as methylacrylate and 1,3-butadiene, after CO-dissociation under UV-light. Unfortunately, the complexes formed appear very labile and their isolation was not successful.

$[\mu\text{-(pdt)Fe}_2(\text{CO})_6]$, which is used as a hydrogenase model, was chosen as a precursor for the synthesis of $[\mu\text{-(pdt)Fe}_2(\mathbf{PN})(\text{CO})_4]$ and $[\mu\text{-(pdt)Fe}_2(\mathbf{PN})_2(\text{CO})_2]$. Both complexes were structurally characterized by means of single crystal X-ray diffraction. The most basic site in $[\mu\text{-(pdt)Fe}_2(\mathbf{PN})(\text{CO})_4]$ is the nitrogen atom in the pyridine ring, as was confirmed by reaction with different protic reagents, while \mathbf{PNH}^+ was always formed exclusively. Two equivalents of the \mathbf{PN} compound could be coordinated to $[\text{W}(\text{CO})_6]$ after dissociation of four CO molecules by irradiation with UV light. Even after very long reaction times and an excess of \mathbf{PN} ligand, a third equivalent could not displace the last two CO molecules under the given conditions, probably due to steric hindrance.

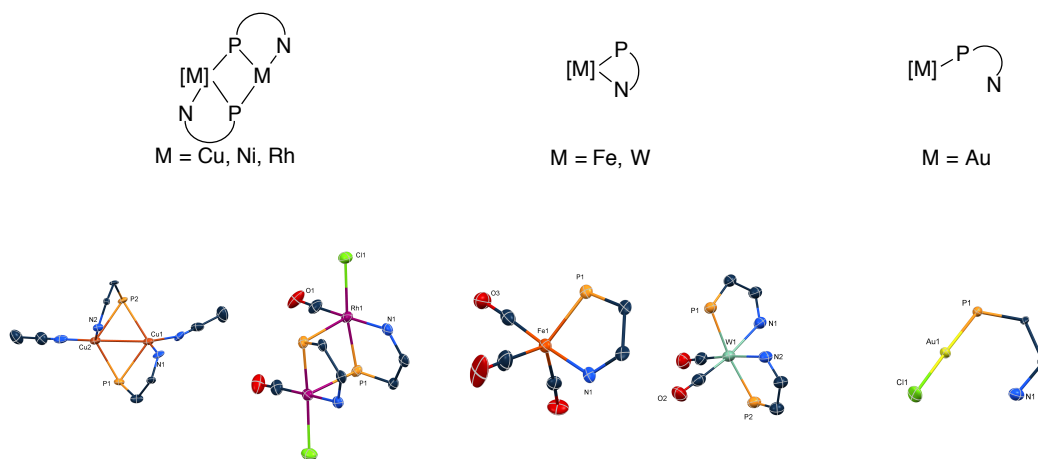


Figure 5.1 The different \mathbf{PN} -coordination modes obtained with the complexes prepared in this work

Figure 5.1 summarizes the different coordination modes the \mathbf{PN} phosphinine adopts in the complexes prepared in this work. This clearly shows that the pyridyl-substituted phosphorus heterocycle results in a good candidate for the preparation of a wide range of transition metal complexes that range from dimers, monomers and eventually bimetallic complexes. With the results in literature and the ones obtained here, it appears that the \mathbf{PN} phosphinine still has a very interesting chemistry that still remains open for further exploration and investigation in the future.

In chapter two, four new λ^4 -phosphinines were synthesized by reacting the 2,4-diphenyl-6-tolylphosphinine with ferrocenyllithium (**17**) and the \mathbf{PN} phosphinine with methylolithium (**18**), phenyllithium (**19**) and ferrocenyllithium (**20**). The corresponding lithium salts were obtained quantitatively according to $^{31}\text{P}\{^1\text{H}\}$ NMR spectroscopy. While **17** shows only one $^{31}\text{P}\{^1\text{H}\}$ NMR signal even at $T = -100\text{ }^\circ\text{C}$, **18**, **19** and **20** show two singlets at lower temperatures (coalescence

temperature = -94 °C, -79 °C, and -81 °C, respectively). This demonstrates that the phosphorus atom undergoes a dynamic inversion at the phosphorus atom, which energetic barrier is rather low (approximately 36 kJ/mol). The pyridyl ring increases the inversion barrier in comparison with the non-functionalized anionic phosphinine **17**, as only one species was detected even at $T = -100$ °C.

Compound **21** and **19** were reacted with water and MeOH separately. The symmetrical anion **21** was converted to two different species: the corresponding *Z*-1,2-dihydrophosphinine and the *E*-1,2-dihydrophosphinine isomers. In the case of the reaction with water, the *Z*-isomer is the major species (94%) but when **21** reacted with MeOH, the *Z*-isomer and the *E*-isomer are formed almost in a 50:50 ratio. This could be explained by the subtle interplay, which exists between the pK_a values of the generated 1,2-dihydrophosphinine species and the pK_b values of the formed base (LiOH or LiOMe). Quenching the lithium salts with water leads preferentially to the kinetic product, while quenching with MeOH clearly leads ultimately to the thermodynamic product. For the case of **19**, the same behavior was observed only that the unsymmetrical nature of the ligand led to two more species present in solution. These are the kinetic and thermodynamic products (*Z*- and *E*-isomers) from the protonation of the P=C bond either on the side of the pyridyl ring or on the side of the phenyl-ring in 2- and 6-positions of the heterocycle ring, respectively.

Compounds **19-21** were coordinated to Rh(I) fragments. [(cod)Rh(**19**)] was formed quantitatively and appears to be fairly stable toward water under argon. Ligand **19** is coordinated in a chelating-fashion, yielding a neutral rhodium complex. For the case of **20**, it was assumed that when reacted with [Rh(cod)₂]BF₄, a neutral complex of the type [(cod)Rh(**20**)] is formed, which would immediately react with traces of water from the solvent or the glass wall under formation of the rhodium cationic complex [(cod)Rh(H-**20**)]BF₄ (**27**). In this case, a proton has been added to the P=C double bond of the coordinated ligand as confirmed crystallographically. The lithium salt **21** forms a neutral Rh-complex when reacted with [Rh(cod)₂]BF₄, where the ligand is coordinated *via* the delocalized π -system in a η^5 -fashion. Apparently, the absence of a hetero-donor functionality favors this type of coordination over a η^1 -P-mode. Interestingly, when two equivalents of [Rh(cod)₂]BF₄ were mixed with **20**, complex **28** was formed, where the phosphorus atom is bound to one Rh center in a η^1 -mode and the delocalized π -system within the heterocycle is coordinated to a second rhodium center in a η^5 -fashion. This type of ligand confirms that the presence of a hetero-donor group forces the coordination chemistry to metal centers in a chelating mode. Nevertheless, the π -system remains available for the coordination to a second metal center.

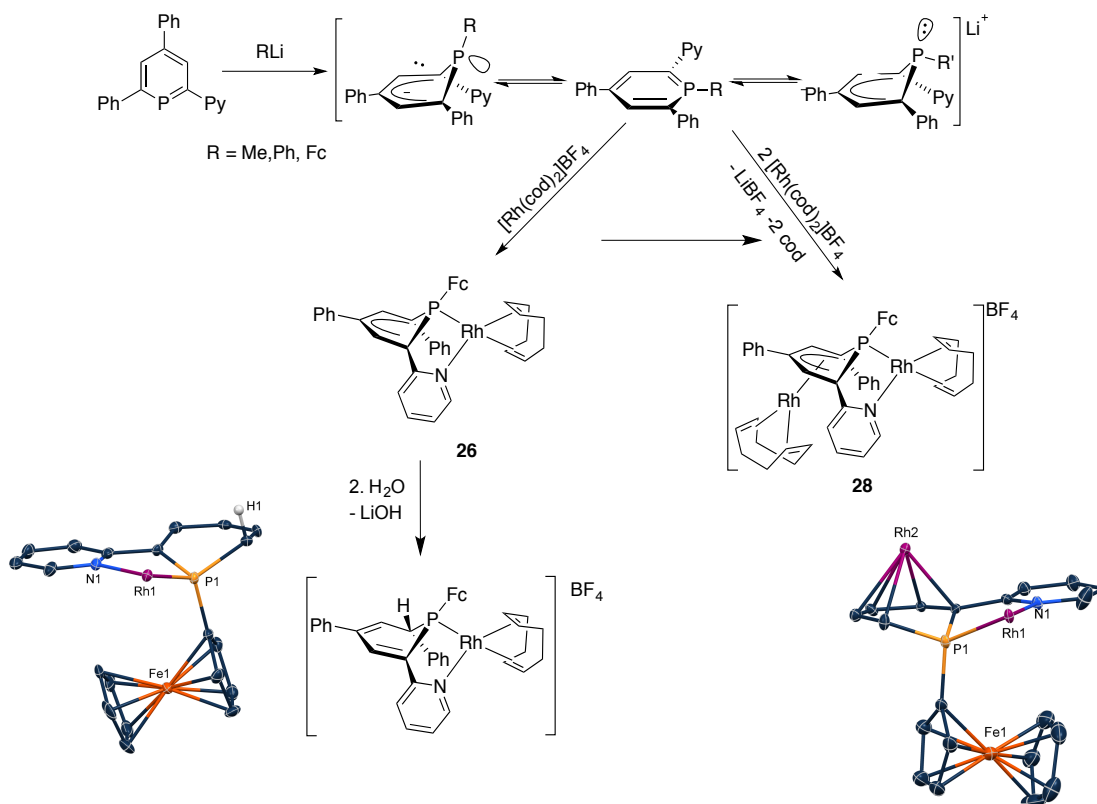


Figure 5.2 Synthesis of λ^4 -phosphinines and coordination chemistry towards Rh of the Fc-substituted anionic phosphinine

In chapter 4 the first pyridyl-substituted phosphabarrelene is presented. The formation of the two enantiomers of the obtained phosphabarrelene was confirmed by means of $^{31}\text{P}\{^1\text{H}\}$ NMR spectroscopy after adding and enantiomerically pure acid, which protonated the nitrogen from the pyridyl ring yielding two diastomeric ionic pairs, which gave two different signals in the spectrum. DFT calculations showed that the phosphorus lone pair of the phosphabarrelene is represented by the HOMO-2, which is energetically not available for oxidation with selenium or sulfur. The coordination chemistry of the **PN** phosphabarrelene (**1**) was explored and five complexes could be fully characterized. The gold complex $[\text{Au}(\mathbf{1})\text{Cl}]$ is a linear complex, where the ligand is coordinated only *via* the phosphorus lone pair. Two Rh-complexes were synthesized: $[(\text{cod})\text{Rh}(\mathbf{1})]\text{BF}_4$ and $[\text{Rh}(\mathbf{1})(\text{CO})\text{Cl}]$. In both cases, the phosphabarrelene heterocycle is coordinated in a chelating fashion *via* both the P and the N atom. A mixture of $[\text{W}(\text{CO})_6]$ and **1** in THF under UV irradiation yields the octahedral complex $[\text{W}(\text{CO})_4(\mathbf{1})]$, where the ligand also adopts a chelating coordination fashion. $[\text{Fe}(\text{CO})_3(\mathbf{1})]$ was synthesized and purified by means of column chromatography. The NMR spectroscopy analysis suggests the formation of a chelated complex with a dynamic behavior in solution.

UV-irradiation of a solution of **1** led to at least 5 different species observed in the $^{31}\text{P}\{^1\text{H}\}$ NMR spectrum. Contrary to the observations made during irradiation of solutions of phosphabarrelene-based complexes, two species were detected by $^{31}\text{P}\{^1\text{H}\}$ NMR spectroscopy in a ratio of 80:20. The major species of the reaction mixtures of $[\text{Rh}(\mathbf{1})(\text{CO})\text{Cl}]$ and $[\text{W}(\text{CO})_4(\mathbf{1})]$ could be isolated and crystallographically characterized. The corresponding products showed the rearrangement of the phosphabarrelene ligand into a phosphasemibullvalene, which remained coordinated to the metal fragment in a chelating mode. The mechanism of the rearrangement is proposed, which explained the formation of two main isomers (the major and minor species detected in the $^{31}\text{P}\{^1\text{H}\}$ NMR spectra of the reaction mixtures). The comparison between the IR CO-stretching frequencies in $[\text{Rh}(\mathbf{1})(\text{CO})\text{Cl}]$ and $[\text{Rh}(\text{phosphasemibullvalene})(\text{CO})\text{Cl}]$ reveals that the phosphasemibullvalene is a slightly better net-donor than phosphabarrelene **1**.

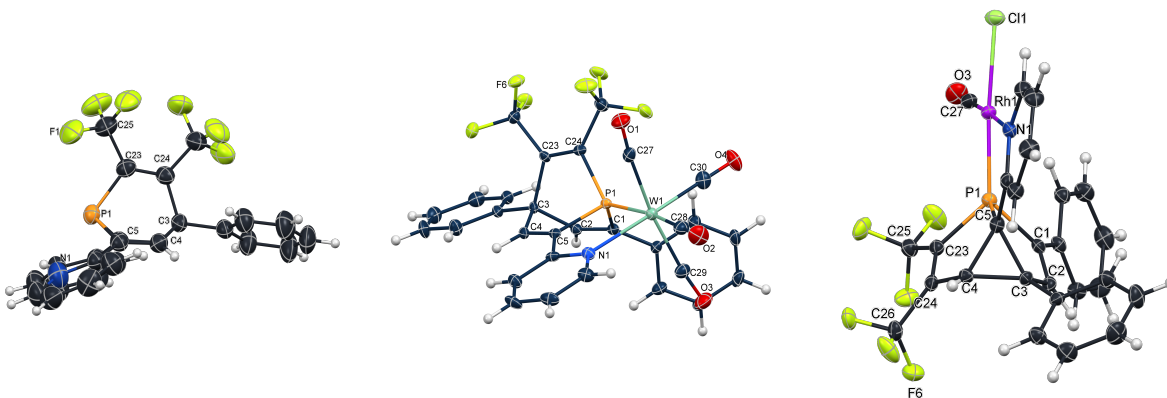


Figure 5.3 The pyridyl-substituted phosphabarrelene (left), its tungsten-carbonyl complex (middle) and the Rh-phosphasemibullvalene complexes (right).

It has been demonstrated that three novel classes of pyridyl-substituted phosphorus ligands can be obtained from the **PN** phosphinine, all of them having very different electronic and steric properties. On one hand, the pyridyl-functionalized λ^4 -phosphinines, which are anionic ligands that can coordinate two metal centers, one *via* the phosphorus atom and one *via* the delocalized charge along the phosphinine skeleton. When a second donor-functionality is present in the ligand structure, the coordination *via* the phosphorus atom is preferred. On the other hand, the pyridyl-functionalized phosphabarrelene provides special steric demand in a phosphorus cage, which can be taken in advantage for the design of complexes with specific characteristics. Moreover, from this phosphabarrelene, the pyridyl-substituted phosphasemibullvalene ligand can be obtained, which again offers different properties from the other class of molecules. In this case, a steric

demanding compound with better net-donor abilities can be used as ligand for transition metal complexes. In all cases, the pyridyl-functionality enhances the stability of the transition metal complexes prepared, when compared to the examples on the non-functionalized phosphorus analogues of the compounds reported in this work.